Elucidating BAP1-microRNA regulatory networks in mesothelioma.

Zohra Butt

Thesis submitted in accordance with the requirements of the University of Liverpool for the degree of Doctor in Philosophy

March 2018

Elucidating BAP1-microRNA regulatory networks in mesothelioma.

Zohra Butt

Abstract

BRCA-1 Associated Protein 1 (BAP1) is a nuclear deubiquitylase (DUB) frequently inactivated by mutation in specific cancers including malignant pleural mesothelioma (MPM). Mutations cause loss of nuclear BAP1 expression or catalytic inactivation and, as BAP1 regulates both ubiquitylation and transcription, its loss in cancer may dysregulate expression of specific proteins, and potentially non-coding RNAs such as miRNAs. To begin to address these questions, the proteome response to *BAP1* mutation was previously profiled in isogenic MeT5A mesothelial cells, and an unbiased DUB siRNA screen revealed that BAP1 regulates cellular abundance of the histone deacetylase HDAC2. In this thesis, I set out to (1) validate BAP1-dependent protein expression in isogenic MeT5A *BAP1*-mutant cells and patient-derived MPM cell lines, (2) address the mechanism by which BAP1 regulates HDAC2, and (3) to identify BAP1-miRNA regulatory networks in MPM.

Profiling the effect of BAP1-deficiency on the MeT5A proteome had revealed alterations in cytoskeletal and metabolic pathways. I verified reduced expression of glycolytic enzymes but increased expression of TCA cycle and associated anaplerotic pathway proteins in MeT5A *BAP1*-mutant cells. Altered expression of certain cytoskeletal proteins correlated with BAP1-status in a panel of patient-derived MPM cell lines, confirming responses to BAP1 loss in isogenic cell models may be evident on more complex genetic backgrounds.

Altered expression of HDAC2 is reported in cancer and our siRNA screen suggested this may be linked to BAP1 status. I found that BAP1 depletion regulates HDAC2 transcript abundance rather than protein stability, and that BAP1 status influences the response of MPM cell lines to HDAC inhibitors.

As BAP1 can influence transcription, I next explored the idea that BAP1 may also regulate expression of miRNAs. I used a NanoString platform to screen for BAP1-dependent miRNAs in isogenic MeT5A mesothelial cells. In total, ~400 unique miRNAs were identified and, compared with parental cells, 113 miRNAs were significantly modulated ($P \leq 0.05$, >1.5-fold) in BAP1-deficient cells. Unsupervised hierarchical clustering generated five distinct clusters, including a large group from the chromosome 14q32.31 miRNA tumour-suppressor locus that was downregulated in BAP1-deficient cells. Gene ontology analysis suggested these miRNAs may affect the cytoskeleton and transcriptional regulation. I then used the Nanostring platform to profile miRNAs in a panel of 20 MPM cell lines. I observed differential miRNA expression in MPM cell lines grouped by BAP1 status, including downregulation of the ch14q32.31 locus.

As loss of BAP1 protein may be more frequent than the reported mutation rate in MPM, post-transcriptional regulation of BAP1 may also be of importance in cancer. To explore this idea, I used computational algorithms to predict miRNA target sites in the BAP1 3'UTR. Several candidate miRNAs were identified, including members of the miR-125 and miR-200 families. We found significantly increased expression of miR-125b-5p in BAP1-deficient isogenic cells ($P \leq 0.01$) and an inverse correlation between miR-125b-5p and BAP1 protein expression ($R^2=0.85$) in MPM cell lines. In addition, a miR-125b-5p mimic could reduce BAP1 expression, suggesting that miR-125b-5p may act as a post-transcriptional modulator of BAP1, operating in a double-negative feedback loop to control BAP1 expression.

Together, the data in this thesis show that BAP1 deficiency leads to a significant deregulation of proteins involved in cytoskeletal and metabolic pathways, a reduction in HDAC2 transcript abundance, and profoundly altered miRNA expression profiles. My data suggest for the first time that BAP1-dependent miRNAs may in part account for the BAP1-deficient MPM phenotype and could provide new biomarkers for BAP1 loss.

Acknowledgements

I would like to thank my supervisors Professor Judy Coulson and Dr. Joseph Sacco. Without your unwavering support and guidance, I would not be the research scientist I am today. I came into your lab as a physiologist longing to escape the field of calcium signalling, and over the past three years you have patiently guided me down the path of molecular biology and cancer research, albeit with some speed bumps along the way! You have taught me the value of an inquiring mind and demonstrated immense passion and work ethic that I can only hope to emulate in my future endeavours.

I am extremely grateful to my parents, Samina and Ejaz, for their constant faith in my ability and for supporting me, even when you weren't quite sure what I've been doing the past three years! To my sisters Aisha, Mariam and Henna, my eternal champions. To Aisha, thank you for your words of encouragement, and for insisting on attending every graduation to cheer me on even when I was unimpressed. To Mariam, thank you for being you. We both made it! To Henna, for your constancy and for providing a laugh or two when it was most needed, even if it was at your expense. My remaining siblings Kasim, Ibrahim, Umar and Aaliyah, I hope I have made you proud.

Thank you to Jenna Kenyani for being *"my post doc"* and for your relentless teasing, I will miss your presence the most. A huge thank you to Andrew Fielding for being the fountain of knowledge for our lab. Thank you to Sarah Taylor for embodying the northern powerhouse we all needed. I extend my thanks to Matthew, Dorota, Francesca, Sarah, Neil, Nathan and to all my colleagues on 5th floor for making my PhD that much more enjoyable. To my friends in Red Block, I have appreciated the chatter and cups of tea. A special mention to Shiquan Wong, thank you for putting up with me. To my exceptional boyfriend Selim Kimyongur, for everything you have done and continue to do for my happiness. Thank you for keeping me fed these past few months!

Finally, I dedicate this thesis to my best friend, Bushra Sharif. We have made this journey together and this achievement is as much yours as it is mine. You have always been a source of love and inspiration, a testament to the wonderful person that you are.

Table of Contents

List of figures

List of tables

List of appendices

List of abbreviations

Abbreviation	Description
3'UTR	3’ untranslated region
5-Aza-CdR	5-aza-2′-deoxycytidine
aa	Amino acid
ACTB	Beta-actin
Ago	Argonaute
ALDOC	Aldolase C
APC/C	Anaphase-promoting complex
APF-1	ATP-dependent proteolysis factor 1
ARP	Actin-related proteins
Asp	Aspartate
ASS1	Argininosuccinate synthase 1
ASXL	Additional sex comb-like proteins
ath	Arabidopsis thaliana
BAP1	BRCA1-associated protein 1
BARD1	BRCA1 associated RING domain 1
BCA	Bicinchoninic acid
BCL2	B-cell lymphoma 2
BLF	British Lung Foundation
Bp	Base pair
BR	Biological replicate
BRCA1	Breast cancer 1
BSA	Bovine serum albumin
CCNE1	Cyclin E1
ccRCC	Clear cell renal cell carcinomas
CDKN2A	Cyclin dependent kinase inhibitor 2A gene
cel	Caenorhabditis elegans
CGR	University of Liverpool Centre for Genomic Research
Ch	Chromosome
CHFR	Checkpoint With Forkhead And Ring Finger Domains
CHOP	C/EBP homologous protein
CLL	B-cell chronic lymphocytic leukaemia
CM	Cutaneous melanoma
COPD	Chronic obstructive pulmonary disease
CRC	Colorectal cancer
CT	Computerised tomography
CTLA-4	Cytotoxic T lymphocyte antigen-4
Cu	Copper
CUL	Cullin
Cys	Cysteine
DAVID	Database for Annotation, Visualisation and Integrated Discovery
DDX	DEAD-box
DSB	Double strand break
DUB	Deubiquitylating enzyme
ECACC	European Collection of Authenticated Cell Cultures
ECM	Extracellular matrix
EGF	Human epidermal growth factor

EGFR	Epidermal growth factor receptor
EMT	Epithelial-to-mesenchymal transition
ENO2	Enolase 2
EPP	Extrapleural pneumonectomy
EZH2	Histone methyltransferase enhancer of zeste homolog 2
FBL	Feedback loop
FBS	Fetal bovine serum
FC	Fold change
FFL	Feedforward loop
FFPE	Formalin-fixed, paraffin-embedded
FN1	Fibronectin
FOV	Fields of view
FOX	Forkhead box
G6P	Glucose-6-phosphate
GADD34	Growth arrest and DNA damage 34
GO	Gene ontology
H2AK119ub1	Monoubiquitylation of histone H2A at lysine 119
H3K27me3	Trimethylation of histone H3 at lysine 27
H4K20me1	Methylation of histone H3 at lysine 20
HAT	Histone acetyl transferase
HBM	Host cell factor 1 binding motif
HCF-1	Host cell factor 1
HCL	Hierarchical clustering
HDAC	Histone deacetylase
HDAC2	Histone deacetylase 2
HDACi	Histone deacetylase inhibitor
HECT	Homologous to the E6AP Carboxyl Terminus
His	Histidine
HK2	Hexokinase 2
HR	Homologous recombination
ICAM1	Intercellular adhesion molecule-1
IG-DMR	Intergenic differentially methylated region
IHC	Immunohistochemistry
INO80	Human inositol auxotrophy 80
IR	Ionising radiation
ISG15	Interferon-stimulated gene 15
JAMM	JAB1/MPN/MOV34 family
JOS	Josephins
K	Lysine
KLF5	Krüppel-like zinc-finger transcription factor 5
LATS1/2	Large tumour suppressor kinase 1 and 2
M1	N-terminal methionine
mAb	Monoclonal antibodies
MDM2	Mouse Double Minute 2
MesobanK	Mick Knighton Mesothelioma Tissue Bank
MeV	Multiple Experiment Viewer
MINDY	Motif-interacting with Ub (MIU)-containing novel DUB family
miRNA	MicroRNA
miRNome	Global miRNA expression profiles
MM	Malignant mesothelioma

MPM	Malignant pleural mesothelioma
mTOR	Mammalian target of rapamycin
MULE	Mcl-1 ubiquitin ligase E3
NAD	Nicotinamide adenine dinucleotide
NEDD8	Neural precursor cell expressed developmentally down-regulated protein 8
NF-kB	Nuclear factor kappa-light-chain enhancer of activated B cells
NF2	Neurofibromatosis type 2 gene
NGS	Next generation sequencing
NLS	Nuclear localisation signal
NS	NanoString
NS1	NanoString nCounter cartridge 1
NS2	NanoString nCounter cartridge 2
NS3	NanoString nCounter cartridge 3
NSCLC	Non-small cell lung cancer
OCT4	Octamer-binding transcription factor 4
OGT	O-linked beta-N-acetylglucosamine transferase
osa	Oryza sativa
OTUD	Ovarian tumour proteases
OXPHOS	Oxidative phosphorylation
P-bodies	Processing bodies
P53	cellular tumour antigen P53
PARP	Poly ADP ribose polymerase
PBA	Phenylbutyric acid
PBS	Phosphate-buffered saline
PcG	Polycomb group
PD-1	Programmed death receptor-1
PDAC	Pancreatic ductal adenocarcinoma
PEG	Polyethylene glycol
PFS	Progression free survival
PGAM1	Phosphoglycerate mutase 1
PGC1α	peroxisome proliferator activator receptor-γ co-activator 1α
PGM2	Phosphoglucomutase 2
PI3K	Phosphoinositide 3-kinase
PPP	Pentose phosphate pathway
PR-DUB	Human polycomb repressive deubiquitylase complex
PRC1	Polycomb repressive complex 1
PRC2	Polycomb repressive complex 2
pre-miRNA	Precursor miRNA
pri-miRNA	Primary miRNA
PTM	Post-translational modification
PYGL	Glycogen phosphorylase L
qRT-PCR	Quantitative reverse-transcription PCR
rAAV	Recombinant adeno-associated virus
RBR	RING-between-RING
RCC	Reporter code count
RIN	RNA integrity number
RING	Really Interesting New Gene
RISC	RNA-induced silencing complex
RLIM	RING finger LIM domain-binding protein

RNA-Seq	RNA sequencing
RT	Reverse transcriptase
rTRAIL	Tumour necrosis factor (TNF)-related apoptosis-inducing ligand
SAHA	Suberoylanilide hydroxamic acid
SDS-PAGE	Sodium dodecyl sulfate polyacrylamide gel electrophoresis
SERPIN	Serine protease inhibitor
SETD2	histone methyl transferase SET domain containing 2
siBAP1	BAP1 siRNA
siC	siRNA control
SILAC-MS	Stable isotope labeling with amino acids in cell culture with mass spectrometry
siRNA	Short interfering RNA
SMRP	Soluble Mesothelin-Related Peptide
SNORDs	Small nucleolar RNAs
SUCLG2	Succinate-CoA ligase GDP-forming beta subunit
SUMO	Small ubiquitin-related modifier
TALEN	Transcription Activator-Like Effector Nuclease
TBS	Tris Buffered Saline
TBS-T	Tris Buffered Saline-Tween
TF	Transcription factor
TMA	Tissue microarray
TNF	Tumour necrosis factor
TPDS	Hereditary tumour predisposition syndrome
TSA	Trichostatin A
TSG	Tumour suppressor gene
Ubls	ubiquitin-like proteins
UCH	Ubiquitin carboxy-terminal hydrolase
ULD	UCH37-like domain
ULK2	Unc-51 like autophagy activating kinase 2
UPP	Ubiquitin-proteasome pathway
USP	Ubiquitin specific protease
UVM	Uveal melanoma
VAT-PP	Video-assisted thoracoscopic partial pleurectomy
VEGF	Vascular endothelial growth factor
WT	Wild-type
YY1	Yin yang 1
ZEB1	Zinc finger E-box-binding homeobox 1
ZFN	Zinc Finger Nuclease

Chapter 1: Introduction

1.1 Malignant pleural mesothelioma (MPM)

1.1.1 Clinical presentation

1.1.1.1 Affected organs

Malignant mesothelioma (MM) is a rare and aggressive cancer arising from mesothelial cells that line the surface of various body cavities. There are four anatomical sites where mesothelioma can develop, pleura, peritoneum, pericardium and the tunica vaginalis testis. Malignant pleural mesothelioma (MPM) is the most common form of this disease (~80%), followed by peritoneal localisation (~20%) (van Meerbeeck et al., 2011). Pericardial and tunica vaginalis testis presentations are extremely rare, accounting for <1% of all mesotheliomas (Mezei et al., 2017). This thesis will only address MPM.

1.1.1.2 Epidemiology

The background incidence of MPM in the UK is very low. There were 2,600 new cases of MPM diagnosed in the UK in 2014, representing <1% of the total cancer cases for that year, yet accounting for 2% of all cancer deaths in the UK, highlighting the dismal prognosis of this disease (Cancer Research UK). Exposure to asbestos is the principal causative agent in MPM, and as most asbestos exposure was work-related prior to UK legislation banning its industrial use in 1999, MPM is classified as an occupational disease in the majority of cases (Owen, 1964; Newhouse and Thompson, 1965; Elmes and Wade, 1965). The UK incidence rate of MPM has risen 67% since the early 1990s, reflecting the long latency period of MPM from first exposure to asbestos to initial diagnosis, which averages around 40 years (range 15–67 years) (Robinson, 2012). Because of the long latency period and national differences in the timing of reduction or ban of asbestos use, MPM incidence is expected to peak within the next few decades worldwide (Bianchi and Bianchi, 2014). In countries where asbestos continues to be mined and used (India, China, Russia, Vietnam, Zambia) MPM is likely to be a significant health burden in the decades to come (Kao et al., 2010). This underlines the ongoing importance of research directed towards early diagnosis and disease management of MPM.

1.1.1.3 Diagnosis

Diagnosing MPM represents a clinical challenge as the signs and symptoms are relatively non-specific and can be seen with almost any intrathoracic disease process. The clinical

manifestations of MPM usually develop insidiously and often include dyspnoea and chest pain. Chest X-ray usually shows a unilateral pleural effusion or thickening. Chest X-ray alone is insufficient for diagnosis of MPM and chest computerised tomography (CT) scan is usually performed. Observation of a "rind-like" tumour along the pleural cavity together with pleural thickening is suggestive of the disease (Eibel et al., 2003; Wang et al., 2004). However, a thoracoscopy to obtain a tissue biopsy for immunohistochemistry (IHC) analysis is required for the formal and relatively accurate (>90%) diagnosis of MPM (see section 1.1.3.2) (Husain et al., 2018). This comes with its own complications such as tumour seeding, and as MPM mainly affects elderly patients often presenting with significant comorbidities, tumour biopsies are not always available as these patients are unable to tolerate the surgical procedure (van Zandwijk et al., 2013). As such, there are ongoing efforts to focus on identifying non-invasive molecular biomarkers to guide diagnosis and patient management.

1.1.2 Therapy

1.1.2.1 Standard clinical management

MPM treatment options include three main modalities; surgery, radiotherapy and chemotherapy. Surgery aims to either cure the disease or control the symptoms. It is most beneficial for patients who present with early stage disease, improving symptoms such as dyspnoea and chest pain, but as for any diffuse cancer, microscopic disease is rarely eradicated with surgery (Sugarbaker and Wolf, 2010). The primary surgical treatments are lung-sparing pleurectomy with or without decortication, video-assisted thoracoscopic partial pleurectomy (VAT-PP), or complete lung removal with extrapleural pneumonectomy (EPP). However, in view of the high morbidity following EPP (Treasure et al., 2011) and lack of efficacy of VAT-PP in controlling pleural effusion in MPM patients (Rintoul et al., 2014), the optimal surgical management of MPM remains unclear.

MPM represents a challenge for radiotherapy, as the tumour encases the lungs making it difficult to irradiate disease while avoiding toxicity to normal lung and cardiac tissue. Radiotherapy is largely palliative, aimed at pain relief, but is also used to prevent the occurrence of subcutaneous metastasis developing along chest drainage sites (Boutin et al., 1995). The chemotherapeutic regimen considered to be the standard of care for the palliation of MPM is a combination of pemetrexed and cisplatin. Compared to cisplatin alone, this combination improves patient survival by two to three months (Vogelzang et al., 2003). Nevertheless, the median survival time with combination chemotherapy is

twelve months (Vogelzang et al., 2003), and fewer than 15% of patients treated with surgical resection live beyond three years (Schipper et al., 2008).

1.1.2.2 Clinical trials and emerging therapies

There remains a lack of effective biomarker targeted therapies for MPM, although new targets are now being identified and trials starting. Recently, immunotherapy targeting immune checkpoints such as cytotoxic T lymphocyte antigen-4 (CTLA-4) and/or programmed death receptor-1 (PD-1) with monoclonal antibodies (mAb) has shown promising early results MPM. MAPS2 is the largest phase II clinical trial of immune checkpoint inhibitors in MPM to date (Scherpereel, 2017). Initial findings were reported at ASCO last year, and support clinically meaningful activity for either anti-PD-1 mAb nivolumab alone or in combination with anti-CTLA-4 mAb ipilimumab in the second line setting. Combination therapy showed greater efficacy with a response rate of 26% versus 17%, and median progression free survival of 5.6 months compared to 4 months for nivolumab alone.

Vascular endothelial growth factor (VEGF) is produced by a variety of tumours, including MPM, and stimulates neovascularisation of tumours (Ohta et al., 1999). Numerous clinical trials have evaluated the effect of bevacizumab, a mAb directed against VEGF, alone and in combination with chemotherapy in MPM, with mixed results (Jackman et al., 2008; Kindler et al., 2012; Ceresoli et al., 2013). All chemotherapy combinations with addition of bevacizumab failed to meet primary endpoints of improvement in progression free survival (PFS), compared to the standard regimen of pemetrexed and cisplatin. However, in a phase III trial evaluating the role of bevacizumab in combination with pemetrexed and cisplatin, a statistically significant improvement in median PFS (9.2 vs. 7.3 months) and median overall survival (18.8 vs. 16.1 months) was observed as compared to patients who received pemetrexed and cisplatin (Zalcman et al., 2016). As such, the National Comprehensive Cancer Network, representing 27 of the United States' leading cancer centres, now recommends bevacizumab/pemetrexed/cisplatin as a first-line therapy option for patients with unresectable MPM who are candidates for bevacizumab (Ettinger et al., 2016).

Epigenetic regulators are also emerging as interesting cancer targets. Histone deacetylase (HDAC) inhibitors (HDACi) are under investigation in multiple tumour types (Eckschlager et al., 2017), and HDACi trials in MPM are of relevance to chapter 4 of this thesis. Other

targeted agents in development include the proteasome inhibitor bortezomib, and mesothelin-specific antibodies (Hassan et al., 2007a; Hassan et al., 2007b).

Though in its infancy, the ability to target microRNAs (miRNAs) also holds promise for molecular intervention in MPM, examples including the restoration or inhibition of miRNA expression in MPM using miRNA mimics and inhibitors, respectively (van Zandwijk et al., 2017) (see section 1.4.5.2).

1.1.3 Pathology

1.1.3.1 Histological subtypes

According to the World Health Organisation classification of tumours of the lung and pleura, there are three major histological subtypes of MPM: epithelioid (60%), sarcomatoid (20%) and biphasic (20%), which is a mix of both epithelioid and sarcomatoid histologies (Travis, 2014). The desmoplastic type is very rare (1%). It is important to differentiate MPM tissue on this basis as histological subtype is the strongest and most consistent predictor of survival in MPM (Scherpereel et al., 2010); epithelioid patients survive on average nine months longer than sarcomatoid patients (Bibby et al., 2016; Law et al., 1982; Johansson and Linden, 1996).

1.1.3.2 Biomarkers

A biomarker-directed approach is attractive in MPM diagnostics to identify "at risk" individuals and patients with early stage MPM. For this purpose, serum and pleural effusion markers have been investigated, but the diagnostic accuracy for the more promising biomarkers such as mesothelin, osteopontin, and fibulin-3 for discriminating between MPM and other intrathoracic diseases are variable (van der Bij et al., 2011). Mesothelin is the most widely studied, it is a cell surface glycoprotein that is highly expressed in MPM (Robinson et al., 2003). Soluble Mesothelin-Related Peptide (SMRP), a splice variant of mesothelin, is the only marker with FDA approval for monitoring of treatment response and disease progression in epithelioid and biphasic MPM (Robinson et al., 2003). However, a large meta-analysis reported poor sensitivity (32%) at 95% specificity, so negative results are of little value (Hollevoet et al., 2012). IHC markers have utility in distinguishing MPM from lung adenocarcinoma or metastasis from other sites. A wide panel of immunohistochemical stains which include both mesothelial markers (calretinin, cytokeratin-5 and wilms tumour-1) and adenocarcinoma markers are used to differentiate the neoplastic cells as being either of mesothelial or epithelial in origin, as MPM is

particularly liable to misdiagnosis as metastatic lung adenocarcinoma (van Zandwijk et al., 2013). Other findings suggest that loss of nuclear BRCA1-associated protein 1 (BAP1) staining may be useful as a diagnostic and prognostic biomarker in MPM (see section 1.3.2.3), and staining for ER stress-responsive transcription factor C/EBP homologous protein (CHOP) and growth arrest and DNA damage 34 (GADD34) phosphatase may prove useful for MPM prognosis and for informing the classification of MPM histopathology, respectively (Dalton et al., 2013).

1.1.4 Genomic landscape of MPM

In an effort to identify novel therapeutic targets in MPM, several studies have reported on the genomic background of MPM, as reviewed in (Hylebos et al., 2016). The mutational burden of MPM is relatively low (Bueno et al., 2016). Nevertheless, genetic analyses of MPM samples have identified several key genetic mutations, including frequent somatic inactivation of a number of tumour suppressor genes such as cyclin dependent kinase inhibitor 2A gene (CDKN2A) (Prins et al., 1998), neurofibromatosis type 2 gene (NF2, also known as merlin) (Sekido et al., 1995), and BRCA1-associated protein 1 gene (BAP1, see section 1.3.2) (Bott et al., 2011). Mutations in other genes have been associated with MPM albeit at lower frequency, including the tumour suppressor p53, large tumour suppressor kinase 1 and 2 (LATS1/2), histone methyl transferase SET domain containing 2 (SETD2), unc-51 like autophagy activating kinase 2 (ULK2), members of the DEAD-box (DDX) helicase family DDX3X and DDX51, and cullin 1 (CUL1), a component of an E3 ligase complex (Bueno et al., 2016; Guo et al., 2015a). In addition, frequent losses of chromosome arms 1p, 3p, 4q, 6q, 9p, 13q, 14q, and 22q and gains of chromosome arms 1q, 5p, 7p, 8q, and 17q have been reported in MPM (Jean et al., 2012). Although these studies were limited by small sample sizes and in some cases matched normal samples were missing, overall some interesting candidate driver genes have been detected for further research in MPM.

My protein of interest, BAP1, is also a deubiquitylating enzyme (DUB), therefore in the next section I will introduce the ubiquitin system.

1.2 Reversible ubiquitylation

1.2.1 Ubiquitin

Ubiquitin research started in the late 1970s following complementary discoveries of a small, universally-present protein of unknown function, termed ubiquitin (Goldstein et al.,

1975) and ATP-dependent proteolysis factor 1 (APF-1) (Ciechanover et al., 1980; Hershko et al., 1980). This new protein was shown to interact with a lysine residue of the chromatin-associated protein, histone H2A (Goldknopf and Busch, 1977) and was covalently conjugated to proteins before their degradation *in vitro* (Ciechanover et al., 1980) (Hershko et al., 1980). Soon afterwards, APF-1 and ubiquitin were shown to be the same protein (Wilkinson et al., 1980), bringing together two previously independent processes: protein degradation and chromatin-associated ubiquitin. Since then, the ubiquitin field has expanded immensely, including work stemming from discoveries for the requirement of the ubiquitin system for intra-cellular proteolysis, cell viability, and cell cycle progression (Ciechanover et al., 1984; Finley et al., 1984). Altogether, this has yielded the modern paradigm for the importance of regulated proteolysis in control of protein levels, as a discrete process from their control by transcription and protein synthesis.

In mammals, ubiquitin is encoded by four fusion genes, as monomeric ubiquitin-ribosomal protein fusions (Baker and Board, 1991; Redman and Rechsteiner, 1989) or tandem ubiquitin coding units (Wiborg et al., 1985); in each case, proteolytic processing of the initial translation product is required to produce functional ubiquitin. Ubiquitin is a 76-amino acid protein with a globular conformation and a molecular weight of approximately 8.5 kDa (Vijay-Kumar et al., 1987). It exists in cells as either monomers in the "free ubiquitin pool", or covalently conjugated to other proteins (Monia et al., 1989). The ubiquitin molecule is the most abundant representative of a larger family of ubiquitin-like proteins (Ubls). Ubls, including small ubiquitin-related modifier (SUMO), neural precursor cell expressed developmentally down-regulated protein 8 (NEDD8) and interferon-stimulated gene 15 (ISG15), share common structural features to ubiquitin and are similarly ligated to substrate proteins (Burroughs et al., 2012; Hochstrasser, 2009).

1.2.2 Ubiquitin conjugation

Ubiquitylation is a post-translational modification involving the covalent attachment of ubiquitin to substrate proteins via the sequential action of E1 (ubiquitin-activating), E2 (ubiquitin-conjugating) and E3 (ubiquitin ligase) enzymes (Ciechanover et al., 1982; Hershko et al., 1980; Hershko et al., 1983). These enzymes facilitate the formation of an isopeptide bond between the C-terminus of ubiquitin and the amine group of a lysine side chain residue of a substrate protein. As reviewed in (Clague et al., 2015), the human genome encodes for eight E1 enzymes, approximately forty E2 enzymes and more than six hundred E3 ligases (Clague et al., 2015). E3 ligases provide much of the specificity in the

ubiquitin system as they can interact with both the E2-ubiquitin conjugate and the substrate protein to which ubiquitin is to be transferred. Mechanistically, E3s have been classified into three families, the Really Interesting New Gene (RING), the Homologous to the E6AP Carboxyl Terminus (HECT) and RING-between-RING (RBR) (Morreale and Walden, 2016).

In its basic form, the concerted action of E1, E2 and E3 enzymes result in the conjugation of a single ubiquitin monomer to a substrate protein, termed "monoubiquitylation". Similarly, a substrate protein can be monoubiquitylated on multiple separate lysine residues, termed "multi-monoubiquitylation". The initial monoubiquitylation can be extended by peptide linkages of further "free" ubiquitin molecules to any of the seven lysine residues (K6, K11, K27, K29, K33, K48, K63) or the N-terminal methionine (M1) present in a substrate-attached ubiquitin, a process termed "polyubiquitylation". This produces polyubiquitin chains of various topologies, which are identified by the residue involved in the linkage e.g. K48-linked chains. Chain diversity is further increased by their architecture. In "homotypic" chains, all ubiquitin subunits are connected through the same lysine or methionine residue. In contrast, "heterotypic" chains contain multiple lysine linkages between ubiquitin subunits and may be mixed or branched. Mixed chains are composed of different linkages, but each ubiquitin is modified with one other ubiquitin molecule. In branched chains, a single ubiquitin molecule is modified with two or more ubiquitin molecules. The complexity of ubiquitin chains and their physiological relevance have been comprehensively reviewed (Akutsu et al., 2016; Li and Ye, 2008; Komander and Rape, 2012).

1.2.3 Functions associated with monoubiquitin and polyubiquitin chains

As ubiquitin contains seven lysine residues and ubiquitylation has been demonstrated to occur through each of them, this generates the potential for highly diverse modifications of target proteins. Monoubiquitylation has emerged as a regulator of gene transcription, subcellular localisation and activity of cellular proteins. Histone monoubiquitylation, particularly on H2A and H2B, can alter the structure of chromatin to repress or promote gene transcription, respectively (Meas and Mao, 2015). Furthermore, monoubiquitylation can serve as a signal to trigger the regulated internalisation of plasma membrane proteins, and can also regulate the activity of components of the endocytic machinery (Hicke, 2001). Proper cellular localisation of a protein is a primary means of regulating its activity and many strategies, including monoubiquitylation, have evolved to ensure precise spatial regulation. Monoubiquitylation can affect the function of nuclear DUBs towards specific

substrate proteins through regulation of their sub-cellular compartmentalisation (see section 1.3.3).

Specific biological roles are associated with the different polyubiquitin chain topologies. The cellular functions for K48- and K63-linked polyubiquitin chains were the first to be described, they are the two most abundant polyubiquitin chain types (Swatek and Komander, 2016). K48-linked chains were shown to target substrate proteins to the 26S proteasome for degradation (Chau et al., 1989). Whilst initially thought to be exclusive to the function of K48-linked chains, recent work now suggests that all chain types except for K63 are recognised by the proteasome and may target proteins for degradation (Jacobson et al., 2009; Xu et al., 2009). Of note, a role for K11-linked chains has been recognised during cell cycle progression, where they target cell cycle regulators for degradation (Min et al., 2015). In human cells, K11-linked chains are preferentially produced during mitosis and early G1, during which the anaphase-promoting complex (APC/C) E3 ligase recruits E2 ligases to generate heterotypic K11- and K48-branched chains on substrates (Jin et al., 2008; Meyer and Rape, 2014). This modification leads to the recognition of polyubiquitylated substrates and their rapid degradation by the proteasome.

In contrast, K63-linked polyubiquitin chains do not target substrate proteins for proteasomal degradation, instead substrates are delivered to the endosomal-lysosomal pathway (Nathan et al., 2013). The early endosome is the "sorting station" of the cell where internalised cargo, such as plasma membrane receptors, channels and lipid membranes are sorted for degradation in late endosomes/lysosomes or for recycling back to the plasma membrane (Jovic et al., 2010). Several studies demonstrate an important role for K63-linked ubiquitylation in protein sorting at the endosome (Lauwers et al., 2009), targeting internalised proteins to the lysosome (Huang et al., 2006; Barriere et al., 2007), and the internalisation step of endocytosis (Geetha et al., 2005; Duncan et al., 2006).

K63-linked polyubiquitylation can also serve a function in DNA repair (Spence et al., 1995), autophagy (Geisler et al., 2010) and the cellular response to hypoxia (Ferreira et al., 2015). Importantly, K63-linked chains are crucial for the regulation of nuclear factor kappa-light-chain enhancer of activated B cells (NF-kB) signalling. NF-kB is a transcription factor and central regulator of a wide range of biological pathways, including immune and inflammatory responses, cell survival, and senescence (Wertz and Dixit, 2010). In brief, K63-linked polyubiquitination initiates a series of phosphorylation events leading to the

translocation of NF-kB into the nucleus to enable its roles in gene regulation (Chen and Chen, 2013). It is now known that NF-kB activation involves at least two other types of ubiquitin chains on adaptor proteins, M1-linked linear ubiquitin chains (Rahighi et al., 2009) and heterotypic K48/K63-branched chains (Ohtake et al., 2016). This highlights another example of how ubiquitylation controls transcriptional regulation.

1.2.4 Deubiquitylation and the deubiquitylases

Importantly, ubiquitylation is a reversible process. Ubiquitin is removed from substrates through the action of DUBs. They do this by hydrolysing the isopeptide or peptide bond between ubiquitin and the substrate protein, and between ubiquitin monomers in polyubiquitin chains (Reyes-Turcu et al., 2009). Also, as outlined in section 1.2.1, ubiquitin is synthesised *de novo* as fusion proteins, either ribosomal protein-fused or strings of consecutive ubiquitin units, which must be cleaved by DUBs to produce free ubiquitin monomers. The human genome encodes ~100 DUBs that are subdivided into six families based on the nature of their catalytic domains: ubiquitin specific proteases (USPs), ubiquitin carboxy-terminal hydrolases (UCHs), motif-interacting with Ub (MIU)-containing novel DUB family (MINDYs), ovarian tumour proteases (OTUDs), Josephins (JOSs), and the JAB1/MPN/MOV34 family (JAMMs) (Abdul Rehman et al., 2016; Clague et al., 2013). These families are additionally differentiated into metalloproteases (JAMMs) or cysteine proteases (USPs, UCHs, OTUs, JOSs and MINDYs) with differing DUB enzyme mechanics. Metalloproteases contain a zinc ion within their active site which facilitates the activation of water molecules for subsequent ubiquitin chain hydrolysis. In distinction, cysteine proteases contain a catalytic triad comprising cysteine, histidine and aspartate, which together facilitate nucleophilic attack of the ubiquitin linkage (Komander et al., 2009a).

The degree of linkage specificity varies between DUB families. The MINDYs are a newly discovered family of DUBs that are highly selective for binding K48 polyubiquitin chains with at least four ubiquitin moieties (Abdul Rehman et al., 2016; Kristariyanto et al., 2017). Several of the JAMM metalloproteases exhibit greater specificity towards K63-linked ubiquitin chains than any of the other five DUB families (Ritorto et al., 2014). OTU family members OTU7B and OTUB1 display a distinct preference towards K11- and K48-linkages, respectively, whilst most USPs can cleave multiple different ubiquitin chain linkages thereby showing little or no preference for a specific chain linkage (Bremm et al., 2010; Edelmann et al., 2009; Ritorto et al., 2014). The JOSs are the smallest DUB family with only four members with their functions poorly understood. Ataxin-3 is the best studied of the

four, with preferential specificity for K63-linked polyubiquitin chains, however it shows even greater activity towards heterotypic chains containing both K48- and K63-linkages (Winborn et al., 2008).

The different DUB families are the subject of many recent reviews (Komander et al., 2009a; Komander, 2010; Clague et al., 2013; Maurer and Wertz, 2016). For the purposes of this thesis, I will highlight the UCH family, of which my DUB of interest, BAP1, is a member.

1.2.4.1 The UCH family of deubiquitylases

To date, four UCH enzymes have been identified, UCHL1 (Doran et al., 1983), UCHL3 (Wilkinson et al., 1989), UCHL5 (Lam et al., 1997) and BAP1 (Jensen et al., 1998). Structurally, the most prominent feature of UCH enzymes is an active-site crossover loop over the core N-terminal UCH domain, which forms upon ubiquitin binding (Johnston et al., 1999; Misaghi et al., 2005). This structure poses a significant steric obstruction as folded, ubiquitylated proteins are too big to enter through the crossover loop. Indeed, UCHL1 and UCHL3 (which contain only the UCH domain) have negligible enzyme activity against folded substrates or polyubiquitin chains of any linkage type *in vitro* (Komander et al., 2009b; Popp et al., 2009). It is thought that UCHL1 and UCHL3, with their restricted accessibility, instead act on ubiquitylation sites on unfolded regions of proteins and process *de novo* ubiquitin chains to replenish the free ubiquitin pool. In comparison, the proteasome-associated DUB UCHL5, and BAP1, which are larger proteins with N-terminal UCH domain and C-terminal extensions (Eletr and Wilkinson, 2014), have longer active-site crossover loops thus allowing cleavage of complex polyubiquitylated substrates (Clague et al., 2013). BAP1 also shows a preference for cleaving monoubiquitin, which is important for its function as a transcriptional regulator (see section 1.3.4.1)

DUBs themselves are also regulated through ubiquitylation. Within the UCH family, UCHL1 is monoubiquitylated at multiple lysine residues surrounding the active site, including K157 of the crossover loop, thus affecting its catalytic activity and impairing its ability to bind ubiquitylated substrates (Meray and Lansbury, 2007). Interestingly, UCHL1 can self-regulate this process via auto-deubiquitylation in a regulatory feedback loop. Like UCHL1, BAP1 is also multi-monoubiquitylated, in this case impairing its nuclear function, which BAP1 counteracts through auto-deubiquitylation (see section 1.3.3).

1.3 BRCA1-Associated Protein 1 (BAP1)

1.3.1 Functional domains

BAP1 is a ~90 kDa protein composed of an N-terminal catalytic UCH domain, followed by a region harbouring various protein-protein interaction domains and two C-terminal nuclear localisation signals (NLS) (Fig. 1.1). These domains are important for BAP1 function as a DUB within the nucleus, as mutations in the UCH or NLS domains result in the loss of DUB activity or nuclear localisation, respectively (Ventii et al., 2008). BAP1 also has a host cell factor 1 (HCF-1) binding motif (HBM), which it uses to bind to and deubiquitylate the transcriptional regulator HCF-1, and regions of interaction with the breast cancer 1 (BRCA1) - BRCA1 associated RING domain 1 (BARD1) heterodimer (BRCA1-BARD1) tumour-suppressor complex, additional sex comb-like proteins (ASXL1/2), forkhead box K1 and K2 (FOXK1/K2) and yin yang 1 (YY1) transcription factors, exemplifying the diverse functional roles of BAP1 in transcription.

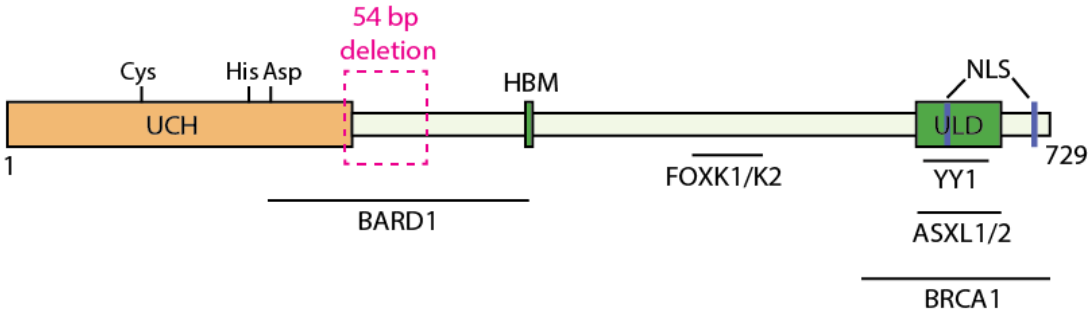

Figure 1.1: Schematic representation of BAP1 illustrating its functional domains and regions of interaction with other proteins.
BAP1 is a 729-amino acid protein belonging to the UCH family. The N-terminal UCH catalytic domain (1-250) contains the BAP1 catalytic triad Cys95, His169 and Asp184. BAP1 has two C-terminal NLS (656-661 and 717-722), a HBM domain (363-366), and a ULD domain of unknown function. BAP1 can interact with various proteins and transcription factors at the following regions: BARD1 (182-365), FOXK1/K2 (477–526), BRCA1 (598-729), ASXL1/2 (635–693) and YY1 (642–686). A novel isoform (BAP1Δ) with a 54 base pair (bp) deletion has been identified. UCH, ubiquitin carboxy-terminal hydrolase; Cys, cysteine; His, histidine; Asp, aspartate; BARD1, BRCA1 associated RING domain 1; HBM, HCF-1 binding motif; FOXK1/K2, forkhead box K1 and K2; NLS, nuclear localisation signal; ULD, UCH37-like domain; YY1, yin yang 1; ASXL1/2, additional sex comb-like proteins, BRCA1, breast cancer 1.

1.3.2 BAP1 is a tumour suppressor gene

The *BAP1* gene is located on chromosome region ch3p21.1, a genomic region that is known to be highly enriched for tumour suppressor genes (TSG) (Angeloni, 2007). No single characteristic defines a TSG, but classical features include: (a) mutated in cancer or in

inherited syndromes that predispose to cancer, (b) detectable loss of function mutations accompanied by loss of heterozygosity which can inactivate the growth suppressive activity of the protein (c) the ability to inhibit tumour growth *in vitro* upon restoration of protein expression and (d) mice with null mutations in the putative TSG show a predisposition to cancer (Guo et al., 2014).

Loss of heterozygosity and homozygous deletions of ch3p21 are frequently seen in a wide spectrum of epithelial cancers. In fact, ch3p deletions are detected in almost 100% of small-cell lung cancer and clear cell renal cell carcinomas (ccRCC), >90% non-small-cell lung cancer (NSCLC) cell lines and >80% of breast carcinomas (Angeloni, 2007). In another study, ch3p21.1 losses were also observed in 30% of MPMs (Bott et al., 2011). A seminal paper by Jensen *et al.* identified *BAP1* as a novel TSG, describing its location to ch3p21.2 – ch3p21.31 and identifying somatic *BAP1* deletions/mutations in lung carcinoma cell lines (Jensen et al., 1998). The group also showed that BAP1 could suppress breast cancer cell growth in soft agar. BAP1-mediated growth suppression was also observed in an *in vivo* model, the exogenous expression of wild-type (WT) *BAP1* in a *BAP1*-null cell line NCI-H226 suppressed proliferation in culture and reduced tumour growth in athymic nude mice (Ventii et al., 2008). Its tumour suppressive role was attributed to a functional NLS and to its deubiquitylating activity against substrates involved in DNA damage repair and cell cycle regulation (Ventii et al., 2008). It is important to note that there is some ambiguity in the literature surrounding the classification of NCI-H226, it is claimed to be an MPM or NSCLC cell line.

Nevertheless, the function of BAP1 in cancer is controversial. Paradoxically for a TSG, MPM cell lines containing WT *BAP1* showed decreased proliferation upon BAP1 knockdown, and the reintroduction of WT *BAP1* in *BAP1*-null MPM cell lines resulted in an increase in cell proliferation (Bott et al., 2011). In breast cancer cells, BAP1 was shown to have oncogenic functions, promoting cell proliferation by stabilising Krüppel-like zinc-finger transcription factor 5 (KLF5) via deubiquitylation (Qin et al., 2015). KLF5 is highly expressed in basal-like breast cancer and promotes breast cancer cell proliferation, survival, migration and tumour growth (Zheng et al., 2009; Liu et al., 2009b).

Somatic *BAP1* mutations in MPM were first reported in 2011 by Bott *et al.* (Bott et al., 2011). Using a candidate gene sequencing approach, they examined MPM tumours for mutations in genes located in chromosomal region ch3p21, and discovered that the gene showing

the highest rate of mutation was *BAP1*, with somatic mutations in 12 of 53 (23%) MPMs thereby implicating *BAP1* as a driver gene in MPM. In accordance with these results, somatic *BAP1* mutations were detected in 22% (4/18) (Testa et al., 2011) and 20% (24 of 121) (Zauderer et al., 2013) of sporadic MPM. In fact, these figures may be an underestimation as they come from a single molecular technique such as Sanger sequencing which can miss large DNA deletions. Studies that have used an integrated molecular approach that includes sequencing methodologies in conjunction with BAP1 IHC, record a *BAP1* mutation rate of >50% in sporadic MPM (Nasu et al., 2015; Lo Iacono et al., 2015). Furthermore, Pena-Llopis *et al*. detected somatic *BAP1* mutations in 14% (24/176) of ccRCC (Pena-Llopis et al., 2012). Harbour *et al*. reported inactivating somatic *BAP1* mutations in 47% (28/60) of uveal melanomas (UVM), with a much higher frequency (27/34, 79%) in metastasising UVM (Harbour et al., 2010). Less commonly, somatic *BAP1* mutations can also occur in distinct melanocytic tumours such as atypical spitz nevi (2/18, 11%) and in sporadic primary cutaneous melanomas (CM) (3/60, 5%) (Wiesner et al., 2012). Indeed, the spectrum of *BAP1*-mutated tumours is limited but varied.

Recent *in vivo* studies using genetically engineered *Bap1*-mutant mouse models provide solid evidence for its role in tumourigenesis and as an important TSG. In one study, homozygous mice were found to be embryonic lethal, indicating an essential survival role for the gene, and the generation of *BAP1*-deficient mice by conditional *BAP1* KO gave rise to features mirroring human myelodysplastic syndrome (Dey et al., 2012). In a different study, it was discovered that heterozygous *BAP1*-mutant ($BAP1^{+/-}$) mice were more susceptible to MM development, particularly of the peritoneum, upon exposure to asbestos. $BAP1^{+/-}$ mice showed greater than 2-fold increase in MM incidence, as well as decreased survival after asbestos exposure, compared to WT littermates (Xu et al., 2014), indicating that genetics may modify susceptibility to MPM. PCR analysis of DNA from MM cells of $BAP1^{+/-}$ mice showed reduced signal for the residual *BAP1* WT allele, indicating *BAP1* biallelic inactivation had occurred, consistent with its proposed role as a tumour predisposition gene (see section 1.3.2.1).

1.3.2.1 *BAP1* tumour predisposition syndrome

Coinciding with the first reports of somatic *BAP1* mutation in MPM, Testa *et al.* reported the first description of an association between germline *BAP1* mutations and familial MPM (Testa et al., 2011). They discovered germline heterozygous *BAP1* mutations cause a hereditary tumour predisposition syndrome (TPDS) associated with an increased risk in

families of developing MPM and other types of cancers, such as UVM, ccRCC, CM and breast cancer. This has stemmed from the work of Carbone *et al.* who discovered the existence of several familial clusters of MPM, implying that a family's genetic status had a role in determining susceptibility to MPM (Carbone et al., 2007). The same group have since identified germline *BAP1* mutations in two U.S. families (Family W and L) with high incidence of MPM. A germline splice-site mutation at the *BAP1* intron 6/exon 7 boundary in DNA from the W family was shown to lead to aberrant skipping of exon 7 during mRNA processing and predicted protein truncation. A nonsense mutation in *BAP1* exon 16 was present in the L family, creating a premature stop codon leading to a predicted protein truncation. Published simultaneously, another study described germline *BAP1* mutations in two families with atypical melanocytic tumours, UVMs and CMs (Wiesner et al., 2012). Since then, the syndrome has expanded with evidence of germline *BAP1* mutation leading to basal cell carcinoma, ccRCC, cholangiocarcinoma, meningioma and other malignancies (De La Fouchardiere et al., 2015; Wadt et al., 2015; Farley et al., 2013; Popova et al., 2013; Abdel-Rahman et al., 2011)

Importantly, the study demonstrated a high MPM incidence in the presence of germline *BAP1* mutation, in spite of very modest asbestos exposure, implying that *BAP1* could modulate asbestos-related carcinogenesis (Testa et al., 2011). Independent animal models have supported the notion that *BAP1* is a TSG whose mutations predispose to MM (Xu et al., 2014) and that low doses of asbestos might be sufficient to trigger MPM in the presence of a genetic predisposition (Napolitano et al., 2016). Indeed, two *BAP1*-mutant mouse models with engineered mutations analogous to Family W and L, showed a 2-fold higher incidence of MM development upon asbestos exposure, compared to WT littermates (Kadariya et al., 2016). Surprisingly, MPM patients with germline *BAP1* mutation and *BAP1* TPDS have a better prognosis compared to patients with sporadic MPM that retain BAP1 expression, showing up to a 7-fold increase in survival (Baumann et al., 2015; Ohar et al., 2016). Additionally, analysis of high risk MPM families have highlighted differences in clinical features with the presence of germline *BAP1* mutation. Overall, *BAP1*-mutant carriers are younger at the age of MPM diagnosis (58 vs. 68 years) compared to non-carriers, and tumours are predominantly of the epithelioid subtype.

1.3.2.2 *BAP1* mutation profiles in different cancers

According to the COSMIC and cBioPortal databases (Forbes et al., 2008; Gao et al., 2013; Cerami et al., 2012), which catalogue mutations found in cancer cell lines and patient

tumour samples, the percentage that harbour *BAP1* mutations are greatest in MPM (30.6%), UVM (31.5%) and ccRCC (13.6%) (Fig. 1.2). As discussed above, in the literature these represent the tumours classically associated with *BAP1* mutations (Bott et al., 2011; Harbour et al., 2010; Pena-Llopis et al., 2012). In contrast, *BAP1* mutations were less common in lung carcinoma (1.5%), as reflected in the literature (Andrici et al., 2016), and breast carcinoma (0.6%) (Forbes et al., 2008). Different types of mutation can occur in the *BAP1* gene, including: single base-pair substitutions leading to nonsense, missense or synonymous mutations; in-frame or frameshift mutations caused by insertions or deletions; splice-site mutations that alter exon inclusion; nonstop extensions where single base-pair substitutions occur within stop codons allowing continued and inappropriate translation of mRNA; whole gene deletions; and complex mutations with several changes at a specific location (Fig 1.2).

BAP1 mutations span the length of the protein structure and there is little clustering of mutations around specific amino acids or even within specific BAP1 domains (Fig 1.2). Overall, frameshift mutations caused by deletion, missense or nonsense substitutions are the most common sequence alterations across the five tumour types, especially in MPM, UVM and ccRCC. The predicted consequence of most frameshift deletions is BAP1 protein truncation, leading to loss of the NLS and/or the C-terminal protein binding domains. Nonsense substitutions can lead to premature stop codons and consequently the induction of nonsense-mediated decay to eliminate these mRNA transcripts (Hug et al., 2016). This reduces BAP1 protein level or generates unstable BAP1 protein if the mRNA is translated. As discussed in section 1.3.1, BAP1 is a predominantly nuclear DUB, the NLS transports BAP1 into the nucleus and within proximity of its substrates. Therefore, nuclear exclusion of BAP1 on loss of the NLS would render it unable to perform its nuclear functions. Missense mutations in the BAP1 UCH domain, which are least commonly seen in MPM than other tumours (Fig. 1.2), are predicted to interfere with the ubiquitin cleavage activity of BAP1.

Specific *BAP1* mutations occur at a low frequency, although there are some examples of recurrent alterations. For example, in MPM at amino acid position one there are two recorded incidences of a whole gene deletion and one of a homozygous in-frame deletion of 125 amino acids, the likely phenotypic consequence is that no BAP1 protein is produced. A higher frequency deletion at Serine520 has been recorded in ccRCC, which causes a frameshift that generates a truncated BAP1 protein lacking the NLS and corresponding

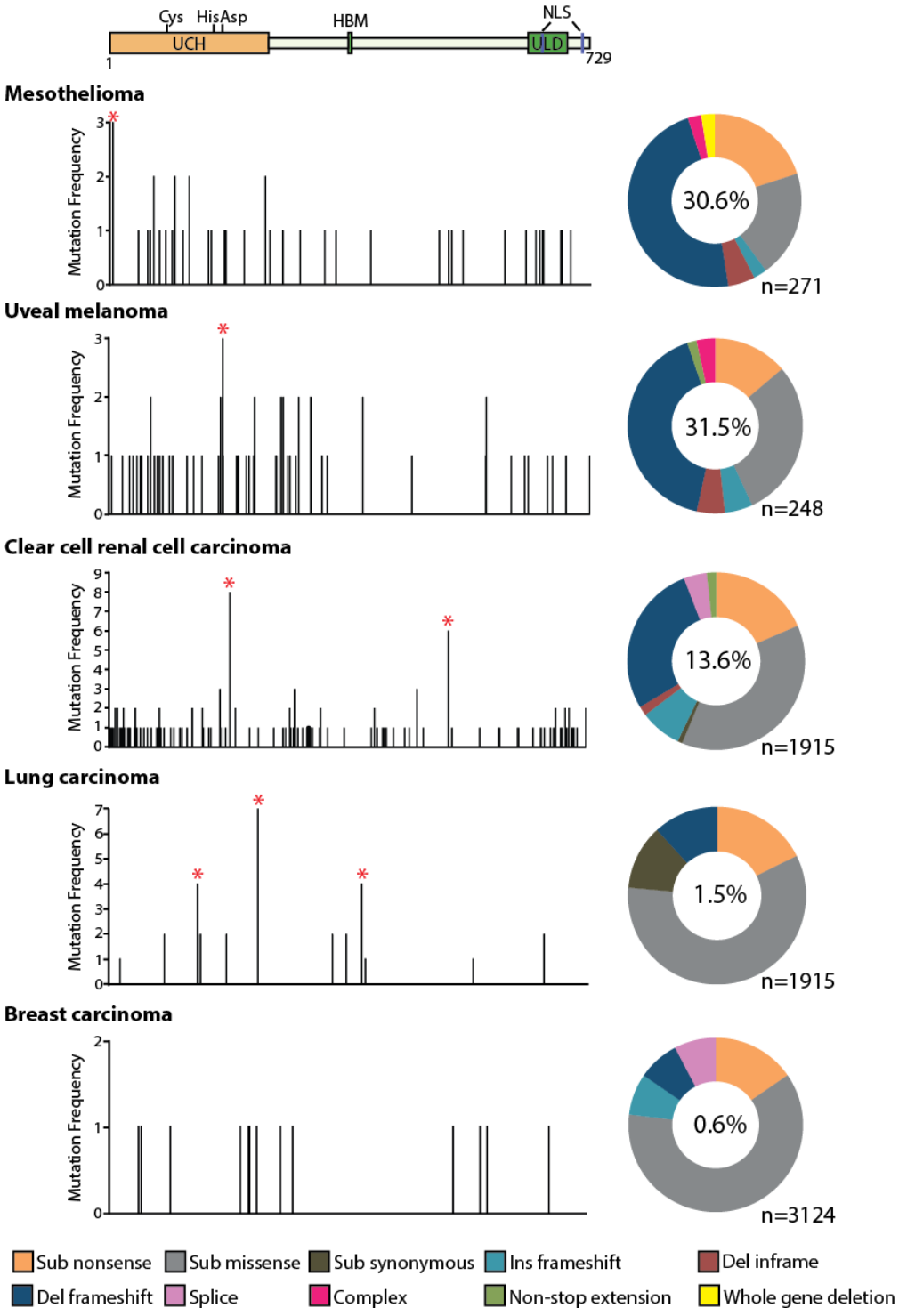

Figure 1.2: Mapping BAP1 mutations from cancer cell lines and tumour samples to its amino acid sequence

BAP1 mutations of varying frequency were identified in the five tumour types (COSMIC and cBioPortal, accessed July 2015). Of the 247 tumours with BAP1 mutations, 3.6% are heterozygous mutations and 15.8% are homozygous mutations. The pie charts depict the spectrum of BAP1 mutations that are found in each tumour type. N represents the total number of tested samples, and the proportion of those that are mutated are expressed as a percentage. Red asterisks highlight the mutations referred to in main text. Sub: substitution

nuclear functions, together with the C-terminal BRCA1 protein-binding domain. A relatively frequent nonsense substitution at Arginine385 is recorded in lung carcinoma, which is likely to result in the complete loss of the BAP1 C-terminal domain.

Aside from deletions, missense substitutions are the most frequent sequence alteration. In UVM, there is a missense substitution that changes Serine172 to an Arginine, in ccRCC a change from Glycine185 to Arginine, and in lung carcinoma, two different missense mutations that change Proline135 to Arginine and Arginine227 to Histidine. The fact that these missense substitutions all occur within the catalytic UCH domain of BAP1 could lead to interesting phenotypic consequences at the protein level. With all the domains intact, a protein product is likely to be produced, however BAP1 deubiquitylating activity is likely to be impaired.

1.3.2.3 BAP1 as a cancer biomarker

Recent studies have suggested a role for BAP1 IHC staining as a diagnostic and prognostic marker. Negative nuclear staining for BAP1 is already proposed as a reliable indicator of BAP1 mutation in MPM biopsies (Nasu et al., 2015). One study showed that loss of IHC staining for BAP1, while not definitive, can be used to support the diagnosis of MPM in pleural effusion cytology specimens (Andrici et al., 2015). In a large retrospective study of 143 MPMs, negative nuclear staining for BAP1 occurred in 62% of MPM specimens and was significantly associated with the presence of *BAP1* mutation, epithelioid subtype and a better prognosis (Righi et al., 2016). In agreement, there is a higher frequency of *BAP1* mutation in epithelioid MPM compared to sarcomatoid MPM (Cigognetti et al., 2015; McGregor et al., 2015; Pulford et al., 2017). Thus, an argument has been made to perform BAP1 IHC as part of the routine diagnostic work-up of patients with MPM, predominantly to predict outcome but also potentially as an adjunct for genetic testing for germline *BAP1* mutation (Farzin et al., 2015).

Interestingly, 25% of MPM tumours with otherwise normal BAP1 status failed to display IHC staining for BAP1, raising the possibility of post-transcriptional or post-translational repression of BAP1 in a subset of MPM tumours (Bott et al., 2011). The possibility that BAP1 could be inactivated or downregulated in cancer by non-genetic mechanisms is a hypothesis that is explored in chapter 7.

The use of liquid biopsies is a concept that relies on the analysis of circulating tumour cells or other cellular components, such as circulating tumour DNA, miRNAs, micro-vesicles or exosomes, in bodily fluids to provide information on cancer diagnosis and development (Alix-Panabieres and Pantel, 2013). This approach could potentially complement, or even serve as an alternative for tissue biopsy, which can be invasive, risky, and painful for the patient. As loss of BAP1 protein can support a diagnosis of MPM, surrogate markers for BAP1 loss that are detectable by liquid biopsy, such as miRNAs, could hold value as non-invasive diagnostic or prognostic biomarkers in MPM (see section 1.4.5.1).

1.3.2.4 Exploiting loss of BAP1 therapeutically

There are an exclusive set of driver genes that are frequently mutated in MPM, including *BAP1*. As such, there has been increased focus on BAP1 and its associated signalling pathways as potential therapeutic targets. BAP1-dependencies are described as the specific vulnerabilities conferred on the tumour cell as a consequence of *BAP1* genomic alteration. These vulnerabilities create a dependency of the tumour cells on a cellular pathway or process and the genes or proteins involved in them. The discovery of BAP1 dependencies are important if these alterations can sensitise tumour cells to current drug therapies.

LaFave *et al.* sought to identify mechanisms by which BAP1 loss leads to transformation, in the hope of identifying therapeutic vulnerabilities or synthetic lethalities in *BAP1*-mutant MPM cells (LaFave et al., 2015). In their study, they observed that *BAP1* mutation in MPM cells, typically resulting in loss of BAP1 protein, increased the expression of a subunit of the polycomb repressive complex 2 (PRC2), the histone methyltransferase enhancer of zeste homolog 2 (EZH2) (see section 1.3.4.1). This led to an increase in histone H3 methylation marks and enhanced repression of PRC2 targets. In an earlier study, EZH2 was found overexpressed in ~80% of primary MPMs compared with normal mesothelial cells, and its loss by shRNA knockdown decreased histone methylation levels and significantly inhibited tumourigenicity of MPM cells (Kemp et al., 2012). It has been proposed that BAP1 plays a role in sensitisation to drugs that target epigenetic regulators such as EZH2. Indeed, MPM cells that lack BAP1 are sensitive to EZH2 pharmacologic inhibition, suggesting a novel therapeutic approach where the BAP1 status of MPM patients can be exploited for treatment selection (LaFave et al., 2015). A phase II trial investigating the effect of EZH2 inhibitor Tazemetostat as second-line therapy in patients with BAP1-deficient relapsed or

refractory MPM is currently underway, this trial may inform a novel epigenetic therapy for BAP1-mutant MPM (Epizyme Inc, 2016).

In a recent study to determine if the mutational status of MPM could predict response to existing anti-cancer compounds, the authors discovered that a subset of MPM cell lines with loss of function *BAP1* mutations demonstrated increased sensitivity to the death receptor agonist recombinant tumour necrosis factor (TNF)-related apoptosis-inducing ligand (rTRAIL) (Kolluri et al., 2018). rTRAIL agonists selectively induce apoptosis in cancer cells, but has shown limited clinical efficacy in trials and to date there has been no investigation of rTRAIL therapy in MPM. The study proposes that BAP1 modulates rTRAIL sensitivity through PR-DUB activity by impinging on the expression of apoptosis pathway components. The association was also observed across 25 patient-derived MPM cell lines, human tumour explants and mouse MPM xenograft models, again providing support for the potential use of BAP1 functional status to stratify MPM tumours for rTRAIL therapy.

Due to the important role BAP1 plays together with BRCA1 in homologous recombination (HR) repair (see section 1.3.4.2) (Yu et al., 2014), poly ADP ribose polymerase (PARP) inhibitors were tested for their efficacy in *BAP1*-mutant tumour cells. PARP inhibition has generated mixed results in *BAP1*-mutant cells; one report observed no differential sensitivity between *BAP1*-WT and *BAP1*-mutant MPM cells treated with the PARP inhibitor MK4827 (Merck) (Bott et al., 2011), whereas increased sensitivity to another PARP inhibitor Olaparib was observed in homozygous *BAP1*-mutant chicken DT40 cells, compared to WT and heterozygous *BAP1*-mutant cells (Yu et al., 2014). A recent study by Parrotta *et al*. has highlighted the importance of an alternative splice variant of BAP1 in conferring sensitivity to PARP inhibition (see section 1.3.3) (Parrotta et al., 2017). They discovered that MPM cells expressing >20% of the BAP1 splice isoform (BAP1Δ) were more sensitivie to Olaparib, whilst the ratio of BAP1Δ: full length BAP1 isoform governed sensitivity to combination treatment with Olaparib and GDC0980, a dual phosphoinositide 3-kinase-mammalian target of rapamycin (PI3K-mTOR) inhibitor. It is possible that stratifying patients based on their BAP1Δ expression may improve clinical responses to PARP/PI3K-mTOR inhibitors.

1.3.3 Regulation of BAP1

BAP1 function may be regulated and diversified through expression of alternative isoforms, post-translational modifications (PTMs), or interaction with regulatory proteins and complexes. Recently, a novel BAP1 isoform (BAP1Δ) has been identified, with a 54 base-pair

deletion in exon 9 of BAP1, spanning the last 12 amino acids of the catalytic region and part of the BARD1 interaction domain (Fig. 1.1) (Parrotta et al., 2017). Although its relevance to BAP1 biology requires further investigation, BAP1Δ localises to the nucleus and may interfere with the nuclear functions of full length BAP1 in a dominant-negative manner, as BAP1Δ exhibited reduced DUB activity towards ubiquitinated histone H2A (see section 1.3.4) (Parrotta et al., 2017). Alternative splice variants are not unusual in cancer as the capacity to generate protein diversity can often confer a survival advantage (Paronetto et al., 2016). Whether this is the case for BAP1Δ remains to be elucidated.

BAP1 can be phosphorylated on multiple residues, leading to various functional consequences in DNA repair (see section 1.3.4.2) and gene silencing (see section 1.3.5). Studies have shown that BAP1 is phosphorylated at Ser592 in S-phase during replication stress (Eletr et al., 2013), and after ionising radiation (IR) treatment (Stokes et al., 2007; Yu et al., 2014). It is proposed that phosphorylation of BAP1 at Ser592 is a regulatory mechanism to control BAP1 function in HR DNA repair (Ismail et al., 2014), and to promote its interaction with other HR factors to facilitate recruitment to double-strand breaks following IR (Yu et al., 2014). Indeed, Yu *et al*. identified six IR-induced phosphorylation sites in BAP1, including Ser592, and showed that mutation of these inhibited BAP1 recruitment to DNA double strand break (DSB) sites (Yu et al., 2014). The phosphorylation of BAP1 at Thr493 is important for its interaction with the transcription factor FOXK2 and for its recruitment to FOXK2 target gene promoters (see section 1.3.5) (Okino et al., 2015).

BAP1 protein is largely confined to the nucleus, where it assembles in high-molecular-weight multi-protein complexes with transcriptional regulators to influence processes such as cell growth and proliferation and chromatin-associated processes such as transcription. The ubiquitin conjugating enzyme UBE2O regulates the shuttling of BAP1 between the nucleus and the cytoplasm by multi-monoubiquitylating its NLS leading to cytoplasmic sequestration, an activity which is antagonised by BAP1 autodeubiquitylation (Mashtalir et al., 2014). Although the significance of cytoplasmic BAP1 remains unclear, one study has suggested a possible interaction between BAP1 and ER channels that control pro-apoptotic Ca^{2+} flux from the ER (Bononi et al., 2017a).

A global proteomic analysis of DUBs and their associated protein complexes was performed by Sowa *et al*. to facilitate the understanding of DUB regulation, their biological function and targets (Sowa et al., 2009). Their software platform CompPASS employed an

unbiased comparative methodology to identify and score high-confidence candidate interacting proteins for 75 human DUBs, from parallel proteomic data sets generated through anti-tag immunoprecipitation and mass spectrometry (Jackson, 2009). The study revealed high-confidence interactions between BAP1 and several proteins, including ASXL1, ASXL2, HCF-1, O-linked β-N-acetylglucosamine transferase (OGT), FOXK1, FOXK2 and YY1 (see section 1.3.4). BAP1 interacts with polycomb group (PcG) proteins including the three humans homologs ASXL1, ASXL2 and ASXL3 (Katoh, 2013). The interaction between BAP1 and ASXL1 is critical for the catalytic activity of BAP1 as part of its function within the PR-DUB complex (see section 1.3.4.1) (Sahtoe et al., 2016), illustrating an essential mode of regulation for BAP1 through its protein-protein interactions.

1.3.4 BAP1 and chromatin modulation

Reversible ubiquitylation was initially viewed as a mechanism to target proteins for degradation, counteracted by the action of DUBs. This idea has now evolved as it is appreciated that reversible ubiquitylation can regulate a myriad of cellular processes, including the control of gene expression. One way that gene expression is regulated is through chromatin remodelling. Four core histone proteins (H2A, H2B, H3 and H4) are involved in the structural organisation of chromatin and each can undergo various covalent post-translational modifications such as (de)methylation, (de)acetylation, (de)phosphorylation and (de)ubiquitylation on specific residues to alter the chromatin structure, resulting in transcriptional activation or repression (Kouzarides, 2007).

1.3.4.1 BAP1 and H2A monoubiquitylation in transcriptional regulation

PcG proteins are transcriptional repressors first described in *Drosophila* as key regulators of epigenetic silencing of homeotic gene expression during development (Lewis, 1978). PcG proteins are found in large multi-protein complexes that catalyse post-translational modifications of histone proteins resulting in gene silencing. In mammals, two main repressive PcG complexes exist, polycomb repressive complex 1 (PRC1) and 2 (PRC2).

PRC2 and PRC1 are responsible for histone methylation and ubiquitylation, respectively (Fig. 1.3A*i*). EZH2 is a component of the PRC2 complex, it mediates the trimethylation of histone H3 at lysine 27 (H3K27me3), triggering the recruitment of the PRC1 complex through recognition of this histone mark by RYBP (see Fig. 5.13). Following this, the BMI1/RING1 E3 ligase component of the PRC1 complex facilitates chromatin repression and gene silencing through the monoubiquitylation of histone H2A at lysine 119

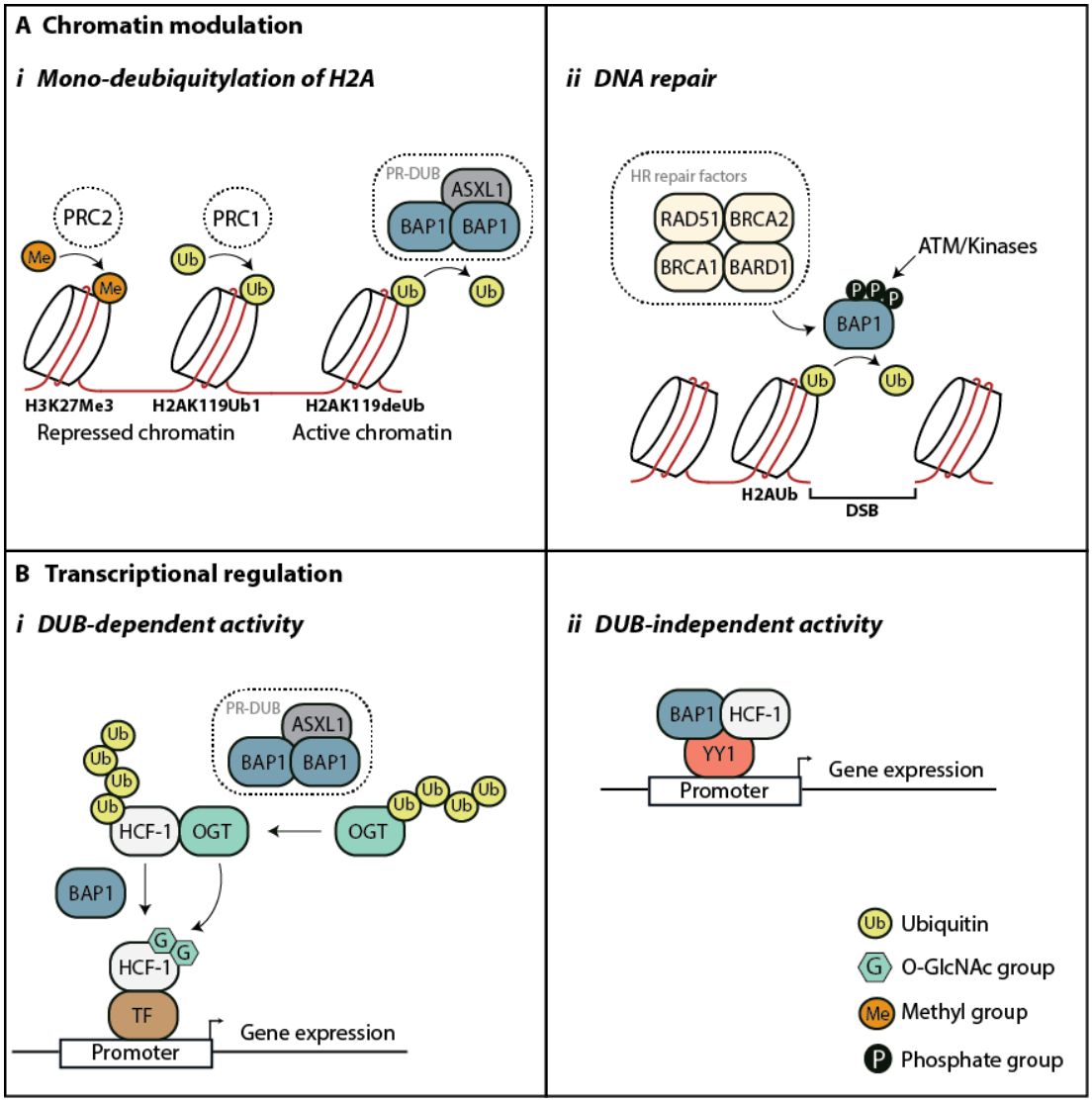

Figure 1.3: Functional roles of BAP1

A *i* BAP1 associates with ASXL1 to form the polycomb repressive deubiquitylase (PR-DUB) complex, which in turn deubiquitylates histone H2A. The PR-DUB complex opposes the activity of PRC1 and PRC2, de-repressing gene silencing caused by histone H2A ubiquitylation. ***A ii*** BAP1 can regulate the response to DNA double strand breaks (DSB). BAP1 is phosphorylated by ATM and multiple kinases, promoting its recruitment to the site of DNA damage and the recruitment of other DNA repair factors. BAP1 will deubiquitylate histone H2A at DSB sites. **B *i*** Through the PR-DUB complex BAP1 can also deubiquitylate OGT, a protease responsible for the O-GlycNAcylation and protein maturation of chromatin associated protein HCF-1. HCF-1 is also a substrate for the deubiquitylation activity of BAP1. ***B ii*** BAP1 also forms a ternary complex with HCF-1 and the transcription factor YY1, resulting in its recruitment to various gene promoters and leading to BAP1-activated gene expression. BAP1, BRCA1 associated protein 1; ASXL1, additional sex combs like 1; OGT, O-linked β-N-acetylglucosamine transferase; HCF-1, host cell factor 1; PRC1/2, polycomb repressive complex 1/2; YY1, yin yang 1.

(H2AK119ub1). Interestingly, H3K27me3 marks were increased in *BAP1* knockout hematopoietic cells, primarily at gene promoter regions of EZH2-dependent genes, suggesting BAP1 may regulate EZH2 activity and the expression of EZH2 targets (LaFave et al., 2015). The expression of BAP1 increases repressive H4K20me1 marks at the EZH2 locus, these are recognised by PRC1 subunit L3MBTL2 to maintain chromatin repression. BAP1 co-occupies the EZH2 locus with L3MBTL2 thereby ultimately controlling the transcription of EZH2 by deubiquitylating and stabilising L3MBTL2. As such, BAP1 depletion enhances EZH2 transcriptional output through reduced L3MBTL2 stability (LaFave et al., 2015).

It is thought that the compaction of nucleosomes and restricted accessibility to RNA polymerase complex contribute to the PRC1 mechanism of gene silencing (Simon and Kingston, 2009). Within the human polycomb repressive deubiquitylase (PR-DUB) complex, BAP1 opposes the action of PRC1 by deubiquitylating histone H2A (Fig. 1.3A*i*) (Scheuermann et al., 2010). For BAP1 to deubiquitylate histone H2A, it requires auto-recruitment to nucleosomes via its C-terminal extension (710-729 aa) and enzyme activation by ASXL1 (Sahtoe et al., 2016). The interaction between BAP1 and ASXL1 is critical for the catalytic activity; ASXL2 and ASXL3 can also activate BAP1 through a shared conserved DEUBAD domain thereby increasing its affinity for H2AK119ub1 (Sahtoe et al., 2016). Mass spectrometry analysis has also revealed BAP1 and the ASXL proteins complex together in a ratio of ~2:1, indicating that BAP1 is dimeric within the PR-DUB complex (Kloet et al., 2016).

Polycomb gene silencing is a dynamic balance between H3 trimethylation by PRC2 and demethylation by a range of specific histone lysine demethylases, and H2A monoubiquitylation by PRC1 and deubiquitylation by PR-DUB (Scheuermann et al., 2010; Shi, 2007). BAP1 knockdown has been shown to alter expression of several polycomb target genes (Bott et al., 2011), thereby implicating transcriptional dysregulation as a potential pathogenic mechanism in *BAP1*-mutated tumours.

1.3.4.2 BAP1 and the BRCA1/BARD1 complex in DNA repair

BAP1 was originally identified in a yeast two-hybrid screen as a protein that interacted with the RING finger domain of BRCA1 (Jensen et al., 1998). BRCA1 exists as a heterodimer with BARD1 through its RING domain, and this tumour suppressor complex has ubiquitin E3 ligase activity during the DNA damage response (Greenberg et al., 2006). Although BAP1 does not regulate the deubiquitylation of BRCA1, it can disrupt BRCA1 autoubiquitylation

and function by binding to and deubiquitylating BARD1. This abolishes the E3 ligase activity of BRCA1/BARD1 by perturbing heterodimer formation (Nishikawa et al., 2009). It is thought that BAP1 can function in the DNA damage response as down-regulation of BAP1 in HeLa cervical carcinoma cells by short hairpin RNAs resulted in S-phase retardation and hypersensitivity to ionising radiation, mimicking a phenotype similar to BRCA1 or BARD1 deficiency (Nishikawa et al., 2009). It was suggested that BRCA1-mediated E3 ligase activity and BAP1-mediated deubiquitylation together may regulate this cellular process.

Indeed, upon investigation of the cellular role of BAP1 in DSB repair, an enrichment of BAP1 was observed near DSB sites after IR treatment, which correlated inversely with H2A ubiquitylation levels (Yu et al., 2014). Crucially, ATM-dependent phosphorylation of BAP1 is important for cell survival after IR treatment and promotes BAP1 recruitment to DSB sites for H2A deubiquitylation (Fig. 1.3A*ii*). RAD51 and BRCA1 promote DSB repair through HR and are recruited to DSB sites (Price and D'Andrea, 2013). BAP1 depletion reduced the number of RAD51 and BRCA1 foci near DSB sites in irradiated fibroblast cells, potentially through an effect on gene expression governing BRCA1 recruitment on chromatin.

1.3.4.3 BAP1 and INO80 in DNA replication

BAP1 can also function as a chromatin-targeting factor to maintain genomic stability during normal DNA replication. In this process, nucleosomes are disassembled ahead of the replication fork for elongation and reassembled behind the replication fork to restore pre-replication chromatin structure. The chromatin remodelling complex human inositol auxotrophy 80 (INO80) promotes replication fork progression during normal DNA synthesis in human cells, but it was unclear how the complex was targeted to these forks. It was discovered that BAP1 stabilises INO80 by deubiquitylation and importantly, it recruits INO80 to replication forks through an interaction with H2AUb, via a mechanism which remains to be elucidated (Lee et al., 2014). In this scenario, there was no evidence of histone H2A deubiquitylation by BAP1, but BAP1 may instead function as a platform for INO80 to associate with chromatin and increase DNA accessibility ahead of the replication fork, or to restore pre-replication chromatin behind the fork. The study suggests that BAP1 can contribute to cell proliferation by promoting replication fork progression, which is somewhat paradoxical for its tumour suppressive function, but relevant to a role in suppressing genomic instability.

1.3.5 Other transcriptional roles for BAP1

In addition to its roles in H2A deubiquitylation, BAP1 regulates transcription through a variety of other mechanisms. Within the PR-DUB complex, BAP1 deubiquitylates and stabilises O-linked β-N-acetylglucosamine transferase (OGT), a protease responsible for the O-GlcNacylation (a form of glycosylation) and the proteolytic maturation of HCF-1 (Capotosti et al., 2011; Dey et al., 2012) (Fig. 1.3B*i*). Activated HCF-1 recruits OGT to O-GlcNacylate the transcription factor peroxisome proliferator activator receptor-γ co-activator 1α (PGC1α). This enables BAP1 to deubiquitylate and stabilise PGC1α, promoting gluconeogenesis. HCF-1 is a chromatin-associated protein; it cannot bind DNA directly nevertheless it can influence transcription through its recruitment to gene promoters by transcription factors that contain a HBM motif, and by functioning as a scaffold to recruit histone-modifying enzymes to these promoters (Tyagi et al., 2007). In this way, HCF-1 can both positively and negatively regulate the expression of genes involved in diverse cellular processes such as cell cycle progression and cell proliferation. HCF-1 is also a BAP1 substrate; BAP1 can bind HCF-1 via its HBM domain and deubiquitylate HCF-1 by preferentially removing K48-linked polyubiquitin chains (Fig. 1.3B*i*). In this context, the deubiquitylation of HCF-1 is a crucial step in BAP1-regulated cell growth; BAP1 can promote cell proliferation by accelerating G1/S progression via HCF-1 activation (Machida et al., 2009; Misaghi et al., 2009). In contrast, BAP1 is also involved in cell growth suppression mediated by BRCA1-BARD1 complex, thus the association of BAP1 with its interaction partners governs its functional output.

As nearly all cellular BAP1 is complexed with HCF-1, it was postulated that HCF-1 could represent a major scaffold protein for BAP1, helping to coordinate the association of BAP1 with other interacting partners to form specific transcription regulatory complexes (Yu et al., 2010). YY1 is a zinc finger protein with fundamental roles in embryogenesis, differentiation, replication and cell proliferation (Gordon et al., 2006). YY1 can activate or repress gene transcription depending on which transcriptional activators or repressors it is associated with, and to what gene promoters it is bound. BAP1 interacts directly with the zinc finger region of YY1 via its C-terminal domain, and consistent with its speculated role as a scaffold protein, HCF-1 is required for the formation of this ternary complex *in vivo* (Fig. 1.3B*ii*). BAP1-interacting proteins are known to be involved in chromatin-associated processes, aiding in the recruitment of BAP1 to specific promoters to activate transcription. Indeed BAP1/HCF-1/YY1 form a complex on chromatin, with YY1 targeting BAP1 to specific gene-regulatory regions, such as the *cox7c* gene promoter, which encodes a subunit of the

mitochondrial enzyme cytochrome c oxidase (Yu et al., 2010). Additionally, gene pathway analysis indicated that this ternary complex appears to control a number of different processes including cell cycle progression, cell survival, and metabolism (Yu et al., 2010). Similarly, the transcription factor FOXK2 has been reported to function as a chromatin-targeting factor for BAP1 (Ji et al., 2014). FOXK2 recognises BAP1 phosphorylated at Thr493 thereby recruiting it to FOXK2 binding regions on *MCM3*, *CDC14A* and *CDKN1B* genes (Okino et al., 2015). BAP1 represses these FOXK2 target genes by suppressing PRC1-mediated BMI1/RING1 E3 ligase activity. A surprising result given that BMI1/RING1 and H2A ubiquitylation is generally associated with chromatin repression and gene silencing (Fig. 1.3A*i*), it nevertheless raises the interesting possibility of PRC1-dependent activation of gene expression in BAP1-mutated cancers.

1.3.6 Other cellular roles for BAP1

Recently, several studies have been published describing novel functional roles for BAP1 (Baughman et al., 2016; Bononi et al., 2017a; Bononi et al., 2017b; Dai et al., 2017; Hebert et al., 2017). These roles range from BAP1 regulation of metabolism, intracellular calcium homeostasis, unfolded protein response, cytoskeletal organisation and cell motility. I will discuss these functional roles in greater detail and their implications in the context of my findings in chapters 3 and 5.

1.4 miRNAs

1.4.1 Biogenesis and functionality

miRNAs are short non-coding RNAs of 19-25 nucleotides that bind to the 3' untranslated regions (UTRs) of target mRNAs to downregulate gene expression at a post-transcriptional level (Bartel, 2004). miRNA genes are transcribed in the nucleus by RNA polymerase II or III to generate a primary miRNA (pri-miRNA) transcript (Lee et al., 2004; Borchert et al., 2006). A microprocessor complex containing the RNase III enzyme Drosha cleaves the transcript to form precursor miRNA (pre-miRNA) (Han et al., 2004). Pre-miRNA is then exported to the cytoplasm by exportin-5, where it is processed by RNase III enzyme Dicer into a mature miRNA duplex (Hutvagner et al., 2001). The duplex unwinds, and the functionally mature miRNA strand is incorporated into the RNA-induced silencing complex (RISC) whilst the passenger strand is often degraded. The thermodynamic stability of the strands determines which arm of the duplex will be incorporated into the RISC as the mature miRNA (Schwarz et al., 2003). The argonaute (Ago) proteins constitute the major functional

element of the RISC, and the sequence-specific repression of complementary target RNAs is mediated by the RISC through the binding of the Ago protein to the miRNA (Peters and Meister, 2007).

Within target mRNA, the "seed region" is a sequence of approximately seven nucleotides that is essential for miRNA binding (Lewis et al., 2003). A mature miRNA contained in the RISC complex is guided towards complementary mRNA targets, where the "seed sequence" (residues 2-8 at the 5' end) of the mature miRNA base pairs with the seed region of target genes. This can result in mRNA cleavage and subsequent degradation if there is complete complementarity, or translational repression with incomplete complementarity (Bartel, 2009; Filipowicz et al., 2008). Distinct cytoplasmic foci known as processing bodies (P-bodies) function as sites of general mRNA turnover and for storage of mRNA transcripts targeted for translational repression by miRNAs (Liu et al., 2005).

In mammals, miRNA-mRNA binding is generally the result of imperfect complementary base pairing, while in contrast, near-perfect complementary base pairing is most common in plants (Bartel, 2004). The imperfect nature of miRNA-target binding enables a single miRNA to target multiple mRNAs. There is also a degree of redundancy between miRNA that can target a single protein. In addition, individual mRNAs frequently contain more than one miRNA binding site, therefore miRNAs have the potential to regulate numerous cellular pathways and processes through targeting multiple mRNAs. Indeed, it has been estimated that miRNAs can regulate about two-thirds of all protein-coding genes in the mammalian genome (Friedman et al., 2009). This can create a complex regulatory network between miRNA-mRNA that can act in a tissue-specific and cell-state dependent manner (Lu et al., 2005). Disrupting this highly complex miRNA regulatory network can induce abnormal cell behaviour and disease pathogenesis (Li et al., 2010). As such, dysregulated miRNA expression is a common feature in cancers (Farazi et al., 2013), where miRNAs can act as either tumour suppressors or oncogenes ("oncomiRs") depending on the nature of their target genes.

1.4.2 miRNA nomenclature

Criteria and conventions for miRNA identification and naming are described in (Ambros et al., 2003). In miRNA databases, the names or identifiers of human miRNAs are of the form hsa-mir-125a-5p/3p. "hsa" signifies the organism, in this case homosapiens, "mir" refers to the gene locus and the pre-miRNA, whereas the mature miRNA is designated "miR", and

the number refers to the order of discovery. miRNA genes can also be annotated with an additional lower-case letter, for example hsa-miR-125a and hsa-miR-125b, these denote closely related mature sequences that are expressed from separate pre-miRNA. Often, the letters are used to differentiate among multiple members of the same miRNA family. The 5p/3p refers to the 5'- or 3' arm of the precursor sequence from which the mature miRNA is derived. Additionally, distinct precursor sequences or genomic loci that express identical mature sequences get numbered suffixes, for instance, hsa-mir-121-1 and hsa-mir-121-2 produce the same mature microRNA product: hsa-miR-121. The global miRNA expression profile in a specific genome is termed the "miRNome".

1.4.2 Regulation of miRNA expression

Although a considerable number of known miRNAs are universally expressed across human tissues, a growing body of research has revealed the highly tissue-specific nature of miRNA expression (Landgraf et al., 2007; Ludwig et al., 2016). This is unsurprising as different tissues have specialised functions and would therefore express a specific set of protein coding and miRNA genes for the regulation of these functions. Tissue-specific miRNA expression profiles have been determined for normal tissues and for various tumour types (Farazi et al., 2013).

The genes in which miRNAs are encoded are known as the host genes. It is thought that the majority of mammalian miRNAs appear to be located within introns of protein coding or non-coding genes (Rodriguez et al., 2004), which may have implications for their transcriptional regulation as they are transcriptionally linked to the expression of their host genes. These miRNAs are termed intragenic miRNAs. In contrast, intergenic miRNAs have their own gene promoters and so are expressed independently of nearby protein coding genes, and can be regulated through these promoters by specific transcription factors (Gulyaeva and Kushlinskiy, 2016). Almost half of all miRNA genes are organised in polycistronic clusters and are therefore co-expressed, suggesting that members of the same miRNA family may evolve simultaneously and share functional features (Kim et al., 2009; Baskerville and Bartel, 2005). Interestingly, several lines of evidence have recently emerged to suggest that miRNAs participate in regulatory loops with transcription factors to modulate their own expression, as discussed in more detail in section 7.1.

For both intra- and intergenic miRNAs, mutations in the DNA sequences of host genes or in the mRNA seed region are able to impact the biogenesis and function of miRNAs (Mishra

et al., 2008). Any disruption of host gene expression is also likely to affect intragenic miRNA expression; a gain-of-function mutation may enhance miRNA expression and consequently its regulatory effects towards it targets, whereas a loss-of-function mutation may abrogate miRNA expression and its target regulation. Additionally, mutation in the mRNA seed region may result in the escape from translational inhibition or degradation of the mRNA transcript by a miRNA (Chin et al., 2008).

Similarly to protein-coding genes, miRNA gene expression can also be regulated by methylation of their promoter regions (Han et al., 2007). DNA methylation indirectly influences the regulation of the miRNA target genes; promoter hypermethylation leads to silencing of miRNA genes and consequently an overexpression of target genes, whereas hypomethylation leads to miRNA gene re-expression and target gene repression. Various miRNA genes are affected by epigenetic inactivation due to aberrant hypermethylation, which is characterized as a mechanism of miRNA silencing in cancer (Guo et al., 2015c; Lujambio et al., 2007). At the post-transcriptional level, the expression of miRNAs can be regulated through changes in miRNA processing and stability. Their expression can also be downregulated due to dysregulation of the biogenesis machinery, such as losses or gains in Drosha, Dicer and Ago (Gulyaeva and Kushlinskiy, 2016). Overall, tumours frequently exhibit global downregulation of mature miRNAs, due to a combination of chromosomal deletion, mutation and epigenetic silencing (Jansson and Lund, 2012).

1.4.3 miRNAs in cancer biology

The first description of miRNA dysregulation in cancer was in B-cell chronic lymphocytic leukaemia (CLL), where the miR-15a/16-1 cluster was found to be deleted in the majority of CLL patients, resulting in elevated B-cell lymphoma 2 (BCL2) levels (Calin et al., 2002). This prompted the idea that each tumour type could possess a distinct miRNA signature that distinguishes it from normal tissues, and even other cancer types. In support of this, several studies have described altered miRNA expression in diverse types of cancers, compared with normal cells from the same tissue, as reviewed in (Iorio and Croce, 2017). Interestingly, the same group also revealed that miRNA genes are frequently located at fragile sites or in genomic regions that are prone to alterations in cancer (Calin et al., 2004), thus increasing their susceptibility to mutation and deletion. However, the combination of deletion plus mutation in miRNA genes are rare events (Calin et al., 2005), instead epigenetic regulation of miRNA expression is likely to be a major mechanism governing changes in miRNA function in cancer cells (Calin and Croce, 2006).

miRNAs have been proposed to contribute to tumourigenesis as upregulated miRNAs often act as oncomiRs whilst downregulated miRNAs possess tumour suppressive functions. However, the classification of miRNAs as one or the other can be difficult because of the intricacies of their expression patterns, which can differ for specific tissues and cellular states. Coupled with the fact that one miRNA can target multiple mRNA transcripts, it is possible for a single miRNA to function as a tumour suppressor in one context, and an oncomiR in another (MacFarlane and Murphy, 2010).

1.4.4 Potential for miRNA therapy in cancer

The rationale for using miRNAs as therapeutic agents is based on the findings that miRNA expression is dysregulated in cancer compared to normal tissues, and that cancer phenotypes can be altered by targeting miRNA expression (Rothschild, 2014). Current approaches for miRNA therapy in cancer involve either the restoration of tumour suppressive genes by inhibition of oncogenic miRNAs using miRNA inhibitors, or inhibition of oncogenes by treatment with "miRNA mimics" (Shah et al., 2016).

miRNA inhibitors are chemically synthesised, single-stranded oligonucleotides complementary to endogenous miRNA, which sequester miRNA so it cannot be processed by the RISC complex. There is a plethora of miRNA inhibitors, such as anti-miR oligonucleotides or antagomiRs, locked nucleic acids, miRNA sponges and miRNA masks (as reviewed by (Shah et al., 2016)). AntagomiRs have been used with relative success, the silencing of miR-10b with antagomiRs in a mouse breast cancer model was associated with reduced metastasis, both *in vitro* and *in vivo* (Ma et al., 2010). miRNA mimics are chemically modified RNA duplexes that can be loaded into the RISC complex to achieve downstream inhibition of target mRNAs. They represent an alternative to restore the normal function of downregulated miRNAs. Numerous studies have validated the efficiency of miRNA replacement therapy in *in vitro* and *in vivo* models, and in patients (see section 1.4.5.2) (Esquela-Kerscher et al., 2008; Esposito et al., 2014; Reid et al., 2013). The manipulation of miRNA expression in patient tumours represents a novel therapeutic tool, however the major challenge facing miRNA therapeutics is in the effective *in vivo* delivery of these agents to specific sites in the body.

1.4.5 miRNAs in MPM

In the first study to show dysregulated expression of miRNAs in MPM, Guled *et al.* compared miRNA expression profiles in MPM tumour samples compared with miRNAs in normal human pericardium, and between different histological subtypes of MPM, identifying a number of miRNAs related to MPM tumourigenesis and a set of miRNAs that can differentiate between MPM subtypes (Guled et al., 2009). Ivanov *et al.* have previously reported a downregulation of miR-31 due to deletions on chromosome 9p21.3 in approximately 54% of tumours from MPM patients, making this miRNA one of the most commonly deleted in MPM. miR-31 re-expression reduced proliferation through cell cycle arrest, and inhibited migration and invasion of MPM cells. miR-31 has also been linked with chemotherapy resistance in MPM. Moody *et al.* suggest the loss of miR-31 in MPM tumours may confer a chemosensitive phenotype, and as many MPM patients are inherently resistant to chemotherapy, stratifying patients based on high miR-31 levels could enhance the efficacy of chemotherapy following administration of miRNA inhibitors to silence miR-31 expression (Moody et al., 2017).

Although upregulated miRNA expression has been reported in MPM, such as increased expression of the miR-17-92 oncogenic cluster (Busacca et al., 2010; Balatti et al., 2011), the reduced expression of a variety of miRNAs in MPM seems to be associated with the characteristic biological changes observed in this cancer. miR-29c-5p is downregulated in MPM cell lines compared with normal mesothelial controls, with its overexpression able to inhibit proliferation and invasion of MPM cells *in vitro*. Asbestos-induced genomic changes in MPM often involves promoter hypermethylation (Christensen et al., 2008); the DNA methyltransferases responsible are targets of miR-29c-5p. They were shown to be downregulated following miR-29c-5p overexpression, implying that epigenetic regulation of MPM is a major function of miR-29c-5p (Pass et al., 2010).

The tumour suppressive functions of the let-7 family were first described in lung cancer (Takamizawa et al., 2004), and while there have been no reports of let-7 downregulation in MPM, it is suggested that the transcriptional upregulation of let-7 family members is involved in the attenuation of RAS activity and the impairment of anchorage-independent growth of MPM cells (Khodayari et al., 2011). MPM cells exhibit a propensity to migrate and locally invade surrounding tissue, and increased levels of epithelial-to-mesenchymal transition (EMT) markers in sarcomatoid MPM cells is thought to be associated with the aggressive, invasive nature of this subtype (Schramm et al., 2010). Evidence suggests that

changes in the expression of EMT-related genes are associated with dysregulated miRNA expression in MPM, with miR-205 and miR-145 expression showing an inverse correlation with EMT markers vimentin, zinc finger E-box-binding homeobox 1 (ZEB1) and octamer-binding transcription factor 4 (OCT4).

miR-34 and miR-15 families are well-described tumour suppressive miRNAs that are downregulated in many cancers because of chromosomal deletion or promoter methylation (Hermeking, 2010; Calin et al., 2002). Altered expression of these miRNAs have also been reported in MPM, the co-transcribed miR-34b/miR-34c cluster is silenced by methylation in the majority (85%) of MPM tumours (Kubo et al., 2011), and members of the miR-15 family were all detected at significantly lower levels in MPM cell lines and tissues compared with normal controls (Reid et al., 2013). MPM cell metabolism is another biological feature influenced by changes in miRNA expression, Tomasetti *et al*. showed that various stress stimuli induced the downregulation of miR-126 in MPM cells, consequently reducing mitochondrial respiration and promoting glycolysis in these cells (Tomasetti et al., 2014).

miRNA expression profiling of MPM has identified signatures associated with all stages of tumourigenesis, from cancer initiation, to development and metastasis. Understanding these miRNA signatures can inform on the consequences of their loss, and suggest novel targets for therapy and disease screening, which may help to improve patient survival for this cancer.

1.4.5.1 miRNAs as potential biomarkers in MPM

microRNAs have also been proposed as biomarkers for cancer due to their stability in a range of clinical samples (Nouraee and Calin, 2013). Recent studies have investigated their potential to provide diagnostic or prognostic information, either in the tumour itself or in blood samples and bodily fluids (Reid, 2015). Two independent studies demonstrating that microRNAs could be a useful tool to aid diagnosis focused on the ability of the miR-200 family to discriminate MPM from lung adenocarcinoma (Gee et al., 2010; Benjamin et al., 2010). Their test combines the significantly lower expression of all members of the miR-200 family, together with miR-192, miR-203, miR-205 in MPM, and the significantly higher expression of miR-193 and miR-152 families in MPM than is seen in lung adenocarcinomas: the miR-192/200c/193a signature is reported to provide 95% specificity in distinguishing MPM from lung adenocarcinoma (Benjamin et al., 2010). This assessment is now the basis

of a USA-regulations compliant diagnostic test offered by Rosetta Genomics (Benjamin et al., 2010).

Interestingly, miRNA expression profiles seem capable of complementing existing standard biomarkers such as mesothelin (Santarelli et al., 2011), thereby improving the accuracy of MPM diagnosis. miRNA-based biomarker tests could add relevant adjunct information in MPM and increase the probability of reaching the right diagnosis between MPM and adenocarcinoma, and between MPM subtypes. Negative nuclear staining for BAP1 is already proposed as a reliable indicator of BAP1-mutated MPM and an important adjunct to support MPM diagnosis. Therefore, the potential association of altered miRNA expression with tumourigenic mechanisms such as mutation in a MPM driver gene like *BAP1*, increases the likelihood of the miRNA(s) having a diagnostic value for MPM. As such, there is the possibility that altered miRNA expression profiles in *BAP1*-mutated MPMs could function as non-invasive surrogate biomarkers for *BAP1* loss in MPM.

1.4.5.2 miRNA-based therapies in MPM

The MesomiR-1 phase I clinical trial represents the first clinical experience of a miRNA replacement therapy in MPM (van Zandwijk et al., 2017). It was previously shown that the miR-16 family is downregulated in MPM, and restoration of expression with a miR-16 mimic led to a pronounced inhibition of MPM cell growth *in vitro* (Reid et al., 2013). From this, the commencement of the MesomiR-1 trial aiming to assess the safety and activity of miR-16 mimics in MPM has shown good tolerance and early signs of anti-tumour activity in humans (van Zandwijk et al., 2017). miR-16 mimics were delivered intravenously by loading the mimic into TargomiR minicells. Minicells are anucleate, nano-sized (400 nm in diameter) cells derived from bacteria, that can be packaged with various types of cargo and targeted to tumour cells via antibodies specific for tumour cell-surface receptors, in this case the epidermal growth factor receptor (EGFR) (MacDiarmid and Brahmbhatt, 2011).

Out of 22 patients who were assessed for response by pleural CT, fifteen had stable disease and one patient achieved an objective partial response to TargomiR treatment and showed substantial improvement in pulmonary function. Although results will need to be confirmed in larger studies, the study provides important safety data for TargomiRs as a therapeutic approach and shows encouraging anti-tumour activity in patients with refractory MPM.

In this chapter, I have presented an overview of MPM and highlighted the need for novel and non-invasive biomarkers to support early diagnosis. I have also discussed reversible ubiquitylation, with a particular focus on DUBs and the functions of BAP1. I have also described the genomic landscape of MPM, including the association between somatic and germline *BAP1* mutations and high MPM incidence. Finally, I have introduced the idea of miRNA dysregulation in cancer, and how differential miRNA expression has potential diagnostic value in MPM.

1.5 Project aims

1.5.1 Outstanding questions

MPM is a rare and aggressive cancer with poor prognosis and limited treatment options. A new wave of MPM research is now focussed on identifying therapeutic vulnerabilities that can sensitise this chemo-resistant tumour to current and newer chemotherapeutics. Although the mutation burden in MPM is low, there are an exclusive set of driver genes that are frequently mutated in MPM, including *BAP1*. Genetic inactivation of *BAP1* (see section 1.3.2) is well characterised, but alternative epigenetic mechanisms for *BAP1* inactivation, such as gene promoter methylation or the post-transcriptional repression by miRNAs are unexplored in MPM.

The literature surrounding BAP1 biology has exploded over recent years, with new roles still being discovered in different tumour types that can be conflicting in nature. This suggests that there are critical differences in tissue specificity in *BAP1*-mutant tumours, and that BAP1 functions may be highly context-dependent. As such, there is a need for better *in vitro* models for the appropriate cell context under investigation, particularly for MPM. The recent availability of well-characterised, patient-derived MPM cell lines through MesobanK, a bioresource facilitating the availability of MPM tissue, blood and cell lines for basic science, translational and clinical research (see section 3.1) (Rintoul et al., 2016), has improved the outlook for pre-clinical mechanistic studies in MPM. However, in order to establish the effect of a single gene mutation on MPM biology, this lab had utilised recombinant adeno-associated virus (rAAV)-mediated genome editing (Horizon Discovery) to engineer clinically relevant *BAP1*-mutated isogenic cell lines from MeT5A mesothelial cells (see section 3.1) (Kenyani et al., manuscript in prep). Alleles were sequentially targeted with a predisposition point mutation as seen in the Family W genome, and a promoter trap to mimic biallelic *BAP1* inactivation. These isogenic MeT5A *BAP1*-mutant cell lines were

used to profile the BAP1-dependent proteome in the search for synthetic lethal interactions, and this data was independently validated in this study.

The MPM research community is beginning to identify therapeutic targets that may be stratified according to BAP1 status (see section 1.3.2.4), however conclusive data from clinical trials are still lacking and other targets remain to be discovered, particularly in the emerging field of epigenetics. This lab has previously identified a link between BAP1 and histone deacetylase 2 (HDAC2) (section 4.1), but the mechanisms of action and the implications for HDACi in MPM were unknown.

Protein expression may be influenced by BAP1 on a number of levels, including through BAP1-regulated deubiquitylation, or through the transcriptional regulation of both coding and non-coding RNAs. The consequences of genetic *BAP1* inactivation on protein-coding gene expression in MPM (see section 1.3.4) is well documented. To date, there has been no investigation of the BAP1-dependent transcription of miRNAs and their consequent effect on cell biology. To this end, the isogenic MeT5A *BAP1*-mutant cell lines were used to explore for the first time the BAP1-dependent miRNome in a context of *BAP1*-deficient MPM. Currently, there are no surrogate liquid biopsy markers for *BAP1* loss, which could potentially enable stratification of BAP1 status via a simple blood test. miRNAs are stable in a range of clinical samples including liquid biopsies, therefore characterising a robust miRNA signature for *BAP1*-deficient MPM could hold great value as non-invasive diagnostic or prognostic biomarkers in MPM.

1.5.2 Specific aims

1. One of the major aims of this study was to validate the *BAP1*-responsive proteome in isogenic MeT5A *BAP1*-mutant cell lines, as part of a larger study to identify BAP1-dependencies that might influence MPM cell physiology and drug sensitivities (Kenyani et al., manuscript in prep) (Chapter 3). Following this, I aimed to explore the functional relevance of the *BAP1*-responsive proteome in a panel of patient-derived MPM cell lines of known BAP1 status and histologies, in order to infer the functional consequences of these expression changes in MPM (Chapter 3).

2. In the same vein, as part of another study investigating the link between BAP1 and HDAC2 (Sacco et al., 2015), I aimed to investigate the mechanism by which BAP1

regulates HDAC2 expression and the consequences of BAP1 loss-of-function for HDACi treatment in MPM (Chapter 4).

3. Furthermore, I investigated for the first time the *BAP1*-responsive miRNome in MPM, by profiling miRNA expression in isogenic MeT5A *BAP1*-mutant cell lines using the NanoString platform (Chapter 5). I aimed to expand the exploration of the *BAP1*-responsive miRNome across a large panel of patient-derived MPM cell lines, to explore any association of differential miRNA expression with BAP1 status and histological subtype (Chapter 6).

4. Lastly, I aimed to investigate the regulation of BAP1 by miRNAs in MPM, by exploring the correlative relationships between candidate miRNA expression and BAP1 status and histology across the large panel of patient-derived MPM cell lines, and through functional assays using miRNA mimics to manipulate miRNA expression (Chapter 7).

Chapter 2: Materials and Methods

2.1 Cell biology

2.1.1 Cell culture

Unless otherwise stated, all cell culture plastic ware was purchased from Corning (NY, USA). All cell culture media and fetal bovine serum (FBS) were from Gibco (Invitrogen, Paisley, UK). In every case, FBS was heat-inactivated at 55°C for 25 mins before its addition to cell culture media.

The non-malignant, SV40-transformed human pleural mesothelial cell line MeT5A was acquired from the American Tissue Culture Collection (ATCC, VA, USA). MeT5A were cultured in Medium-199 containing 1 g/L D-Glucose, supplemented with 10% FBS, 2% HEPES (Invitrogen), 0.1 mg/ml recombinant human epidermal growth factor (EGF) (Peprotech, London, UK), 10 mg/ml Hydrocortisone (Sigma-Aldrich, MO, USA), 10 mg/ml Insulin (Sigma-Aldrich), 0.1% Trace Elements B (CellGro, VA, USA) and 2 mg/ml Selenous Acid (Sigma-Aldrich). Isogenic BAP1 mutant cell lines previously engineered from MeT5A by gene-editing (see chapter 3), were cultured in Medium-199 as above, supplemented with 0.7µg/ml Puromycin (Sigma-Aldrich) for the *BAP1*$^{w-/+}$ cell line, and with 0.7µg/ml Puromycin and 0.1mg/ml G418 (ForMedium, Norfolk, UK) for BAP1$^{w-/KO}$ cell lines.

The human mesothelioma cell lines MSTO-211H, NCI-H2052, NCI-H2452, NCI-H28 and NCI-H226 were acquired from ATCC (hereafter referred to as ATCC cell lines) and cultured in RPMI-1640 media containing 2 g/L D-Glucose, supplemented with 10% FBS. Fifteen patient-derived, low-passage human mesothelioma cell lines were acquired from the Mick Knighton Mesothelioma Tissue Bank (MesobanK) (Rintoul et al., 2016), and are hereafter referred to as MesobanK cell lines. Ten of these cell lines ("#" designation) were cultured in RPMI-1640 media containing 2 g/L D-Glucose, supplemented with 10% FBS, and the remaining five cell lines ("MESO" designation) were cultured in RPMI-1640 GlutaMAX™ media containing 2 g/L D-Glucose, supplemented with 10% FBS, 20 ng/ml EGF, 1 µg/ml Hydrocortisone and 2 µg/ml Heparin (Sigma-Aldrich), according to the protocols from the two labs that derived these cell lines (Al-Taei et al., 2012; Chernova et al., 2016).

All cell lines routinely underwent mycoplasma testing using the EZ-PCR Mycoplasma Test Kit (Geneflow, UK) and STR profiling using the GenePrint 10 system (Promega, WI, USA).

Cells were propagated in culture for a limited number of passages in a humidified incubator at 37°C with 5% CO_2. Upon reaching 80% confluency in 100mm dishes, cells were washed with phosphate-buffered saline (PBS, Gibco) to remove any traces of serum. Cells were lifted from the dish following minimal incubation with 0.05% trypsin-EDTA (Gibco) and re-seeded into new dishes in fresh media at the ratios described in Table 2.1.

2.1.1.1 Freezing and thawing of cell lines

All cell lines were regularly frozen and stored in liquid nitrogen. Regular freezing ensured passage numbers were kept low. To freeze cells, a confluent (80%) T75 cm^2 flask was washed with PBS, trypsinised and then inactivated with complete medium. Cells were then collected in a 50 ml sterile tube and centrifuged for 5 min at 300g to pellet cells. Media was discarded, and the cells were resuspended in 10 ml of freezing media (media with 15% FBS, 5% DMSO, 10 mM HEPES pH 7.4). Cryovials (Corning) were labelled with appropriate identifying information and current passage number, and 1 ml of the cell suspension was added to each cryovial. Cryovials were stored at -80°C for at least 24 hrs in a Mr Frosty freezing container, which ensures gentle lowering of cellular temperature at a rate of 1 °C/min. After equilibrating at -80°C, cryovials were moved into liquid nitrogen for long term storage.

Cells were reconstituted by removal from liquid nitrogen and quick thawing to 37°C. The defrosted cell suspension was added to a T25 cm^2 tissue culture flask containing 10 ml warm complete media. Cells were then incubated at 37°C with 5% CO_2. After 24 hrs, media was refreshed on the cells to remove any residual DMSO.

2.1.2 RNA interference

RNA interference can be used to interfere with the function of an endogenous gene (Fire et al., 1998). siRNA transfections were performed in either 6-well plates or 60mm dishes. siRNA oligonucleotide sequences are listed in Table 2.2. Forward transfection protocols were employed in Chapter 4 to introduce siRNA into cultured cells, as per the manufacturer's instructions. MSTO-211H cells were seeded in 6-well plates or 60 mm dishes at 1.5 x 10^5 or 3.3 x 10^5 cells per well, respectively, in full growth medium one day prior to siRNA transfection. Immediately before transfection, media was replaced with 800 µl (6-well plate) or 1.8 ml (60 mm dish) of growth media with no FBS or other supplements. siRNAs were transfected into cells using the Oligofectamine transfection reagent (Invitrogen), at a final siRNA concentration of 45 nM. Briefly, two solutions were prepared

Cell Line	Source	Isolated from	Histological Subtype	Age	Gender	Split Ratios
MeT5A	ATCC	Pleural fluid	Transformed normal mesothelial	N/A	M	1:3 over 2 days
BAP1$^{w-/+}$	Isogenic *BAP1*-mutant cell lines derived from MeT5A*			N/A	M	1:2 over 2 days
C5.1 *BAP1*$^{w-/KO}$				N/A	M	1:2 over 2 days
C3.1 *BAP1*$^{w-/KO}$				N/A	M	1:2 over 2 days
MSTO-211H	ATCC	Pleural fluid	Biphasic	62	M	1:3 over 2 days
NCI-H2052		Pleural fluid	Epithelioid	65	M	1:2 over 3 days
NCI-H2452		Tumour tissue	Epithelioid	N/A	M	1:3 over 3 days
NCI-H28		Pleural fluid	Epithelioid	48	M	1:3 over 3 days
NCI-H226		Pleural fluid	Epithelioid	N/A	M	1:3 over 3 days
#2	MesobanK (Al-Taei et al., 2012)	Tumour tissue	Biphasic	41	F	1:4 over 3 days
#15		Tumour tissue	Epithelioid	68	M	1:4 over 3 days
#19		Tumour tissue	Biphasic	71	M	1:5 over 3 days
#24		Tumour tissue	Sarcomatoid	68	M	1:2 over 3 days
#26		Tumour tissue	Biphasic	66	M	1:3 over 3 days
#30		Tumour tissue	Epithelioid	60	M	1:3 over 3 days
#34		Pleural fluid	Sarcomatoid	53	M	1:3 over 3 days
#38		Tumour tissue	Epithelioid	63	M	1:3 over 3 days
#43		Tumour tissue	Epithelioid	56	M	1:3 over 3 days
#52		Tumour tissue	Epithelioid	57	F	1:2 over 3 days
MESO-3T	MesobanK (Chernova et al., 2016)	Tumour tissue	Epithelioid	56	M	1:3 over 3 days
MESO-8T		Tumour tissue	Epithelioid	77	M	1:3 over 2 days
MESO-12T		Tumour tissue	Epithelioid	78	M	1:3 over 3 days
MESO-14T		Tumour tissue	Epithelioid	59	M	1:3 over 3 days
MESO-23T		Tumour tissue	Epithelioid	68	M	1:3 over 3 days

Table 2.1: Cell line information for MeT5A wildtype and Isogenic BAP1 mutant cell lines, ATCC and MesobanK mesothelioma cell lines.
N/A: not available. *(Kenyani et al., manuscript in prep)

Protein	Oligo	Product Number	Target Sequence	Working Concentration
AllStars Negative Control	Non-targeting (siC)	SI03650318	N/A	45 nM
BAP1	#3 (siBAP1_3)	SI00066710	5'-CGCUGGUGCUGGA AGCAAATT-3'	45 nM
BAP1	#5 (siBAP1_5)	SI03036390	5'-GGUGAACCGUCAG ACAGUATT-3'	45 nM

Table 2.2: siRNA oligo sequences

Forward siRNA Transfection			
6-well plate		60mm dish	
Solution A	**Solution B**	**Solution A**	**Solution B**
2.5 µl siRNA	4.1 µl Oligofectamine	5.5 µl siRNA	9 µl Oligofectamine
180 µl OptiMEM	18.4 µl OptiMEM	396 µl OptiMEM	40.5 µl OptiMEM

Table 2.3: Reaction mixes for forward transfection of siRNAs.
siRNA stock concentration: 20 µM.

for siRNA transfection, the volumes for each component are listed in Table 2.3 for a 6-well plate or 60mm dish. Solution B was added to solution A and incubated for 20 mins at room temperature before 200 µl (6-well plate) or 450 µl (60 mm dish) of transfection complexes were added drop-wise to the cells. After 4 hrs incubation, FBS was added to the cells to a final concentration of 10%. The media was replaced the following day with full growth media. Cells were harvested 72 hrs after transfection for analysis by qRT-PCR or immunoblotting.

2.1.2.2 Reverse siRNA transfection

A reverse transfection protocol was employed in Chapter 7 to introduce siRNA into cultured cells. Reverse transfection was performed using Lipofectamine RNAiMAX transfection reagent (Invitrogen) and a final siRNA concentration of 45 nM. Two solutions were prepared for siRNA transfection, the volumes for each component are stated in Table 2.4 for a 6-well plate. Solution A was added to solution B at 1:1 ratio and incubated for 10 mins at room temperature, before 150 µl of the transfection complexes were added to a 6-well plate. MSTO-211H cells were trypsinised, counted and 2.8 x 10^5 cells seeded onto the transfection complexes in 2 ml of full growth media. Cells were harvested 72 hrs after transfection for analysis by immunoblotting.

Reverse siRNA Transfection: 6-well plate	
Solution A	**Solution B**
9.68 µl siRNA	9 µl Lipofectamine RNAiMAX
150 µl OptiMEM	150 µl OptiMEM

Table 2.4: Reaction mixes for reverse transfection of siRNA.
siRNA stock concentration: 20µM.

2.1.3 Reverse transfection of miRNA mimics

The overexpression of mature miRNAs was achieved by transfecting MPM cell lines with miRNA mimics (Qiagen) (see section 1.4.4). Reverse transfection of the miR-125b-5p mimic (MSY0000423) was performed using the Lipofectamine RNAiMAX transfection reagent. AllStars Negative Control siRNA (siC) and BAP1 #3 siRNA oligo (siBAP1_3) were used as controls in miRNA mimic experiments, as described in section 2.1.2.2. Two solutions were prepared for mimic transfections, as detailed in Table 2.5 for a 6-well plate. Solution A was added to solution B at 1:1 ratio and incubated for 10 mins at room temperature to allow formation of transfection complexes, before 150 µl were plated into 6-well plates. MSTO-211H cells were trypsinised, counted and then seeded onto the transfection complex at 2.8 x 10^5 cells/2 ml per well, and incubated for 72 hrs under normal growth conditions. Cells were incubated for 72 hrs under normal growth conditions prior to harvesting and analysis by immunoblotting.

miRNA mimic reaction mix	
Solution A	**Solution B**
1.08 µl miRNA mimic	9 µl Lipofectamine RNAiMAX
150 µl OptiMEM	150 µl OptiMEM

Table 2.5: Reaction mixes for reverse transfection of miRNA mimics.
Stock mimic concentration: 20 µM. Final concentration of miRNA mimic: 5 nM

2.1.4 Drug treatment of cells

2.1.4.1 Cycloheximide chase

MSTO-211H cells were seeded at 3.3 x 10^5 cells per 60 mm dish, and transfected the next day in standard media with 45 nM siRNA using Oligofectamine (section 2.1.3. 1). 72 hrs later, cycloheximide (Sigma-Aldrich) was added to cells at a final concentration of 10 µg/ml for 0.5 hr, 1 hr, 2 hrs, 4 hrs or 6 hrs before the cells were lysed in Laemilli buffer (section 2.3.1) and processed for immunoblotting (sections 2.3.2 – 2.3.4).

2.1.4.2 Proteasome inhibition

MSTO-211H or NCI-H28 cells were seeded at 1 x 10^6 cells per 60 mm dish. The following day, cells were treated with 50 nM epoxomicin (Calbiochem, CA, USA) for 6 hrs. For siRNA knockdown prior to epoxomicin treatment, MSTO-211H cells were seeded at 2.0 x 10^5 cells per well in a 6-well plate, transfected the following day with 45 nM siRNA using Oligofectamine then, 72 hrs later, cells were treated with 50 nM epoxomicin for 6 hrs. Cells were lysed in Laemilli buffer (section 2.3.1) and processed for immunoblotting (sections 2.3.2 – 2.3.4).

2.1.4.3 HDAC inhibition

To assay the effect of HDAC inhibition on cell viability, 4000 cells/well were seeded in 100 µl of cell culture medium in 96-well white-walled, clear-bottomed plates and incubated overnight at 37°C with 5% CO_2. The following day, the HDAC inhibitors vorinostat or mocetinostat (Selleck Chemicals, TX, USA) were added to cells in fresh media at a range of concentrations for 48 hrs (vorinostat: 100, 20, 10, 5, 2, 1, 0.5, 0.1 µM, mocetinostat: 40, 20, 10, 5, 2, 1, 0.5, 0.1 µM). The final DMSO concentration in all wells was 0.1%. Cell viability was measured using the CellTitre-Glo luminescent cell viability assay (Promega), as described in section 2.1.5.

2.1.5 Cell viability assays

Cell proliferation and viability was monitored using CellTitre-Glo luminescent cell viability assay (Promega), which estimates the number of viable cells by quantifying the cellular level of ATP. 1500 cells/well were seeded in 100 µl of cell culture medium in 96-well white-walled, clear-bottomed plates and incubated at 37°C with 5% CO_2. Luminescence measurements were taken at 4 hrs post seeding (T0) and then at 24 hr intervals over 5 consecutive days. Prior to these measurements, the plates were placed at room temperature for 30 mins. 100 µl of CellTitre-Glo reagent was added directly to cells and incubated for 10 mins in the dark with mixing to allow for cell lysis and the generation of a luminescent signal, which was detected using a Glomax multi-detection system (Promega, emission wavelength: 560 nm).

2.1.6 Flow cytometry

To determine the cell cycle distribution profile of the isogenic *BAP1*-mutant cell lines, exponentially growing cells were fixed in 80% ethanol/PBS prior to propidium iodide (PI, Sigma-Aldrich) staining (50 µg/µl) to determine DNA content (Fulwyler, 1965). PI-labelled

cells were gated on single cells and the fluorescence of single cells was quantified using a BD FACScalibur™ system (BD Biosciences, UK). The percentage of cells at each phase of the cell cycle (G_1/ G_0, S or G_2/M) was quantified based on DNA content.

2.2 Molecular biology

2.2.1 RNA Extraction

To avoid sources of RNase contamination, only RNase-free certified filter tips and tubes were used for RNA extraction, which was carried out in a designated workspace for RNase-free work, and all instruments and surfaces were treated with an RNase cleaning product RNaseZap (Thermo Fisher Scientific, MA, USA).

2.2.1.1 Total RNA extraction for mRNA analysis

Total RNA extraction was performed using the RNeasy mini kit and QIAshredder columns (Qiagen, Germany) with on-column DNase digestion in accordance to the manufacturer's protocol. Briefly, samples were lysed and homogenized in guanidine thiocyanate-containing buffer and beta-mercaptoethanol to release RNA and inactivate RNases (Chomczynski and Sacchi, 1987). Lysates were spun through QIAshredder columns to remove cellular debris. Ethanol was added to the lysates prior to addition to RNeasy spin columns, to promote the selective binding of RNA to the RNeasy silica membrane, followed by DNAse digestion. Total RNA was eluted in 30 µl RNAse-free water (Qiagen) and the concentration (ng/µl) and purity were determined using a Nanodrop 1000 spectrophotometer (section 2.2.2.1). The RNA integrity of total RNA was also assessed by gel electrophoresis. RNA samples were stored at -80°C.

2.2.1.2 Total RNA extraction for miRNA analysis

To enrich for small RNAs <200 nucleotides (such as miRNAs), total RNA extraction was performed using QIAzol lysis reagent and the miRNeasy mini kit (Qiagen) with on-column DNase digestion as above. Briefly, samples were lysed and homogenized in QIAzol lysis reagent containing phenol and guanidine thiocyanate, designed to release RNA, inhibit RNases, and to remove cellular DNA and proteins from the lysate by organic extraction. After addition of chloroform, the homogenate was separated into aqueous and organic phases by centrifugation. RNA partitions to the upper, aqueous phase, while DNA partitions to the interphase and proteins to the lower, organic phase or the interphase. The upper, aqueous phase was collected, and ethanol added to promote the selective binding of all

RNA molecules >18 nucleotides upwards to the RNeasy spin column silica membrane. The lysate was applied to the RNeasy spin column, followed by followed by DNAse digestion. Total RNA was eluted in 30 µl RNAse-free water and the concentration (ng/µl) and purity of RNA was determined in three quality control assays as described in section 2.2.2. RNA samples were stored at -80°C.

2.2.2 Quality assessment of total RNA

2.2.2.1 NanoDrop 1000 spectrophotometer

Nucleic acids were quantified using UV absorption measured at 260 nm by the NanoDrop 1000 spectrophotometer (Thermo Fisher Scientific). The concentration of nucleic acid was determined using the Beer-Lambert law, which predicts a linear relationship between absorbance and concentration: $A = \varepsilon cl$ where A = absorbance, ε = extinction coefficient, c = concentration in M^{-1} cm^{-1} and l = path length. In addition, absorbance at 280 nm and 230 nm was measured to assess protein or organic compound contamination. The A260/280 ratio was used to determine protein contamination of a RNA sample, whereas the A260/230 ratio indicates the presence of organic contaminants. For pure RNA, a ratio of ≥1.8 was considered acceptable, and all samples satisfied these criteria.

2.2.2.2 Qubit fluorometer

Total RNA, following the miRNA extraction method, was quantified using a Qubit 2.0 fluorimeter (Thermo Fisher Scientific) and Qubit RNA BR Assay Kit (Thermo Fisher Scientific), at the University of Liverpool Centre for Genomic Research (CGR). This method utilises fluorescent dyes that bind specifically RNA, providing greater specificity than UV absorbance–based quantification, where DNA, RNA, protein, free nucleotides or excess salts may all contribute to the absorbance at 260nm. Total RNA was measured relative to RNA standards of known concentration.

2.2.2.3 Agilent 2100 bioanalyser

The quality and integrity of total RNA, following the miRNA extraction method, was confirmed using an Agilent 2100 bioanalyser and RNA 6000 Pico Kit (both Agilent Technologies Inc, CA, USA), at the CGR. The bioanalyser examines RNA fragments following electrophoretic separation based on their size. The bioanalyser software generates an electropherogram, which provides a visual assessment of the quality of the RNA sample, and the trace was used to produce an RNA Integrity Number (RIN) for each sample. The RIN software algorithm allows for the classification of total RNA based on a numbering system

of 1 – 10, with 1 being the most degraded and 10 being the most intact. A RIN ≥7 is indicative of high quality intact RNA, and all samples met this criterion.

2.2.3 Reverse transcription

A dedicated hood was used to set up reactions for cDNA synthesis and PCR amplification (Temin and Mizutani, 1992). To avoid RNase contamination, only RNase-free certified filter tips and tubes were used. All instruments and surfaces were treated with RNaseZap. To avoid cross-contamination of DNA templates, the hood work surface and all equipment were irradiated with UV light for 30 mins prior to use.

2.2.3.1 cDNA synthesis from mRNA

cDNA was reverse transcribed from 1 µg total RNA with RevertAid H-minus M-MulV reverse transcriptase (Fermentas, Thermo Fisher Scientific) and an oligo-dT primer (Promega). Briefly, 1 µg RNA and 0.5 µg oligo-dT primer were incubated at 70°C for 5 mins then snap chilled on ice, to ensure the primer annealed to the 3' polyadenylated tail of mRNAs. A reaction mix containing 4 µl reverse transcriptase buffer (1X) (Fermentas), 2 µl of 10 mM polymerase chain reaction (PCR) nucleotides (Promega) and 0.5 µl of 40 µg RNasin (Promega) was then added. After 5 mins incubation at 37°C, 1 µl RevertAid H-minus M-MulV reverse transcriptase (200 units/µl) was added to each sample and cDNA synthesised for 1 hr at 42°C. Denaturation at 70°C for 10 mins and snap-cooling the samples on ice deactivated the reverse transcriptase and minimised secondary structure of the cDNA, which was diluted 1:5 in RNase-free water (Sigma-Aldrich) and stored at -20°C until further use. Reactions were prepared from RNA without addition of reverse transcriptase (RT-) for use as negative controls, to ensure all PCR amplicons are derived from cDNA and not from contaminating genomic DNA.

2.2.3.2 cDNA synthesis from mature miRNAs

cDNA was reverse transcribed from 2 µg total RNA using miScript II RT Kit (Qiagen). Mature miRNAs were polyadenylated by poly(A) polymerase and reverse transcribed into cDNA using oligo-dT primers containing 5' universal tags (Fig. 2.1). Briefly, 2 µg RNA was added to 2 µl reverse transcriptase mix (1X) containing poly(A) polymerase, 4 µl HiSpec buffer (5X) which facilitates the selective conversion of mature miRNAs and certain small nuclear/nucleolar RNAs into cDNA, and 2 µl oligo-dT primers (10X). The reaction volume was made up to 20 µl with RNase-free water. cDNA was synthesised for 1 hr at 37°C, followed by heat-inactivation of the reverse transcriptase at 95°C for 5 mins. cDNA was then

diluted 1:100 in RNAse-free water (Sigma-Aldrich) and stored at -20°C until further use. Reactions without addition of reverse transcriptase (RT-) were generated for use as negative controls.

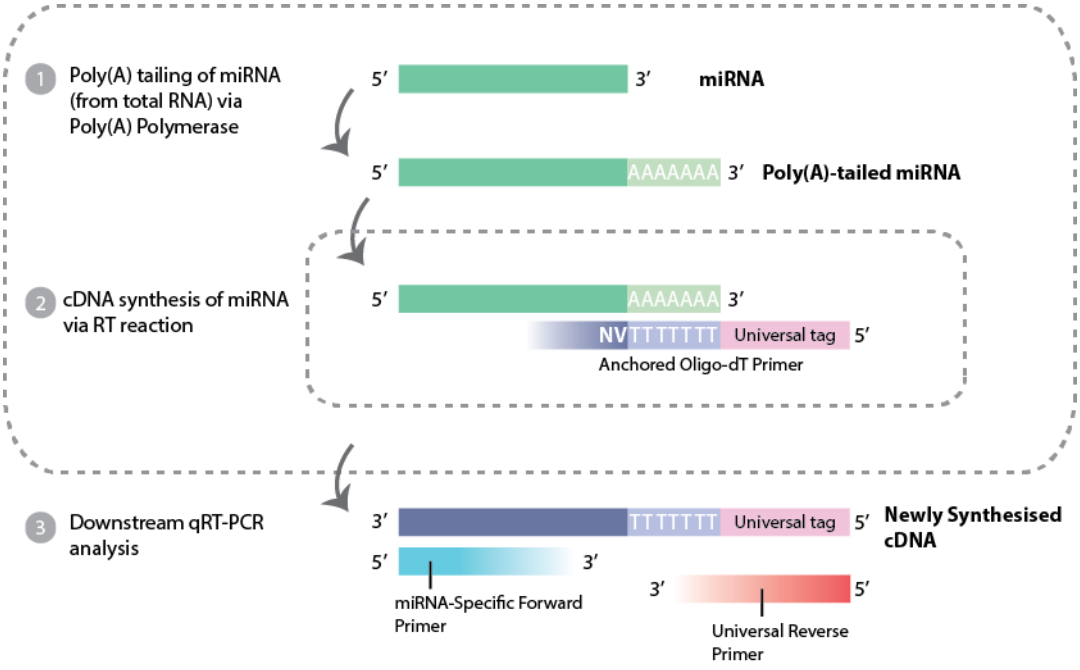

Figure 2.1: Schematic of the miScript PCR system for reverse transcription and quantification of mature miRNA.
cDNA is generated from total RNA containing miRNAs using the miScript II RT kit, and amplified by qRT-PCR using the miScript SYBR Green PCR Kit (both Qiagen). Mature miRNAs are approximately 22 nucleotides in length, therefore the first step involves elongating the miRNA by adding a poly(A) tail at the 3′ end of each RNA molecule with poly(A) polymerase. The polyadenylated miRNA is primed for cDNA synthesis using anchored oligo-dT primers. The primer anneals to the 3′ poly(A) tail and includes degenerate bases like dN (dA, dT, dG or dG) and dV (either dG, dA or dC) at its 3′ end, to lock the priming site immediately upstream of the poly(A) tail. This modification prevents poly(A) slippage events which can occur when tandem repeats are found at the site of replication. In addition, the oligo-dT primer also contains additional bases that create a universal sequence tag on each cDNA strand that is synthesised. The universal tag is at the 5´-end of the cDNA, and is recognised by the miScript Universal Primer (reverse primer) in subsequent PCR cycles. miScript Primer Assays contain forward primers that are specific for the target miRNA sequences of interest. Adapted from (Abm, 2018)

2.2.4 qRT-PCR

2.2.4.1 Quantitation of mRNA expression

Quantitation of mRNA expression was performed by qRT-PCR (Saiki et al., 1985) using SYBR green supermix and a CFX Connect real-time PCR detection system (both Bio-Rad, CA, USA). Each reaction contained 4 µl of cDNA (from section 2.2.3.1, diluted 1:4 in RNase-free water) 0.15 µl forward and reverse primers (20 µM stock concentration, final concentration 300 nM) and 5 µl of SYBR green supermix (2X). Reactions were made up to a final volume of 10 µl with RNase-free water. The PCR primer pairs used are shown in Table 2.6.

Samples were arranged in triplicates on a white-walled 96-well PCR plate and firmly sealed with a plastic cover (both Bio-Rad). After a denaturation step at 95°C for 3 min, samples underwent 2-step amplification at 94°C (30 secs) and 60°C (60 secs) for 40 cycles. Melt curves were analysed after 40 cycles to assess whether the assay had produced a single, specific product. The quantitation cycle (Cq) values for test genes were compared to the reference gene β-actin (ACTB) using the $2^{-[\Delta\Delta Cq]}$ Livak method (Livak and Schmittgen, 2001) for relative gene expression, which relates the qRT-PCR signal from the test gene in a test sample, to that of an untreated control.

mRNA Target	Primer pairs	Annealing temperature (°C)	Product length (bp)
BAP1	BAP1for: 5′-CAGCCCTGAGAGCAAAGGATATG-3′ BAP1rev: 5′-ATGGTCCGCACTGCACTAAG-3′	62	129
ACTB (β-actin)	ACTBFnew9-06: 5′-CACCTTCTACAATGAGCTGCGTGTG-3′ ACTBRnew9-06: 5′-ATAGCACAGCCTGGATAGCAACGTAC-3′	59	158
HDAC1	HDAC1for: 5′-ACGGGATTGATGACGAGTCCTATG-3′ HDAC1rev: 5′-TGAGCCACACTGTAAGACCACC-3′	62	100
HDAC2	HDAC2for: 5′-TTACTGATGCTTGGAGGAGGTGGC-3′ HDAC2rev: 5′-TGGACACCAGGTGCATGAGGTAAC-3′	64	181

Table 2.6: Primer pairs used for PCR amplification.
bp: base pairs.

2.2.4.2 Quantitation of miRNA expression

Quantitation of miRNA expression was performed by quantitative reverse-transcription PCR (qRT-PCR) using miScript SYBR Green PCR Kit (Qiagen) and a CFX Connect real-time PCR detection system (Bio-Rad). Each reaction contained 2.5 µl of cDNA (from section 2.2.3.2, diluted 1:100 in RNase-free water), 2.5 µl miScript primer assay (10X) which contained miRNA-specific forward primers, 2.5 µl miScript universal reverse primer (10X), which anneals to the unique sequence from the universal tag (Fig. 2.1), and 12.5 µl of QuantiTect SYBR green master mix (2X). Reactions were made up to a final volume of 25 µl with RNase-free water. The primers are listed in Tables 2.7 and 2.8.

Samples were arranged in triplicate on a white-walled 96-well PCR plate and firmly sealed with a plastic cover (both Bio-Rad). After an initial 15 min activation step at 95°C, samples underwent 3-step cycling at 94°C (15 secs), 55°C (30 secs) and 70°C (30 secs) for 40 cycles. Melt curves were analysed after 40 cycles to assess whether the assay had produced a single, specific product. In routine analysis, the Cq values for test genes were normalized to the mean value of reference genes SNORD95 and SNORD96A, and relative expression represented as $2^{-[\Delta\Delta Cq]}$.

Mature miRNA Target	Forward Primer Sequence	Catalogue number
hsa-miR-10a-5p	5'-UACCCUGUAGAUCCGAAUUUGUG-3'	MS00031262
hsa-miR-10b-5p	5'-UACCCUGUAGAACCGAAUUUGUG-3'	MS00031269
hsa-miR-125a-5p	5'-UAAUACUGCCUGGUAAUGAUGA-3'	MS00003423
hsa-miR-125b-5p	5'-UCCCUGAGACCCUAACUUGUGA-3'	MS00006629
hsa-miR-127-3p	5'-UCGGAUCCGUCUGAGCUUGGCU-3'	MS00003437
hsa-miR-141-3p	5'-UAACACUGUCUGGUAAAGAUGG-3'	MS00003507
hsa-miR-200a-3p	5'-UAACACUGUCUGGUAACGAUGU-3'	MS00003738
hsa-miR-200b-3p	5'-UAAUACUGCCUGGUAAUGAUGA-3'	MS00009016
hsa-miR-200c-3p	5'-UAAUACUGCCGGGUAAUGAUGGA-3'	MS00003752
hsa-miR-429	5'-UAAUACUGUCUGGUAAAACCGU-3'	MS00004193
hsa-miR-31-5p	5'-AGGCAAGAUGCUGGCAUAGCU-3'	MS00003290
hsa-miR-34c-5p	5'-AGGCAGUGUAGUUAGCUGAUUGC-3'	MS00003332
hsa-miR-376b-3p	5'-AUCAUAGAGGAAAAUCCAUGUU-3'	MS00007399
hsa-miR-377-3p	5'-AUCACACAAAGGCAACUUUUGU-3'	MS00004095
hsa-miR-381-3p	5'-UAUACAAGGGCAAGCUCUCUGU-3'	MS00004116
hsa-miR-656-3p	5'-AAUAUUAUACAGUCAACCUCU-3'	MS00005355

Table 2.7: Forward primer sequences for qRT-PCR assays of mature miRNA expression.
Distinct bases between closely related miRNAs are underlined

Small nucleolar RNA controls	Catalogue number
SNORD61	MS00033705
SNORD68	MS00033712
SNORD95	MS00033726
SNORD96A	MS00033733

Table 2.8: Forward primer sequences for small nucleolar RNA (SNORD) housekeeping genes used for miRNA qRT-PCR.

2.2.5 NanoString nCounter human v3 miRNA expression assay

The nCounter human v3 miRNA expression assay is a hybridization-based profiling method for detecting the expression of ~800 miRNAs in total RNA samples enriched for small RNAs (see section 5.1 for further details on this assay). The nCounter human v3 miRNA expression assay kit was sourced from NanoString Technologies (WA, USA) and the assay was performed in accordance to the manufacturer's instructions. Data collection was performed by the nCounter prep station and the nCounter digital analyser (both NanoString Technologies) in the CGR.

Total RNA including miRNAs were extracted as detailed in section 2.2.1.2. RNA concentration and integrity were assessed using a Qubit fluorometer and Agilent bioanalyser as detailed in sections 2.2.2.2 and 2.2.2.3, respectively. 100 ng of total RNA in 3 µl RNAse-free H_20 was used as input material for the first NanoString nCounter assay which is described in Chapter 5 (NS1). For subsequent assays detailed in Chapter 6 (NS2 and NS3), 300 ng/3 µl of total RNA per sample was used as input material to increase the binding density of sample to the surface of the nCounter cartridge (see section 2.2.5.3 – 2.2.5.4) and to increase the chances of detecting a higher abundance of miRNAs. The protocol below is for one set of 12 reactions performed on one NanoString nCounter cartridge.

2.2.5.1 miRNA sample preparation

The sample preparation involved annealing an oligonucleotide bridge to a portion of both the target mature miRNA and the specific miRtag oligonucleotide sequence to generate a duplex for ligation (Fig 2.2). miRNA controls were included in the sample preparation to monitor ligation efficiency and specificity throughout the reaction. The annealing master mix was prepared by combining 13 µl annealing buffer, 26 µl of nCounter miRNA tag reagent and 6.5 µl of miRNA assay controls (diluted 1:500 in RNAse-free water). 3.5 µl of the annealing master mix was pipetted into 0.2 ml strip tubes with individual caps, and 3 µl

(100 or 300ng) of RNA sample was added to each tube. The strip tubes were placed in a Veriti Thermal Cycler with a heated lid set at 70°C (Thermo Fisher Scientific) to initiate the annealing protocol shown in Table 2.9.

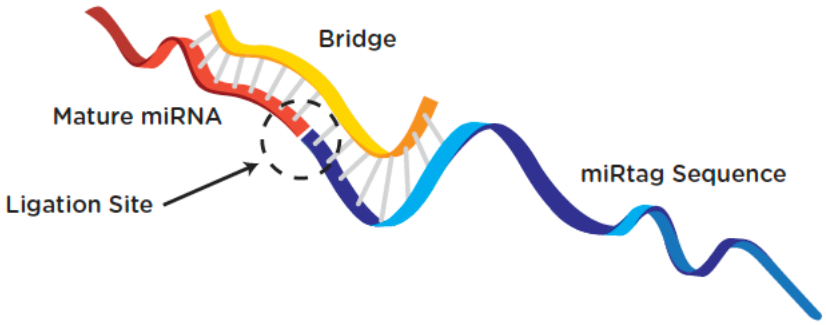

Figure 2.2: Specific capture of miRNA targets via ligation.
Unique oligonucleotide tags (miRtag, blue) are specifically ligated (circular region) onto the 3' end of target miRNAs (red) so that short RNA targets can be detected by nCounter probes. Ligation specificity is ensured by the oligonucleotide bridge (yellow) sequence that is complementary to each mature miRNA and the connected miRtag. Image reproduced from NanoString.

Temperature	**Time**
94°C	1 min
65°C	2 min
45°C	10 min
48°C	hold
Total Time	**13 min**

Table 2.9: nCounter annealing protocol

The ligation master mix was prepared by combining 19.5 µl polyethylene glycol (PEG) and 13 µl ligation buffer. Following completion of the annealing protocol, 2.5 µl of the ligation master mix was pipetted into each tube and incubated at 48°C for 5 mins. 1 µl ligase was then added to each tube and the ligation protocol initiated as shown in Table 2.10. After completion, 1 µl ligation clean-up enzyme was added to each tube and the purification protocol initiated as detailed in Table 2.11 to remove any unligated tags in each reaction. Upon completion, 40 µl RNase-free H_20 was added to each sample ready for the hybridization protocol.

Temperature	Time
48°C	3 min
47°C	3 min
46°C	3 min
45°C	5 min
65°C	10 min
4°C	hold
Total Time	**24 min**

Table 2.10: nCounter ligation protocol

Temperature	Time
37°C	2 hrs
70°C	10 min
4°C	hold
Total Time	**2 hrs 10 min**

Table 2.11: nCounter purification protocol

2.2.5.2 Hybridisation of reporter and capture probes

The hybridization master mix was prepared by adding 130 µl of hybridization buffer to 130 µl of the reporter codeset. The reporter codeset consists of hundreds of probes that hybridise specifically to complementary target miRNA and are identified by the digital signal from the unique molecular barcodes on their 5' end. 20 µl of master mix was added to nCounter strip cap tubes. Samples from the miRNA sample preparation protocol were denatured at 85°C for 5 mins, snap-cooled on ice and a 5 µl aliquot from each sample was added to the hybridization mastermix in each tube. 5 µl of the capture probeset was added to each tube immediately before placing at 65°C in a Veriti Thermal Cycler for 18.5 hr incubation. The capture probeset contain probes which carry a biotin label on their 3' end, these also hybridise to complementary sequences on target miRNAs in the sample to aid the immobilization of the miRNA-reporter probe complex onto the surface of the nCounter cartridge for data collection. Once removed from the thermal cycler, the samples were transferred onto the nCounter prep station for post-hybridisation processing.

2.2.5.3 Post-hybridisation processing and data collection

Post-hybridisation processing and data collection used two instruments, the nCounter prep station and the nCounter digital analyser (both NanoString Technologies), respectively. Strip cap tubes containing the hybridized samples were transferred onto the prep station and excess probes were washed away using a two-step magnetic bead purification. To briefly describe the automated process, magnetic beads containing

sequences that are complementary to the capture probe were used to bind the hybridized samples, wash steps removed any excess reporter probes and non-target cellular transcripts. The hybridised samples were then eluted off the beads and again hybridized to magnetic beads containing sequences complementary to the reporter probes, thus allowing excess capture probe to be removed in subsequent washing steps. The hybridized samples were again eluted off the beads and immobilized onto the surface of the nCounter cartridge for data collection by the nCounter Digital Analyser. The analyser images each lane on the cartridge using a microscope objective and CCD camera, and tabulates the raw counts for each unique barcode representing a mature miRNA. The data produced by the nCounter Digital Analyzer are exported as a Reporter Code Count (RCC) file. One RCC file is produced for every cartridge lane, which represents a single sample, and contains the barcode counts for each miRNA gene and controls in that lane.

2.2.5.4 NanoString nSolver analysis software

Data analysis was performed using the nSolver analysis software (NanoString Technologies). The software offers various methods for background subtraction, normalisation and for calculating fold change estimates from the data (see chapter 5 for an in-depth description of this workflow). Following the import of RCC files, the software assesses each file for the following QC metrics: image quality, with the percentage fields of view (FOV) successfully scanned >75%, binding density of probes to the cartridge surface within each sample lane between 0.05 – 2.25 spots per square micron, and positive control linearity, with an R^2 value >0.95 for the correlation between counts observed for the positive controls. If a sample performed outside these ranges, it was flagged by the software. Data for all lanes on each cartridge passed these QC checks and was processed as described in chapters 5 and 6.

2.3 Protein biochemistry

2.3.1 Laemmli lysis

Whole cell extracts were prepared by direct addition of hot Laemmli buffer (50 mM Tris pH 6.8, 2% SDS, 10% glycerol) (Laemmli, 1970). Briefly, cells were grown as a monolayer in 6-well plates, 60 mm or 100 mm dish, and were washed twice in PBS before cell lysis. PBS was aspirated from each well/dish, which were then transferred onto a heat block at 110°C before the immediate addition of 150 µl (6-well plate), 350 µl (60 mm dish) or 500 µl (100 mm dish) of preheated (110°C) Laemmli buffer. The surface of the plate/dish was scraped with a rubber policemen, and the lysate collected into a 1.5 ml microcentrifuge tube with

a screw cap. Samples were incubated at 110°C for 10 mins with intermittent vortexing every 2 mins to shear chromatin. A 20 µl aliquot of each cell lysate was diluted 1:5 in double-distilled H_2O (ddH_2O) for determination of protein concentration (see section 2.3.2).

2.3.2 Protein determination and sample preparation

The total protein concentration of cell lysates was determined using a bicinchoninic acid (BCA) assay (Thermo Fisher Scientific). The principle of this method is that proteins reduce copper (Cu) ions from Cu^{2+} to Cu^{+} in an alkaline solution, so that the amount of Cu^{2+} reduced results in a purple product that is proportional to the amount of protein present in the cell lysate. The resulting colorimetric change is measured at 562 nm, and the amount of protein present can be calculated by comparing the absorption reading to solutions of bovine serum albumin (BSA) standards of known concentrations (Smith et al., 1985).

The BCA assay was performed according to the manufacturer's instructions, using BSA to generate a standard curve (working range: 20 – 2000 µg/ml). The standards and the cell lysates were arranged in triplicate on a round-bottomed, clear 96-well plate. 10 µl of diluted cell lysate (section 2.3.1) and 10 µl of each standard was plated per well. 200 µl of BCA reagent (50:1 reagent A:B) was added per well and incubated for 25 mins at 37°C. The resulting colourimetric change was measured at 562 nm using a Glomax multi-detection system (Promega). Following protein quantification, cell lysates were supplemented with 10X sample buffer (312.5mM Tris-base pH 6.8, 50% glycerol, 1M DTT and 1% bromophenol blue) and stored at -20°C until use. For immunoblotting, 25-30 µg cell lysates were made to equal volumes with 10X sample buffer, and then denatured at 98°C for 5 mins.

2.3.3 Sodium dodecyl sulfate polyacrylamide gel electrophoresis (SDS-PAGE)

SDS-PAGE involves the separation of proteins based on their size (Shapiro et al., 1967). 10% 10-well acrylamide mini gels were poured as detailed in Table 2.12 and run using a Bio-Rad Mini-Protean® 3 system with electrophoresis buffer containing 50 mM Tris HCl, 38 mM glycine and 0.1% SDS. Alternatively, precast NuPAGE® Novex™ Bis-Tris 4-12% 20-well gradient gels were run in a Novex™ Bolt™ Mini Gel tank (Invitrogen) with NuPAGE® MOPS buffer (1X) containing 200 µl NuPAGE® antioxidant (both Invitrogen). For electrophoresis, 25-30 µg of protein from each sample and two molecular weight markers, Perfect Protein (Novagen, Merck-Millipore, MA, USA) and Rainbow Marker (GE Healthcare IL, USA) were loaded onto gels and separated by electrophoresis at 200V for 1 hr. Pre-cast gels were

utilised for protein samples from cycloheximide chase experiments and for large MPM cell line panels. Otherwise, protein samples were separated on self-poured acrylamide gels.

Reagent	10% acrylamide resolving gel	4% acrylamide stacking gel
ProtoGel (ml)	6.7	1.3
Resolving buffer (ml)	5.2	-
Stacking buffer (ml)	-	2.5
ddH_20 (ml)	7.9	6.1
10% APS (µl)	150	50
TEMED (µl)	15	10

Table 2.12: Constituent volumes for 10% acrylamide mini gel

2.3.4 Immunoblotting

Following SDS-PAGE, proteins were transferred by immunoblotting (Towbin et al., 1979; Burnette, 1981) onto a BioTrace™ nitrocellulose membrane (VWR, PA, USA, 0.2 µM pore size), using Genie® electrophoretic transfer apparatus (Idea Scientific, MN, USA) at 24V for 75 mins in fresh transfer buffer containing 25 mM tris-glycine and 20% methanol. The pre-soaked transfer membrane was positioned onto the gel, and the gel/membrane assembly was sandwiched between pre-soaked Whatman filter paper (VWR) and blotting pads (Idea Scientific). Trapped air bubbles were removed by gently rolling over the surface of the Whatman filter paper and blotting pads. Following transfer, the membrane was stained using Ponceau-S (Sigma-Aldrich) to visualize protein bands and assess the homogeneity of the transfer process. Membranes were de-stained by rinsing in distilled water until the background was clear. Membranes were then incubated in a blocking buffer of either 5% milk powder (Marvel, BC, Canada) or 5% BSA (First Link Ltd, UK) in Tris Buffered Saline-Tween 20 (TBS-T, 20mM Tris-base pH 7.6, 137 mM NaCl, 0.1% Tween-20) for 1 hr. Primary antibodies were diluted in the same buffer used for the blocking step, and the membranes were incubated with the primary antibody with gentle rocking for either an hour at room temperature, or overnight at 4°C. See Table 2.13 for details of primary antibody concentrations and conditions. Membranes were subsequently washed twice in TBS-T and incubated with a secondary antibody (Table 2.14) for 1 hr at room temperature and protected from light. Secondary antibodies were diluted in the same buffer as used for the primary antibody. The membranes were then washed twice in TBS-T and twice more in TBS (20mM Tris-base (pH 7.6), 137mM NaCl), each step for 10 minutes with gentle rocking. Protein bands were visualized using the LI-COR Odyssey 2.1 infrared imaging system

Protein	Company	Catalogue Number	Species	Dilution	Antibody Blocking Buffer (in 5% TBS-T)
ALDOC	Santa Cruz	sc-12066	Goat	1:500	BSA
ASS1	Millipore	MABN704	Mouse	1:500	BSA
ß-actin **(45 min RT)**	Abcam	ab6276	Mouse	1:20,000	Milk
	Sigma-Aldrich	A2066	Rabbit	1:20,000	Milk
BAP1	Santa Cruz	sc-28383	Mouse	1:250	Milk
BCL2	Abcam	ab692	Mouse	1:500	Milk
CCNE1	Cell Signaling	#4129	Mouse	1:1000	Milk
DHFR	Abcam	ab124814	Rabbit	1:10,000	BSA
E-Cadherin	CR-UK	-	Mouse	1:1000	Milk
ENO2	Cell Signaling	#9536	Rabbit	1:100	BSA
FN1	Sigma-Aldrich	F3648	Rabbit	1:1000	Milk
HDAC1	Santa Cruz	sc-6298	Goat	1:2000	Milk
HDAC2	Santa Cruz	sc-7899	Rabbit	1:2000	Milk
ICAM1	Santa Cruz	sc-8439	Mouse	1:100	BSA
OGT	Cell Signaling	#5368	Rabbit	1:1000	BSA
P53	Santa Cruz	sc-126	Mouse	1:1000	Milk
SERPINE1	Abcam	ab82218	Mouse	1:1000	BSA
PGAM1	Abcam	ab96622	Rabbit	1:1000	BSA
PGK1	Abcam	ab113687	Mouse	1:500	BSA
PYGL	Sigma-Aldrich	HPA004119	Rabbit	1:100	BSA
RRM1	Cell Signaling	#3366	Rabbit	1:1000	BSA
SERPINB6	Santa Cruz	sc-398487	Mouse	1:100	Milk
SUCLG2	Santa Cruz	sc-99646	Goat	1:5000	Milk
USP8	R&D Systems	AF7735	Sheep	1:1000	Milk
Vimentin	Cell Signaling	#5741	Rabbit	1:1000	BSA

Table 2.13: Primary antibodies used in this study.
Unless otherwise stated, all primary antibody incubations were performed overnight at 4°C. RT: room temperature.

(LI-COR, NE, USA). 16-bit images were analysed and quantified using the Odyssey ImageStudio Lite software (LI-COR, NE, USA).

Secondary Antibody	Company	Catalogue Number	IRDye	Dilution
Donkey α-mouse	LI-COR	926-68022	680LT	1:15,000 for 1 hr RT protected from light
		926-32213	800CW	
Donkey α-rabbit		926-68023	680LT	
		926-32213	800CW	
Donkey α-goat*		926-32214	800CW	

Table 2.14: Secondary antibodies used in this study.
*Secondary antibody recognises primary antibodies raised in sheep. RT: room temperature.

2.4 Bioinformatics and statistical analysis

2.4.1 Collation of mutation data

To generate a survey of BAP1 mutations (Fig. 1.3) mutation data for the BAP1 gene in cancer tissues and cancer cell lines was collated from two open access databases, COSMIC (Forbes et al., 2017) and cBioPortal (Gao et al., 2013; Cerami et al., 2012). Data were extracted in July 2015 from the following primary tissue types and histology: pleura - mesothelioma, eye - uveal tract, malignant melanoma, kidney - clear cell renal cell carcinoma, lung - adenocarcinoma, breast – carcinoma. The data included the total number of samples analysed and their sample IDs, the number of mutated samples, the type of mutation, and the amino acids affected. Mutation frequencies were calculated by dividing the total number of mutated samples by the total number of samples analysed. To avoid the same data being represented twice, where possible sample IDs and the amino acid mutation were compared, and redundancy removed from the datasets.

2.4.2 miRNA target prediction

TargetScan Human 7.1 (http://www.targetscan.org/), PicTar (http://pictar.mdc-berlin.de/), miRDB (http://mirdb.org/miRDB/) and microRNA.org (http://www.microrna.org/microrna/) were used in Jan 2016 to search for human mature miRNAs predicted to target human BAP1. Each database uses its own algorithm to identify potential miRNA binding sites in the BAP1 mRNA sequence, by searching for the presence of conserved sites on the BAP1 3' UTR that match the seed region of each miRNA.

The miRWalk2.0 (http://zmf.umm.uni-heidelberg.de/apps/zmf/mirwalk2/index .html) database was used in Dec 2016 to gather information on predicted and validated miRNA target genes. miRBase miRNA accession numbers provided the input for the

"Validated Target" module, to generate lists of official gene symbols for miRNA-target genes.

2.4.3 Hierarchical clustering

To identify similarities between groups of data within a large dataset, data values in the form of $\log_2$ ratios for fold changes in miRNA expression, or P-values ($\log_{10}$), were entered into Multiple Experiment Viewer (MeV, Version 10.2, http://mev.tm4.org). A two-dimensional heat map was generated with double gradient colour scales of blue and yellow, or green and red. Unsupervised hierarchical clustering analysis was performed on either the gene list and the sample list, or both, which generated a dendogram tree using the average linkage method of clustering and Pearson correlation distance metric. The "leaves" of the dendogram tree, i.e. genes or samples, were displayed in a linear order. For clustering shown in chapters 5 and 6, optimal leaf ordering of the gene and sample tree was performed to maximize the similarity of adjacent rows and columns in the clustering.

2.4.4 Gene ontology (GO) analysis

To perform enrichment analysis on miRNA-gene targets, gene sets were interrogated using the Database for Annotation, Visualisation and Integrated Discovery (DAVID; https://david.ncifcrf.gov/). Official gene symbols were uploaded into DAVID and annotated by GO terms encompassing biological processes, cellular compartments or molecular functions. An enrichment threshold EASE score of 1.0 was applied. Data were downloaded in the functional chart format with GO terms and their corresponding P-values to indicate the strength of the enrichment for a gene list in the annotation category.

2.4.5 Statistical analysis

Statistical analyses were applied in all cases where at least three independent experiments were performed. Statistical analyses were performed using GraphPad Prism Version 6.00 for Mac. For experiments with three or more samples a one-way ANOVA was performed, coupled with Dunnett's post-hoc test. Gaussian distribution was confirmed by the D'Agostino & Pearson omnibus normality test. Paired or unpaired t-tests, and Mann Whitney U tests were used when analysing the statistical significance of the means of two populations.

Chapter 3: Characterising BAP1 status and validating BAP1-dependencies in cellular models of mesothelioma

3.1 Introduction

The development of commercially available and well characterised tumour cell lines has been an important tool for the study of tumour pathogenesis, the identification of disease biomarkers and predicting responses to drug treatment. Tissue biobanks like the ATCC and European Collection of Authenticated Cell Cultures (ECACC) are repositories for biological material including tumour cell lines that can be propagated over multiple passages in tissue culture. However, unlike lung cancer, where the current collection of tumour cell lines are in the hundreds (Gazdar et al., 2010), relatively few established MPM cell lines are available for *in vitro* culture. Recently, there has been a move to generate better pre-clinical models for *in vitro* mechanistic studies, through genome-editing or establishing low-passage tumour cell lines. The latter stemmed from findings of increased genomic instability during tissue culture expansion, which can compromise the usefulness of data generated from commercially available tumour cell lines (Tsuji et al., 2010; Chernova et al., 2016). MesobanK UK (http://www.mesobank.com) is an initiative to facilitate the availability of quality assured MPM tissue, blood and cell lines for basic science, translational and clinical research (Rintoul et al., 2016). This bioresource was established in 2012 through funding from the British Lung Foundation (BLF) and the Mick Knighton Mesothelioma Research Fund.

Despite the recent availability of well characterised MPM cell lines through MesobanK, these panels remain difficult models in which to establish the effect of a single gene mutation, due to their heterogeneous genetic backgrounds. Genome-editing, to mutate a single gene on an otherwise genetically identical background, can create isogenic cell panels better suited to address such questions. Previous work in the Coulson lab utilised recombinant adeno-associated virus (rAAV)-mediated genome editing (Horizon Discovery) to generate BAP1-mutated isogenic cell lines from MeT5A mesothelial cells (Kenyani et al., manuscript in prep). Unlike other genome editing methods using engineered nucleases such as CRISPR-Cas9, Transcription Activator-Like Effector Nucleases (TALENs) or Zinc Finger Nucleases (ZFNs), rAAV-mediated genome editing relies on homologous recombination without inducing a DSB (Gaj et al., 2016). The rAAV viral vector delivers single-stranded DNA into the nucleus of a cell, which is then incorporated into the genome

using the cell's endogenous homologous recombination repair system. The single-stranded DNA has been engineered with the desired sequence alteration flanked by homology arms, which facilitate pairing of the vector genome with homologous chromosomal sequences at the target locus. The vector genome carrying the sequence alteration is then incorporated into one strand at the target locus using recombination cross-over events, then the repair pathway copies the sequence alteration into the other strand. The end result is the introduction of a sequence change, for example point mutations, indels and selection markers, into the host genome (Russell and Hirata, 1998; Khan et al., 2011).

As described in section 1.3.2, germline *BAP1* mutations predispose to *BAP1* TPDS and somatic mutations lead to loss of nuclear BAP1 protein expression in ~50% of MPM (Bott et al., 2011). With this in mind, two rAAV genome editing cassettes were designed to sequentially introduce *BAP1* mutations that mimic these clinical manifestations (Fig. 3.1). In the first instance, a *BAP1*-haploinsufficient cell line was produced (henceforth referred to as *BAP1*$^{w-/+}$) by targeting one *BAP1* allele with the predisposition mutation documented in the germline of Family W members that developed MPM (Testa et al., 2011). This splice-site mutation in intron 6 leads to a frameshift causing exon 7 skipping and a predicted premature stop codon. Following clonal selection and sequence validation of this first allelic mutation, a promoter trap was introduced into the second BAP1 allele to mimic BAP1-deficient MPM with biallelic inactivation of BAP1. Two independent isogenic clonal cell lines (henceforth referred to as C5.1 (*BAP1*$^{w-/KO}$) and C3.1 (*BAP1*$^{w-/KO}$)) were sequence verified (Kenyani et al., manuscript in prep). A major advantage of these isogenic cell lines for *in vitro* research is that they are genetically identical to the parental mesothelial cell line, except for the engineered *BAP1* mutations that are clinically relevant to the tumorigenesis of MPM. However, it is important to acknowledge that both isogenic *BAP1*$^{w-/KO}$ clones still show residual BAP1 expression upon promoter trapping (see section 3.4), as such *BAP1* double mutation essentially denotes knock-down of BAP1.

The subsequent cellular vulnerabilities that transpire following BAP1 loss through mutation in MPM are not fully understood. This lab is interested in identifying these BAP1-dependencies and understanding the means by which MPM cells adapt to loss of BAP1 to survive. Changes in protein expression upon BAP1 loss could potentially be exploited for therapeutic benefit, especially if these represent proteins that are already targeted by established chemotherapeutics.

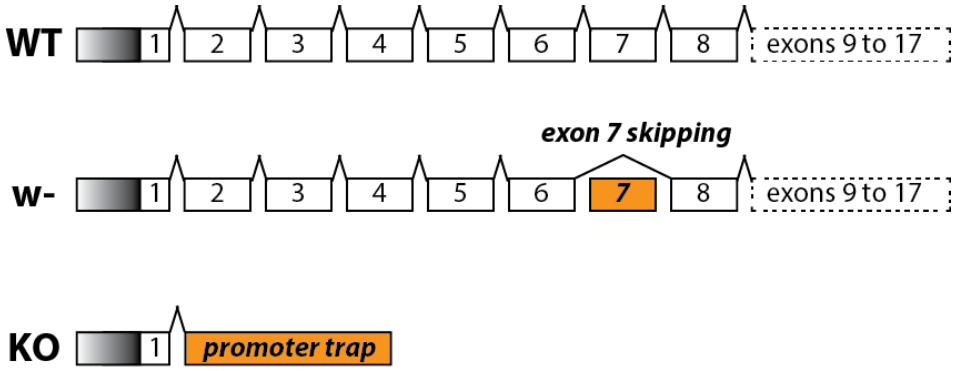

Figure 3.1: The exon structure of BAP1 transcripts following gene editing.
Schematic of the exon structure of BAP1 transcripts showing altered splicing by the w- mutation and expression of the promoter trap. WT: wildtype, w-: w-family splice site mutation, KO: knockout. Black: 5' UTR of exon 1, orange: abnormalities in transcripts expressed from gene edited alleles.

Therefore, to begin the search for cellular BAP1-dependencies in MPM, a triplex stable isotope labeling with amino acids in cell culture with mass spectrometry (SILAC-MS) approach was used to profile the effect of BAP1-deficiency on the MeT5A proteome (work undertaken by Dr. Jenna Kenyani). Parental MeT5A (*BAP1*$^{+/+}$) and isogenic *BAP1*$^{w-/+}$ cells were compared with the isogenic *BAP1*$^{w-/KO}$ clones C3.1 or C5.1. The method involves culturing cells in a medium supplemented with amino acids containing either light, medium or heavy isotopes, which are incorporated during protein synthesis. When peptides are analysed by MS, the source of the sample is distinguished by the mass difference, and the relative abundance of proteins in each cell line is determined based on relative intensities of the light, medium and heavy peptides. In summary, 1922 proteins were identified, 18% of which were modulated, i.e. up- or down-regulated >1.5-fold in C5.1 (BAP1$^{w-/KO}$) cells relative to the MeT5A (*BAP1*$^{+/+}$) and/or *BAP1*$^{w-/+}$ cells. Functional annotation of these modulated proteins revealed marked enrichment of biological processes and molecular functions that affect the regulation of actin cytoskeleton and cellular metabolism (Fig. 3.2).

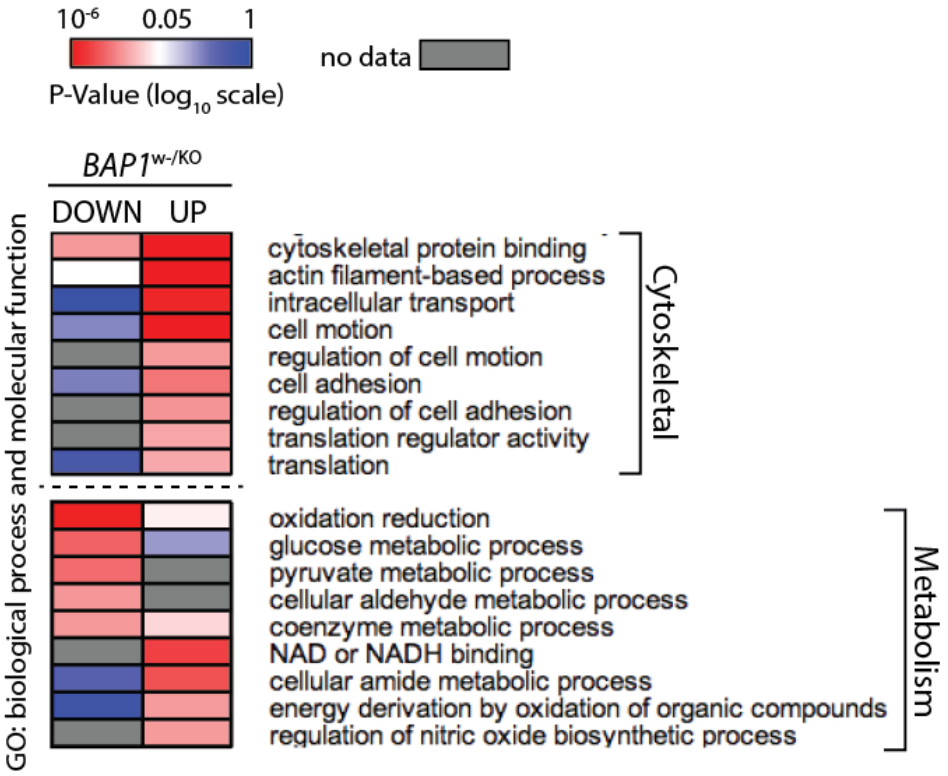

Figure 3.2: BAP1-responsive proteins in isogenic *BAP1*-mutant MeT5A cells are enriched for specific cellular processes and functions.
Heat map summarising enriched GO terms (biological process and molecular function) from proteins that were up- or down-regulated by >1.5-fold in isogenic BAP1-mutant cell line C5.1 (*BAP1*$^{w-/KO}$). Colour scale indicates significance for the enriched GO terms amongst up- or down-regulated proteins. Adapted from (Kenyani et al., manuscript in prep)

3.2 Aims and objectives

As part of this larger study to profile the effect of BAP1-deficiency on the MeT5A proteome, I set out to validate candidate BAP1 responses in the isogenic MeT5A cell lines and explore their relevance in patient-derived MPM cell lines. My principal objectives were:

1. To measure the growth characteristics and BAP1 expression of isogenic MeT5A *BAP1*-mutant cell lines.
2. To characterise BAP1 expression in a panel of patient-derived MPM cell lines from the ATCC and MesobanK.
3. To validate candidate BAP1-dependent protein expression in the isogenic MeT5A *BAP1*-mutant cell line, and to compare expression of these candidates in patient-derived MPM cell lines with differing BAP1 status.

3.3 Strategy and workflow for characterisation of BAP1-dependent protein expression in *BAP1*-mutant cell lines

The strategy adopted here mirrors that used later in this thesis to explore BAP1-dependent miRNA expression (chapters 5 and 6). During the discovery phase, an 'omics platform (in this case SILAC-MS) was used to profile BAP1-dependency in isogenic parental and *BAP1*-mutated cells (Fig. 3.3A). Initial validation of selected hits from the 'omics platform was undertaken in the isogenic cell model using directed assays (in this case western blotting). Hits of interest were then examined in a panel of patient-derived MPM cell lines of known BAP1 status, to determine the relevance of identified BAP1-dependencies across cancer cells with other genetic alterations.

During the work for this thesis, I utilised MPM cell lines from various sources, and these cell lines were acquired at different stages during my study (Fig. 3.3B). The isogenic MeT5A *BAP1*-mutant cell lines were established prior to the start of my study, and five commercially available MPM cell lines from ATCC were available in the lab. Subsequently, we acquired 15 additional patient-derived MPM cell lines from MesobanK UK. Consequently, specific groups of cell lines were available for analyses performed in different chapters of this thesis (Fig. 3.3B). I initially contributed towards the characterisation of BAP1-dependency in the isogenic MeT5A *BAP1*-mutant cell lines, with the intention to validate findings in the panel of patient-derived cell lines from ATCC and MesobanK. The cell lines from MesobanK are considered good models for their original tumours (Rintoul et al., 2016); they were passaged between six and nine times after isolation from primary tumour surgical tissue or pleural fluid before we acquired them, and were minimally passaged in our hands for experimental use.

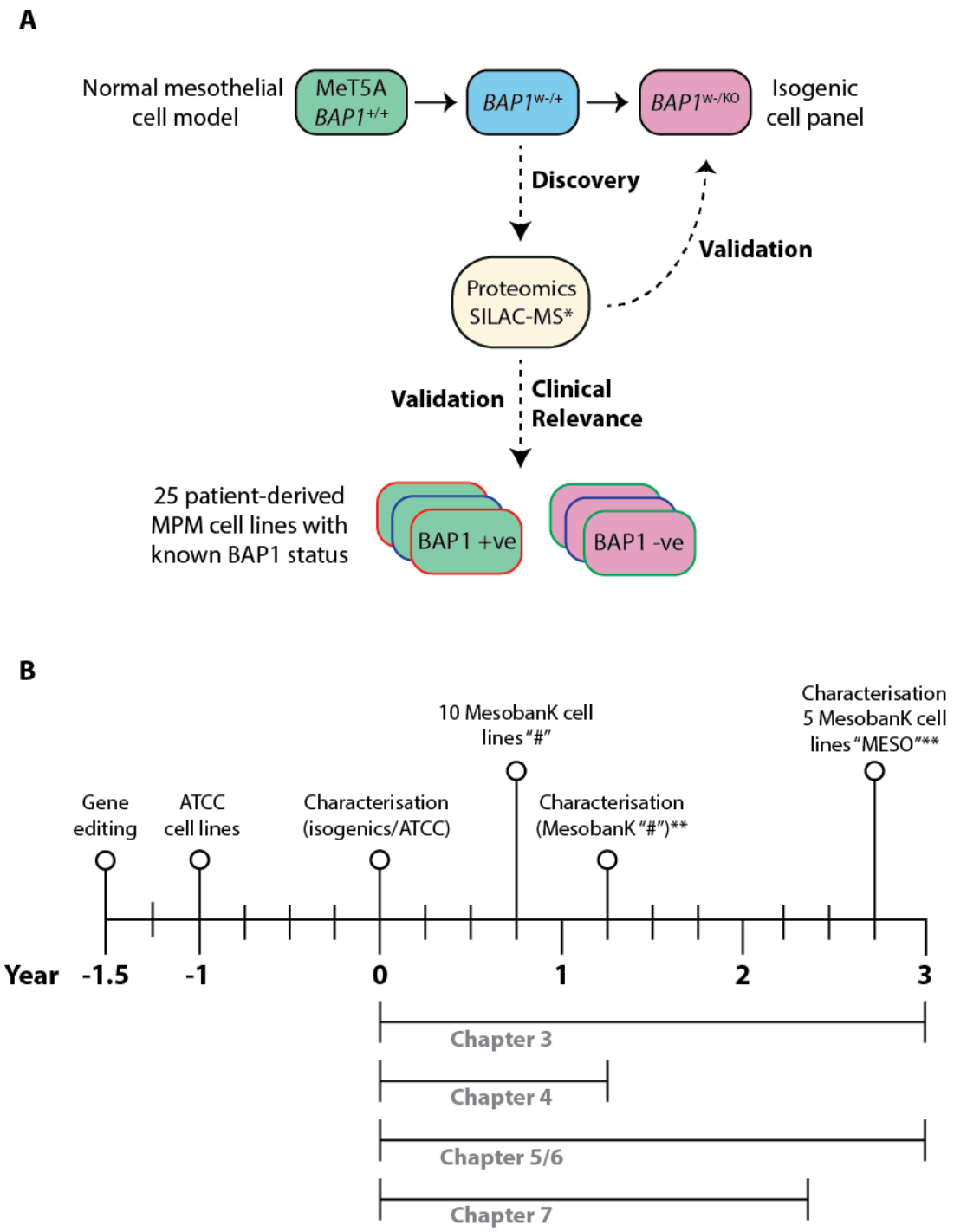

Figure 3.3: Summary of the workflow and timeline for acquisition/characterisation of the isogenic *BAP1*-mutant and MPM cell lines.
A Flow diagram illustrates how cell lines were utilised in this study to characterise and validate BAP1-dependencies. *Work was undertaken by Dr. Jenna Kenyani.
B Timeline of events displaying when each cell line panel was acquired and how they were integrated into this study. **Shared effort with Dr. Sarah Taylor.

3.4 Isogenic MeT5A *BAP1*-mutant cell lines with reduced BAP1 protein exhibit reduced cell growth and accumulation in S-phase

The initial characterisation of isogenic MeT5A *BAP1*-mutant cell lines involved analysing their BAP1 protein expression level (Fig. 3.4A), measuring their growth rate *in vitro* (Fig. 3.4B) and establishing their cell cycle distribution (Fig. 3.4C). Relative to the parental cell line MeT5A (*BAP1*$^{+/+}$), mutation of one BAP1 allele in the *BAP1*$^{w-/+}$ cell line resulted in significantly decreased BAP1 protein expression, to 69% of that in parental MeT5A (*BAP1*$^{+/+}$) cells (Fig. 3.4A). Mutation of the second allele in clone C5.1 (*BAP1*$^{w-/KO}$) further decreased BAP1 protein expression to 37%. In contrast, the clone C3.1 (*BAP1*$^{w-/KO}$) expressed 77% BAP1 protein relative to MeT5A (*BAP1*$^{+/+}$), comparable to the level observed in the *BAP1*$^{w-/+}$ cell line. Despite progressive reduction in BAP1 protein expression with successive allele mutation for *BAP1*$^{w-/+}$ and C5.1 (*BAP1*$^{w-/KO}$), loss of BAP1 protein remained incomplete in both *BAP1*$^{w-/KO}$ clones. We believe this is due to incomplete mis-splicing of the w-allele.

BAP1 deficiency resulted in a slower rate of cell growth (Fig. 3.4B). At day 5, *BAP1*$^{w-/+}$ and C3.1 (*BAP1*$^{w-/KO}$) showed a significant reduction in cell number compared to the MeT5A (*BAP1*$^{+/+}$). Growth curves for C5.1 (*BAP1*$^{w-/KO}$) cells also reflect a similar growth profile to the C3.1 (*BAP1*$^{w-/KO}$) clone (Kenyani et al., manuscript in prep). Furthermore, slowed growth was associated with accumulation in S-phase of the cell cycle, with 22% and 29% of cells in S-phase, respectively, compared with 20% of MeT5A (*BAP1*$^{+/+}$) cells (Fig. 3.4C).

3.5 Validating effects of BAP1-deficiency on the MeT5A proteome

3.5.1 Isogenic MeT5A *BAP1*-mutant cell lines significantly deregulate proteins involved in the actin cytoskeleton

Profiling the C5.1 (BAP1$^{w-/KO}$) cell proteome by SILAC-MS revealed altered expression of key actin cytoskeletal regulatory pathways (Fig. 3.2). Upregulated proteins in C5.1 (*BAP1*$^{w-/KO}$) cells were significantly over-represented in functions such as cytoskeletal protein binding (Fig. 3.2), defined as the selective interaction with any protein component of the cytoskeleton. Other enriched GO terms included actin-filament based processes that can impact on the organisation of the actin cytoskeleton, cell motion and cell adhesion (Fig. 3.2). Relevant proteins chosen here for validation by immunoblotting included the extracellular matrix (ECM) component fibronectin (FN1) and intercellular adhesion molecule-1 (ICAM1). Components of the actin-related proteins-2/3 (ARP2/3) complex and members of the serine protease inhibitor (SERPIN) family were also chosen for validation.

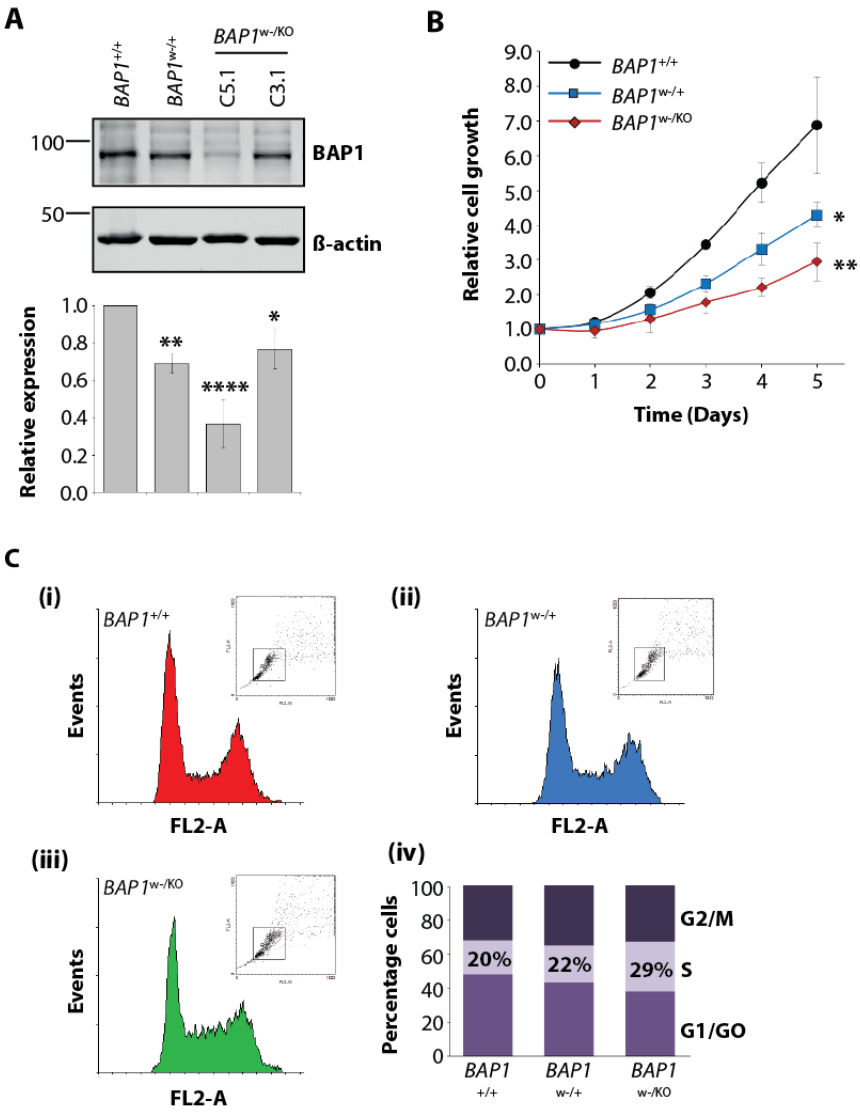

Figure 3.4: Isogenic MeT5A BAP1-mutant cell lines exhibit a reduction in growth and slowed S-phase progression.

A Representative immunoblot of MeT5A (*BAP1*$^{+/+}$) and isogenic BAP1-mutant cell lines *BAP1*$^{w-/KO}$, C5.1 (*BAP1*$^{w-/KO}$) and C3.1 (*BAP1*$^{w-/KO}$). Quantification of BAP1 protein normalised to ß-actin and relative to MeT5A (*BAP1*$^{+/+}$): mean expression from three independent experiments, error bars show standard deviation (SD), *P≤0.05, **P≤0.01 and ****P≤0.0001 compared to MeT5A (*BAP1*$^{+/+}$) by one-way ANOVA and Dunnett post-hoc test. **B** Proliferation of MeT5A (*BAP1*$^{+/+}$), (*BAP1*$^{w-/KO}$) and C3.1 (*BAP1*$^{w-/KO}$) measured by CellTitre-Glo viability assay. Mean values were normalised to the signal at Day 0, error bars show SD for three independent experiments, *P≤0.05 and **P≤0.01 compared to MeT5A (*BAP1*$^{+/+}$) at Day 5 by one-way ANOVA and Dunnett post-hoc test. **C** Flow cytometry analysis of the cell cycle distribution for **(i)** MeT5A (*BAP1*$^{+/+}$) **(ii)** *BAP1*$^{w-/KO}$ and **(iii)** C3.1 (*BAP1*$^{w-/KO}$). PI-labelled cells were gated for single cells, and a minimum of 10,000 events used for analysis. **(iv)** The distribution of cells between G1/GO, S and G2/M. Values were plotted from one experiment.

Active ARP2/3 complexes are responsible for actin filament nucleation and branching for cell motility (Pollard and Beltzner, 2002), whilst SERPIN family members regulate numerous biological pathways including ECM composition (Al-Mamun et al., 2016). SILAC-MS showed increased expression in C5.1 (BAP1$^{w-/KO}$) cells vs. MeT5A (*BAP1*$^{+/+}$), for the majority of these proteins, but decreased expression for SERPINB6 (Fig. 3.5A). It was confirmed that both FN1 and ICAM1 (Fig. 3.5C and 3.5D) were upregulated in C5.1 (*BAP1*$^{w-/KO}$) cells when compared to MeT5A (*BAP1*$^{+/+}$) cells by immunoblotting, although the increase in FN1 expression was substantially smaller than suggested by SILAC-MS. ARPC2, an ARP complex subunit, and the actin-related protein ARP3 were also upregulated in C5.1 (*BAP1*$^{w-/KO}$) cells (Fig. 3.5E). SERPINE1 (also known as PAI-1) protein expression was substantially higher in C5.1 (*BAP1*$^{w-/KO}$) cells (Fig. 3.5F), in contrast to decreased expression of SERPINB6 in C5.1 (*BAP1*$^{w-/KO}$) cells (Fig. 3.5G).

3.5.2 Isogenic MeT5A *BAP1*-mutant cell lines downregulate glycolytic metabolism enzymes but upregulate TCA cycle and anaplerotic enzymes

Moving on to consider cellular metabolism, SILAC-MS had revealed proteins that were downregulated in C5.1 (*BAP1*$^{w-/KO}$) cells were significantly associated with GO terms relating to glycolytic, pyruvate and aldehyde metabolism and oxidoreductase enzyme function (Fig. 3.2). In contrast, upregulated proteins were significantly associated with GO terms relating to fatty acid amide metabolism, nitric oxide biosynthesis and oxidation of organic compounds such as pyruvate in the TCA cycle and NAD/NADH (Fig. 3.2). Overall, glycolysis and TCA cycle enzymes were differentially expressed in C5.1 (*BAP1*$^{w-/KO}$) cells relative to MeT5A (*BAP1*$^{+/+}$). The most notable trend from this data was the downregulation of key glycolysis/gluconeogenesis enzymes, and in contrast the increased expression of many enzymes that drive the TCA cycle (Kenyani et al., manuscript in prep).

Proteins that were selected to be validated by immunoblotting are indicated in Fig 3.6. SILAC-MS showed increased expression in C5.1 (BAP1$^{w-/KO}$) cells vs. MeT5A (*BAP1*$^{+/+}$), for the TCA cycle enzyme succinate-CoA ligase GDP-forming beta subunit (SUCLG2) and the urea cycle enzyme argininosuccinate synthase 1 (ASS1), together with phosphoglucomutase 2 (PGM2) and glycogen phosphorylase L (PYGL) that are involved in metabolism of glucose-1-phosphate (Fig. 3.7A). Decreased expression of glycolytic enzymes aldolase C (ALDOC), phosphoglycerate mutase 1 (PGAM1) and enolase 2 (ENO2) was also detected by SILAC-MS (Fig. 3.7A). Immunoblotting for these enzymes confirmed a substantial >6-fold increase in PGM2 expression in C5.1 (*BAP1*$^{w-/KO}$) cells relative to MeT5A (*BAP1*$^{+/+}$). In contrast, no change

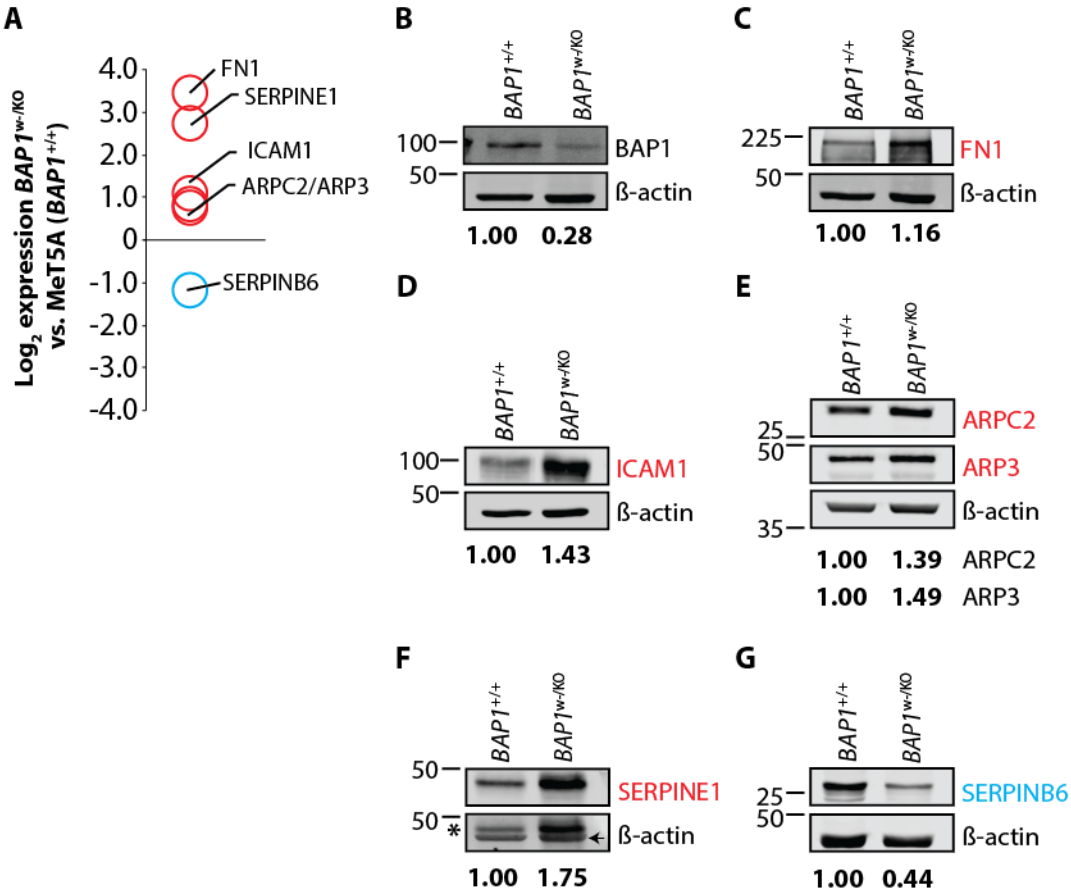

Figure 3.5: BAP1 deficiency in MeT5A significantly deregulates proteins involved in cytoskeletal pathways.
A Line plot showing cytoskeletal proteins that responded by >1.5 fold in C5.1 (*BAP1*$^{w-/KO}$) cells vs. MeT5A (*BAP1*$^{+/+}$) as determined by SILAC-MS (work undertaken by Dr. Jenna Kenyani). **B-G** immunoblots validate the expression changes of **B** BAP1, **C** FN1, **D** ICAM1, **E** ARPC2 and ARP3, **F** SERPINE1 and **G** SERPINB6 in MeT5A (*BAP1*$^{+/+}$) and C5.1 (*BAP1*$^{w-/KO}$) cells. Quantification of protein expression, normalised to ß-actin and relative to MeT5A (*BAP1*$^{+/+}$), from one biological replicate are stated below each immunoblot. *SERPINE1 immunoreactive band.

in PYGL protein expression was observed in C5.1 (*BAP1*$^{w-/KO}$) cells (Fig. 3.7B). Immunoblotting also confirmed that the glycolytic enzymes ALDOC, PGAM1 and ENO2 were substantially decreased in C5.1 (*BAP1*$^{w-/KO}$) cells, to 20-30% of the level detected in MeT5A (*BAP1*$^{+/+}$). In contrast, the expression of TCA/anaplerotic enzymes SUCLG2 and ASS1 was higher in C5.1 (*BAP1*$^{w-/KO}$) cells than MeT5A (*BAP1*$^{+/+}$) (Fig. 3.7C). Overall, the majority of BAP1-dependent metabolic enzymes followed up by immunoblotting confirmed downregulation of enzymes involved in glycolytic metabolism, but upregulation of enzymes that ultimately drive the TCA cycle.

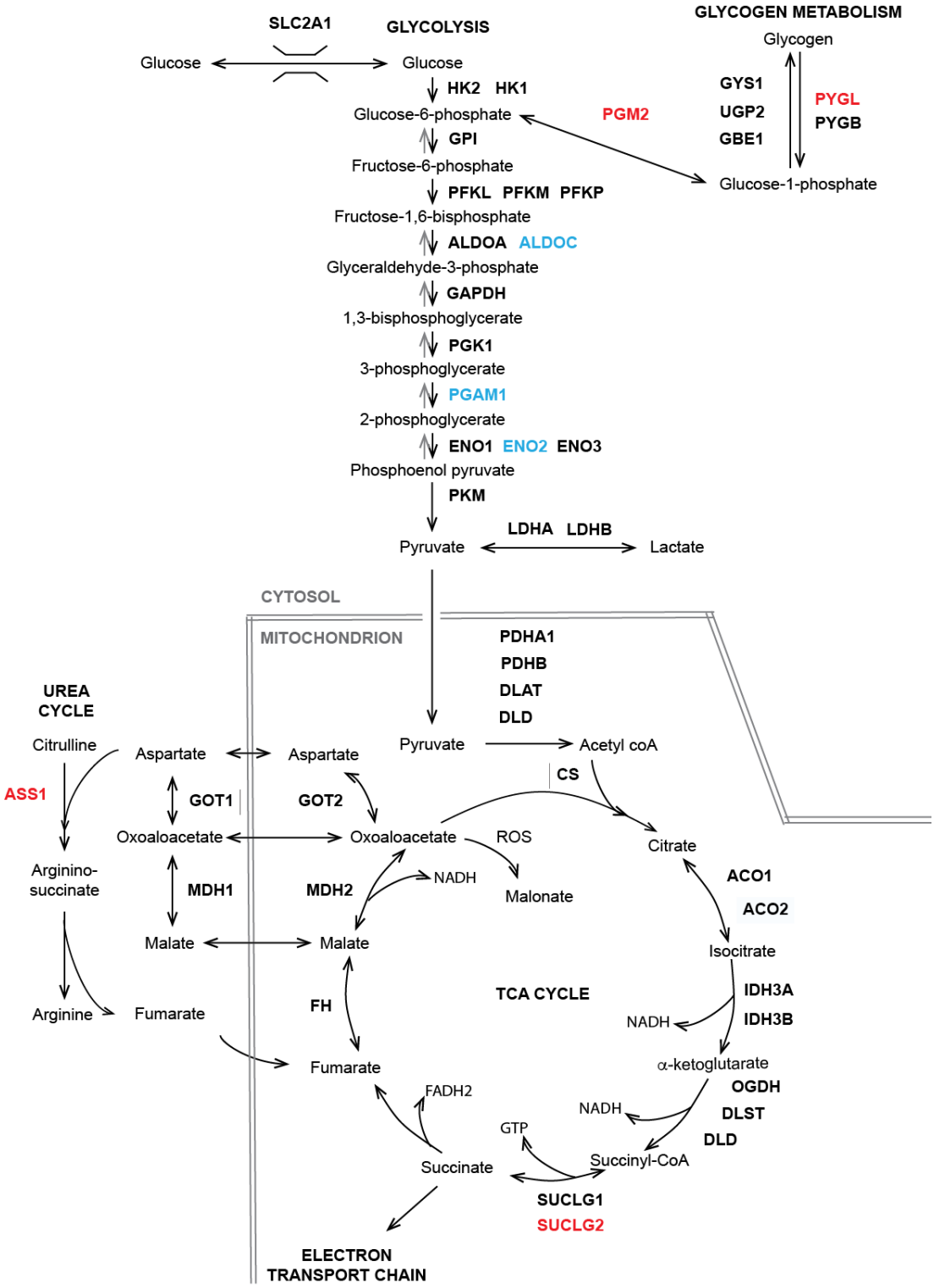

Figure 3.6: BAP1 deficiency in MeT5A impinges on cellular metabolism.
Schematic highlighting alterations in proteins regulating glucose metabolism, the TCA and urea cycles. Proteins that were upregulated (red) and downregulated (blue) in isogenic BAP1-mutant cell line C5.1 (*BAP1*$^{w-/KO}$) relative to (*BAP1*$^{+/+}$), as determined by SILAC-MS, are indicated. These were chosen for validation by immunoblotting. Adapted from (Kenyani et al., manuscript in prep).

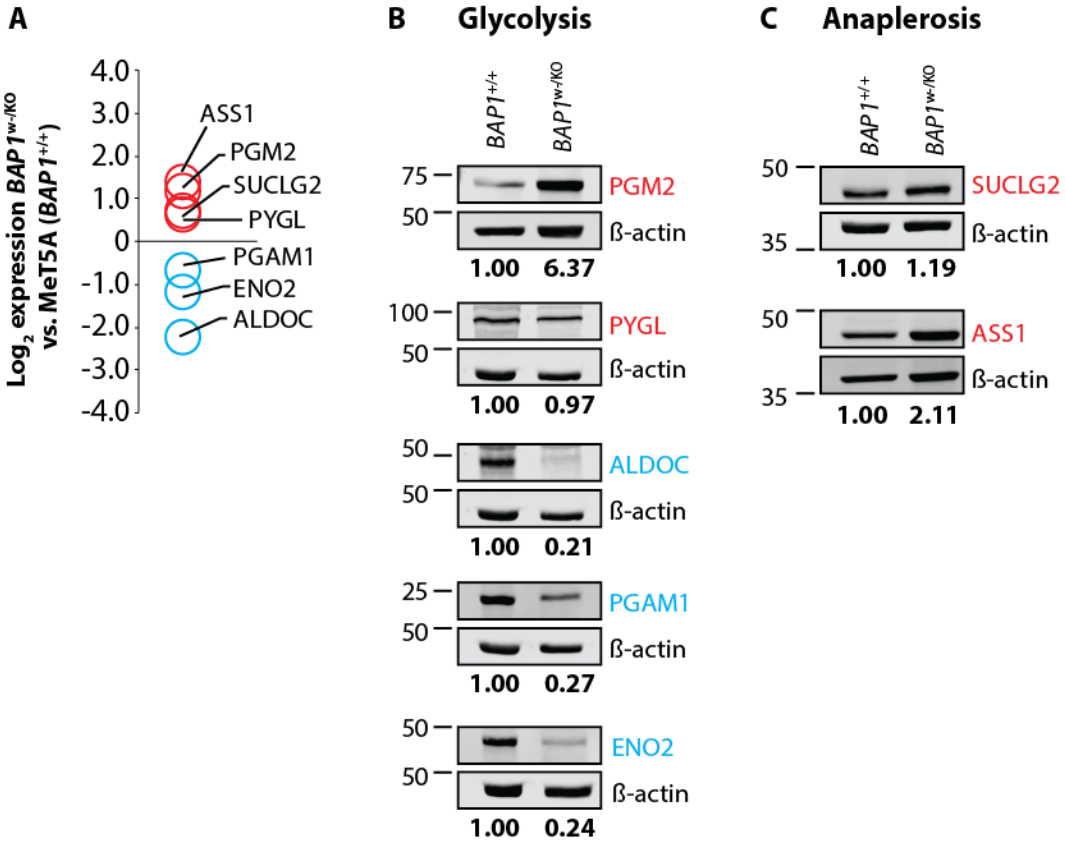

Figure 3.7: BAP1 deficiency in MeT5A deregulates expression of enzymes involved in glycolysis and anaplerosis.
A Line plot showing selected metabolic enzymes responding by >1.5 fold in C5.1 (*BAP1*$^{w-/KO}$) cells vs. MeT5A (*BAP1*$^{+/+}$) as determined by SILAC-MS. **B-C** Immunoblots to validate the expression changes of **B** glycolytic enzymes PGM2, PYGL, ALDOC, PGAM1 and ENO2 and **C** TCA/urea cycle enzymes SUCLG2 and ASS1 in MeT5A (*BAP1*$^{+/+}$) and C5.1 (*BAP1*$^{w-/KO}$). Quantification of protein expression, normalised to ß-actin and relative to MeT5A (*BAP1*$^{+/+}$), from one biological replicate are stated below each immunoblot.

3.6 Characterising BAP1 mRNA and protein expression in a panel of patient-derived MPM cell lines

Next, I assessed the BAP1 status of a panel of MPM cell lines from ATCC and MesobanK (Fig. 3.8), with the aim of using these cell lines to validate BAP1-dependent protein changes identified in C5.1 (*BAP1*$^{w-/KO}$) cells. I initially assessed the BAP1 mRNA and protein expression in these MPM cell lines. The BAP1 mutation status of MPM cell lines from MesobanK was not known at the time this work was undertaken, and the assignment of BAP1 status was based on *in vitro* catalytic activity, as determined by detection of BAP1 binding to the active-site directed probe, HA-Ub-PA, via immunoblotting (work undertaken by Dr. Sarah Taylor) (Kenyani et al., manuscript in prep).

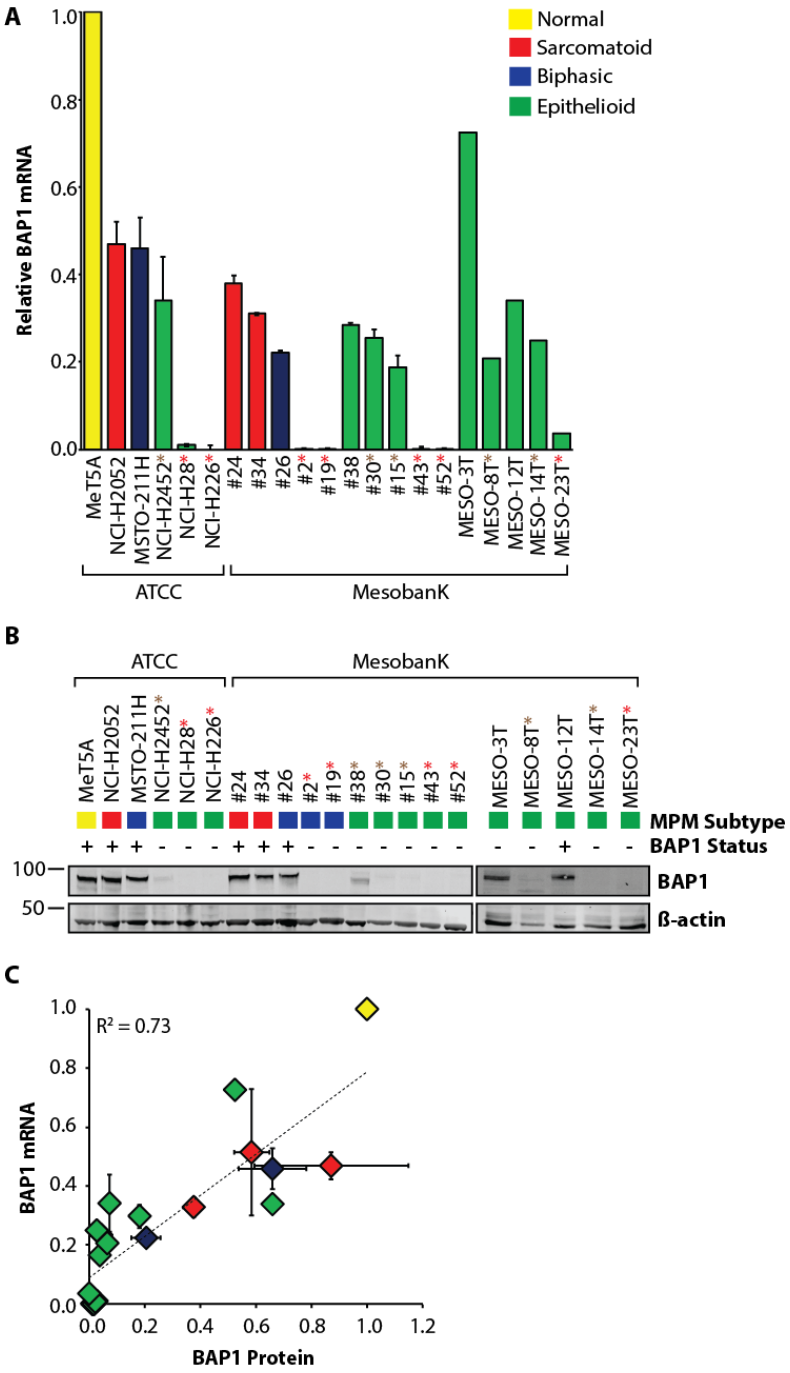

Figure 3.8: Characterising BAP1 expression in a panel of MPM cell lines.
A panel of MPM cell lines were sourced from ATCC and MesobanK. **A** Quantification of BAP1 transcript levels, normalised to ß-actin and relative to MeT5A (*BAP1*$^{+/+}$), where displayed error bars show SD for three independent experiments. Where no error bars are displayed n=1 **B** Representative immunoblot displaying BAP1 protein expression. In **A** and **B** red asterisks signify "BAP1 null" cell lines with no detectable BAP1 mRNA or protein, brown asterisks signify 20-40% BAP1 mRNA expression but <10% BAP1 protein expression relative to MeT5A (*BAP1*$^{+/+}$). **C** Scatter plot displaying expression of BAP1 protein, normalised to ß-actin and relative to MeT5A (*BAP1*$^{+/+}$) (from **B**, X-axis) versus BAP1 mRNA from (from **A**, Y-axis). Plus and minus signs indicate BAP1 status, based on *in vitro* catalytic reactivity towards the active-site directed probe, HA-Ub-PA. Colour coding indicates the histological subtypes of MPM.

Cell lines were also classified into their histological subtypes, as BAP1 gene mutations leading to loss of nuclear BAP1 protein expression are more frequently observed in epithelioid MPM (Yoshikawa et al., 2012).

All MPM cell lines expressed less BAP1 mRNA than MeT5A (*BAP1*$^{+/+}$) cells (Fig. 3.8A) and fell into two distinct groups, where BAP1 mRNA was detectable (albeit to varying levels) or undetectable. The seven cell lines in the latter group are indicated by red asterisks in Fig 3.8A, NCI-H28, NCI-H226, #2, #19, #43, #52 and MESO-23T. These seven cell lines also showed no BAP1 protein expression (Fig. 3.8B), and are all likely to harbour BAP1-mutations, as is known to be the case for NCI-H28 and NCI-H226. In general, there was good correlation between BAP1 mRNA and protein expression (Fig. 3.8C). However, there were a few exceptions, notably NCI-H2452, #15, #30, #38, MESO-8T and MESO-14T (indicated by brown asterisks in Fig 3.8). These cell lines show between 20-40% BAP1 mRNA expression but <10% BAP1 protein expression relative to MeT5A (*BAP1*$^{+/+}$). NCI-H2452 have a missense mutation in the BAP1 catalytic domain resulting in an inactivated (and possibly an unstable) protein. MPM cell line #38 displayed an immunoreactive band for BAP1 at a lower molecular weight than expected (Fig. 3.8B) and BAP1 in this cell line was catalytically inactive (work performed by Dr Sarah Taylor), suggesting it could harbour a truncating and/or catalytic site mutation in *BAP1*. Although full length BAP1 protein was expressed in MESO-3T, this was also catalytically inactive, suggestive of a catalytic site mutation. Overall, loss of active BAP1 protein was common in the epithelioid MPM cell lines examined (12/13). In contrast, in the sarcomatoid and biphasic MPM cell lines, 100% (3/3) and 50% (2/4) of cell lines expressed active BAP1 protein, respectively.

3.7 Validating BAP1-dependencies in a panel of patient-derived MPM cell lines

Having validated the SILAC-MS proteomic analysis by confirming differential expression of selected cytoskeletal and metabolic enzymes in the MeT5A *BAP1*-mutant cell lines by immunoblotting (section 3.5), I broadened the analysis of enriched cytoskeletal (Fig. 3.9) and metabolic proteins (Fig. 3.10 and 3.11) by assessing their expression in the panel of MPM cell lines by immunoblotting. In contrast with the isogenic MeT5A cell model, these patient-derived cell lines are more representative of MPM and will carry a variety of other genetic alterations that characterise the disease. At the time this work was undertaken, 15 MPM cell lines were available in our lab, these were classified by histological subtype and divided into BAP1-positive or BAP1-negative groups, in order to visualise the relationship between BAP1 status and expression of the candidate proteins (Fig. 3.9 – 3.11).

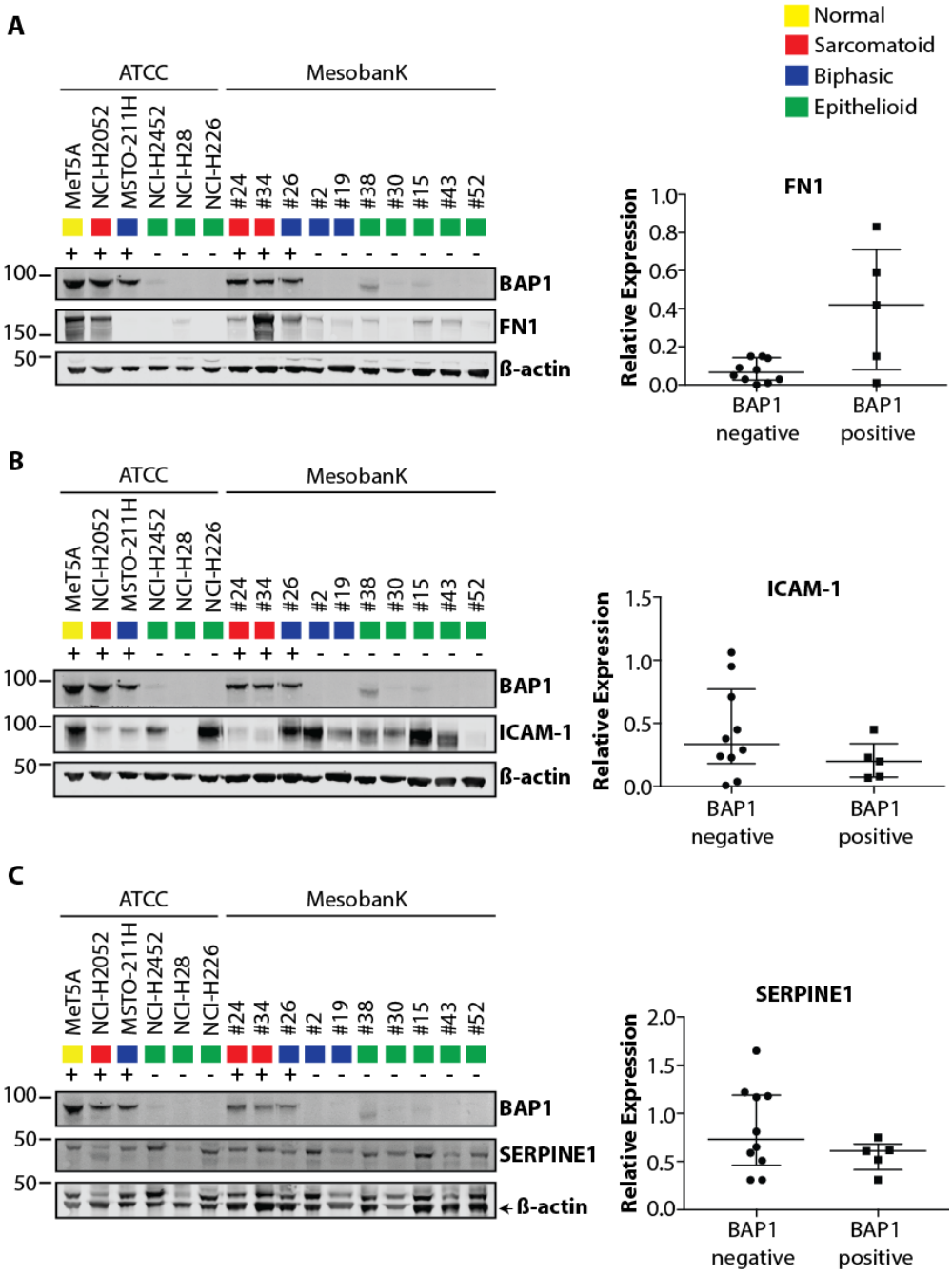

Figure 3.9: Expression of ICAM1 and SERPINE1, but not FN1, are inversely related to BAP1 positivity in a panel of MPM cell lines.
Immunoblots **(A-C, left)** and scatter dot plots **(A-C, right)** displaying relative protein expression are shown for BAP1, FN1, ICAM1 and SERPINE1 in MPM cell lines. Scatter dot plots show median with interquartile range. Protein expression was quantified from a single experiment, normalised to ß-actin and shown relative to MeT5A (*BAP1*$^{+/+}$). No significant differences in protein expression between BAP1-negative and BAP1-positive cell lines by unpaired t-test.

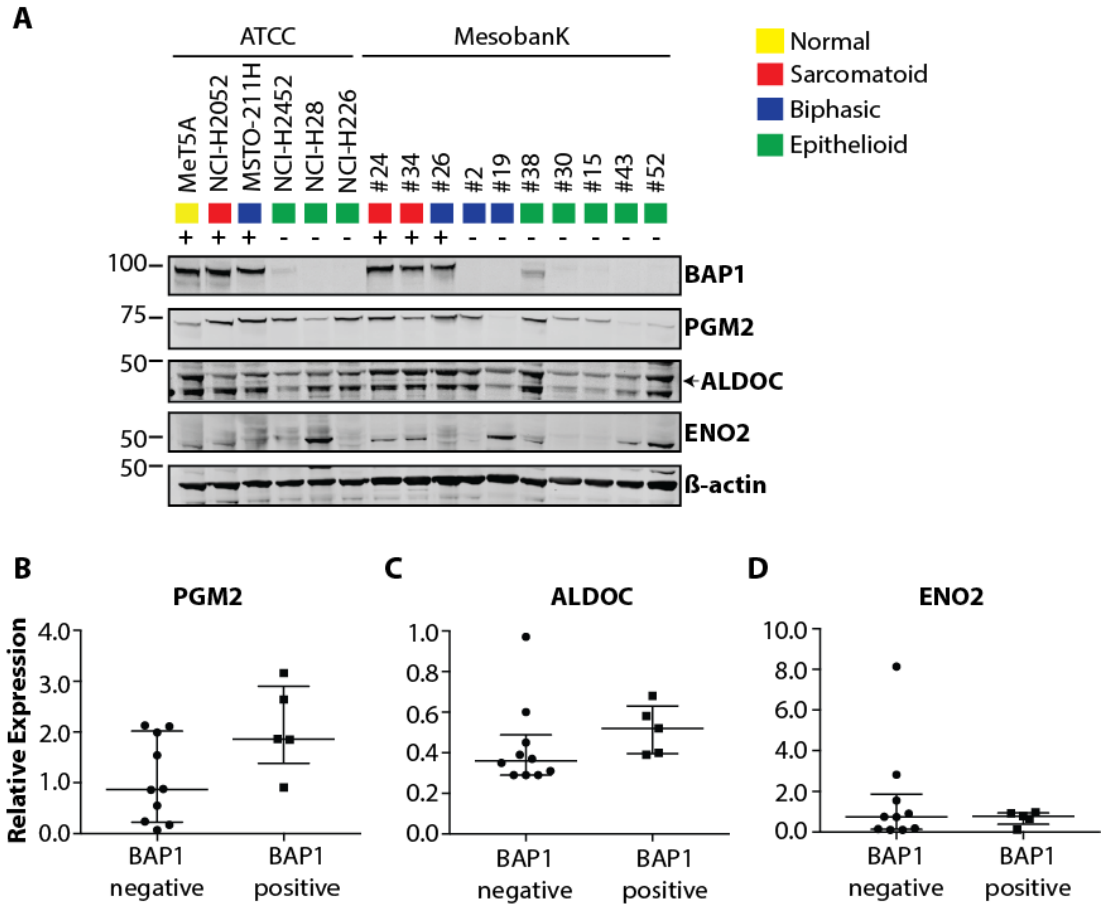

Figure 3.10: Expression of glycolytic proteins in *BAP1*$^{w-/KO}$ MeT5A cells is not recapitulated in BAP1 negative MPM cell lines.
Immunoblots **(A)** and scatter dot plots displaying relative protein expression **(B-D)** are shown for BAP1, PGM2, ALDOC and ENO2 in MPM cell lines. Scatter dot plots show median with interquartile range. Protein expression was quantified from a single experiment, normalised to ß-actin and shown relative to MeT5A (*BAP1*$^{+/+}$). No significant differences in protein expression between BAP1-negative and BAP1-positive cell lines by unpaired t-test (PGM2) and Mann Whitney U test (ALDOC and ENO2).

FN1 expression was higher in C5.1 (*BAP1*$^{w-/KO}$) than parental cells (Fig 3.5C). However, BAP1-negative MPM cell lines showed reduced expression of FN1 overall when compared to BAP1-positive cell lines (Fig 3.9A). Expression differences were less clear for ICAM1 (Fig. 3.9B) and SERPINE1 (Fig. 3.9C) when comparing the two groups of MPM cell lines. However, in agreement with the response in C5.1 (*BAP1*$^{w-/KO}$) cells (Fig 3.5), there are a subset of BAP1-negative MPM cell lines that show higher expression of these proteins when compared to BAP1-positive cell lines. I also assessed the expression of selected glycolytic enzymes (Fig. 3.10) and anaplerotic enzymes (Fig. 3.11) in the MPM cell panel. In contrast to the increased expression seen in C5.1 (*BAP1*$^{w-/KO}$) cells (Fig 3.7B), PGM2 expression was generally higher in BAP1-positive cell lines than BAP1-negative cell lines (Fig. 3.10A and B), whilst both ALDOC

(Fig. 3.10C) and ENO2 (Fig. 3.10D) showed little difference in their expression profiles between BAP1-negative and BAP1-positive cell lines. Turning to the anaplerotic enzymes, ASS1 generally recapitulated the increase observed in C5.1 (*BAP1*$^{w-/KO}$) cells (Fig 3.7C) in BAP1-negative MPM cell lines (Fig. 3.11A), whereas median SUCLG2 expression was lower in BAP1-negative cell lines and highly variable across both groups of cell lines (Fig. 3.11B). Overall, amongst the proteins selected for validation, the cytoskeletal protein responses to *BAP1* genome-editing were validated in the isogenic MeT5A cells and in most cases across the MPM cell line panel. However, with the exception of ASS1, the expression profiles for selected glycolytic and anaplerotic enzymes in MPM cell lines did not reflect the profiles from *BAP1* genome-edited MeT5A cells.

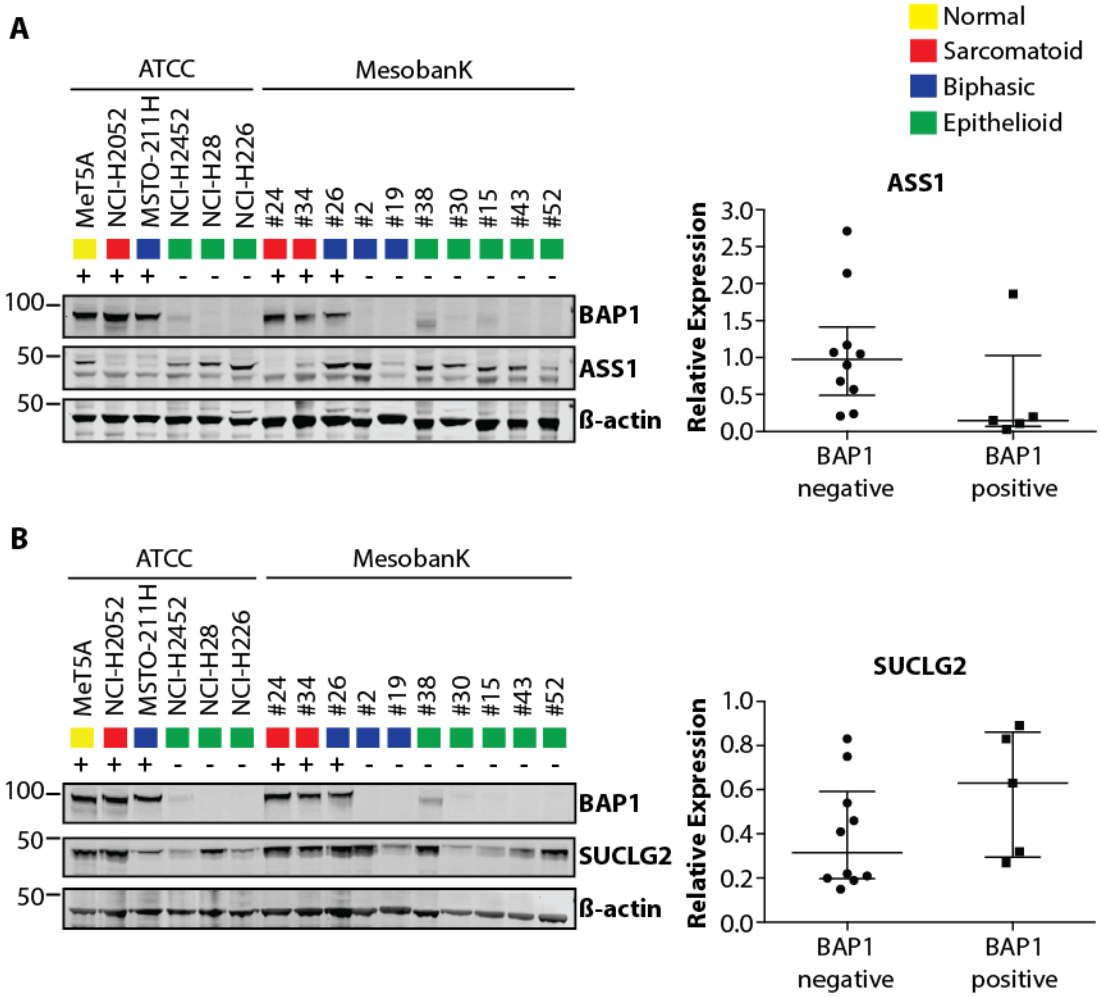

Figure 3.11: Expression of ASS1, but not SUCLG2, is inversely related to BAP1 protein status in a panel of MPM cell lines.
Immunoblots **(A-B, left)** and scatter dot plots displaying relative protein expression **(A-B, right)** are shown for BAP1, ASS1 and SUCLG2 in MPM cell lines. Scatter dot plots show median with interquartile range. Protein expression was quantified from a single experiment, normalised to ß-actin and shown relative to MeT5A (*BAP1*$^{+/+}$). No significant differences in protein expression between BAP1-negative and BAP1-positive cell lines by unpaired t-test.

3.8 Discussion

In this chapter I have highlighted my contributions to a larger study that aimed to characterise BAP1-dependencies in *BAP1*-mutant cell lines (Kenyani et al., manuscript in prep). This study utilised SILAC-MS to profile the BAP1-dependent proteome in isogenic MeT5A parental and *BAP1*-mutated cells. Changes to the C5.1 (*BAP1*$^{w-/KO}$) cell proteome, compared to parental cells, included the significant upregulation of proteins involved in actin cytoskeletal regulatory pathways, significant downregulation of glycolytic enzymes and the significant upregulation of enzymes that drive the TCA cycle. Following this discovery phase, I validated selected protein changes in C5.1 (*BAP1*$^{w-/KO}$) cells by immunoblotting and sought to infer the relevance of these changes by validating their expression across a panel of MPM cell lines with known BAP1 status, also by immunoblotting. Overall, the cytoskeletal protein changes identified in the C5.1 (*BAP1*$^{w-/KO}$) cells were recapitulated in both cell models, with the exception of FN1. However, the majority of the metabolic enzymes demonstrated opposing or varying expression profiles in *BAP1*-negative MPM cell lines compared to that of C5.1 (*BAP1*$^{w-/KO}$) cells, with the exception of ASS1.

In order to identify BAP1-dependencies in MPM, this lab generated isogenic cell lines in a mesothelial background by introducing a series of mutations reflective of the clinical manifestations of *BAP1*-haploinsufficiency (*BAP1*$^{w-/+}$) and biallelic *BAP1* inactivation (*BAP1*$^{w-/KO}$). Through rAAV genome-editing of MeT5A (*BAP1*$^{+/+}$) cells, BAP1 expression was reduced to ~40% in isogenic MeT5A *BAP1*-mutant cell line C5.1 (*BAP1*$^{w-/KO}$). We hypothesised that there is incomplete mis-splicing of the w-allele, and an alternative splice site has been accessed to retain BAP1 expression from this allele. The incomplete loss of BAP1 protein is perhaps unsurprising when considering results from genome-wide CRISPR/Cas9 screens, which have listed the BAP1 gene as one of ~1500 human "essentiality" or "fitness" genes required for cell viability (Shalem et al., 2014; Hart et al., 2015). This could suggest that complete loss of BAP1 may be deleterious for cells in certain contexts, therefore retaining some BAP1 expression can confer a survival advantage. Indeed, mouse *Bap1* gene deletion is lethal during embryogenesis, *Bap1*$^{-/-}$ embryos are not detected past embryonic day E9.5 suggesting BAP1 is essential for mouse embryonic development (Dey et al., 2012). Nevertheless, the isogenic MeT5A cell lines are a good model of stable, long term *BAP1* deficiency, forgoing the need for RNAi methodologies which can generate off-target effects.

It is important to note that the isogenic MeT5A *BAP1*$^{w-/KO}$ cell lines C5.1 and C3.1 have significant passage number differences compared to the parental MeT5A (*BAP1*$^{+/+}$) cell line and the heterozygous *BAP1*$^{w-/+}$ cell line, which may represent a potential source of variation. As the *BAP1*$^{w-/+}$ cell line was derived from parental MeT5A (*BAP1*$^{+/+}$) cells, and both C5.1 (*BAP1*$^{w-/KO}$) and C3.1 (*BAP1*$^{w-/KO}$) cell lines were subsequently derived from the *BAP1*$^{w-/+}$ cell line, the significant passage number differences between cell lines are the result of sequential rounds of genome editing. Ensuring a clonal population of each of the isogenic MeT5A *BAP1*-mutant cell lines was one method to combat variation within and between the cell lines. Other means of reducing potential sources of variation between the cell lines would be to culture the parental MeT5A and heterozygous *BAP1*$^{w-/+}$ cell lines to a similar passage number to that of the C5.1 (*BAP1*$^{w-/KO}$) and C3.1 (*BAP1*$^{w-/KO}$) cell lines prior to their experimental use.

Initial characterisation of the isogenic MeT5A cell lines included an assessment of their growth patterns and cell cycle distribution. I discovered that the sequential editing of *BAP1* alleles and consequent reduction in BAP1 protein expression slowed the rate of MeT5A cell proliferation. Given the fact that C5.1 (*BAP1*$^{w-/KO}$) cells show downregulated expression for glycolysis enzymes, and the proliferation assay utilised for the assessment of cell growth is ATP-dependent (see section 2.1.5), these results could reflect low metabolism rather than actual cellular proliferation. As such, alternative supporting observations such as cell count using a cytometer and/or visual inspection of cellular morphology could be implemented to increase confidence in this result.

Although the slowed rate of MeT5A cell proliferation as a consequence of *BAP1* genome editing is somewhat counterintuitive on loss of a tumour suppressor, the observed growth phenotype could be explained by their cell cycle progression. The cell cycle distribution of isogenic MeT5A *BAP1*-mutant cell lines showed an increase in the number of cells in S-phase, compared with the parental cell line. This is consistent with a previous study where knockdown of BAP1 in the BAP1-positive MPM cell line MSTO-211H caused an accumulation of these cells in S-phase (Bott et al., 2011). Conversely in the same study, when the *BAP1*-null MPM cell line NCI-H28 was transfected with WT BAP1, the number of cells accumulating in S-phase decreased. It was hypothesized that BAP1 loss may contribute to a delayed but more permissive G1/S checkpoint, so that all cell growth is reduced.

Mechanistically, the specific cellular functions of BAP1 could also explain the slowed S-phase progression on BAP1 mutation. BAP1 was initially characterised as a DUB that could interact with the BRCA1-BARD1 tumour suppressor complex (Nishikawa et al., 2009). This complex has E3 ubiquitin ligase activity, an important requirement for its tumour suppressive function during the DNA damage response. Although BAP1 cannot deubiquitylate BRCA1 (Mallery et al., 2002), it can modulate its E3 ligase activity by binding and deubiquitylating BARD1 (Nishikawa et al., 2009). Interestingly, the inhibition of BAP1 by shRNA in HeLa cells can lead to an impairment of the DNA damage response coupled with slowed S-phase progression, which is also seen in situations of BARD1 or BRCA1 deficiency (Nishikawa et al., 2009).

The isogenic MeT5A *BAP1*-mutant cell lines are a novel tool to investigate BAP1 dependencies in MPM. They differ from the parental MeT5A cell line by the mutation of interest which has been precisely integrated into their genomes. However, these cell lines capture only a small part of the genetic landscape of MPM, as such, a larger panel of patient-derived MPM cell lines (Chernova et al., 2016; Al-Taei et al., 2012) was acquired for the purpose of validating experimental findings from isogenic MeT5A cells. I showed that these MPM cell lines varied in their BAP1 mRNA and protein status and showed overall good correlation between the two. These MPM cell lines are also distinguished by their histology, which is important as MPM is a heterogeneous disease and it would be prudent to identify expression level differences between MPM tumours of different histological subtypes. There are now published data from Kolluri *et al.* detailing BAP1 expression by western blotting and nuclear IHC staining for the MPM cell lines derived from MesobanK (Kolluri et al., 2018). Most of their BAP1 expression data is in agreement with our findings, with the exceptions of #15, #30, #38 and MESO-3T. The authors have classified these cell lines as BAP1-positive, yet in our hands these are BAP1-negative cell lines based on *in vitro* catalytic reactivity of BAP1 towards the active-site directed probe, HA-Ub-PA. It is important to investigate DUB catalytic activity as it is an important component governing BAP1 cellular function. Any loss of catalytic activity could be suggestive of a catalytic site mutation, which we predict to be the case for #38 and MESO-3T (see section 3.6).

Analysis of the C5.1 (*BAP1*$^{w-/KO}$) cell proteome by SILAC-MS had revealed altered expression of key actin cytoskeletal regulatory pathways (Fig. 3.2) (Kenyani et al., manuscript in prep). Here, it was confirmed by immunoblotting that the expression of several cancer-associated proteins increased upon BAP1 loss. Negative correlation of ICAM1 and SERPINE1 with BAP1

expression was validated in both the isogenic MeT5A cells and patient-derived MPM cell lines. In contrast, FN1 expression was markedly reduced in BAP1-negative MPM cell lines when compared to BAP1-positive cell lines.

High ICAM1 and SERPINE1 expression has been associated with local invasion and metastasis in various tumour types (Mendez et al., 2009; Liu et al., 2008; Rosette et al., 2005). Degradation of the ECM facilitates the migration of tumour cells to other tissues and structures. SERPINE1 regulates this process by inducing cell detachment from the ECM, thereby promoting migration and tumour invasion (Duffy et al., 2008). The process of cell migration from the blood through endothelium into tissue is termed extravasation, and leukocytes such as neutrophils are one a prominent type of extravasating cell. Cancer cells can utilise neutrophils for their own extravasation; neutrophils facilitate the contact between cancer cells and the endothelium by acting as linkers (Strell et al., 2007). Cancer cells can lack β2-integrins which are the ligands for ICAM1 on the endothelium. Instead, they express ICAM1 and adhere to neutrophils which subsequently connect them to the endothelium (Strell et al., 2007). BAP1 has not previously been associated with the regulation of these proteins, however in agreement with a potential role in regulating the invasive capacities of cancer cells, there are various studies that indicate BAP1 is a metastasis suppressor, particularly in UVM, where BAP1 inactivation is associated with metastasis development and worse prognosis (Harbour et al., 2010; Njauw et al., 2012).
In the MPM cell panel, FN1 did not recapitulate the change seen on gene-editing. Of interest, FN1 expression was lowly expressed in all MPM cell lines compared to MeT5A (*BAP1*$^{+/+}$), but within the cell panel the sarcomatoid MPM cell lines showed greater FN1 expression compared to epithelioid MPM cell lines, where expression was low or undetectable. Gain of FN1 is one of the defining features of EMT, it alters ECM composition and is believed to contribute to the invasive properties of cancer (Jung et al., 2015). However, MPM cells exhibit a propensity for highly invasive local growth into surrounding tissue with a weak ability for metastasis (Elmes and Simpson, 1976), which may potentially explain the lower expression of FN1 in MPM cells on average, compared to MeT5A (*BAP1*$^{+/+}$). FN1 expression in MeT5A (*BAP1*$^{+/+}$) is unsurprising as mesothelial cells are capable of producing FN1 (Kinnula et al., 1998). The higher expression of FN1 in sarcomatoid MPM cells compared to epithelioid MPM cells could be a reflection of the more aggressive, invasive nature of this subtype (Schramm et al., 2010). It is possible that the BAP1-dependent effect on FN1 is context-specific in MPM, as there is subtype variation between the two proteins.

A recently published study has taken a different approach to profile the BAP1-dependent proteome, in this case WT BAP1 was reintroduced into a BAP1-null, epithelioid MPM cell line NCI-H226 (pCDH1_BAP1^{wt}) (Hebert et al., 2017). Of note, their study identified through SILAC-MS similar pathways affected by BAP1 status, revealing a significant enrichment for proteins involved in cytoskeleton organisation amongst others. Although we both report significantly increased expression for components of the ARP family, in contrast they report significantly upregulated protein expression of the SERPINB family, including SERPINB6 that was downregulated in C5.1 (*BAP1*$^{w-/KO}$) cells. ICAM1 and FN1 were not detected in their dataset. Importantly, they suggest that these protein changes were related to an increase of cell invasive and migratory capacities when a functional BAP1 protein was expressed. In contrast, in C5.1 (*BAP1*$^{w-/KO}$) cells we predominantly saw increased expression of actin cytoskeleton-related proteins on BAP1 loss. This reinforces the context-specific nature of BAP1 function and highlights the importance of interpreting results from different cancer cell models. It could be argued that the isogenic MeT5A cells are a cleaner model for assessing BAP1-dependencies, as they were derived from a normal mesothelial genetic background, whereas the NCI-H226 (pCDH1_BAP1^{wt}) cells are an established MPM cell line with various genomic instabilities that have been accruing in culture over decades. In support of our isogenic cell model, the C5.1 (*BAP1*$^{w-/KO}$) cells are more representative of the series of events that occur in tumours as they progressively lose both *BAP1* alleles. This cell line was engineered from a *BAP1*-haploinsufficient cell line and underwent biallelic *BAP1* inactivation consistent with *BAP1* being a two-hit TSG (Testa et al., 2011), in comparison, Hebert *et al.* re-introduced BAP1 protein into an MPM cell line that is BAP1-deficient and may have adapted to BAP1 loss overtime.

SILAC-MS analysis of the C5.1 (*BAP1*$^{w-/KO}$) proteome also suggested generally downregulated expression for glycolysis enzymes, and upregulated expression of TCA cycle and anaplerotic enzymes (Kenyani et al., manuscript in prep). Interestingly, expression of early glycolysis enzymes involved in glucose-1-phosphate metabolism increased, in contrast to downstream glycolysis pathway components. There is some evidence suggesting increased expression of enzymes in the first stage of glycolysis can help to re-reroute metabolic flux towards the pentose phosphate pathway (PPP), upon cells experiencing oxidative stress (Kuehne et al., 2015). It is entirely plausible that by losing BAP1 expression, isogenic MeT5A *BAP1*-mutant cell lines elicit a diminished protective response against oxidative stress, thereby upregulating upper enzymatic components of glycolysis and increasing PPP flux. Indeed, MPM pathogenesis is closely associated with

oxidative stress in mesothelial cells (Chew and Toyokuni, 2015), thus under these conditions MPM cells may re-route metabolic flux as a compensatory mechanism for survival. It would be interesting to investigate this further by profiling the expression of PPP enzymes or measuring the generation of NADPH during the rate limiting step of PPP, for analysis of metabolic flux through this pathway in isogenic MeT5A *BAP1*-mutant cell lines.

To meet the growing energy and nutrient demands of enhanced proliferation, cancer cells often undergo metabolic reprogramming to shift ATP generation from oxidative phosphorylation to aerobic glycolysis, despite oxygen availability and functioning mitochondria. Known as the Warburg effect, this results in the metabolism of glucose to lactate via aerobic glycolysis, which is in contrast with the more efficient method of ATP production via mitochondrial oxidative phosphorylation (OXPHOS) (Warburg et al., 1927). In C5.1 (*BAP1*$^{w-/KO}$) cells, the observed increase in expression of TCA and anaplerotic enzymes, which function to replenish the TCA cycle, is in contrast with this phenomenon. It had been assumed that the glycolytic phenotype in cancer is a result of mitochondrial OXPHOS impairment, a view that has been challenged by recent investigations which find that the function of mitochondrial OXPHOS in most cancers is intact (Scott et al., 2011; Lim et al., 2011; Hsu and Sabatini, 2008).

BAP1 has been associated with metabolism in a number of recent publications, but there are conflicting data in different cell models. Hebert *et al*. observed a significantly decreased number of active mitochondria indicative of mitochondrial dysfunction and reduced TCA cycle function after BAP1 re-expression, and highlighted a number of proteins involved in the mitochondrial respiratory chain with reduced expression in their NCI-H226 (pCDH1_BAP1^{wt}) cells (Hebert et al., 2017). In contrast with our data, they observed significantly increased expression of glycolytic enzyme ENO2 and for a different aldolase isozyme ALDOA. It could be argued that an increased glycolytic phenotype in their cell model may represent an artefact of cell culture as another study showed that newly-established patient-derived MPM cell lines from MesobanK exhibit lower rates of glycolysis and OXPHOS compared to the metabolic profile of commercially MPM cell lines from ATCC (Chernova et al., 2016), of which NCI-H226 cells are ascribed.

In a study from the lab that originally documented the germline *BAP1* mutation in Family W, the authors detected altered glycolytic and TCA cycle metabolites in *BAP1*$^{+/-}$ fibroblasts from Family W (analogous to the *BAP1*$^{w-/+}$) and Family L, compared to WT BAP1 fibroblasts,

suggestive of increased aerobic glycolysis and lactate secretion, and reduced OXPHOS and ATP production in *BAP1*$^{+/-}$ fibroblasts (Bononi et al., 2017b). There are several points to consider from their data and in light of our findings, notably we focused on understanding proteome-level adaptation of C5.1 (*BAP1*$^{w-/KO}$) cells compared to *BAP1*$^{+/-}$ cells, therefore our findings are from a background of biallelic *BAP1* inactivation. They obtained similar results in primary human mesothelial cells treated with siRNA to reduce BAP1 protein expression levels. However, we have identified pitfalls in using transient siRNA depletion over long term genetic *BAP1* loss for evaluating BAP1-dependencies (see chapter 4) (Sacco et al., 2015). In agreement with our data in isogenic *BAP1*-mutant cell lines, *in vivo* labelling of the proteome in *BAP1*-knockout mice also report a repression of glycolysis and gluconeogenesis (Baughman et al., 2016), suggesting a reduced glycolytic phenotype in *BAP1*-knockout conditions in line with our data.

In summary, this lab has engineered isogenic MeT5A *BAP1*-mutant cell lines as a precise model to investigate BAP1-dependencies in MPM and profiled their proteome. Among other findings, C5.1 (*BAP1*$^{w-/KO}$) cells show a significantly altered expression of proteins involved in regulating the actin cytoskeleton, differential expression of glycolytic enzymes and increased expression of TCA cycle associated enzymes. I successfully validated a subset of these by immunoblotting in C5.1 (*BAP1*$^{w-/KO}$) cells and recapitulated the expression profiles for selected proteins associated with cytoskeletal pathways in panel of patient-derived MPM cell lines. Although expression changes of selected metabolic enzymes were confirmed by immunoblotting in isogenic MeT5A cells, their expression in the panel of patient-derived MPM cell lines did not reflect BAP1 status. However, as these results are from one biological replicate, there is the need for additional validation of these expression changes. These experiments should be repeated at least thrice to generate meaningful biological conclusions and for statistical analyses of the protein expression data.

One way of using data on BAP1 dependencies (understanding the way cells adapt to loss of BAP1 to survive) is to identify therapies to which they may be preferentially sensitive/resistant. An example of this is the relationship between BAP1 and class 1 HDAC expression, addressed in Chapter 4. Whilst several studies including our own have profiled the BAP1-dependent transcriptome and proteome in different models, there has to date been no attempt to understand how expression of microRNAs may be regulated by BAP1. I address this novel question in Chapters 5 and 6, using a similar strategy of 'omics profiling

(in that case Nanostring) and targeted validation (by qRT-PCR) in isogenic MeT5A cells and the MPM cell panel.

Chapter 4: Investigating BAP1 regulation of Histone Deacetylase 2

4.1 Introduction

HDACs are a group of enzymes that catalyse the removal of acetyl groups from lysine-rich residues on histone tails. This leads to a more closed chromatin structure which is associated with transcriptional repression (De Ruijter et al., 2003). Originally, histones were considered the main targets of HDACs; it is now known that non-histone proteins can also be targeted by HDACs, such that the term lysine deacetylases is a more accurate term for these enzymes (Glozak et al., 2005). There are 18 different HDAC isoenzymes divided into four subclasses: Class 1 (HDAC1, HDAC2, HDAC3 and HDAC8), Class IIa (HDAC4, HDAC5, HDAC7, HDAC9), Class IIb (HDAC6, HDAC10) and Class III Sirtuins (SIRT1-SIRT7) and Class IV (HDAC11). Class III Sirtuins are functionally distinct from the other zinc-dependent isoenzymes as they are nicotinamide adenine dinucleotide (NAD^+)-dependent. Class III Sirtuins are unaffected by conventional HDACi, instead they are inhibited by nicotinamide and other NAD derivatives (Porcu and Chiarugi, 2005). HDACs oppose the activity of histone acetyl transferases (HATs). HDACs and HATs act in concert to maintain the balance between condensed and relaxed chromatin, respectively, thus providing a layer of epigenetic control in the regulation of gene expression.

Class I HDACs are largely localised to the nucleus. HDAC1 and HDAC2 share 83% amino acid homology and are found together in many of the same repressive transcriptional complexes, which suggests a high degree of functional redundancy between the two isoenzymes (Grozinger and Schreiber, 2002). Knockout studies of HDAC1 and HDAC2 revealed their functional roles in the G1/S-phase transition, cell proliferation and apoptosis, and their non-histone protein targets such as p21, p57 and p53 that can regulate these cellular processes (Lagger et al., 2002; Harms and Chen, 2007; Zupkovitz et al., 2010). It is therefore unsurprising that aberrant HDAC1 and HDAC2 regulation can be seen in many human diseases including various cancers (Cress and Seto, 2000). There are a number of studies which demonstrate altered expression of HDAC isoenzymes in a variety of tumour samples. HDAC1 expression is increased in gastric (Choi et al., 2001), colon (Wilson et al., 2006) and breast cancers (Zhang et al., 2005), whilst HDAC2 is overexpressed in cervical (Huang et al., 2005), gastric (Song et al., 2005) and colorectal cancers (Zhu et al., 2004). The transcriptional repression of tumour-suppressor genes as a consequence of HDAC

overexpression, and aberrant targeting of gene promoter regions could be a contributing factor in tumour onset (Gui et al., 2004). As such, HDACs are seen as important therapeutic targets. Indeed, the anti-proliferative effects of HDACi is already well known. Classical HDACi such as suberoylanilide hydroxamic acid (SAHA, marketed as vorinostat) and trichostatin A (TSA) are known as "pan-HDAC" inhibitors as they block all isoenzyme activity except Class IIa HDACs. Vorinostat has been approved for many years for the treatment of cutaneous T-cell lymphoma in a select group of patients (Duvic et al., 2007), but has shown limited efficacy as a single agent in the treatment of solid tumours (Grassadonia et al., 2013). The next challenge in this field is to develop class-specific or isoenzyme-specific HDACi, both as novel tools for investigating the biological functions of different isoenzymes, and for use in the clinic to inhibit HDAC isoenzymes that are associated with specific cancers (Ononye et al., 2012).

HDAC activity can be regulated by post-translational modifications such as acetylation, sumoylation, phosphorylation, nitrosylation, alkylation and ubiquitylation (Segre and Chiocca, 2011). For the latter process of ubiquitylation, various ubiquitin E3 ligases have been identified that target Class I HDACs including HDAC1 (Gaughan et al., 2005; Oh et al., 2009) and HDAC2 (Kramer et al., 2003; Zhang et al., 2011). E3 ubiquitin-protein ligases Checkpoint With Forkhead And Ring Finger Domains (CHFR) and Mouse Double Minute 2 (MDM2) can ubiquitylate and degrade HDAC1, whilst E3 ubiquitin-protein ligases RING finger LIM domain-binding protein (RLIM) and Mcl-1 ubiquitin ligase E3 (MULE) can target HDAC2 for ubiquitination and degradation. When this study began, no DUBs had been identified that could reverse the ubiquitylation of HDAC2.

Previously, our lab had performed an unbiased siRNA screen of 92 human DUBs to identify any that may regulate the expression of HDAC1 or HDAC2 (Sacco et al., 2015). The screen identified BAP1 as a potential DUB that could regulate the cellular abundance of HDAC1 or HDAC2 in a non-small cell lung cancer (NSCLC) cell line.

4.2 Aims and objectives

This lab is interested in identifying BAP1-dependent cellular targets in MPM that can be exploited for therapeutic benefit. As part of a larger study (Sacco et al., 2015), my aim was to investigate the mechanism by which BAP1 regulates HDAC2 expression and the consequences for HDACi treatment. My focus moved experiments into MPM, where loss of BAP1 function is more frequent (see section 1.3.2.2). My principal objectives were:

1. To investigate the co-expression of HDAC1 and HDAC2 protein in a panel of MPM cell lines, and to check their correlation with BAP1 protein status.
2. To examine turnover of HDAC1 and HDAC2 by the ubiquitin-proteasome pathway (UPP) and investigate whether BAP1 regulates this process.
3. To examine whether BAP1 deubiquitylates HDAC2 and thus stabilises its expression.
4. To investigate the effect of BAP1 loss on HDAC transcript levels.
5. To test whether BAP1 loss-of-function alters cancer cell sensitivity to specific HDACi.

4.3 Correlating BAP1 and HDAC2 protein expression in a panel of MPM cell lines

In an unbiased siRNA screen of 92 human DUBs, BAP1 was identified as the DUB whose depletion in A549 NSCLC cells had the greatest effect on the cellular abundance of HDAC1 and HDAC2. BAP1 mutations are uncommon events in lung carcinoma (Andrici et al., 2016), whilst mutations leading to loss of BAP1 function are implicated in a high proportion of MPM cases (Bott et al., 2011; Yoshikawa et al., 2012; Testa et al., 2011). To test the hypothesis that genetic loss of *BAP1* could affect endogenous HDAC protein expression, I analysed the protein expression of BAP1, HDAC2 and HDAC1 a panel of MPM cell lines with differing *BAP1* genetic status by western blotting. At the time of this work, only the MPM cell lines from ATCC were available in the lab (see Fig. 3.2A). MeT5A (*BAP1*$^{+/+}$) cell line was compared to MSTO-211H and NCI-H2052 that retain wild-type BAP1, NCI-H2452 that have a missense mutation in the BAP1 catalytic domain, and NCI-H28 and NCI-H226 that are genetically BAP1-null. BAP1 protein was expressed in the three BAP1 WT (BAP1$^{+/+}$) cell lines and not in the BAP1-null (BAP1$^{-/-}$) cell lines (Fig 3.8C and Fig. 4.1A). MeT5A expressed both HDAC1 and HDAC2, with HDAC1 expressed at varying levels in MPM cell lines, showing no clear correlation with the BAP1 status. In contrast, HDAC2 expression was significantly lower in BAP1$^{-/-}$ MPM cells and overall showed a tight correlation with the BAP1 status (Fig. 4.1B), with the exception of the NCI-H2052 cell line, which has copy number loss of HDAC2 that likely accounts for reduced HDAC2 protein expression in the presence of BAP1. Overall this correlation is consistent with the idea that endogenous BAP1 may regulate the protein expression of HDAC2 in MPM.

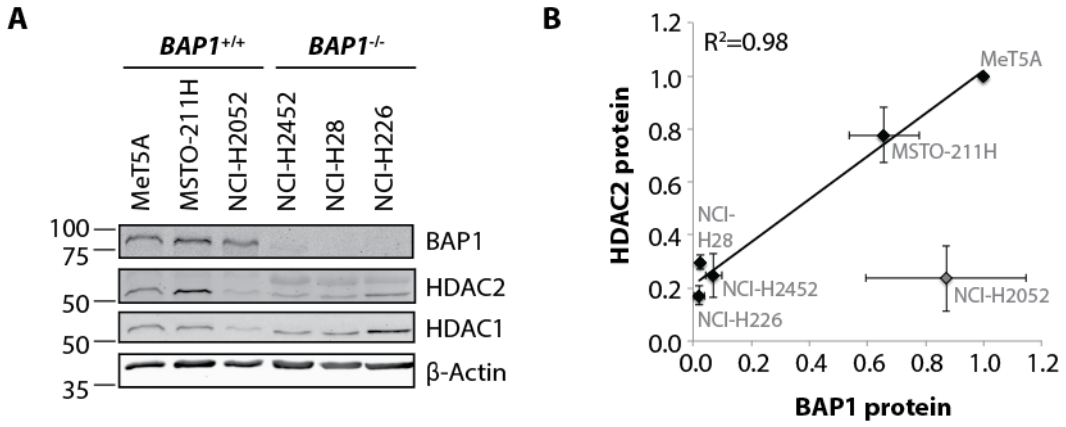

Figure 4.1: Genetic BAP1 loss reduces HDAC2 protein expression in MPM cell lines. **A** Representative immunoblot of BAP1 and HDAC protein expression in the normal mesothelial cell line MeT5A (*BAP1*$^{+/+}$) and a panel of ATCC cell lines indicating their genetic BAP1 status. **B** Quantification of BAP1 and HDAC2 protein expression, relative to MeT5A (*BAP1*$^{+/+}$), demonstrates that BAP1 and HDAC2 protein levels are positively correlated (R^2=0.98) on exclusion of NCI-H2052, which have copy number loss of HDAC2. N = three independent experiments, error bars SD.

4.4 Investigating regulation of HDAC2 by BAP1

4.4.1 BAP1 does not modulate the degradation or stability of HDAC2 protein

Next, I explored the potential mechanisms by which BAP1 could regulate HDAC2 (Fig. 4.2). As a DUB, BAP1 could modulate HDAC2 protein levels by removing polyubiquitin chains, thus regulating its abundance and/or stability. Alternatively, BAP1 has known effects on transcription (see section 1.3.4.1) and could influence the transcription of HDAC2 mRNA. This could occur either indirectly in conjunction with other transcription factors, or through its effect on histones.

Firstly, I investigated whether inhibiting the proteasome with epoxomicin treatment led to an accumulation of HDACs, which would imply these proteins are degraded by the UPP (Fig. 4.3A). In BAP1$^{+/+}$ MSTO-211H cells, treatment with epoxomicin led to a marginal, but non-significant, increase in HDAC2 and HDAC1 protein levels (Fig. 4.3B and C). In BAP1$^{-/-}$ NCI-H28 cells, there was no increase in HDAC protein level in response to epoxomicin, suggesting HDAC protein turnover via the UPP is not a major limiting factor for its expression in this particular cell line (Fig. 4.3B and C).

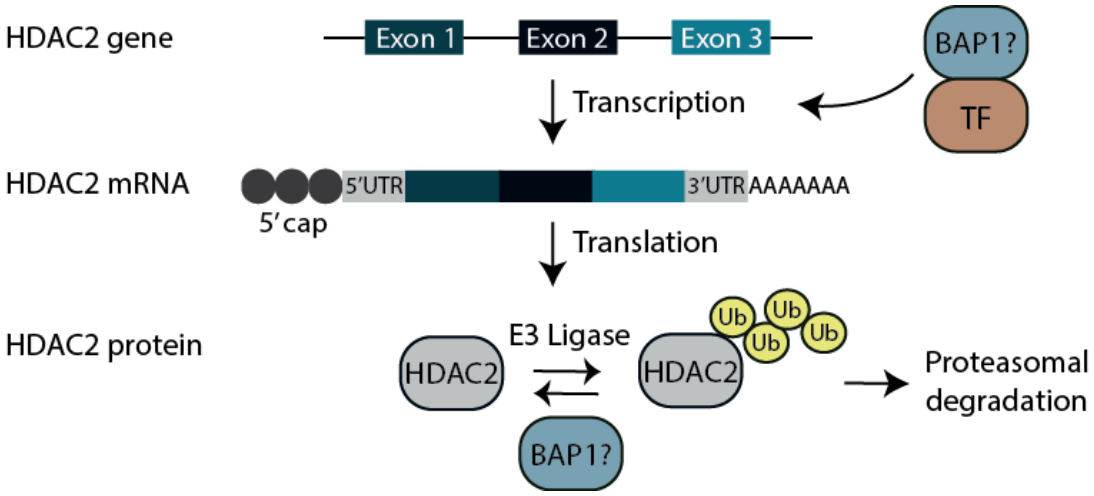

Figure 4.2: Two potential mechanisms for BAP1 regulation of HDAC2.
BAP1 is a deubiquitylase and could therefore modulate HDAC2 protein stability by removing polyubiquitin chains. Alternatively, BAP1 is a known transcriptional regulator and could influence the transcription of HDAC2 mRNA in concert with other transcription factors. Ub: ubiquitin, TF: transcription factors.

To determine whether decreased HDAC2 expression caused by BAP1 depletion can be rescued by proteasome inhibition, the HDAC2 protein level was compared in siRNA control (siC)-transfected and BAP1 siRNA (siBAP1)-transfected MSTO-211H cells treated with epoxomicin (Fig. 4.3D and E). p53 protein levels functioned as a positive control. The p53 expression level was clearly increased with epoxomicin treatment, approximately two-fold relative to the untreated condition, and the increase in p53 protein level was comparable between both knockdown conditions, which used independent siRNA sequences. However, there was no increase in HDAC2 protein level in BAP1-depleted cells with epoxomicin, showing that the BAP1-dependent loss of HDAC2 cannot be rescued by proteasome inhibition. Therefore, it was concluded that BAP1 does not stabilise HDAC2 protein nor protect it from ubiquitin-mediated proteasomal degradation.

In addition, I also examined whether the stability of HDAC2 protein was BAP1-dependent in MSTO-211H cells. These cells were transfected with siC and siBAP1 and treated with cycloheximide, an inhibitor of translation, allowing measurement of the stability of the pre-existing pool of HDAC2 protein (Fig. 4.4A). Both the siRNA transfection and the cycloheximide treatment were effective as seen by loss of BAP1 expression and with p53 degradation over the time-course (Fig. 4.4B).

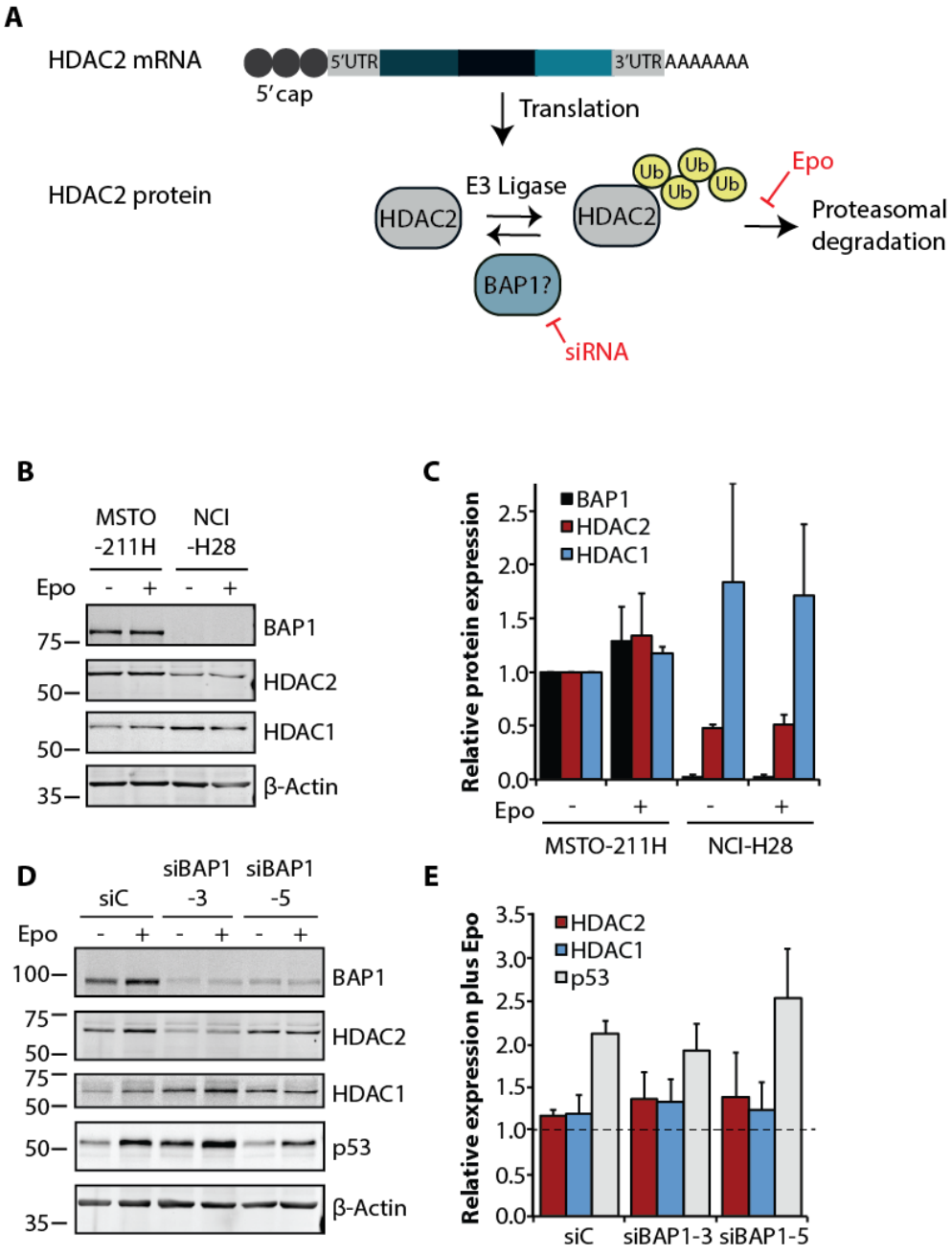

Figure 4.3: BAP1 does not salvage HDAC2 from ubiquitin-mediated proteasomal degradation.

A Proteasome inhibition was induced by epoxomicin (Epo) drug treatment, whilst BAP1 protein levels were decreased by transfection with BAP1 siRNAs. **B** Representative immunoblot of MSTO-211H and NCI-H28 cells treated with 50 nM epoxomicin for 6h prior to cell lysis and immunoblotting. **C** Quantification of protein expression, normalised to actin and relative to the untreated condition. **D** Representative immunoblot of MSTO-211H cells transfected with control or BAP1 siRNAs for 72h, and treated with 50 nM epoxomicin for the final 6h prior to cell lysis and immunoblotting. p53 functioned as a positive control for epoxomicin treatment. **E** Quantification of protein expression, relative to each untreated knockdown condition. N = three independent experiments, error bars show SD, no significant difference by one-way ANOVA and Dunnett's post hoc test.

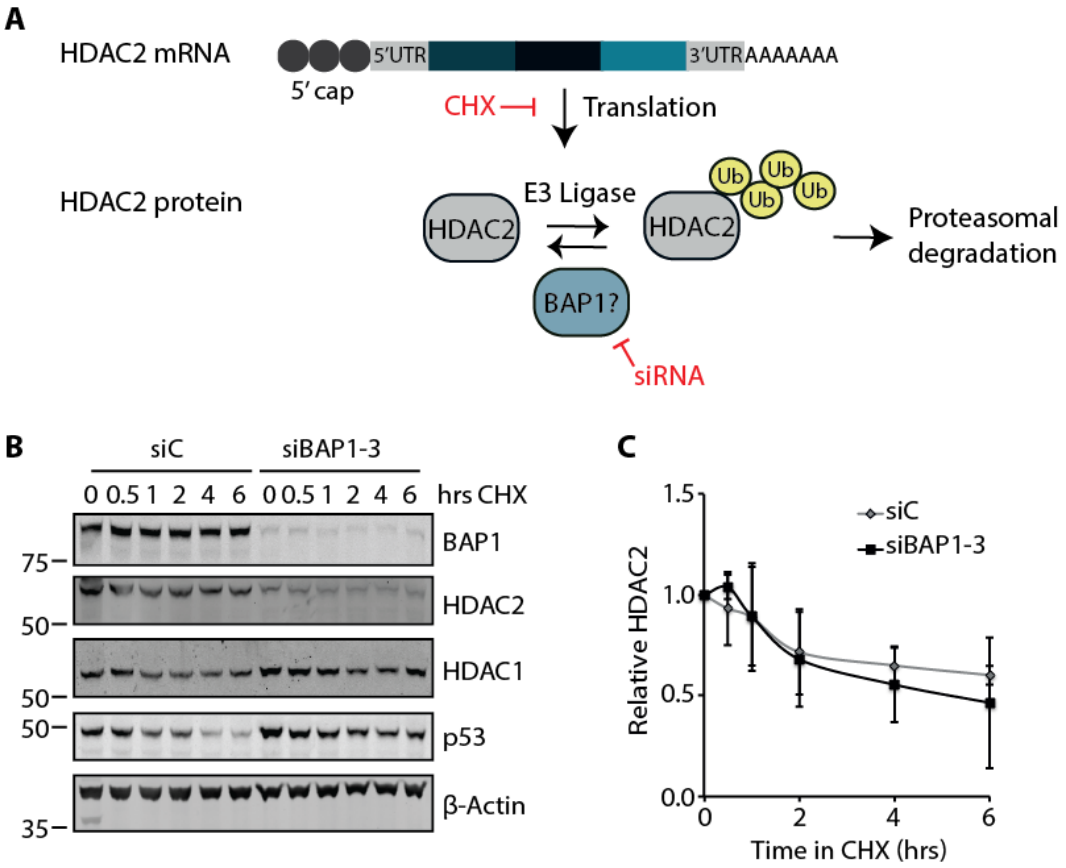

Figure 4.4: Transient BAP1 loss does not affect HDAC2 protein stability.
A Inhibition of translation was induced by cycloheximide (CHX) drug treatment, whilst BAP1 protein levels were decreased by transfection with BAP1 siRNA. **B** Representative immunoblot of MSTO-211H cells transfected with control and BAP1 siRNA for 72h, and treated with 10 μg/ml cycloheximide (CHX) for the indicated time points prior to cell lysis and immunoblotting. p53 functioned as a positive control. **C** Quantification of HDAC2 protein expression relative to actin shows no reduction in HDAC2 protein stability with CHX treatment in BAP1-depleted cells. N = four independent experiments, error bars show SD, no significant differences between samples at each time point by paired t-test.

However, BAP1-depletion did not affect the degradation rate of HDAC2 under conditions where translation was inhibited, as the relative HDAC2 protein level upon BAP1-depletion was comparable to the siC-transfected samples over a six-hour time course (Fig. 4.4C). This further confirmed that BAP1 does not modulate the stability of HDAC2 protein.

4.4.2 BAP1 regulates HDAC2 transcript abundance

As BAP1 has roles in transcriptional regulation, I next investigated the idea that BAP1 might instead control the transcription of HDAC2 (Fig. 4.5A). MSTO-211H cells were transfected with siC, independent siBAP1 sequences, or a pool of siBAP1 sequences, then the relative

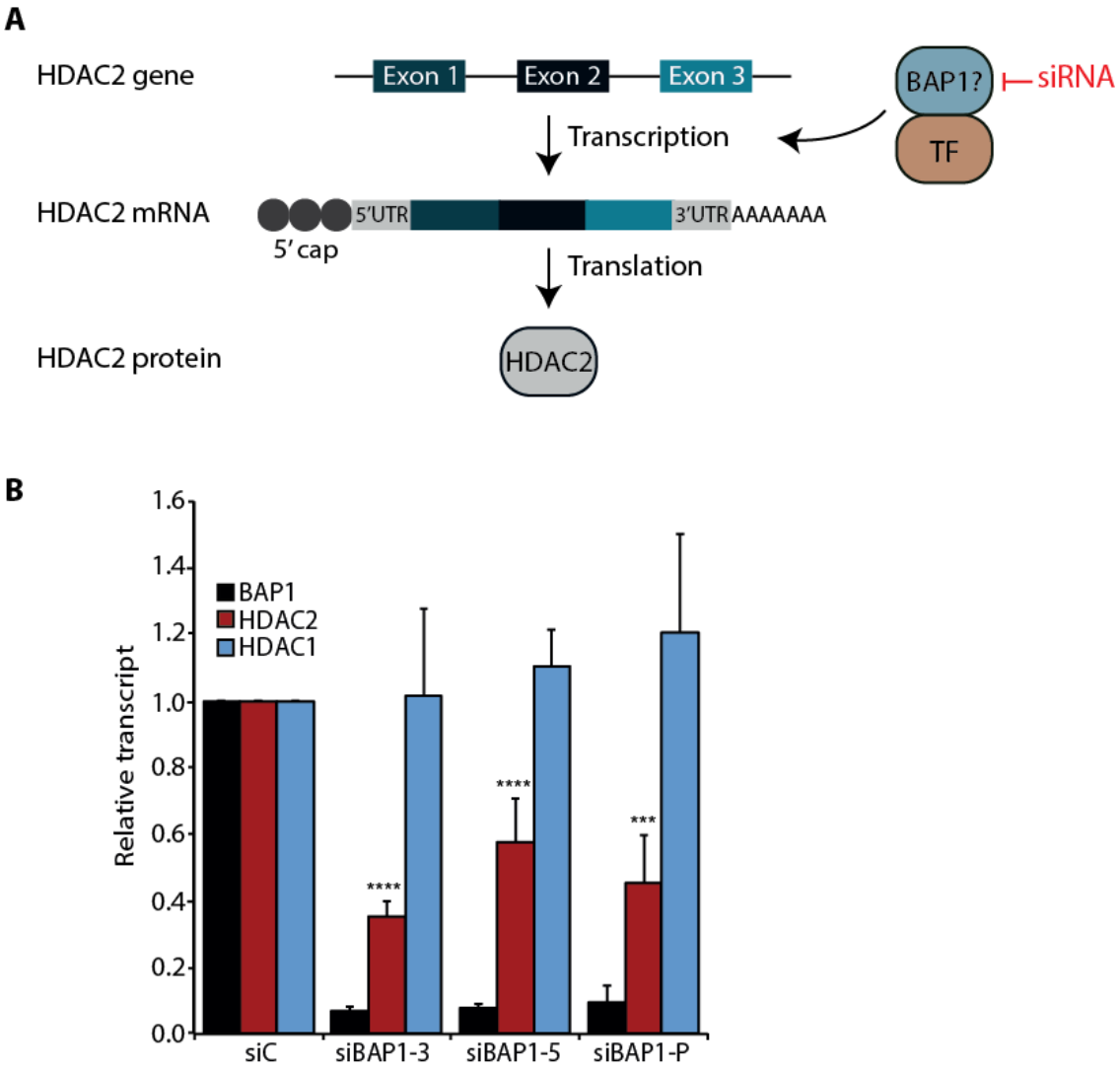

Figure 4.5: BAP1 regulates HDAC2 transcript abundance.
A BAP1 expression was decreased by transfection with BAP1 siRNA. **B** MSTO-211H cells transfected with control, individual BAP1 siRNAs or a pool of siRNAs for 72h before RNA extraction for qRT-PCR. Bar graph shows quantification of BAP1, HDAC1 and HDAC2 transcript levels, normalised to B-actin and expressed relative to the siC control. N = three independent experiments, error bars show SD, one-way ANOVA with Dunnett's post-hoc test, ****P<0.0001, ***P<0.001.

transcript levels of BAP1, HDAC2 and HDAC1 in these samples were measured by qRT-PCR (Fig. 4.5B). In all knockdown conditions, BAP1-depleted cells showed a significant decrease in HDAC2 transcript level when compared to siC. In contrast HDAC1 levels were unaffected by BAP1 depletion. Therefore, this result indicated that BAP1 exerts its effect over HDAC2 by regulating HDAC2 transcript abundance.

4.5 BAP1-mutant MPM and isogenic MeT5A cell lines are more resistant to HDAC inhibition.

Aberrant expression of HDACs is often observed in human disease, particularly cancers, which make them attractive therapeutic targets. HDACi are already in clinical use such as broad-spectrum HDACi vorinostat for the treatment of refractory cutaneous T-cell lymphoma (Duvic et al., 2007). Therefore, an important question is whether genetic loss of *BAP1* and any corresponding changes in HDAC protein expression) may alter the sensitivity of MPM cell lines to HDAC inhibitors. A panel of MPM cell lines from ATCC were treated with mocetinostat, a class 1-specific HDACi, at varying concentrations and cell viability measured after 72 hrs (Fig. 4.6A). *BAP1*$^{+/+}$ MSTO-211H cells with high BAP1 and HDAC2 expression showed the greatest sensitivity to mocetinostat, with an LC50 value of 1.55 μM. In comparison, *BAP1*$^{-/-}$ cell lines NCI-H28 and NCI-H226, with low HDAC2 expression, were more resistant to the effects of mocetinostat, displaying LC50 values of 5.30 μM and 3.34 μM, respectively. Interestingly, the *BAP1*$^{+/+}$ cell line NCI-H2052 (with genetic loss of *HDAC2*) was also resistant to the effects of mocetinostat, with a LC50 value of 3.08 μM.

I also investigated the relationship between BAP1 and HDAC2 protein expression in the isogenic MeT5A BAP1-mutant cell lines *BAP1*$^{w-/+}$ and C3.1 (*BAP1*$^{w-/KO}$) compared to parental MeT5A (*BAP1*$^{+/+}$) (Fig. 4.6B). At the time of this work, only the C3.1 clone (*BAP1*$^{w-/KO}$) was available (see Fig. 3.2A). These cell lines are genetically identical to parental MeT5A cells except for engineered mutations the in BAP1 gene, as such they represent BAP1 haploinsufficiency and BAP1-deficient MPM models, and phenotypic changes can be more easily attributed to genetic BAP1 status. In *BAP1*$^{w-/+}$ cells, I observed a slight increase in HDAC2 and HDAC1 expression relative to MeT5A (*BAP1*$^{+/+}$). In contrast, a reduction in HDAC2 protein expression to ~25% of the level observed in MeT5A (*BAP1*$^{+/+}$) was detected in C3.1 (*BAP1*$^{w-/KO}$) cells. Any changes in HDAC1 expression were less evident in isogenic MeT5A BAP1-mutant cell lines. I also tested whether genetic BAP1 depletion altered sensitivity of isogenic MeT5A cells to HDAC inhibitors (Fig. 4.6C). The loss of BAP1 and decreased expression of HDAC2 corresponded with increased resistance to the HDACi vorinostat in C3.1 (*BAP1*$^{w-/KO}$) cells. These results mirror the findings in MPM cell lines with stable, genetic *BAP1* or *HDAC2* loss.

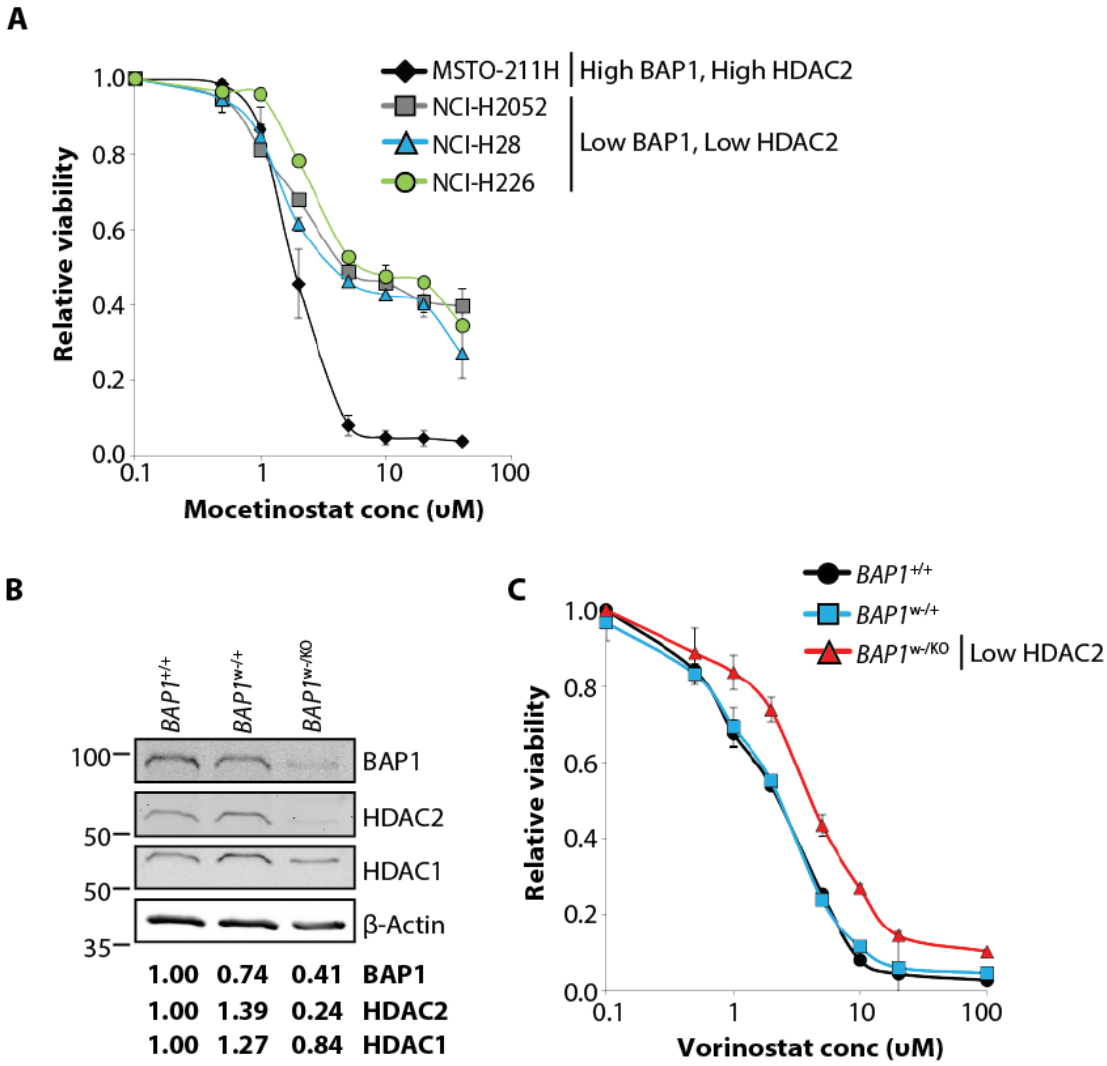

Figure 4.6: BAP1-mutant MPM and isogenic MeT5A cell lines are more resistant to HDAC inhibition.

A Measurement of cell viability in a panel of MPM cell lines with differing BAP1 and HDAC2 protein expression, after treatment with class I HDAC inhibitor mocetinostat at concentrations of 40, 20, 10, 5, 2, 1, 0.5 and 0.1 μM for 72h. Data are normalised to 0.1 μM treatment for each cell line. N = three independent experiments, error bars show SD. **B** Immunoblot of MeT5A (*BAP1*$^{+/+}$) and isogenic BAP1-mutant cell lines *BAP1*$^{w-/+}$ and C3.1 (*BAP1*$^{w-/KO}$) confirming BAP1 deficiency reduces HDAC2 expression. **C** Measurement of cell viability in MeT5A (*BAP1*$^{+/+}$) and isogenic BAP1-mutant cell lines *BAP1*$^{w-/+}$ and C3.1 (*BAP1*$^{w-/KO}$) after treatment with broad-spectrum HDAC inhibitor vorinostat at concentrations of 100, 20, 10, 5, 2, 1, 0.5 and 0.1 μM for 72h. Data are normalised to 0.1 μM treatment for each cell line. N = one experiment, error bars show SD of six technical replicates.

In summary, I set out to investigate how BAP1 may modulate the protein abundance of HDAC2. I have shown that BAP1 does not act as a DUB to protect HDAC2 from ubiquitin-mediated proteasomal degradation, nor does it regulate the stability of this protein. Instead, I found that BAP1 modulates the expression of HDAC2 protein through its regulation of HDAC2 transcript level. Importantly, reduced sensitivity to HDACi in MPM cells with stable, genetic inactivation of BAP1 was mirrored in the isogenic MeT5A cell model of BAP1 loss.

4.6 Discussion

The focus of this chapter was to identify the mechanism by which BAP1 regulates HDAC2 in MPM cells. We had previously identified BAP1 from an unbiased DUB siRNA screen in A549 cells as a candidate regulator of HDAC1 and HDAC2. I have shown that HDAC2 protein is tightly correlated with BAP1 status in a panel of MPM cell lines, and I have viewed the same relationship in an isogenic MeT5A *BAP1*-mutant cell line. Inhibiting the proteasome with epoxomicin showed a marginal increase in HDAC2 protein in *BAP1*$^{+/+}$ MSTO-211H cells, and HDAC2 protein levels were not increased following epoxomicin treatment in BAP1-depleted MSTO-211H cells, suggesting BAP1 does not protect HDAC2 from ubiquitin-mediated proteasomal degradation. Further confirming that BAP1 does not modulate the stability of HDAC2, the depletion of BAP1 levels in MSTO-211H cells did not affect the degradation rate of HDAC2 following cycloheximide treatment. Instead, BAP1 exerts its regulation of HDAC2 by modulating HDAC2 transcript abundance, as BAP1-depleted MSTO-211H cells showed significantly reduced HDAC2 transcript level compared to siC-transfected cells. Importantly, I have shown that genetic *BAP1* or *HDAC2* loss in MPM and isogenic MeT5A cells confer resistance to HDACi. Overall, I demonstrate for the first time that BAP1 modulates the expression of HDAC2, not by direct deubiquitylation but through regulation of the HDAC2 mRNA transcript level and highlight the importance of *BAP1* status in the response to HDACi.

In this study, the genetic inactivation of *BAP1* led to increased resistance to HDACi, whereas MPM cells with siRNA depletion of BAP1 were more sensitive to HDACi (Sacco et al., 2015), illustrating that transient BAP1 loss is not equivalent to genetic BAP1 inactivation in MPM cell lines that have been in long term culture. There is a valid point to be made around inferring results from cells that have undergone transient BAP1 depletion versus cellular adaptation to longer term genetic *BAP1* mutation, the former provides a very limited picture of the genetic background that may drive compensatory mechanisms in cancer. As

such, inferring clinical biomarkers from transient BAP1 depletion might give deceptive results, which is of clinical significance as HDACi such as vorinostat are currently being investigated in clinical trials for UVM in which BAP1 mutations are common (Feun, 2017). There have been poor outcomes from clinical trials of vorinostat in MPM, it was previously evaluated in the VANTAGE-014 phase III clinical trial involving 661 MPM patients with disease progression after chemotherapy, where unfortunately no improvements in overall survival resulted from vorinostat treatment (Krug et al., 2015). In light of our findings where genetic *BAP1* inactivation increased resistance to HDACi, clinical trials in MPM with HDACi might prove more successful if patient recruitment were to take into account the *BAP1* mutation status of individual tumours.

Indeed, well-defined pre-clinical models of genetic *BAP1* loss are needed for the precise screening of biomarkers and new cellular targets that may provide opportunities for synthetic lethal strategies in *BAP1*-mutated cancers such as MPM. In this respect, the isogenic MeT5A *BAP1*-mutant cell lines are a better model to look at cellular adaptation to BAP1 loss and identify drug sensitivities, as this cell model is a more accurate reflection of *BAP1*-deficient MPM than siRNA BAP1 knockdown.

When this study began, no DUBs had been identified that could reverse the ubiquitylation of HDAC2. Subsequent to my work, two studies were published identifying USP17 and USP4 as DUBs that can directly deubiquitylate HDAC2 (Song et al., 2015; Li et al., 2016b). In the former study, the authors reported reduced proteasomal degradation of HDAC2 induced by cigarette smoke extract with USP17 overexpression in airway epithelial cells. In the latter study, USP4-mediated deubiquitylation and stabilisation of HDAC2 inhibited p53 transcriptional and pro-apoptotic functions, and lead to the suppression of NF-κB transcriptional activity in HEK-293T cells. Although we didn't show that BAP1 stabilises HDAC2 protein, we have highlighted an important role for BAP1 in regulating HDAC2 transcript abundance, which may be mediated through alterations of HDAC2 transcript stability.

Mechanistically, BAP1 functions as the deubiquitylase for mono-ubiquitylated histone H2A, and it can also remove polyubiquitin chains from BARD1, BRCA1/BARD1-mediated ubiquitylated products and chromatin-associated protein HCF-1 (Scheuermann et al., 2010; Nishikawa et al., 2009; Machida et al., 2009; Misaghi et al., 2009). We have discovered that BAP1 regulates the expression of another chromatin-associated protein, HDAC2, in this

case by regulating HDAC2 mRNA transcript level. BAP1 is known to influence transcription both dependently and independently of its DUB activity (Fig. 1.3). The removal of mono-ubiquitin from histone H2A activates chromatin, allowing a more permissive environment for transcription to take place. Loss of BAP1 expression and a consequent decrease in its deubiquitylating action on histone H2A would overall reduce BAP1-dependent gene expression, which could be the case for the observed reduction in HDAC2 mRNA level upon BAP1 depletion. BAP1 can also assemble into multi-protein complexes with various transcription factors to promote gene expression (Yu et al., 2010). As such, indirect effects of BAP1 via transcription factors that govern HDAC2 transcription might play a role in this regulatory mechanism.

Another possible mechanism by which HDAC transcript levels may be regulated is through targeting by miRNAs. Transcription factors such as p53 and Myc positively or negatively regulate miRNA expression (Krol et al., 2010). Therefore, I hypothesised that specific miRNAs may be aberrantly expressed in BAP1-null MPM cell lines. If loss of BAP1 caused derepression and upregulation of miRNAs that target HDAC2, this could decrease HDAC2 transcript abundance. Indeed, miRNAs have been predicted to target HDAC2 and many of these have been validated experimentally in various disease states. HDAC2 was previously described as targeted by miR-145 in liver cancer (Noh et al., 2013) and by miR-455 in colorectal cancer (Mao et al., 2017). Recently, miR-223 has been implicated in the pathogenesis of chronic obstructive pulmonary disease (COPD) (Leuenberger et al., 2016). This is a condition characterised by airway obstruction, chronic inflammation and tissue destruction induced by risk factors such as cigarette smoke (Balkissoon et al., 2011). An observed reduction of HDAC2 protein had been previously described in the lung tissue of COPD patients (Ito et al., 2005). Leuenberger et al (2016) discovered HDAC2 mRNA is directly targeted by miR-223 in pulmonary endothelial cells, leading to a significant reduction in HDAC2 protein expression and activity. Furthermore, miR-223 is significantly induced upon exposure to inflammatory cytokines known to be upregulated in COPD patients. There are some parallels between COPD and MPM, both conditions can arise from exposure to asbestos and chronic inflammatory processes have also been identified in MPM (Hillegass et al., 2010).

Investigating the miRNA signature of cell lines with differing genetic *BAP1* status could yield important new insights into the mechanisms by which BAP1 affects cellular functions.

I will explore this avenue further in Chapters 5 and 6, by profiling the BAP1-dependent miRNome in the MeT5A BAP1-deficient isogenic cell model and the panel of MPM cell lines.

Chapter 5: Investigating the BAP1-dependent miRNome in isogenic cell models of BAP1-deficient mesothelioma

5.1 Introduction

miRNA expression profiling provides a wealth of information pertaining to the functional proteome of a cell, as variations in protein expression can be influenced by the expression profiles of one or more miRNAs that regulate them. Since 1993, when the first miRNA was identified, miRNA sequences have been rapidly reported, and there are now 28,645 entries representing hairpin pre-miRNAs in the Sanger miRBase database (http://www.mirbase.org/, version 21, June 2014). These precursors express 35,828 mature miRNA products in 23 species. For *Homo sapiens*, 1881 precursors expressing 2588 mature miRNAs have been submitted to miRBase. Despite the ever-expanding number of miRNAs, deciphering their physiological functions in humans has remained a challenge. Examining the global miRNA expression profile (miRNome) in different physiological conditions or disease states can begin to infer their regulatory roles and function. miRNA expression profiles are commonly altered in human cancers, implying that miRNA dysregulation is an important part of tumour formation, maintenance and metastasis (He et al., 2005; Baranwal and Alahari, 2010; Kuninty et al., 2016). As such, miRNA expression profiling is proving to be clinically relevant to cancer diagnosis and predicting patient outcomes (Takamizawa et al., 2004; Lu et al., 2005; Isayeva et al., 2017).

miRNAs are stable in a range of bodily fluids and specimens such as blood plasma, saliva, urine and formalin-fixed, paraffin-embedded (FFPE) tissue blocks, this has led to considerable interest in their utility as biomarkers for diagnostic and/or prognostic applications in diseases such as cancer (Weber et al., 2010; Liu and Xu, 2011). Technical efforts to improve miRNA expression profiling have produced a wide range of approaches and platforms that are currently available to investigators. Three principal platforms are commercially available for miRNA expression profiling: qRT-PCR, RNA sequencing (RNA-Seq) and hybridisation-based assays (microarrays, NanoString nCounter).

qRT-PCR involves the reverse transcription of mature miRNAs to cDNA, followed by PCR to monitor the real-time accumulation of reaction product. There are several miRNA qRT-PCR assays that are commercially available, with different approaches to priming miRNAs for reverse transcription. In qRT-PCR assays such as Qiagen's miScript PCR system and the

miRCURY™ LNA™ miRNA PCR system, mature miRNAs are polyadenylated to add poly-A tails at their 3′ end prior to cDNA synthesis. In TaqMan Assay-based qRT-PCR, a stem-loop primer adheres to the 3′ end of mature miRNAs which generates a binding site for reverse primers during cDNA synthesis (Schmittgen et al., 2008). There are many advantages to PCR-based approaches. It is a well-established methodology with high sensitivity and specificity, which is conferred during the amplification process by using a forward primer specific for the mature miRNA sequence (Chen et al., 2009). It is a quantitative method, which enables the determination of amounts of amplified cDNA (relative or absolute) in each sample. Laboratories familiar with qRT-PCR would find this approach relatively inexpensive and easy to incorporate into their workflow. A noted disadvantage of this technology are the limits to the number of samples processed per day, in this respect it can only provide medium-throughput for large-scale miRNA profiling experiments, which often involve the expression profiling for hundreds of miRNAs (Git et al., 2010).

Next generation sequencing (NGS) platforms have provided the means to profile miRNA expression by RNA-Seq. In brief, RNA-Seq involves the preparation of a cDNA library from reverse transcribed miRNA, ligation of the cDNA to adaptors with unique barcodes, followed by cDNA immobilization onto a solid-phase or beads for PCR amplification and NGS sequencing (Hafner et al., 2008). These raw sequences can then be aligned to a reference genome sequence to reconstruct which genome regions were being transcribed. This data can be used to annotate expressed gene locations and their relative expression levels. Primarily, the main NGS platforms are Illumina HiSeq 2000 (or Genome Analyser) which uses solid-phase PCR, the Applied Biosystems SOLiD system, Roche Genome Sequencer (454) and Invitrogen's Ion Torrent platform, which all use bead-based emulsion PCR (Pritchard et al., 2012). Major advantages of RNA-Seq are the detection of novel as well as known miRNA sequences, as it is not limited to the detection of selected probes on an array. This method also has greater sensitivity for identifying miRNA sequences that differ by a single nucleotide (Git et al., 2010). However, major limitations remain the high cost, together with the computing power and bioinformatics pipeline required for analysis of RNA-Seq data. Furthermore, absolute quantification of miRNA expression level using RNA-Seq is not possible, as it only provides expression level data relative to the total number of sequence reads for a given sample.

Microarrays provide an intermediate option, using a high-throughput, hybridisation-based platform capable of simultaneously profiling the expression of thousands of miRNAs within

tens of samples in parallel within a single experiment. The microarray workflow does not require reverse-transcription of miRNA into cDNA, instead miRNAs are enzymatically labelled either with a fluorophore-conjugated nucleotide, or with 3′ polyadenylation with poly-A tails followed by ligation of fluorophore-conjugated oligonucleotides. Subsequently, fluorescently-labelled miRNAs are hybridized to DNA-based probes, or beads, on the array (Pritchard et al., 2012). The technology is fairly low-cost but is typically of lower specificity than qRT-PCR or RNA-Seq (Tam et al., 2014). It is also the least quantitative method compared to qRT-PCR and RNA-Seq. Like RNAseq, microarray experiments are unable to provide absolute quantification of gene expression, so data can only be interpreted relative to another reference. Furthermore, gene expression analysis is limited to the set of probes on the microarray which have been designed against known miRNA sequences, as such this method cannot detect novel miRNAs.

The NanoString nCounter platform is an alternative hybridization based technology, based on assignment of a unique barcode, known as a reporter probe, to every gene to be profiled in the assay (Geiss et al., 2008). At its 5′ end, the reporter probe has six positions with differing spatial arrangements of four colours: red, blue, green and yellow. Capture probes, which carry biotin labels on their 3′ end, allow the tripartite complex of miRNA and reporter-/capture probes to immobilize onto the streptavidin-coated surfaces of the cartridge for data collection. The reporter and capture probes hybridize to complementary target miRNA in solution via gene-specific sequences. Each sample is imaged and processed by counting the number of times a unique barcode was detected, thus measuring the expression level of the miRNA that it corresponds to (Geiss et al., 2008).

The assay selected for this study, the NanoString nCounter human v3 miRNA assay, profiles the expression of 798 human endogenous miRNA gene probes and 30 control gene probes. The nCounter platform is comparable to a microarray with hybridization-based technology, high-throughput and no requirement for miRNA amplification by reverse transcription (Tam et al., 2014). However, the number of gene probes in an nCounter assay are typically lower than commercial microarrays, for example Agilent Genomics offers a microarray with 2,549 probes each representing a unique human miRNA. Nevertheless, we decided the nCounter platform was most suited for this study, as it provided a simple bioinformatics pipeline and was cost-effective. It also allows profiling of a greater number of samples in parallel on one cartridge, with up to 12 samples analysed per cartridge. Another advantage of the nCounter technology is its utility for profiling miRNA expression

in FFPE samples, for future translation of the discovery phase reported here. The nCounter assay provides an up-to-date list of miRNA genes from the latest version of Sanger miRBase database at the time of purchase (version 21) (Kozomara and Griffiths-Jones, 2011; Griffiths-Jones et al., 2006; Griffiths-Jones et al., 2008). However, subsets of miRNAs in this assay are included on the basis that there is published evidence to suggest they are clinically-relevant miRNAs, and that they are "high-confidence" miRNAs based on their large numbers of sequence reads from RNA-Seq data (Kozomara and Griffiths-Jones, 2014).

5.2 Aims and objectives

The abnormal expression of miRNAs has been linked to the pathogenesis and progression of various human cancers. A number of studies have profiled the miRNome of MPM, in cell lines or normal and matched tumour tissue samples (Truini et al., 2014). Germline and somatic BAP1 mutations are major drivers of MPM development, and the consequences of BAP1 loss on protein-coding gene expression in MPM are becoming well documented. However, the effect of BAP1 loss on the miRNome in MPM has yet to be elucidated.

The aim of this study was to investigate for the first time the BAP1-responsive miRNome. To this end, I profiled miRNA expression in MeT5A wildtype and isogenic *BAP1* mutant cell lines using the NanoString nCounter platform. Ultimately, the goal was to investigate BAP1-dependent changes to the miRNome in cell lines that represent models of the *BAP1* tumour predisposition syndrome and BAP1-deficient MPM. My objectives in this chapter were to:

1. Profile miRNA expression in MeT5A wildtype and isogenic MeT5A *BAP1*-mutant cell lines.
2. Identify miRNA expression changes in isogenic *BAP1*-mutant cell lines of $\geq$1.5-fold, in combination with expression changes that were statistically significant ($P \leq 0.05$). Henceforth, these miRNAs will be referred to as "significantly modulated" miRNAs.
3. Perform unsupervised hierarchical clustering and gene ontology analysis to infer functions for significantly modulated miRNAs via their predicted gene targets.

5.3 Characterising the BAP1-dependent miRNome in isogenic *BAP1*-mutant cell lines

5.3.1 Overview of NanoString nCounter human v3 miRNA assay workflow

The following workflow was implemented for miRNA expression profiling using the NanoString nCounter platform (Fig. 5.1). Total RNA was extracted from three biological extracts of MeT5A wildtype and isogenic *BAP1*-mutant cell lines. Total RNA concentration was quantified and the quality of RNA confirmed by spectrophotometry and RIN values (Table 5.1). 100 ng of total RNA from each sample was processed for nCounter miRNA expression profiling according to the manufacturer's (NanoString) recommendations.

Initial steps for data analysis involved applying a background subtraction, followed by the normalisation of raw miRNA counts. From this, I established the total number of miRNAs identified in each sample, then narrowed my focus to those miRNAs that were significantly modulated. Next, I performed unsupervised hierarchical clustering on the significantly modulated miRNA list to group similarly changing miRNAs together and annotated these distinct groups or "clusters" by gene ontology (GO), incorporating terms related to biological processes, cellular compartments and molecular functions.

5.3.2 Quality control of samples for miRNA expression analysis

The success of downstream applications like NanoString analysis rely upon having high-quality RNA. As such, the first step in the NanoString nCounter human v3 miRNA assay work-flow was determining the purity of total RNA extracted from MeT5A wildtype and isogenic *BAP1*-mutant cell lines. Total RNA, including small RNAs such as miRNAs, was extracted from cell lines as detailed in section 2.2.1.2. I generated three biological extracts of total RNA from the normal mesothelial cell line MeT5A (*BAP1*$^{+/+}$ wildtype), and the three isogenic cell lines derived from these cells: heterozygous *BAP1*$^{w-/+}$ and two BAP1 double-mutant (*BAP1*$^{w-/KO}$) cell lines C5.1 (*BAP1*$^{w-/KO}$) and C3.1 (*BAP1*$^{w-/KO}$). Initially, the purity of total RNA was determined by NanoDrop where a quality control cut-off of ≥1.80 was applied to ratios of absorbance at 260nm, 280nm and 230nm (Table 5.1). Nucleic acids absorb at 260nm, whereas the contaminating presence of protein and salts are indicated by absorbance at 280nm and 230nm, respectively. In addition, total RNA concentration and quality were further assessed using a Bioanalyser (Agilent) which generated an RNA integrity number (RIN). Samples with RIN score ≥7.0 should ensure good reproducibility and accuracy of downstream gene expression experiments, as there is high confidence of intact RNA (Schroeder et al., 2006; Fleige and Pfaffl, 2006). All samples met both QC criteria.

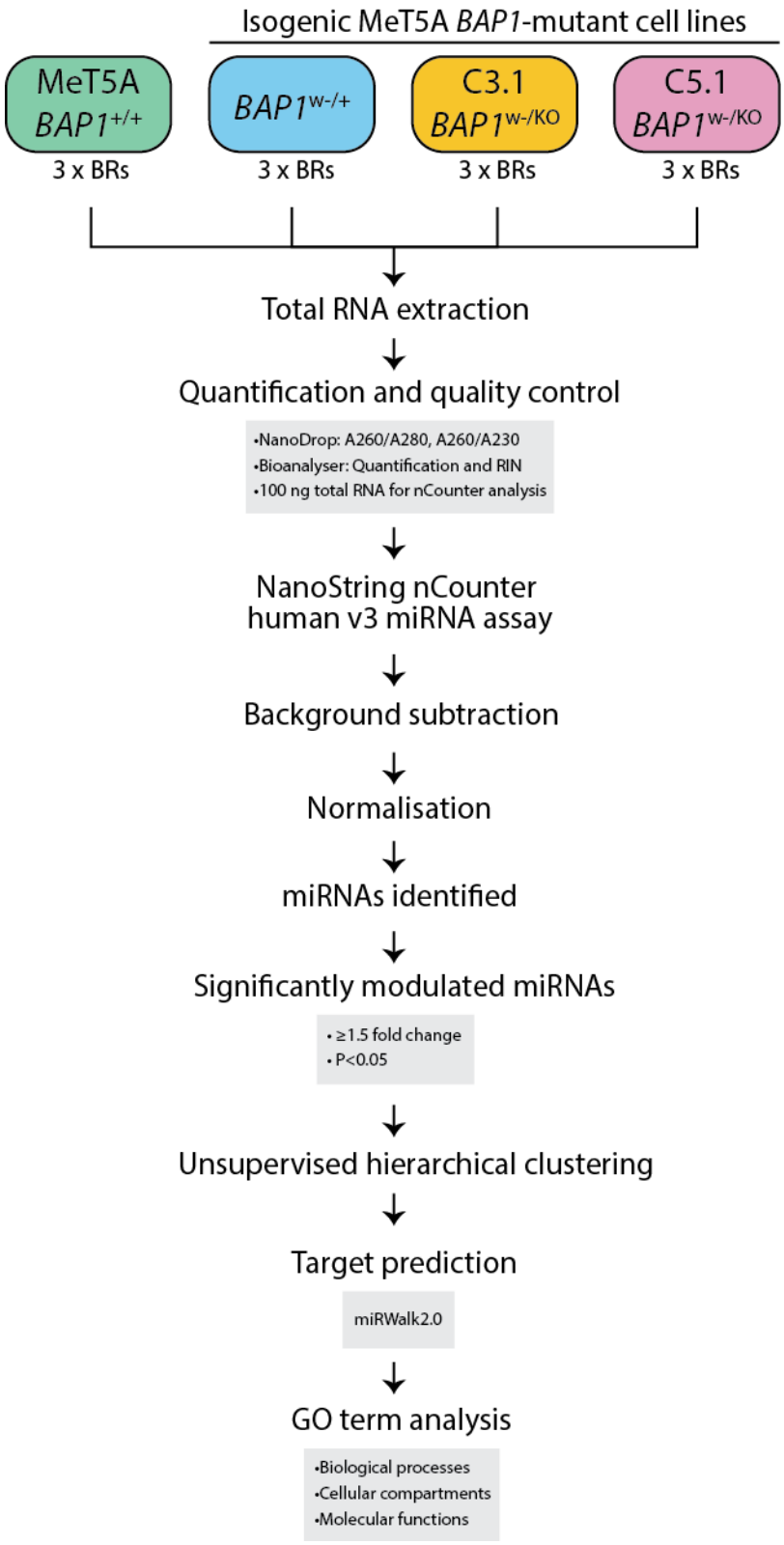

Figure 5.1: Workflow diagram showing the study design and analytical approach for the NanoString nCounter human v3 miRNA assay.

NanoString nCounter cartridge: NS1							
Sample number	Sample name	Biological replicate (BR)	Passage number	NanoDrop ratios		Conc (ng/υl)	RNA integrity number (RIN)
				A260/ A280	A260/ A230		
1	*BAP1*$^{+/+}$	BR1	P39	2.10	1.80	680.0	8.2
2	*BAP1*$^{+/+}$	BR2	P47	2.09	2.20	936.0	7.3
3	*BAP1*$^{+/+}$	BR3	P17	2.13	2.15	664.0	9.4
4	*BAP1*$^{w-/+}$	BR1	P32	2.10	2.19	381.5	9.2
5	*BAP1*$^{w-/+}$	BR2	P33	2.10	2.10	226.1	9.5
6	*BAP1*$^{w-/+}$	BR3	P34	2.11	2.16	436.0	9.3
7	C5.1(*BAP1*$^{w-/KO}$)	BR1	P57	2.16	2.21	195.7	9.2
8	C5.1(*BAP1*$^{w-/KO}$)	BR2	P59	2.10	2.27	303.2	8.7
9	C5.1(*BAP1*$^{w-/KO}$)	BR3	P60	2.15	2.62	280.0	9.0
10	C3.1(*BAP1*$^{w-/KO}$)	BR1	P37	2.06	2.00	213.9	8.1
11	C3.1(*BAP1*$^{w-/KO}$)	BR2	P38	2.10	2.09	560.0	7.6
12	C3.1(*BAP1*$^{w-/KO}$)	BR3	P33	2.12	2.21	395.5	7.6

Table 5.1: RNA sample information for MeT5A wildtype and isogenic *BAP1* mutant cell lines analysed by NanoString nCounter human v3 miRNA assay.
NS1: NanoString nCounter Experiment 1. Sample names reflect the BAP1 status of the MeT5A cell line. Passage numbers indicate the number of passages since the single cell dilution used to establish the clonal cell line. Purity of total RNA (ratios) was determined by NanoDrop spectrophotometer. Total RNA concentration and RNA integrity numbers (RIN) were confirmed by the Agilent 2100 Bioanalyser. Quality criteria of ratios ≥1.80 and RNA integrity numbers (RIN) ≥7.0 were satisfied for all samples.

5.3.3 Options for background subtraction and normalisation of nCounter miRNA expression data

The nSolver™ analysis software (NanoString) enables primary analysis of nCounter miRNA expression data. Before analysis of expression differences between sample groups, nSolver™ allows the user to apply background subtraction and to normalise raw data counts across samples; the options provided are shown in Figure 5.2. There are three methods available for background subtraction: using the negative controls in the nCounter assay (the assay includes eight negative controls that have no target as they recognise synthetic mRNA targets not present in the samples), specifying a user-defined value, or subtracting the value from a blank lane (RNA-free control) on the NanoString cartridge (Fig. 5.2A).

There are three main options which may be utilised for normalisation of background-subtracted raw data counts: positive control normalisation, normalisation to content probes, or specifying a user-defined value (Fig. 5.2B). The nCounter assay has 6 positive control probes in a 4-fold dilution series. These probes are RNA sequences of similar size to a miRNA, that are processed in the same way as miRNAs for the nCounter assay; they are ligated with sequence-specific tags and hybridised to reporter and capture probes, thus they can act as a control for the entire experimental process.

"Content Probes" can be used for normalisation in different ways (1) using the top 100 miRNA genes with the highest counts, (2) using all genes, that is the 798 endogenous miRNAs in the nCounter assay, (3) using probes corresponding to five housekeeping genes, or (4) using three ligation positive and three ligation negative control probes (Fig. 5.2B). The ligation positive control probes recognise synthetic miRNA targets included in the sample preparation, therefore monitoring ligation efficiency. The ligation negative control probes recognise targets not expected to be expressed in samples, therefore monitoring non-specific ligation.

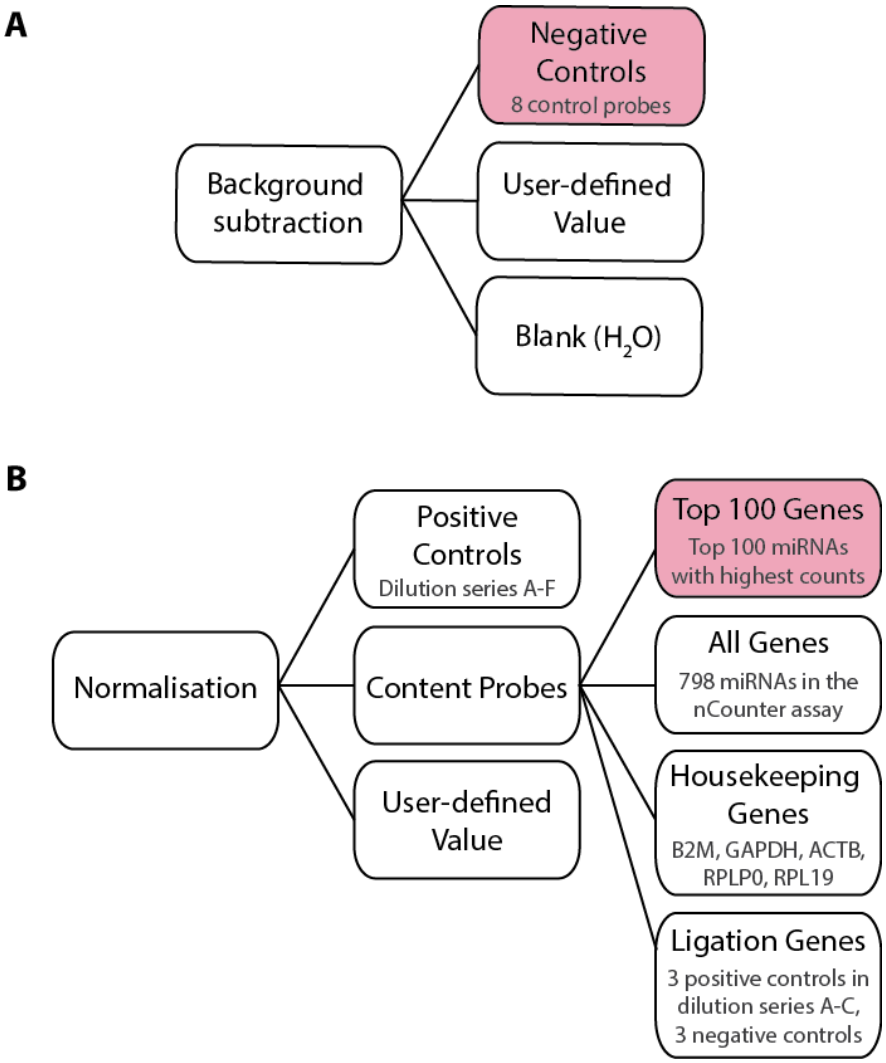

Figure 5.2: Options for background subtraction and data normalisation of NanoString nCounter human v3 miRNA assay data (NS1).
Data analysis was performed using the NanoString nSolver™ software. Alternative options for background subtraction **(A)** and normalisation **(B)** of miRNA data are available within the software. The options chosen for analysis of NS1 are highlighted in pink: the background value for raw data counts was set using the mean of negative controls, and data then normalised to the geometric mean of the top 100 gene probes, i.e. those with the highest counts in the assay.

5.3.4 Assessment of nCounter positive and negative controls

Twelve samples, comprising three biological extracts of MeT5A (*BAP1*$^{+/+}$) and each isogenic MeT5A *BAP1*-mutant cell line, were profiled for the expression of 798 miRNAs and 30 control genes using the NanoString nCounter platform. Firstly, as a quality control measure, I plotted the raw counts for all positive and negative controls included in NS1 nCounter assay (Fig. 5.3). This was performed to visualise counts, identify a value for background subtraction, and confirm linear detection of the positive controls across the 4-fold dilution series. The raw counts for control probes showed little variability across the twelve samples. As expected, the mean raw count for the positive control dilution series decreased linearly until dilution E, which has a mean raw count of 56. The counts had plateaued by dilution F, which represents the least concentrated control probe at 0.125 fM with a mean raw count of 37 (Fig. 5.3A-B). Similarly, the counts for the ligation positive controls decreased linearly across the 4-fold dilution series. The majority of the negative controls have <10 counts, the ligation negative controls also showed a similar expression profile with each control displaying <10 counts.

The eight negative controls reflect the background noise within the nCounter assay. I took the mean value (8.04) from these controls to apply as the threshold above which miRNA expression is detectable, represented by the lower orange dashed line in Figure 5.3A. Below this threshold, a large proportion of miRNAs with very low counts were removed from further analysis, ensuring only miRNAs with counts within the dynamic range (>56 counts) and those that fell within the "lower confidence" zone (8 – 56 counts) were taken forward for further analyses (Fig. 5.3).

Importantly, all positive controls display counts above the threshold for background noise, this includes the lowest input signal from probe F, which implies that the nCounter assay is still sensitive to the detection of miRNA expression at these lower counts (Fig. 5.3 and Fig. 5.4). The 5 spike-in controls are probes that recognise non-mammalian miRNAs that are not expected to be expressed in samples; they recognise miRNAs from the plant species *Arabidopsis thaliana* (ath) and *Oryza sativa* (osa), and the nematode species *Caenorhabditis elegans* (cel) (Fig. 5.3A). These spike-in controls monitor RNA processing steps upstream of the miRNA assay, such as RNA isolation/purification. Three spike-in controls, ath-miR159a, osa-miR414 and osa-miR442 showed counts above the threshold for background noise, with 40, 24 and 14 counts respectively. This could suggest some non-specific cross-species hybridisation with another sequence in the sample. However, I consistently observed

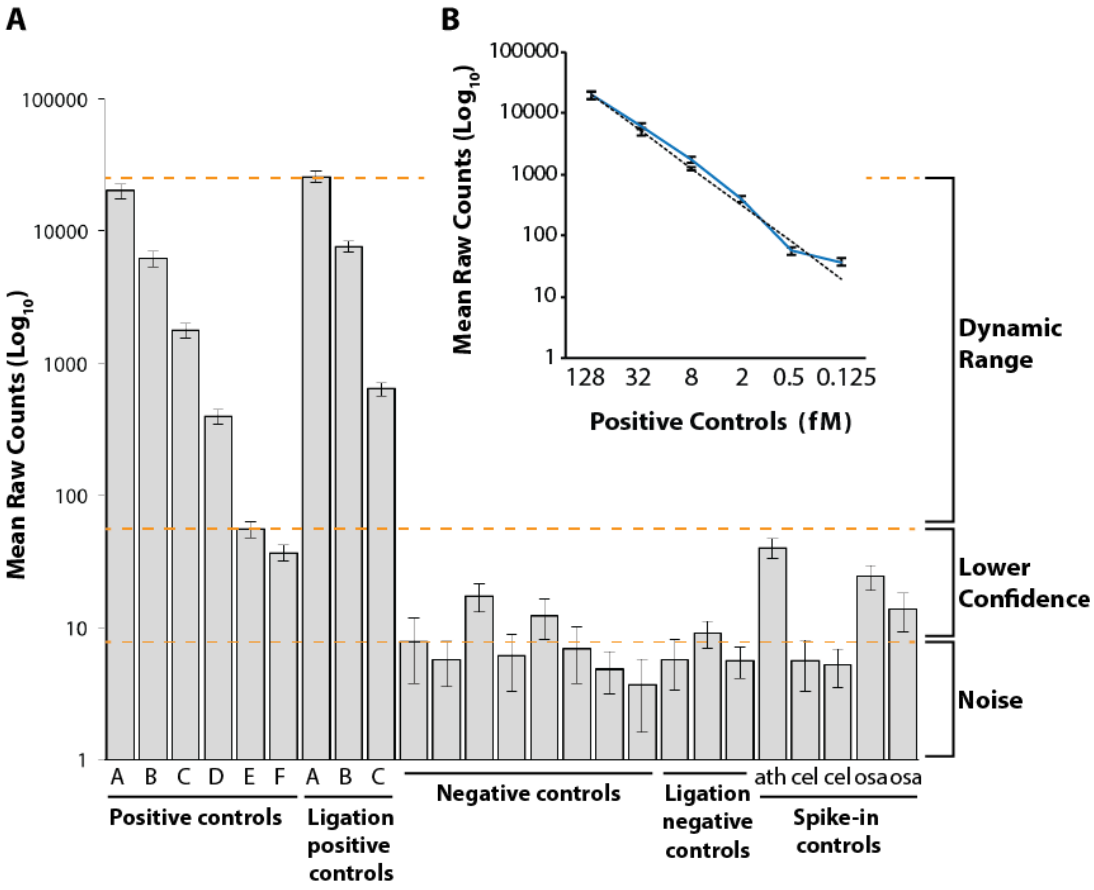

Figure 5.3: Mean raw counts for internal controls within NanoString nCounter human v3 miRNA assay (NS1).
A Bar graph shows mean raw counts for all positive and negative controls on the NS1 nCounter assay (n=12 RNA samples, error bars show SD). The positive control probes are six different RNA transcripts each at one of the following concentrations covering a 4-fold dilution series: A-F 128 fM, 32 fM, 8 fM, 2 fM, 0.5 fM, and 0.125 fM. Three ligation positive control probes are also at the following concentrations: A 128 fM, B 32 fM and C 8 fM. Eight negative controls and three ligation negative control probes have no mRNA or miRNA targets present in the samples. The spike-in controls represent exogenous, non-mammalian RNA transcripts. The orange dashed lines divide the graph into three zones: "Dynamic Range" is indicative of counts >56, "Lower Confidence" represents a range between 8 – 56 counts, and "Noise" is the observed mean raw count for eight negative control probes (8 counts), this value was used for background subtraction. **B** Plot demonstrating quantitative range for raw counts from the positive control 4-fold dilution series. The blue line shows the observed mean raw counts (n=12 samples, error bars show SD), and the black dashed line indicates the expected counts for the input amount. SD: standard deviation.

higher counts for these same three spike-in controls other nCounter assays (see Chapter 6), suggesting this is not exclusive to one particular set of samples or assay.

For each cell line analysed in NS1, the mean raw counts for the six positive and eight negative controls, and for the 798 miRNAs in the assay, were plotted to show their distribution in relation to background counts (Fig. 5.4). The positive controls for each cell line sample were above the threshold for background subtraction, and the majority of the negative controls fell below this threshold.

5.3.5 Comparison of normalisation methods for nCounter miRNA expression data

Data normalisation in miRNA experiments minimises the effect of technical variation between samples and is a pre-requisite for meaningful interpretation of miRNA expression changes. Housekeeping genes are routinely used for normalisation of mRNA data, however there is no consensus about the appropriate normalisation strategy for miRNA data (Schwarzenbach et al., 2015). Thus, I investigated the impact of five different normalisation methods (housekeeping genes, positive and negative ligation genes combined, top 100 genes with the highest counts, "all genes" and positive control genes) on intra-replicate reproducibility of miRNA expression data. Scatter plots (Fig. 5.5 and Appendix Fig. 5.1-5.4) display inter-replicate comparisons of counts for 798 miRNAs from NS1 that have been background subtracted using the mean of the negative controls and normalized using the geometric mean of the content probes for the options summarised in Fig 5.2B. The geometric mean is the *n*th root of the product of *n* numbers, and it is commonly applied to diminish the effect of very high or very low values. This was used as values can vary between 2 and 700,000 counts (NanoString) within the linear dynamic range of the nCounter assay. Since biological replicate samples should, in theory, have similar miRNA expression values, it is reasonable to compare different normalisation techniques by observing the closeness of normalised values in the replicate samples.

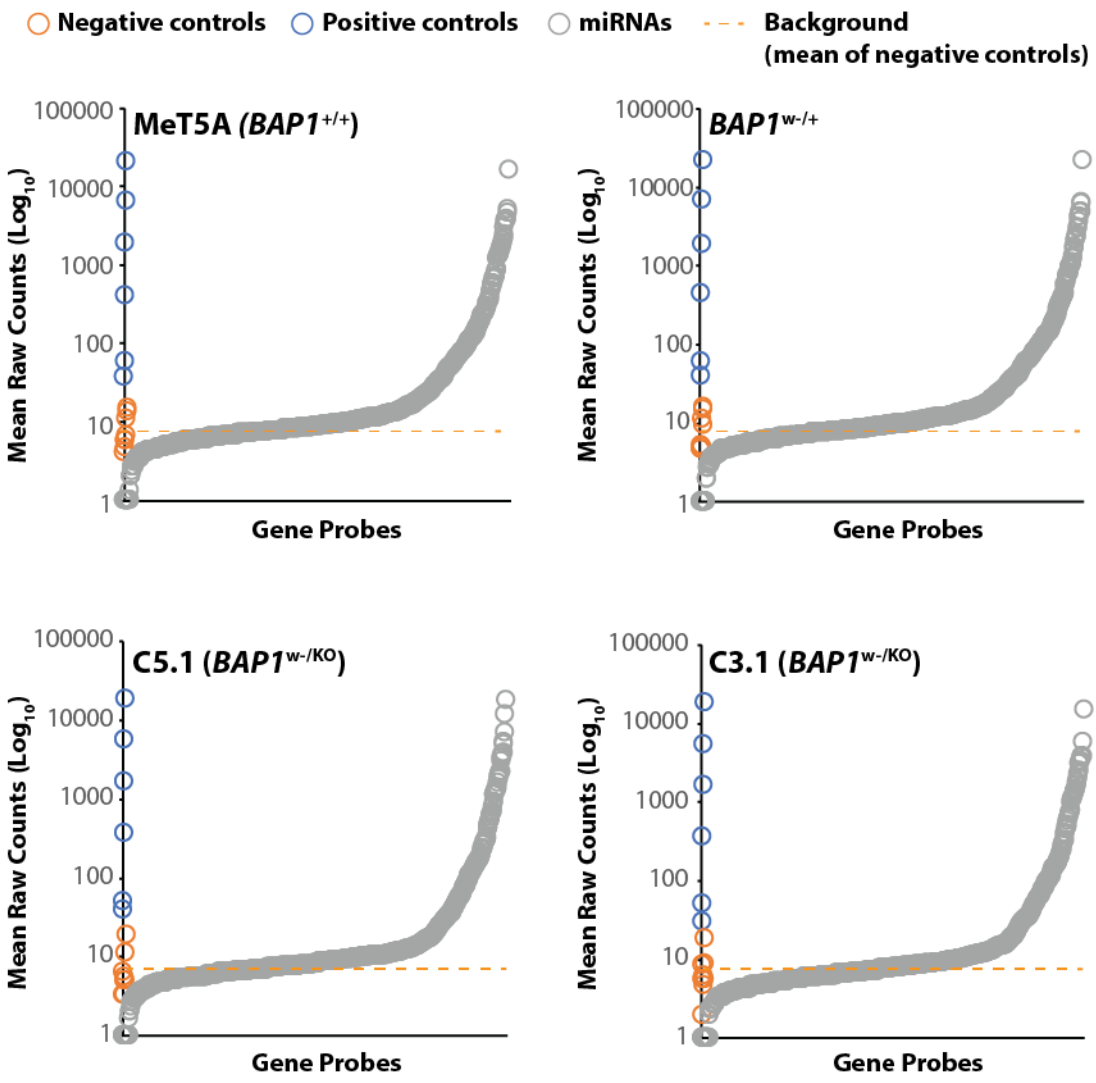

Figure 5.4: Distribution plots of raw counts for miRNAs in NS1.
Distribution plots show the mean raw counts of three biological replicates from MeT5A (*BAP1*$^{+/+}$), and three isogenic *BAP1*-mutant cell lines *BAP1*$^{w-/+}$, C5.1 (*BAP1*$^{w-/KO}$) and C3.1 (*BAP1*$^{w-/KO}$). The mean raw counts are plotted for the 798 miRNAs (grey circles), 6 positive controls (blue circles) and 8 negative controls (orange circles). The orange dashed line indicates the mean counts for negative controls (8.04 counts) to be applied as background subtraction.

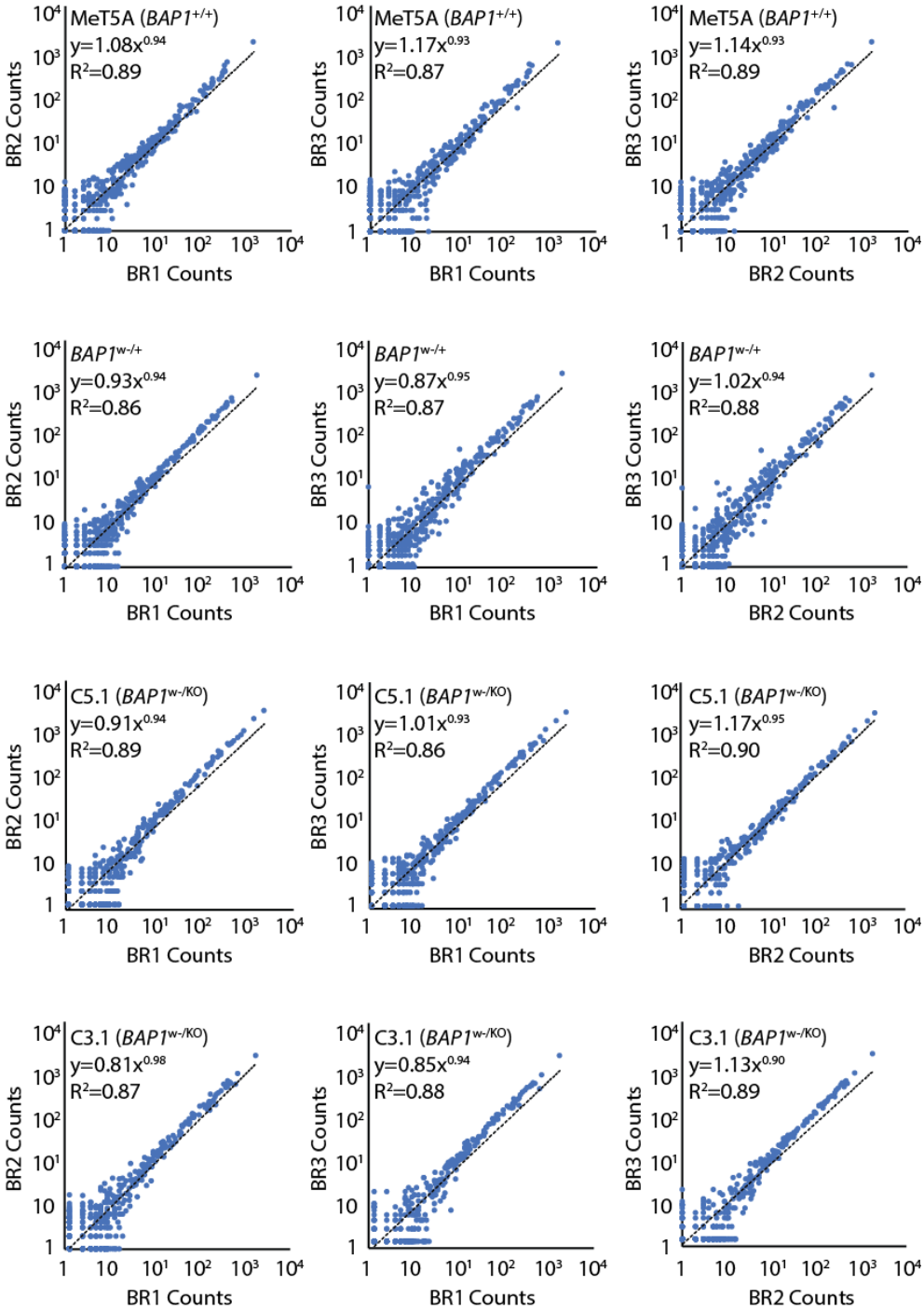

Figure 5.5: Good linear relationships between biological replicates following normalisation of miRNA expression using the top 100 genes.
Scatter plots show inter-replicate comparisons of counts for 798 miRNAs from NS1, following background subtraction and normalisation of miRNA expression to top 100 genes with the highest counts. Comparisons for cell lines MeT5A (*BAP1*$^{+/+}$) and isogenic *BAP1*-mutant cell lines *BAP1*$^{w-/+}$, C5.1 (*BAP1*$^{w-/KO}$) and C3.1 (*BAP1*$^{w-/KO}$) are shown. Power regression equation and R^2 values are displayed. BR: biological replicate.

The five normalisation methods generated values for the slope of the power trendline ranging between 0.90 - 1.05, and R^2 values between 0.86 – 0.91, indicating acceptable linear relationships between biological extracts for each normalisation method (Fig. 5.5 and Appendix Fig. 5.1-5.4). I chose to exclude the method based on the geometric mean of five housekeeping genes (B2M, GAPDH, ACTB, RPLP0, RPL19) as these are endogenous mRNA housekeeping genes more suitable for normalisation of mRNA expression data. In addition, mRNA probes do not undergo ligation and therefore are under different experimental influences. The normalisation method based on the geometric mean of combined positive and negative ligation genes was also excluded as these are exogenous gene probes that control for the initial miRNA ligation step in the nCounter assay only. The geometric mean of the top 100 genes with the highest counts was chosen as the method for normalisation of NS1 miRNA expression data (Fig 5.5). This choice was based on its ability to reduce overall variation between replicate samples as mentioned above, and on two assumptions: (1) in a large-scale miRNA expression profiling study, the number of differentially expressed miRNAs are a minority, the majority of miRNAs are either not expressed or expressed at very low levels (i.e. invariant) and (2) there is no obvious bias in the balance of downregulated miRNAs and up-regulated miRNAs (D'haene et al., 2012). Hence, the geometric mean of the top 100 gene counts can function as a reasonable indicator of the variation in expression level due to technical factors.

5.3.6 Analysis of miRNA expression in nCounter human v3 miRNA assay (NS1)

Following background subtraction and data normalisation, approximately half of the 798 miRNAs represented on the nCounter assay were identified in each cell line when combining the 3 biological replicates, this ranged from 382 – 424 miRNAs (Fig. 5.6A). The overlap between miRNAs identified in the biological replicates for each cell line was evaluated. 60% of the 382 miRNAs identified in MeT5A (*BAP1*$^{+/+}$) samples were identified in all three biological replicates. The proportion was slightly lower for BAP1 mutant cell lines *BAP1*$^{w-/+}$, C5.1 (*BAP1*$^{w-/KO}$) and C3.1 (*BAP1*$^{w-/KO}$), with 58%, 53% and 48%, respectively, identified in all three biological replicates. In each cell line, 70% to 80% of miRNAs were detected in atleast two biological replicates.

I next used a 4-way venn diagram to compare the miRNAs identified in the four different cell lines (Fig. 5.6B). The diagram illustrates the number of miRNAs that were exclusively expressed in the individual cell lines, as well as those displaying overlapping expression. A total of 566 miRNAs were detected in at least one cell line. Of these, 254 miRNAs (45%)

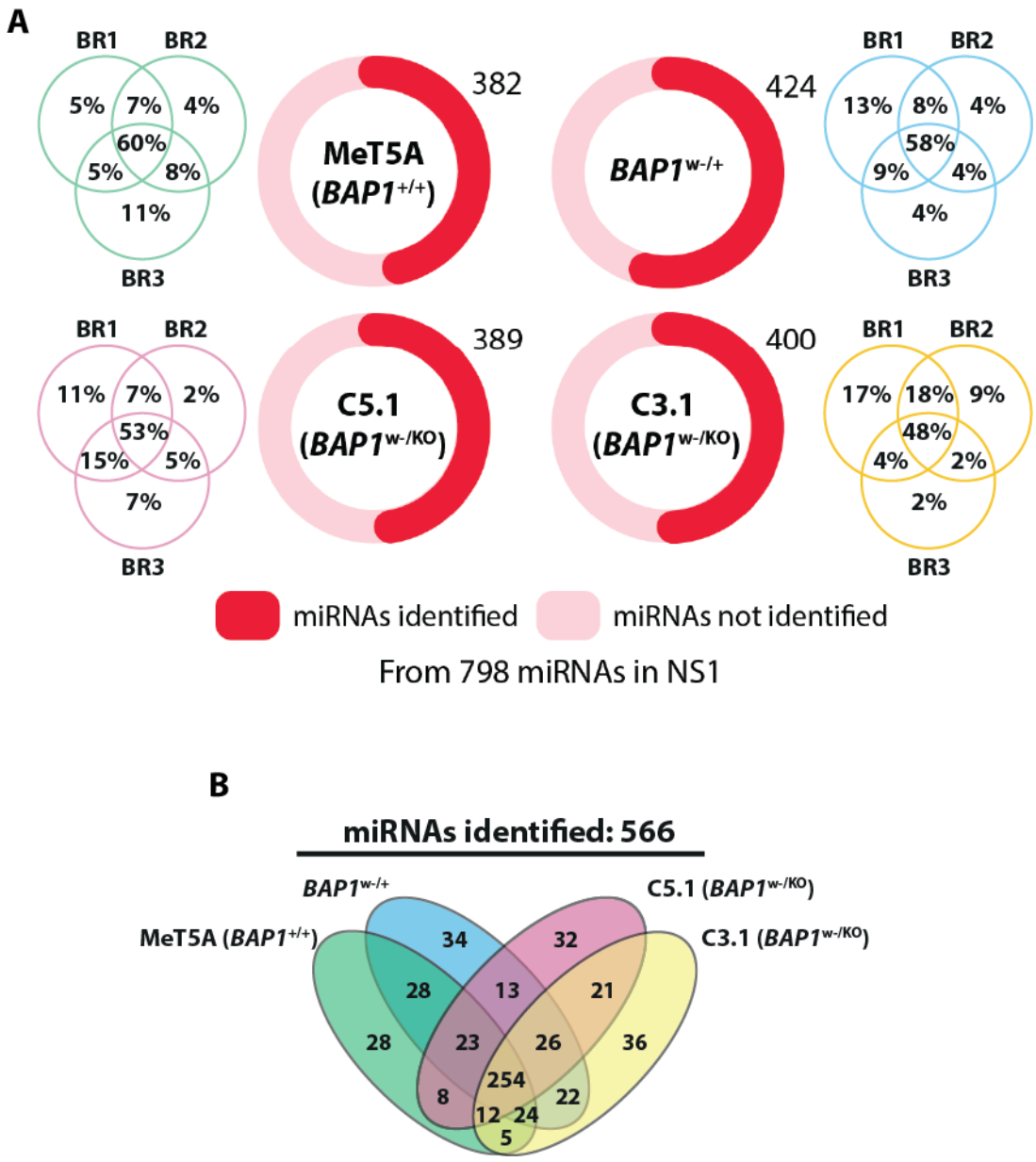

Figure 5.6: Total number of miRNAs identified in isogenic MeT5A BAP1 wildtype and mutant cell lines by the nCounter human v3 miRNA assay (NS1).
A Total number of miRNAs identified in MeT5A (*BAP1*$^{+/+}$), *BAP1*$^{w-/+}$, C5.1 (*BAP1*$^{w-/KO}$) and C3.1 (*BAP1*$^{w-/KO}$) cell lines post-background subtraction and normalisation. For every miRNA, normalised counts were averaged across three biological replicates for each cell line. miRNAs were classed as "identified" if they showed counts ≥2 after normalisation. The 3-way venn diagrams on either side show the overlap between miRNAs identified by these same criteria in each biological replicate. **B** 4-way venn diagram showing the overlap between the total number of miRNAs identified across the different cell lines.

(45%) were commonly expressed by all 4 cell lines, whilst 28, 34, 32 and 36 miRNAs were specific to MeT5A (*BAP1*$^{+/+}$), *BAP1*$^{w-/+}$, C5.1 (*BAP1*$^{w-/KO}$) and C3.1 (*BAP1*$^{w-/KO}$), respectively.

5.3.7 miRNAs are significantly deregulated in isogenic *BAP1*-mutant cell lines

To investigate whether any of the identified miRNAs were regulated by BAP1 loss, the $\log_2$(fold change) was calculated using the parental MeT5A (*BAP1*$^{+/+}$) cell line as the comparator sample. A cut-off for miRNAs exhibiting ≥1.5-fold change in expression levels was applied, in combination with expression level changes that were statistically significant by Welch's unpaired t-test (P≤0.05), which were expressed as $-\log_{10}$(P-Value) in volcano plots to visualise miRNA responses (Fig. 5.7). Setting a fold change cut-off that is large enough to be biologically meaningful for the available data set is important. ≥1.5-fold change in miRNA expression levels is understood to be biologically relevant as the NanoString assay produces one count for one miRNA molecule, which allows the estimation of gene expression and for the elimination of experimental noise. Furthermore, this study and others (Veldman-Jones et al., 2015; Mestdagh et al., 2014) have shown robust reproducibility between biological replicates with the NanoString platform, and the linearity of the internal controls within this study attests to the low degree of experimental noise variance that may otherwise confound fold change estimates.

Those miRNAs that display large magnitude fold changes as well as high statistical significance appear in the upper-left (if expression is significantly downregulated) or upper-right (if expression is significantly upregulated) quadrants of the volcano plot. Few miRNAs were significantly upregulated (solid orange circles) or downregulated (solid blue circles) in the heterozygous *BAP1*$^{w-/+}$ cell line compared to MeT5A (*BAP1*$^{+/+}$) (Fig. 5.7A). In contrast, more miRNAs were significantly up- or downregulated in the *BAP1*$^{w-/KO}$ cell lines C3.1 and C5.1 (Fig. 5.7B-C). Of note, for both *BAP1*$^{w-/KO}$ clones, significantly downregulated miRNAs showed larger magnitude changes in expression than those that were upregulated, with some miRNAs approaching a $\log_2$ 8-fold decrease. Whilst a similar number of miRNAs were significantly upregulated in the *BAP1*$^{w-/KO}$ cell lines, these showed smaller changes in expression, typically between $\log_2$ 2- and 4-fold (Fig. 5.8B-C and Appendix Table 5.1).

In total, 113 miRNAs were significantly modulated in at least one of the isogenic *BAP1* mutant cell lines, with 54 up- and 59 down-regulated relative to MeT5A (*BAP1*$^{+/+}$) (Fig. 5.8 and Appendix Table 5.2). Amongst the downregulated miRNAs, expression of 31 (57%)

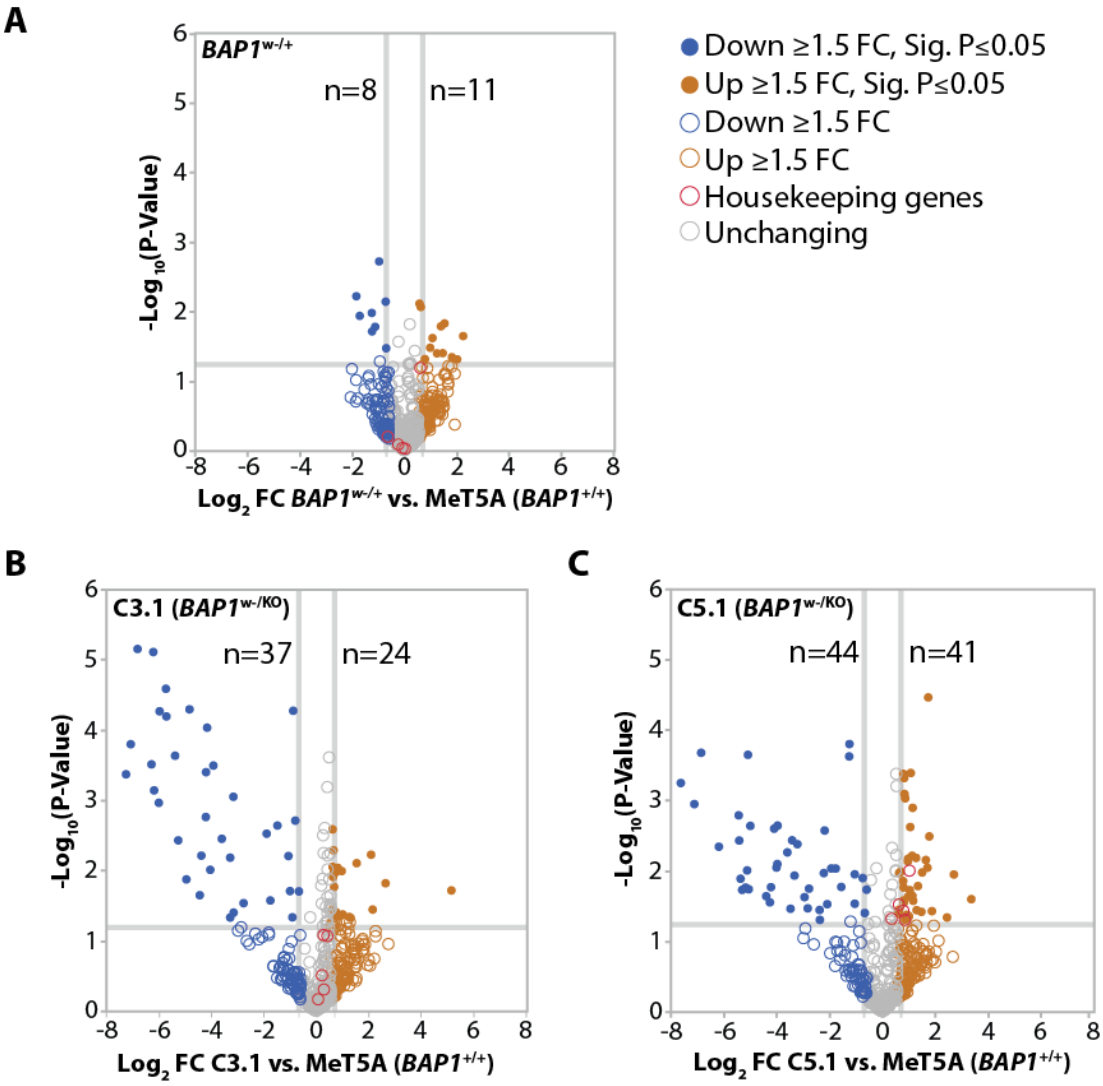

Figure 5.7: Volcano plots illustrate miRNAs that are differentially expressed between isogenic MeT5A BAP1 mutant cell lines.

Volcano plots display mean data from three biological replicates for the isogenic MeT5A BAP1 mutant cell lines *BAP1*$^{w-/+}$ **(A)**, C3.1 (*BAP1*$^{w-/KO}$) **(B)** and C5.1 (*BAP1*$^{w-/KO}$) **(C)**. The x-axis shows $\log_2$ fold change (FC) in miRNA expression vs. the comparator cell line MeT5A (*BAP1*$^{+/+}$). The y-axis is the negative $\log_{10}$ P-Value (a higher value indicating greater significance as measured by Welch's unpaired t-test). miRNAs shown as solid circles represent ≥1.5-FC in miRNA expression vs. MeT5A (*BAP1*$^{+/+}$), with statistical significance (P≤0.05), miRNAs shown with hollow circles have ≥1.5-FC in miRNA expression vs. MeT5A (*BAP1*$^{+/+}$) but have not reached significance (P>0.05). Grey circles represent miRNAs that did not meet FC and significance cut-offs and were therefore classified as unchanging. Housekeeping genes are indicated by red hollow circles. The solid grey lines designate 1.5-FC and P=0.05.

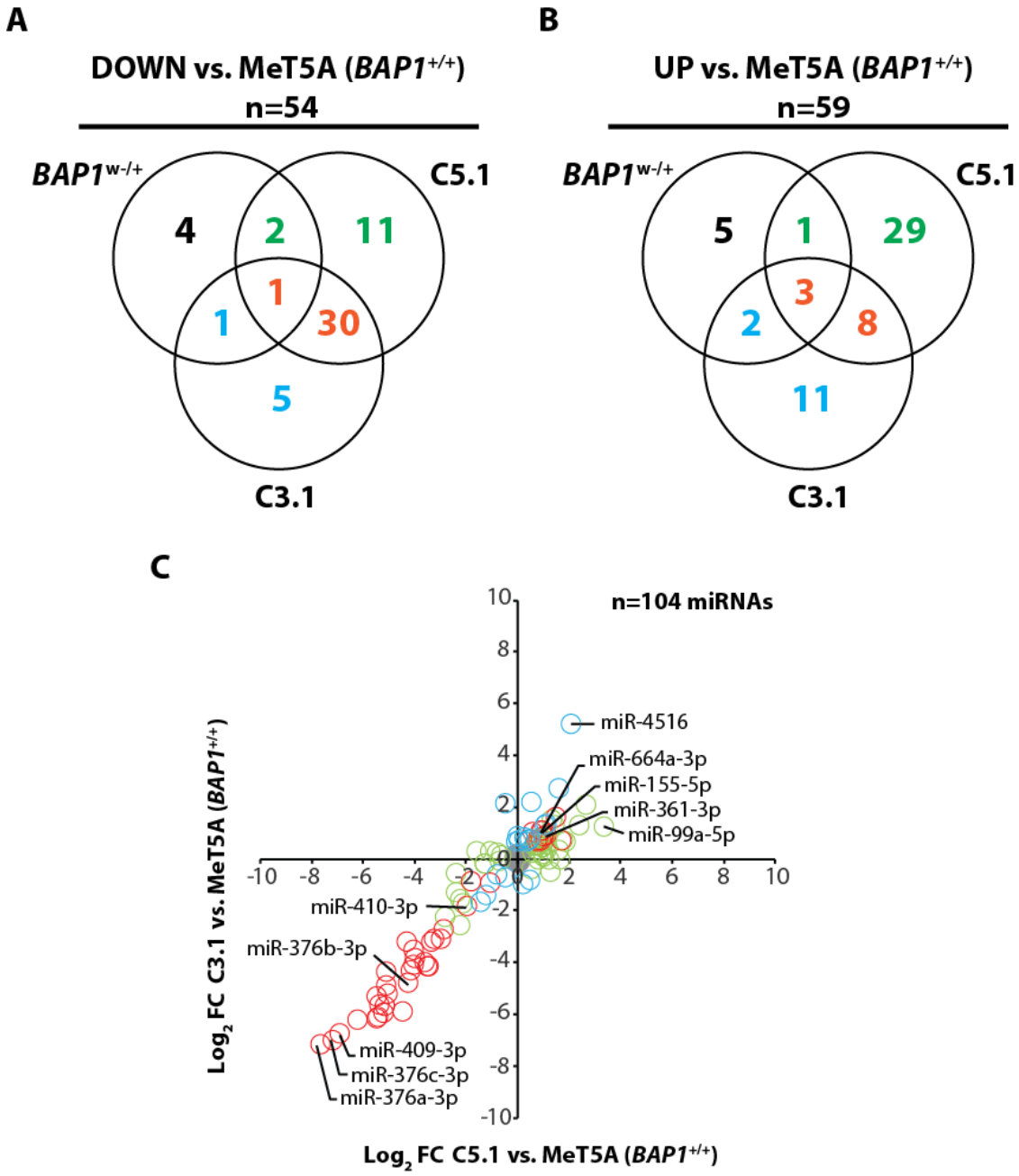

Figure 5.8: Analysis of directional changes in miRNA expression in isogenic MeT5A BAP1 mutant cell lines.

A – B Venn diagrams show the degree of overlap between significantly modulated miRNAs, with down-regulated **(A)** or up-regulated **(B)** expression changes ≥1.5-fold vs. MeT5A (*BAP1*$^{+/+}$) with statistical significance (P≤0.05, Welch's unpaired t-test), for isogenic *BAP1*-mutant cell lines *BAP1*$^{w-/+}$, C5.1(*BAP1*$^{w-/KO}$) and C3.1(*BAP1*$^{w-/KO}$). **C** Scatter plot illustrates the distribution of miRNAs that are up- or down-regulated (≥1.5-fold, P≤0.05) in C5.1 (*BAP1*$^{w-/KO}$) only (green hollow circles), or C3.1 (*BAP1*$^{w-/KO}$) only (blue hollow circles), or in both cell lines (red hollow circles). FC: fold change. Named miRNAs are discussed in section 5.4.

decreased concordantly in both *BAP1*$^{w-/KO}$ cell lines, with 13 (24%) and 6 (11%) miRNAs unique to C5.1 and C3.1, respectively (Fig. 5.8A). There were greater differences between the two *BAP1*$^{w-/KO}$ cell lines when considering the upregulated miRNAs, 30 miRNAs (51%) were significantly modulated only in C5.1, which expressed least BAP1 protein (Fig 3.4), compared to 13 miRNAs (22%) in C3.1 (Fig. 5.8B). However, when fold changes for all 104 miRNAs that were significantly modulated in either *BAP1*$^{w-/KO}$ cell line were compared, it was apparent that most miRNAs respond in a similar manner, even if the expression changes did not satisfy the fold change and significance cut-offs (Fig. 5.8C). Overall, this suggested moderately reduced BAP1 expression could cause substantial miRNA downregulation, whereas some upregulated miRNAs responded in a concentration-dependent manner to BAP1-deficiency.

5.3.8 Hierarchical clustering of significantly modulated miRNAs reveals five distinct clusters

I performed unsupervised hierarchical clustering (HCL) on the 113 significantly modulated miRNA gene list from the isogenic MeT5A samples using Multiple Experiment Viewer (MeV; http://mev.tm4.org), a freely available software that supports the analysis, visualization and stratification of large genomic data sets (Howe et al., 2010). The $\log_2$ fold change vs. MeT5A (*BAP1*$^{+/+}$) for each of the 113 miRNAs are represented in a heatmap, with unsupervised HCL for both the gene list and sample list to build a dendrogram tree of data that clusters similar groups together (Fig. 5.9, left). To aid with visualization, a colour scheme was applied so miRNAs that decreased in expression vs. MeT5A (*BAP1*$^{+/+}$) were shaded blue, and those that increased in expression were shaded orange. As expected, data for the two *BAP1*$^{w-/KO}$ cell lines cluster more closely with each other than with the *BAP1*$^{w-/+}$ cell line. HCL generated five distinct clusters of miRNAs that exhibit similar patterns of response on loss of BAP1.

Overall, two clusters (C1 and C2) generally displayed downregulated expression of miRNAs in isogenic *BAP1*$^{w-/KO}$ cells, and three clusters (C3, C4 and C5) with predominantly upregulated miRNA expression in isogenic *BAP1*$^{w-/KO}$ cells. Amongst these, cluster C4 contained a small number of miRNAs that are upregulated in all three isogenic BAP1 mutant cell lines, cluster C3 showed a large overlap in miRNAs that were upregulated in both isogenic *BAP1*$^{w-/KO}$ cell lines, and cluster C5 contained miRNAs with the largest magnitude changes in C5.1 (*BAP1*$^{w-/KO}$) cells that expresses the least amount of BAP1 protein. Cluster C2 contained a small number of miRNAs with variable expression profiles across the three isogenic BAP1 mutant cell lines, generally these miRNAs displayed

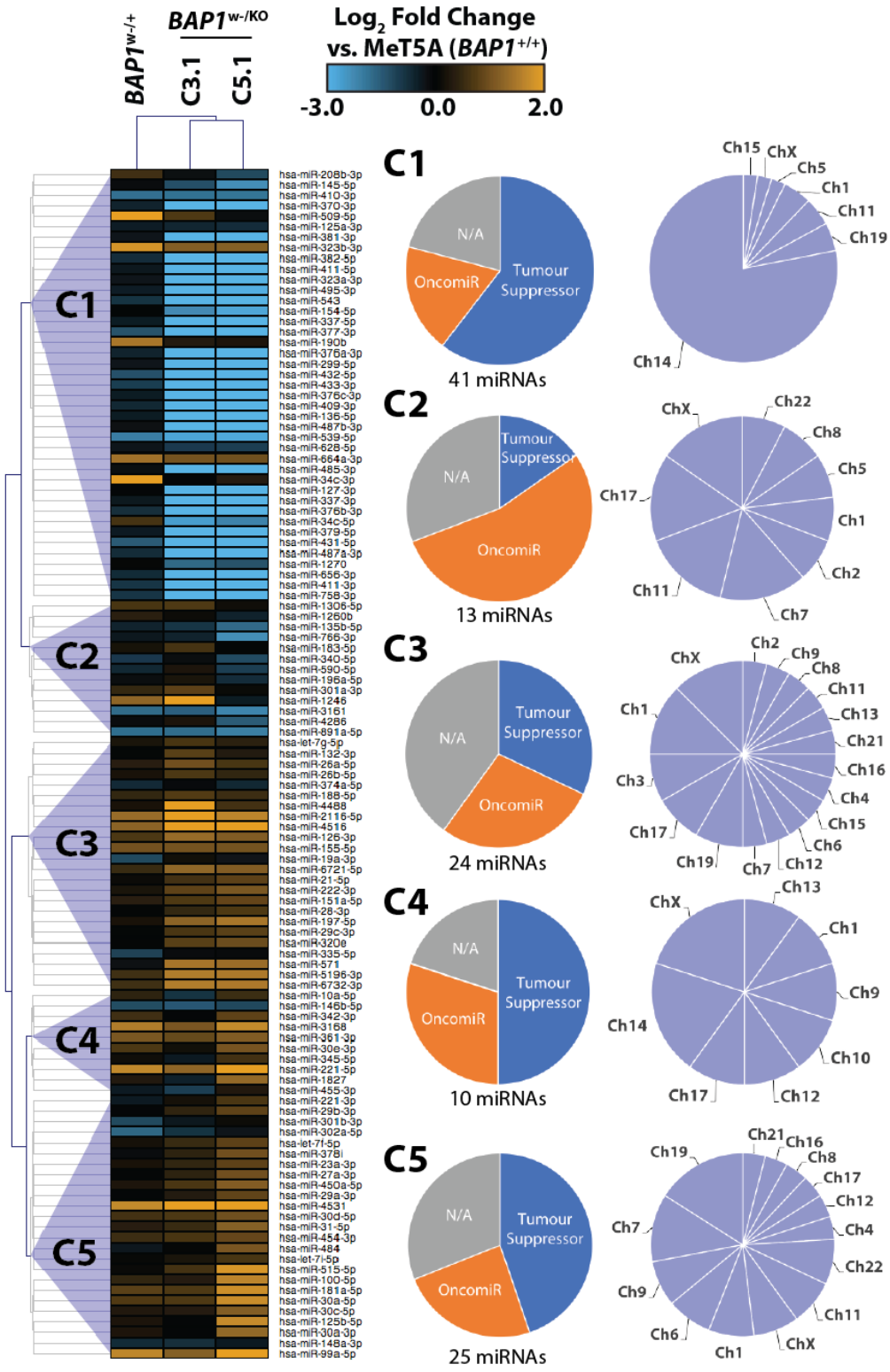

Figure 5.9: Unsupervised hierarchical clustering of 113 significantly modulated miRNAs in isogenic MeT5A BAP1 mutant cell lines.

Heat map generated using Multiple Experiment Viewer (MeV; http://mev.tm4.org) shows log_2 fold changes vs. MeT5A (*BAP1*$^{+/+}$) for miRNAs with expression changes ≥1.5-fold and statistical significance (P≤0.05, Welch's unpaired t-test). For each cluster C1 – C5, the pie charts indicate the proportion of miRNAs annotated with predominantly

oncomiR or tumour suppressive function in cancer (middle), and the chromosomal location of their genes (right). N/A: not available.

downregulated expression in C5.1 (*BAP1*$^{w-/KO}$) cells. The most striking finding from this HCL analysis was the uniform downregulation of the majority of miRNAs in cluster C1 in both the isogenic *BAP1*$^{w-/KO}$ cell lines C3.1 and C5.1; this was not phenocopied by the haploinsufficient *BAP1*$^{w-/+}$ cell line.

For each cluster C1-C5, I used a literature search to annotate whether each miRNA was predominantly described as an oncomiR, tumour suppressor miRNA, or was unstudied (N/A) in cancer (Fig. 5.9, centre). miRNAs were also annotated according to their chromosome location (Fig. 5.9, right). Strikingly, 63% of cluster C1 miRNAs have tumour suppressive function, and 78% are located on chromosome 14. In fact, these chromosome 14 miRNAs are all are located at locus ch14q32.31 (Appendix Table 5.3), with one exception (miR-208b-3p, ch14q11.2). The large bipartite cluster of 51 miRNAs on chromosome 14q32.31 is a well-studied tumour suppressive miRNA cluster that is downregulated in various cancers (Lavon et al., 2010; Shahar et al., 2016; Zehavi et al., 2012).

Cluster C2 represents a smaller group of 13 miRNAs that were mostly downregulated in C5.1 (*BAP1*$^{w-/KO}$) cells. However, the functional profiles for cluster C2 miRNAs were very different to the predominantly tumour suppressive functions of cluster C1 miRNAs; 54% of cluster C2 miRNAs were classified as oncomiRs. The remaining clusters of upregulated miRNAs also contained fewer miRNAs and showed a variable split between oncomiR and tumour suppressive functions, along with a greater spread in their chromosomal distribution (Fig 5.9).

5.3.9 Gene ontology (GO) analysis of miRNA-gene targets

The identification of genes that are targeted by miRNAs is crucial for elucidating their biological functions and interpreting the regulatory networks of miRNA-target interactions. miRWalk2.0 (http://zmf.umm.uni-heidelberg.de/apps/zmf/mirwalk2/index.html) is a database that provides predicted and experimentally validated miRNA binding sites on their target genes. Using this database, I generated a list of miRNA-target gene interactions for each HCL cluster C1-C5. These gene lists were interrogated for enrichment within gene ontology (GO) terms using the Database for Annotation,

Visualisation and Integrated Discovery (DAVID; https://david.ncifcrf.gov/). DAVID uses data-mining to functionally annotate gene lists based on different classifications such as protein domains, tissue expression and importantly gene ontology, which covers terms relating to biological process, cellular compartment and molecular function (Dennis et al., 2003). For each GO term, a P-Value is generated that indicates the strength of enrichment for the gene list within any annotation category.

I extracted a list of significant (P≤0.001) GO terms generated from the gene targets of the miRNAs from each cluster C1-C5, GO terms were retained where significant in at least one cluster, and redundant GO terms were systematically removed from the list. The P-Values were $\log_{10}$-transformed and expressed as a heat map in association with the GO term for each of the five miRNA clusters C1-C5 (Fig. 5.10). Unsupervised HCL was performed to group GO terms with similar significance (P-Value) profiles. The gene targets of cluster C1 miRNAs are highly enriched in the GO terms represented by HCL clusters *f-g*, which include several GO terms relating to known roles for BAP1, such as modulating chromatin (GO: polycomb group (PcG) protein complex) (Scheuermann et al., 2010), the regulation of metabolism (GO: response to glucose) (Bononi et al., 2017b; Baughman et al., 2016; Dai et al., 2017) (Kenyani et al., manuscript in prep) and cytoskeletal pathways (GO: cell motility, focal adhesion) (Hebert et al., 2017; Kenyani et al., manuscript in prep). In fact, GO: focal adhesion is a highly significant term across all five clusters C1-C5, suggesting that the genes enriched in this process are affected by both miRNA induction and repression in response to loss of BAP1.

The gene targets of the cluster C2 miRNAs are highly enriched in the GO terms represented by HCL clusters *a-b*. The GO terms from HCL cluster *a* are significantly enriched in clusters C2 and C5, which are most associated with changes seen in C5.1 (*BAP1*$^{w-/KO}$). The GO terms describe regulatory functions such as RNA processing and turnover, signalling in response to low oxygen, and a known BAP1 function in the cell cycle (GO: G1/S transition of mitotic cell cycle) (Ventii et al., 2008; Nishikawa et al., 2009; Machida et al., 2009). There are fewer significantly enriched GO terms in miRNA clusters C3-C4. The three GO terms significantly associated with cluster C3 (GO: somatic stem cell population maintenance, regulation of cell migration, amino acid transmembrane transporter activity) are highly distinct processes. In cluster C4 the most highly enriched GO term was GO: regulation of transcription – DNA templated.

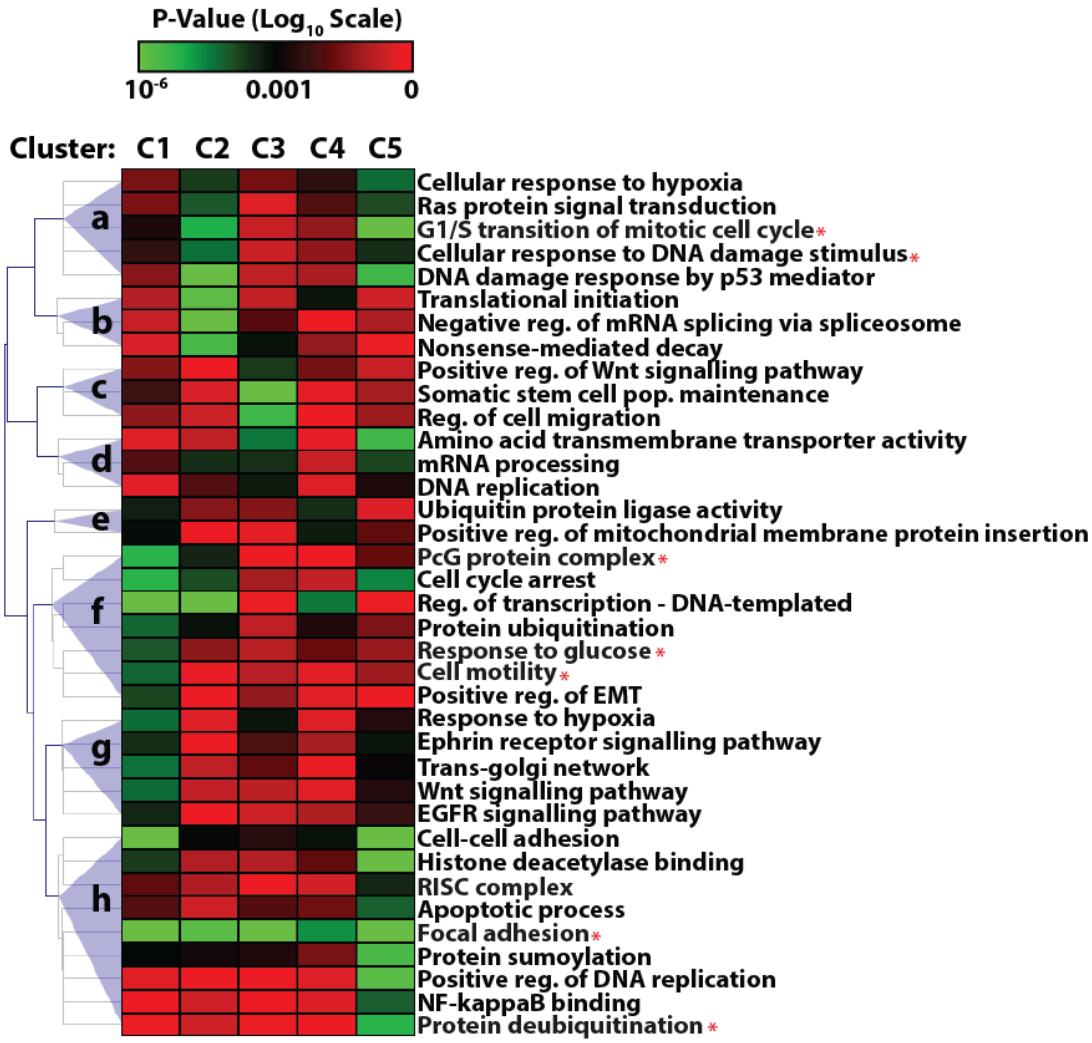

Figure 5.10: Unsupervised hierarchical clustering of significant GO terms associated with the gene targets of significantly modulated miRNAs in isogenic BAP1 mutant cell lines.
Genes encoding validated miRNA targets from hierarchical clusters C1 – C5 in isogenic BAP1 mutant cell lines were curated using miRWalk2.0 (http://zmf.umm.uni-heidelberg.de/apps/zmf/mirwalk/). Functional GO term enrichment analysis (biological process, cellular compartment and molecular function) for validated miRNA-gene targets were performed using the DAVID gene annotation tool (https://david.ncifcrf.gov/). GO terms indicated by red asterisks relate to selected published and predicted roles for BAP1. Statistical significance for the GO terms was determined by modified Fisher's exact test ($P \leq 0.001$). Colour scale limits: green indicates highly significant GO terms ($P \leq 0.001$), black indicates the significance cut-off ($P = 0.001$) and red indicates low or no significance ($P > 0.001$).

The gene targets of cluster C5 miRNAs are highly enriched in the GO terms represented by HCL clusters *a* and *h*. These GO terms describe regulatory functions such as signalling in response to low oxygen (GO: cellular response to hypoxia) and in response to effector proteins (GO: Ras protein signal transduction, NF-kappaB binding). Also described are

known BAP1 functions related to DNA repair (GO: cellular response to DNA damage stimulus (Eletr et al., 2013), DNA damage response by p53 mediator), post-translational modifications (GO: protein deubiquitylation (Jensen et al., 1998), protein sumoylation) and regulation of the cell cycle (GO: G1/S transition of mitotic cell cycle, positive regulation of DNA replication). Other highly enriched GO terms were RNA interference (GO: RISC complex), cytoskeletal pathways (GO: cell-cell adhesion, focal adhesion), programmed cell death (GO: apoptotic process) and interactions with histone deacetylases (GO: histone deacetylase binding).

These data show for the first time that the miRNome is significantly deregulated in isogenic *BAP1*-mutant cell lines, and highlight numerous pathways and processes associated with the target genes of significantly modulated miRNAs. These include many cellular pathways with which BAP1 is already associated through regulation of protein function, and notably several functions identified through analysis of the BAP1-dependent proteome (Chapter 3).

5.3.10 Network maps of the interactions between miRNAs and predicted target genes

Identifying target genes is an important step towards understanding and validating the functions of these BAP1-dependent miRNAs. To better understand the miRNA-gene target interactions I mapped the networks for a selection of GO terms of particular interest for BAP1 biology (GO: PcG protein complex, cell motility, G1/S transition of mitotic cell cycle, protein deubiquitylation, RISC complex) (Fig. 5.11 and Appendix Fig. 5.5). Initially I mapped several miRNA-gene target interactions for cluster C1 (miRNAs displaying uniform downregulation of miRNA expression in both isogenic *BAP1*$^{w-/KO}$ cell lines C5.1 and C3.1), and cluster C5 (miRNAs displaying a dose-dependent upregulation of miRNA expression in C5.1 (*BAP1*$^{w-/KO}$) cells that express the least amount of BAP1 protein).

Visually, the regulatory networks for HCL clusters C1 and C5 are different. They represent both the simplicity and complexity of miRNA network biology, as each miRNA has the potential to target one gene, represented in part by the linear networks in cluster C1 (Fig. 5.11, top), or several different genes as exemplified by the branched networks in cluster C5 (Fig. 5.11, bottom). In theory, as cluster C1 miRNA expression was predominantly downregulated by BAP1 loss, these gene targets would be predicted to show increased expression in BAP1-deficient cells. In contrast, the expression profile of cluster C5 miRNAs were predominantly upregulated on BAP1 loss, so it is predicted that their gene targets

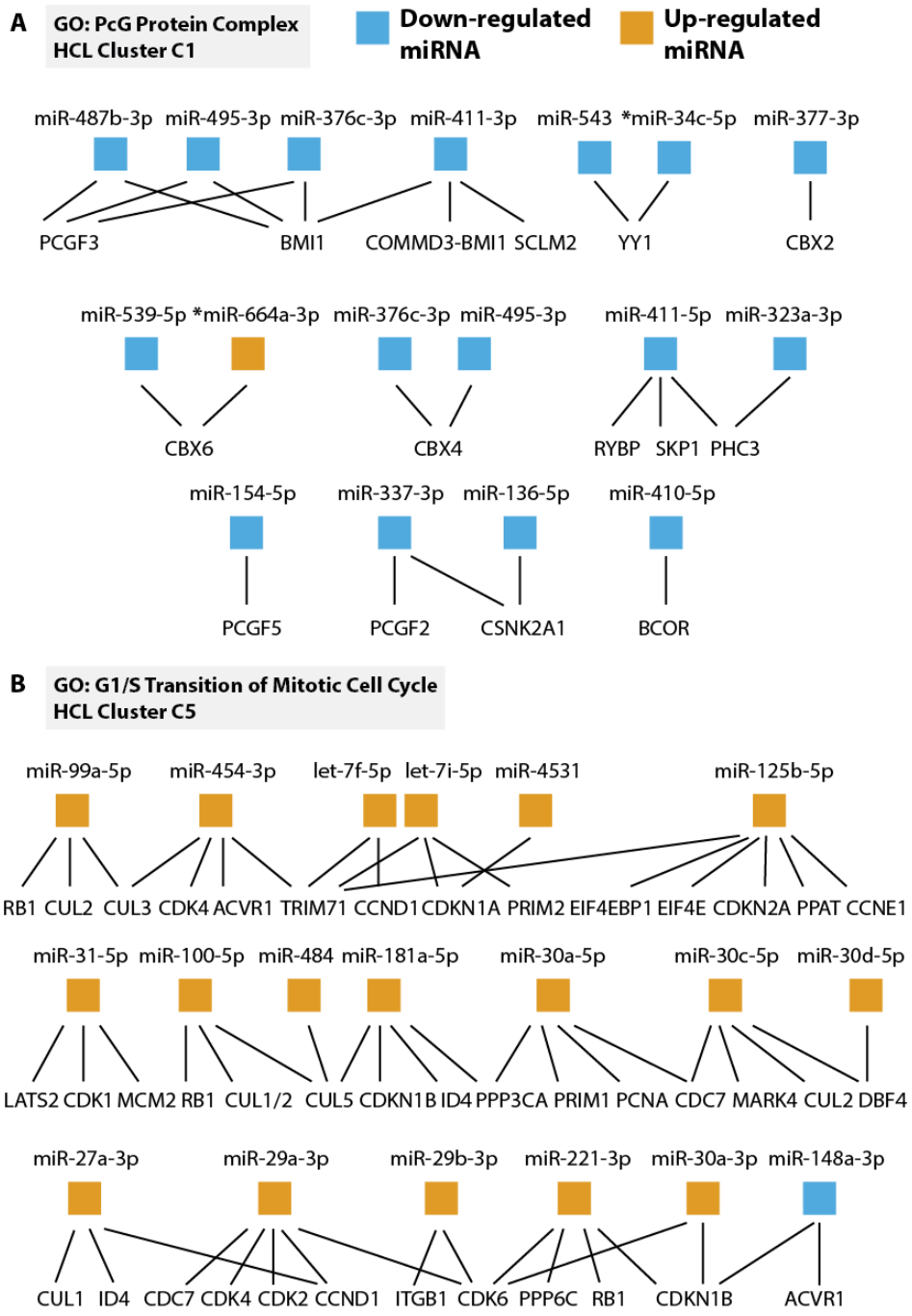

Figure 5.11: Visualisation of miRNA-gene target networks for representative GO terms.

miRNA-gene target interactions for clusters C1 and C5 were extracted from miRWalk2.0 database (http://zmf.umm.uni-heidelberg.de/apps/zmf/mirwalk2 /index.html). Network maps for gene lists enriched within significant GO terms **A** "PcG Protein Complex" and **B** "G1/S transition of mitotic cell cycle" are illustrated. The box beneath each miRNA indicates whether the miRNA was up-regulated (orange) or down-regulated (blue), in both isogenic *BAP1*$^{w-/KO}$ cell lines (cluster 1), or in C5.1 (*BAP1*$^{w-/KO}$) cells (cluster C5). *miRNAs not on ch14q32.31 locus.

would have decreased expression in BAP1-deficient cells. Together, this information can help predict and validate the physiological outcomes of miRNA expression gain or loss for the pathways and processes on which their gene targets converge.

5.4 Discussion

Following the seminal discoveries of miRNA involvement in the pathogenesis of human cancers (Calin et al., 2002; He et al., 2005), it was concluded that most tumour types will display a degree of deregulation of miRNA expression. Using the NanoString nCounter platform, I investigated the possibility of differential miRNA expression in isogenic cell models of BAP1 loss. I found that BAP1 deficiency profoundly altered the miRNome of these cell lines, which included the significant downregulation of a tumour-suppressive miRNA cluster on ch14q32.31 (Fig 5.9). Gene set enrichment analysis indicated that the reprogramming of the miRNome on loss of BAP1 could target key regulators of biological pathways involved in tumorigenesis, such as cell adhesion and migration, proliferation, cell cycle progression and hypoxic response (Fig 5.10).

Several studies have reported miRNA expression profiles in MPM cell lines and tissues (Truini et al., 2014). These reports have highlighted the influence of variables such as histological subtype, sample source (tissue/cell line), sample size, technical issues surrounding statistical analyses and the type of assay used, in generating heterogeneous and often contradictory results regarding miRNA expression in MPM. In my study, I have for the first time directly asked whether BAP1 status affects miRNA profiles by employing isogenic cell lines genetically engineered so that they differ only by the defined mutations in the *BAP1* gene. A major advantage of using this isogenic cellular model of BAP1-deficient MPM is increased confidence in attributing differential miRNA expression profiles as direct or adaptive consequences of BAP1 deficiency.

A major finding from this study was the downregulation of a set of miRNAs from a miRNA cluster mapping to chromosome 14q32 in BAP1-deficient cells (Fig. 5.9). This miRNA cluster is located within the parentally imprinted chromosomal area DLK-DIO3 (*Dlk1-Gtl2* in mouse) and spans the distal portion of chromosome 14 (14q32.1 – 14q32.31, Fig. 5.12). It is a region that holds great biological significance in the fetal development of mice and humans (Cleaton et al., 2016; Da Rocha et al., 2008). Several studies have shown downregulation of miRNAs from this region in different types of cancers, and importantly a tumour suppressive role has been recognized for these miRNAs through their gene

targets. For example, in glioblastoma, the mean expression for ch14q32.31 miRNAs were significantly lower than in matched normal tissue, and their gene targets (including KRAS and EGFR) were upregulated. Importantly, under expression of these miRNAs correlated with poorer prognosis (Shahar et al., 2016).

Importantly, in the context of my study, BAP1 deficiency alone was sufficient to downregulate these tumour suppressive ch14q32.31 miRNAs to mimic a cancer phenotype in MeT5A normal mesothelial cells. As such, these data provide new evidence for a novel mechanism by which BAP1 mutation could contribute to oncogenesis.

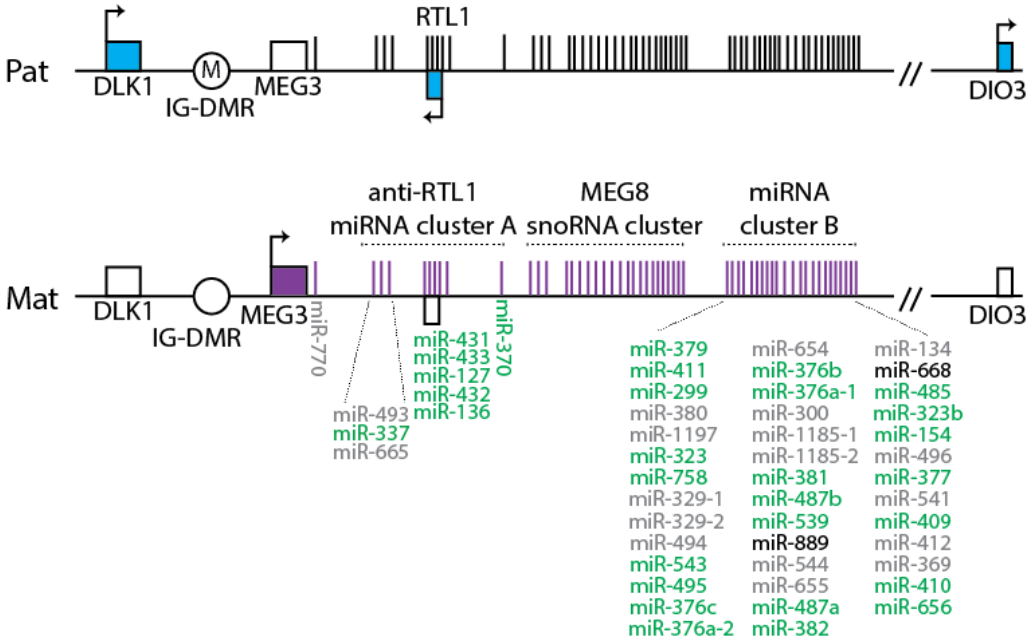

Figure 5.12: Schematic representation of the imprinted DLK1-DIO3 domain on human ch14q32.31.
Genomic organisation of the ch14q32.31 miRNAs within the imprinted DLK1-DIO3 domain. Paternally and maternally expressed genes are shown in blue and purple, respectively. The intergenic germline derived differentially methylated region (IG-DMR) is methylated on the paternal chromosome, denoted by the letter M. The maternally expressed non-coding RNA genes (purple) include maternally expressed gene 3 (MEG3), anti-RTL1 (encodes the smaller miRNA cluster A), maternally expressed gene 8 (MEG8) (encodes small nucleolar RNA (snoRNA) cluster) and the larger miRNA cluster B. miRNAs in green font were identified in this study in HCL cluster C1, these miRNAs showed significantly downregulated expression in isogenic MeT5A *BAP1*-mutant cells. miRNAs in grey were detected but did not meet the fold change and significance cut-offs. miRNAs in black were not detected by the assay. Figure adapted from (Royo and Cavaille, 2008).

The regulation of genomic imprinting in this chromosomal locus is thought to be mediated by a distal element on this locus known as the intergenic differentially methylated region (IG-DMR, Fig. 5.12). In mice, deletion of the hypomethylated form of IG-DMR from the maternal inherited chromosome resulted in the silencing of all maternally expressed imprinted genes from this region, coding for both mRNAs and miRNAs (Seitz et al., 2004). It is hypothesized that the silencing of ch14q32.31 miRNA genes could occur through either chromosomal deletion of IG-DMR, epigenetic modification at this locus by methylation or deacetylation, or both. Indeed, both mechanisms could explain ch14q32.31 miRNA cluster silencing in melanoma cell lines (Zehavi et al., 2012). The study documented loss of heterozygosity and/or complete absence of the IG-DMR, as well as epigenetic silencing of this locus as maternal miRNA genes were re-expressed after treatment with a combination of demethylating and HDAC inhibitors. In epithelial ovarian cancer cell lines, the authors concluded that epigenetic mechanisms were responsible for the downregulation of several miRNAs from this cluster on chromosome 14, as treatment with DNA demethylating agent 5-aza-2'-deoxycytidine (5-Aza-CdR) and the HDAC inhibitor 4-phenylbutyric acid (PBA) upregulated their expression (Zhang et al., 2008). It would be important in future to perform similar analyses in the isogenic MeT5A *BAP1*-mutant cells to establish DNA copy number of the regulatory regions and/or the presence of epigenetic modifications at this locus, to elucidate the mechanism by which this miRNA cluster is silenced by BAP1-deficiency.

Gene ontology analysis can provide an indication of the biological processes affected by the silencing of the miRNA cluster on ch14q32.31. For the cluster C1 miRNAs that map to ch14q32.31, the predicted gene targets were highly associated with biological processes implicated in human carcinogenesis, namely chromatin modulation, cellular metabolism and cell motility (Fig. 5.10). miR-410-3p is a ch14q32.31 miRNA that is significantly downregulated in all isogenic *BAP1*-mutant cell lines, *BAP1*$^{w-/+}$, C5.1 (*BAP1*$^{w-/KO}$) and C3.1 (*BAP1*$^{w-/KO}$) when compared to MeT5A wildtype (*BAP1*$^{+/+}$) cells (Fig. 5.8C). Various cancer types also show a trend for downregulation of this miRNA; miR-410-3p-mediated suppression of cell proliferation and invasion was reported in gliomas (Chen et al., 2012), gastric cancer (Shen et al., 2014) and pancreatic cancer (Guo et al., 2015b). It has been previously shown by qRT-PCR, and within an independent gene expression profiling data set from TCGA, that miR-410-3p expression is downregulated in breast cancer tissues compared to paired normal breast tissue (Zhang et al., 2016). Moreover, miR-410-3p has a tumour-suppressive role in breast cancer through its regulation of cell proliferation and the

EMT phenotype, miR-410-3p overexpression reduced cell growth, invasion, and decreased the expression of EMT markers (Wang et al., 2013). Analysis of the C5.1 (*BAP1*$^{w-/KO}$) cell proteome by SILAC-MS revealed a significant upregulation of proteins involved in actin cytoskeletal regulatory pathways, which have been associated with local invasion and the EMT process (see section 3.8), it may be possible that the upregulation of cancer-associated proteins involved in cytoskeletal reorganisation and invasion upon BAP1 loss is a consequence of the loss of expression and thus regulation by miRNAs such as miR-410-3p.

The miRNAs represented in the example of an HCL Cluster C1 regulatory network (Fig. 5.11, top) are predominantly located on locus ch14q32.31, with two exceptions (miR-34c-5p (Ch11q23) and miR-664a-3p (Ch1q41). In this network, the protein products of the PcG genes targeted by ch14q32.31 miRNAs form the core components of the canonical and non-canonical PRC1 complex (Fig. 5.13). Therefore, not only is the PRC1 complex regulated through the opposing action of BAP1 in the PR-DUB complex, it would seem that the homeostatic balance between chromatin activation and silencing is further modulated by BAP1-dependent miRNAs that can repress the expression of PcG genes. The consequences of ch14q32.31 downregulation is predicted to increase transcriptional repression through increased PRC1 activity, which has implications for tumourigenesis as PRC1 may promote cancer progression by repressing tumour suppressors.

From the list of 30 significantly modulated miRNAs that were uniformly downregulated in *BAP1*$^{w-/KO}$ cell lines C5.1 and C3.1 (Fig. 5.8A and Appendix Table 5.1), ch14q32.31 miRNAs miR-376a-3p, miR-376c-3p and miR-409-3p had the greatest response, showing ~7-fold decrease in expression compared to MeT5A wildtype (*BAP1*$^{+/+}$) (Fig. 5.8C and Appendix Table 5.1). Expression profiling studies have revealed that the miR-376 family, namely miR-376a, miR-376b and miR-376c, show either decreased or increased expression in a range of different types of cancers, indicating the context-dependency of their function as either a tumour suppressors or oncomiRs (Tekirdag et al., 2016). Although downregulation of miR-409-3p has been observed in many cancers (Zheng et al., 2012; Xu et al., 2013; Liu et al., 2015), its role may be disease-dependent, as it is upregulated in prostate cancer where it promotes tumourigenesis through suppression of tumour suppressor genes and induction of EMT (Josson et al., 2015).

At the other end of the spectrum, three miRNAs miR-664a-3p, miR-361-3p and miR-155-5p were significantly upregulated in each of the three isogenic *BAP1*-mutant cell lines, *BAP1*$^{w-/+}$, C5.1 (*BAP1*$^{w-/KO}$) and C3.1 (*BAP1*$^{w-/KO}$), when compared to MeT5A wildtype (*BAP1*$^{+/+}$)

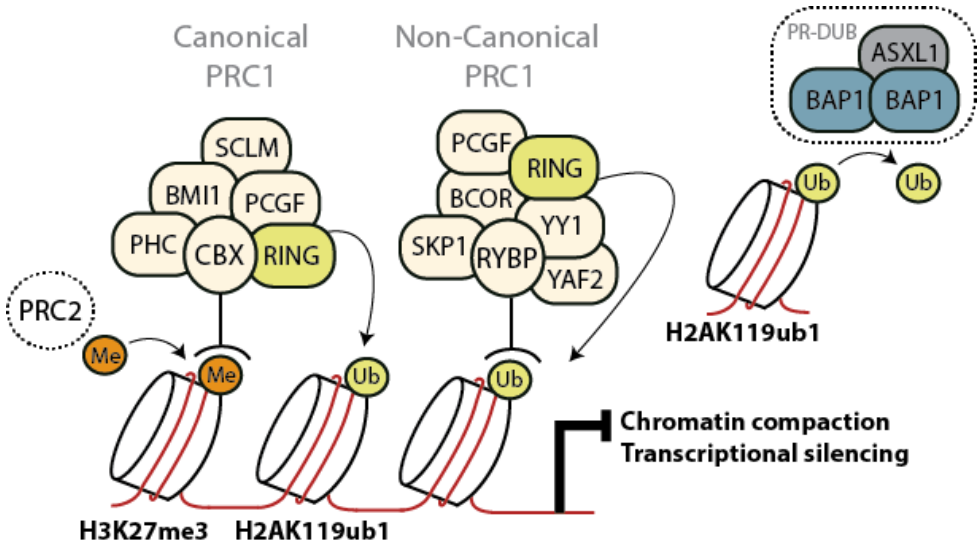

Figure 5.13: A simplified model of polycomb repressive complex 1 (PRC1)-mediated chromatin compaction and gene silencing.
The PRC1 is divided into two subfamilies of canonical (c-PRC1) and non-canonical PRC1 (nc-PRC1). The canonical PRC1 is composed of a RING and PCGF/BMI1 core, and several accessory proteins CBX, PHC and SCLM, each of which have multiple different homologs. The PRC2 complex trimethylates histone H3 at lysine 27 (H3K27me3), CBX proteins are able to recognise and bind to these marks thereby recruiting the c-PRC1 complex and facilitating chromatin repression through the monoubiquitylation of histone H2A at lysine 119 (H2AK119Ub1). The RYBP component of the nc-PRC1 complex can further contribute to transcriptional silencing by recognizing H2AK119ub1 marks. YY1, a DNA binding protein, may also recruit the nc-PRC1 complex to histones via interaction with RYBP and YAF2. The deubiquitylase activity of the polycomb repressive deubiquitylase (PR-DUB) complex opposes PRC1 and de-represses gene silencing caused by histone H2A monoubiquitylation. Figure adapted from (Aranda et al., 2015).

(Fig. 5.8B and Appendix Table 5.1). To date, no study has been published detailing the expression level of miR-664a-3p in cancers. Little is known about miR-361-3p but it has been shown to have decreased expression in NSCLC tissues and cell lines, and is reported to function as a tumour suppressor in this cancer type (Chen et al., 2016).

In contrast, miR-155-5p is well documented as an oncomiR (Jiang et al., 2010b; Gironella et al., 2007) and as a pro-inflammatory miRNA shown to play a critical role in promoting aerobic glycolysis (i.e. the Warburg effect) in breast cancer cells (Jiang et al., 2012). Hexokinases are enzymes that catalyse the first step of glucose metabolism, namely the phosphorylation of glucose to glucose-6-phosphate (G6P) (see Fig. 3.6), which then serves as a metabolite for glycolysis, the PPP and glycogenesis (Roberts and Miyamoto, 2015). In

breast cancer cells exposed to pro-inflammatory cytokines, miR-155-5p appears to promote aerobic glycolysis by upregulating hexokinase 2 (HK2) expression through two distinct mechanisms. First, it promotes HK2 expression by activating its transcriptional regulator STAT3 indirectly through downregulation of a STAT3 inhibitor. Second, miR-155-5p represses expression of miR-143, a negative regulator of HK2, thereby promoting HK2 expression at the post-transcriptional level (Jiang et al., 2012). However, in the context of my work, SILAC-MS analysis of the C5.1 (*BAP1*$^{w-/KO}$) cells showed downregulation of HK2 compared with MeT5A (*BAP1*$^{+/+}$), but upregulated expression of the HK1 isoform (Fig. 3.6). In addition, I observed no significant change in miR-143 expression in C5.1 (*BAP1*$^{w-/KO}$) cells compared with MeT5A (*BAP1*$^{+/+}$). Ultimately, the increased expression of miR-155-5p and its positive regulation of HK2 could be tumour context-specific or restricted to an inflammatory response, which is absent in C5.1 (*BAP1*$^{w-/KO}$) cells.

Looking at the cell lines individually, miR-509-5p, miR-99a-5p and miR-4516 had the greatest response in *BAP1*$^{w-/+}$, C5.1 (*BAP1*$^{w-/KO}$) and C3.1 (*BAP1*$^{w-/KO}$) cell lines, respectively (Fig. 5.8C and Appendix Table 5.1). These miRNAs were significantly upregulated between 2- to 5-fold in their respective cell line, relative to MeT5A wildtype (*BAP1*$^{+/+}$). These responses could be clonal artefacts or dose-dependent responses to loss of BAP1. Little is known about the functions of miR-4516 in cancer. A study evaluating the miRNA profiles of thyroid tumours has shown significantly different expression of miRNAs including miR-4516 between follicular adenomas and follicular variant of papillary thyroid carcinomas, with increased expression of miR-4516 in the latter (Borrelli et al., 2017). In several cancers miR-509-5p and miR-99a-5p behave as tumour suppressive miRNAs, being markedly downregulated in cancer cell lines or tissues, and when overexpressed inhibit cancer cell proliferation, migration and invasion (Li et al., 2017; Song et al., 2017; Wang et al., 2017; Shi et al., 2017).

Similarly, miR-509-5p functions as a tumour suppressive miRNA in the pancreatic ductal adenocarcinoma cell line Panc1 (Hiramoto et al., 2017), where combined overexpression of miR-509-5p and miR-1243 suppressed EMT-related gene expression and induced a mesenchymal-to-epithelial phenotype. Interestingly, the sensitivity of Panc1 cells to gemcitabine was enhanced by combined overexpression of both miRNAs. In my study, mutation of a single *BAP1* allele in MeT5A *BAP1*$^{w-/+}$ cells increased expression of miR-509-5p, a miRNA linked with sensitivity to gemcitabine, an anti-cancer drug used as a second-line treatment for MPM (van Meerbeeck et al., 1999). This may present an opportunity to

investigate whether BAP1-deficiency and associated miR-509-5p overexpression in MPM enhance gemcitabine sensitivity, and whether miR-509-5p levels could be used to stratify MPM patients for treatment with specific therapeutics. Unfortunately, gene probes for miR-1243 were not included in the nCounter assay, but its expression could be investigated by qRT-PCR. The lack of data for miR-1243 highlights the fact that biologically relevant miRNAs may be absent from the Nanostring dataset. Given the success of this initial exploratory study, it may be of interest in future to broaden miRNA analysis in this cell model using an RNAseq platform, and perhaps to also profile lncRNAs.

Although gene ontology analysis allows the biological interpretation of differential gene expression, it is important to note that these interpretations are prediction-based and thus require experimental validation. In the absence of experimental validation, extensive simulation of datasets by Monte-Carlo simulation, where in this case random combinations of miRNA genes and samples are generated, is one method to assess the extent to which gene expression profiles may occur by chance (Ogundijo and Wang, 2017).

In summary, I have shown for the first time that targeted mutation of endogenous BAP1 can significantly alter the miRNome, in MeT5A mesothelial cell lines representing the BAP1 cancer predisposition syndrome (*BAP1*$^{w-/+}$) and BAP1-deficient (*BAP1*$^{w-/KO}$) MPM. Through identifying significantly modulated miRNAs and performing enrichment analysis on their gene targets, I was able to predict cellular processes that may be altered through modulated miRNA expression following loss of BAP1. Alterations in the BAP1-dependent miRNome may contribute to dysregulation the cell cycle, DNA damage response, chromatin modulation and cell motility. I have also shown that the pattern of miRNA expression from ch14q32.31 locus is highly deregulated in BAP1 mutated MeT5A cells, as reported in various tumour types. In chapter 6, I will reiterate the strategy adopted in chapter 3 (see section 3.3), whereby I will investigate the expression and the relevance of the isogenic MeT5A miRNome in patient-derived MPM cell lines with differing BAP1 protein expression. I will also investigate the coordinated expression of BAP1 and ch14q32.31 miRNAs and validate expression changes by qRT-PCR for selected miRNAs from this locus.

Chapter 6: Expanding investigation of the BAP1-dependent miRNome into patient-derived MPM cell lines

6.1 Introduction

Compared with normal cells, cancer cells have undergone an array of genetic and epigenetic modifications that often underlie neoplastic growth, metastasis and drug resistance. Therefore, the usefulness of cancer cell lines as a model system of disease relies on their ability to recapitulate the genomic changes observed in primary tumours from patients. For the purposes of this thesis, I am interested in investigating BAP1-dependencies in MPM. Therefore, the generation of isogenic cell lines was crucial for this research as these cells are genetically identical to their parental cell line except for engineered mutations in BAP1 that are clinically relevant to the tumorigenesis of MPM. For the study in chapter 5, these isogenic cell lines provided a precise model in which to investigate the effect of BAP1 loss on the miRNome, on a mesothelial cell background, from which neoplastic transformation to MPM ensues.

The generation of isogenic cell lines with specific genes inactivated enables target validation and functional studies to be performed far more effectively and with greater confidence in the responses that are produced. Nevertheless, it is important that a sufficient number of cell lines are used to give adequate power to the detection of a particular subset of responses, and that these are shown to be representative over the range of genetic backgrounds for the cancer that is being studied. In this chapter, I have therefore utilised a panel of 20 patient-derived MPM cell lines to broaden knowledge of the miRNA expression profile in MPM (described in section 1.4.5) and to validate the findings from the isogenic MeT5A mesothelial cells described in chapter 5. For these MPM cell lines, BAP1 expression status and *in vitro* catalytic activity are known, so they can be stratified into BAP1-positive or BAP1-negative groups (see Figure 3.8). As is the nature of cell lines established from primary tumours, these cell lines will have varied genetic backgrounds and represent the different histological types of MPM. Whilst this heterogeneity makes miRNA profiles more difficult to interpret in the context of BAP1, together with data from the isogenic *BAP1*-mutated cells, the MPM cell lines may provide greater confidence that specific miRNAs correlate with BAP1 status.

6.2 Aims and objectives

In chapter 5, I investigated differential miRNA expression in isogenic cell models of *BAP1* loss using the NanoString nCounter platform. I found that BAP1 deficiency profoundly altered the miRNome of these cell lines. The aim of this chapter was to explore the BAP1-responsive miRNome across a large panel of MPM cell lines with varying BAP1 status. My objectives were to:

1. Quantify differences in miRNA expression between MPM cell lines within the cell line panel using the NanoString nCounter platform.
2. Identify differential miRNA expression ($\geq$1.5-fold, P$\leq$0.05) in BAP1-negative cell lines compared with BAP1-positive cell lines.
3. Investigate the expression of key miRNAs identified in isogenic *BAP1*-mutant MeT5A cells (NS1 HCL clusters C1 and C3) across the MPM cell line panel.
4. Validate expression levels by qRT-PCR for selected significantly modulated miRNAs identified during the NanoString analyses.

6.3 Analytical approach for NanoString nCounter human v3 miRNA assays NS2 and NS3

Two nCounter assays (named NS2 and NS3) were performed on a panel of MPM cell lines as listed in Table 6.1. Total RNA was extracted from 22 MPM cell lines, with total RNA concentration and RNA quality confirmed by spectrophotometry and RIN values, respectively (Table 6.1). 300 ng of total RNA from each sample was processed for nCounter miRNA expression profiling and analysed using the same NanoString assay and platform as previously described for NS1 (see chapter 5). The analytical workflow is summarised in Figure 6.1.

There were three major points of difference to note between NS2 and NS3, compared to NS1: (1) 300ng total RNA was used vs. 100ng in NS1 (see section 2.2.5) (2) With two exceptions (MSTO-211H and #15), only one replicate for each MPM cell line was analysed on NS2 and NS3, compared with triplicate biological replicates for each isogenic MeT5A cell line on NS1. (3) Lastly, the MPM cell lines were spread out across two cartridges (NS2 and NS3) whereas the NS1 dataset originated from a single cartridge.

NanoString nCounter cartridge: NS2							
Sample number	Sample name	Biological replicate (BR)	Passage number	NanoDrop ratios		Conc (ng/υl)	RNA integrity number (RIN)
				A260/ A280	A260/ A230		
1	#2	BR1	P15	2.09	2.15	292.0	7.1
2	#15	BR1	P20	2.07	2.17	294.0	8.3
3	#19	BR1	P17	2.15	2.05	183.0	8.3
4	#24	BR1	P17	2.14	2.27	330.4	7.7
5	#26	BR1	P14	2.12	2.13	1706	8.0
6	#30	BR1	P14	2.11	2.16	1000	8.8
7	#34	BR1	P13	2.10	2.22	576.0	7.4
8	#38	BR1	P15	2.13	2.10	588.0	7.3
9	#43	BR1	P17	2.10	2.07	908.0	7.9
10	#52	BR1	P16	2.13	2.18	288.4	9.3
11	MeT5A (*BAP1*$^{+/+}$)	BR1	P36	2.10	1.80	680.0	8.2
12	MSTO-211H	BR1	P24	2.10	2.14	1535	9.4

NanoString nCounter cartridge: NS3							
Sample number	Sample name	Biological replicate (BR)	Passage number	NanoDrop ratios		Conc (ng/υl)	RNA integrity number (RIN)
				A260/ A280	A260/ A230		
1	MESO-3T	BR1	P7	2.12	2.19	420.0	8.6
2	MESO-8T	BR1	P8	2.10	2.20	206.0	7.5
3	MESO-12T	BR1	P9	2.09	2.23	832.0	9.1
4	MESO-14T	BR1	P13	2.11	2.01	170.0	9.4
5	MESO-23T	BR1	P16	2.10	2.22	370.0	8.8
6	MeT5A (*BAP1*$^{+/+}$)	BR1	P36	2.10	1.80	680.0	8.2
7	MSTO-211H	BR2	P27	2.11	2.16	1166.4	9.8
8	NCI-H2052	BR1	P34	2.10	2.13	276.0	9.8
9	NCI-H2452	BR1	P20	2.13	2.18	344.0	10.0
10	NCI-H28	BR1	P27	2.10	2.19	276.0	9.5
11	NCI-H226	BR1	P80	2.09	2.21	662.0	9.7
12	#15	BR2	P27	2.09	2.10	816.0	7.4

Table 6.1: Quality control data for MPM cell line RNA for miRNome analysis (NanoString nCounter human v3 miRNA assay).
Sample information for RNA analysed on two cartridges, NS2 (top) and NS3 (bottom). The same biological replicate of normal mesothelial cell line MeT5A (*BAP1*$^{+/+}$) was included on each cartridge as an internal control. Purity of total RNA (ratios) was determined by NanoDrop spectrophotometer. Total RNA concentration and RNA integrity numbers (RIN) were confirmed by the Agilent 2100 Bioanalyser. Quality criteria of ratios ≥1.80 and RIN values ≥7.0 were satisfied for all samples.

To minimise inter-cartridge variability, initial steps for data analysis involved combining the two datasets from NS2 and NS3, before applying background subtraction followed by normalisation of raw miRNA counts (Fig. 6.1). Available options for background subtraction and data normalisation were detailed in section 5.3.3. The mean value for 16 negative controls from samples across both nCounter assays (NS2 and NS3) was applied as the threshold above which miRNA expression was classed as detectable. Next, the "all genes" method i.e. using the geometric mean of all 798 miRNAs within the assay, was used for normalisation of raw miRNA counts. I tested the different normalisation methods and confirmed this caused the least bias in the data (data not shown). An additional argument for applying this method of normalisation, rather than the geometric mean of the top 100 genes used for analysis of NS1, is that when comparing a large number of cell lines that are substantially different from each other, variation in the top 100 genes counts may be expected, so that outliers from one cell line could skew the normalised results for the entire dataset.

Following background subtraction and normalisation, I checked QC criteria and established the total number of miRNAs identified in each sample. Next, I narrowed my focus to miRNAs that were significantly modulated in relation to BAP1 status. MPM cell lines were grouped by BAP1 status and $\log_2$ fold changes in miRNA expression were generated for BAP1-negative versus BAP1-positive MPM cell lines, miRNAs that were up- and down-regulated $\geq$1.5-FC with statistical significance ($P \leq 0.05$) were taken forwards. In parallel, $\log_2$ fold changes in miRNA expression for NS2 and NS3 MPM cell lines were generated versus the MeT5A (*BAP1*$^{+/+}$) sample from within their own nCounter assay. Next, unsupervised hierarchical clustering for the MPM cell line data was performed, to look for trends within the significantly modulated miRNAs from BAP1-negative cell lines, and trends across the MPM cell lines for miRNAs identified in HCL clusters from the NS1 data set in chapter 5. Lastly, changes in miRNA expression identified during this analysis were validated by qRT-PCR in isogenic MeT5A *BAP1*-mutant cell lines and selected MPM cell lines.

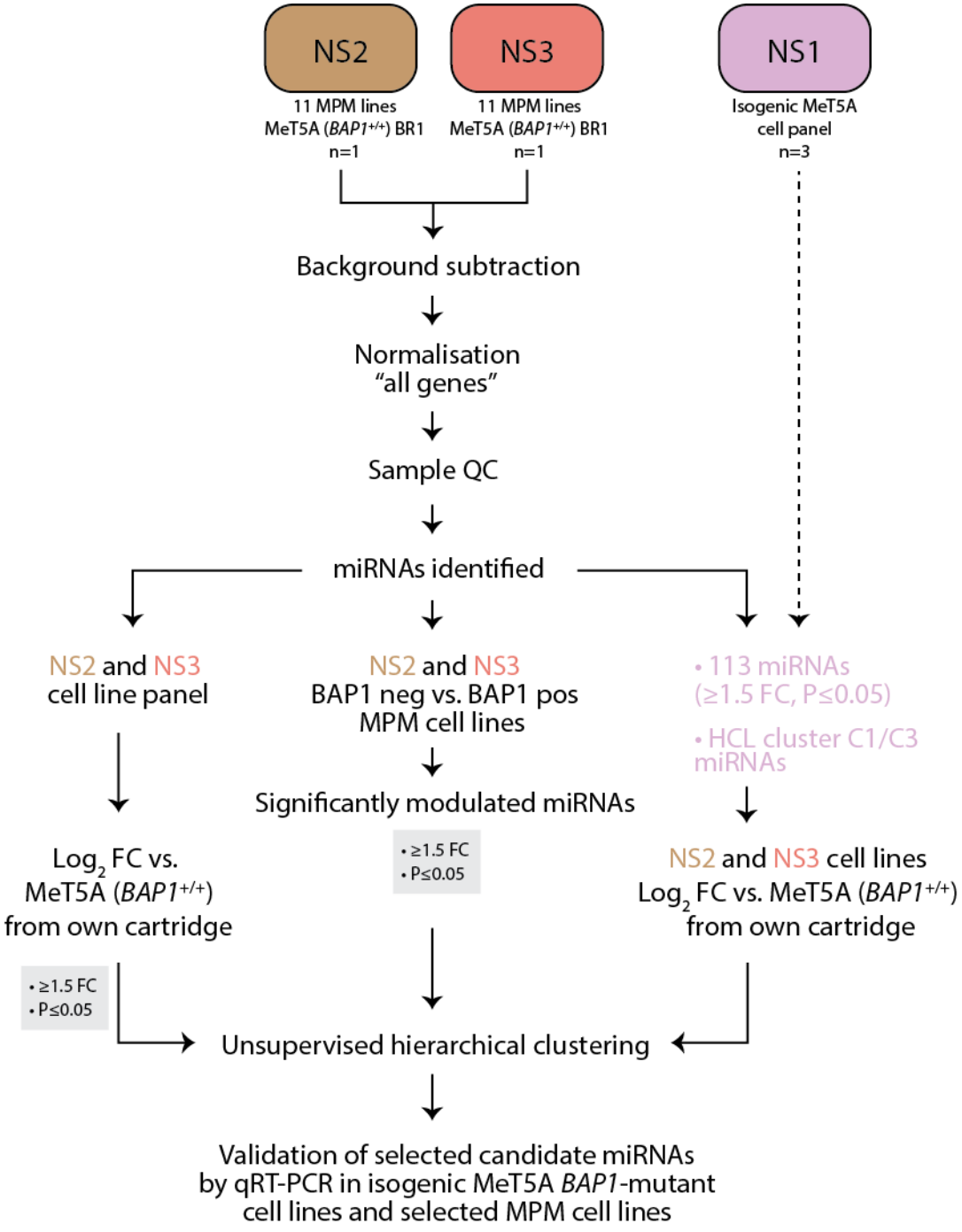

Figure 6.1: Analytical workflow for the NanoString nCounter human v3 miRNA assays NS2 and NS3.
NS2: NanoString nCounter cartridge 2, NS3: NanoString nCounter cartridge 3, BAP1 neg: BAP1 negative, BAP1 pos: BAP1 positive, FC: fold change.

6.4 Assessment of the positive and negative controls following combined analysis of NS2 and NS3

As in chapter 5, the mean raw counts for all positive and negative controls from NS2 and NS3 nCounter assays were plotted (Fig. 6.2), in order to visualise their counts, to confirm the value for background subtraction, and to confirm linear quantification of the positive controls across the 4-fold dilution series. As seen for NS1, the mean raw count for the positive control dilution series decreased linearly until dilution E, which has a count of 23. The counts had plateaued by dilution F, which had a mean raw count of 18 (Fig. 6.2A-B). Similarly, the ligation positive controls decreased linearly across the 4-fold dilution series. All negative control probes showed an expression profile <10 counts, with most falling within the "noise" of the assay. I took the mean value from the negative controls to apply as the threshold above which miRNA expression is detectable, a value of 3 counts. Three spike-in controls, ath-miR159a, osa-miR414 and osa-miR442 showed counts above the threshold for background noise but within the lower confidence zone, as previously observed in NS1 (see section 5.3.4). Only miRNAs with counts above the threshold within the dynamic range, and those that fall within the "lower confidence" zone (Fig. 6.2A) were taken forward for further analyses.

For each cell line in NS2 and NS3, the raw counts for the six positive and eight negative controls, and for 798 miRNAs in the assay were plotted to show their distribution in relation to the controls and the value for background subtraction (Fig. 6.3). As seen in NS1, the counts for positive controls for all cell lines are above the threshold for background subtraction, and the majority of the negative controls fell below this threshold.

6.5 Good reproducibility between biological replicates for cell lines represented on more than one nCounter assay.

The same sample, biological replicate 1 (BR1) of normal mesothelial cell line MeT5A (*BAP1*$^{+/+}$), was included in NS2 and NS3 as an internal control. Three biological replicates of MeT5A (*BAP1*$^{+/+}$) (BR1, BR2 and BR3) formed the internal control in NS1. In addition, two biological replicates of MPM cell lines MSTO-211H and #15 were included in separate nCounter assays, biological replicate 1 (BR1) of MSTO-211H and #15 were investigated in NS2, and biological replicate 2 (BR2) for both cell lines in NS3. Since biological replicates should, in theory, have almost identical miRNA expression values, the closeness of background subtracted normalised counts from these samples was compared to give an overview of inter-cartridge variability.

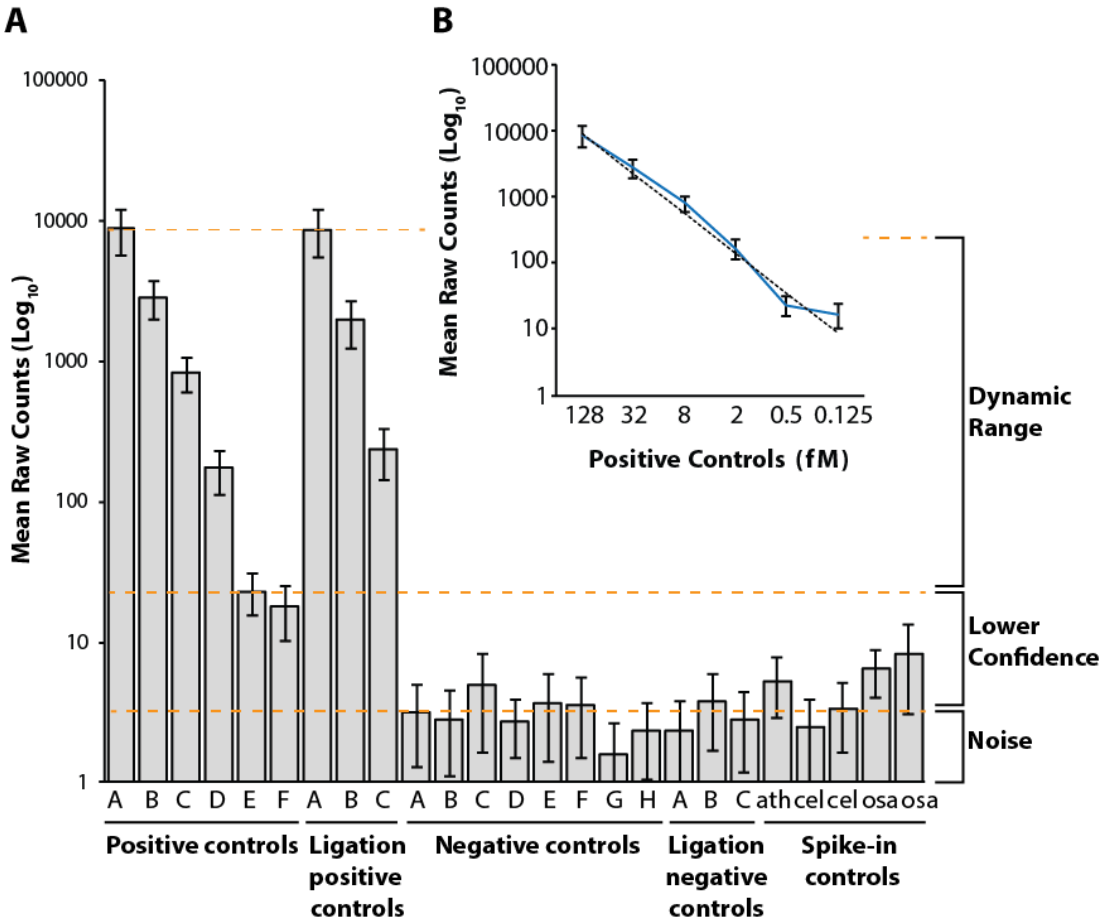

Figure 6.2: Mean raw counts for internal controls within NanoString nCounter human v3 miRNA assays NS2 and NS3.

A Bar graph shows mean raw counts for all positive and negative controls on the NS2 and NS3 nCounter assays (n=24 RNA samples, error bars show SD). The positive control probes are six different RNA transcripts covering a 4-fold dilution series. Three ligation positive control probes are present at the following concentrations: A 128 fM, B 32 fM and C 8 fM. Eight negative controls and three ligation negative control probes have no mRNA or miRNA targets present in the samples. The spike-in controls represent exogenous, non-mammalian RNA transcripts. The orange dashed lines divide the graph into three zones: "Dynamic Range" is indicative of counts >23, "Lower Confidence" represents a range between 3 – 23 counts, and "Noise" is the observed mean raw count for eight negative control probes (3 counts), this value was used for background subtraction. **B** Plot demonstrating quantitative range for raw counts from the positive control 4-fold dilution series. The blue line shows the observed mean raw counts (n=24 samples, error bars show SD), and the black dashed line indicates the expected counts for the input amount. SD: standard deviation.

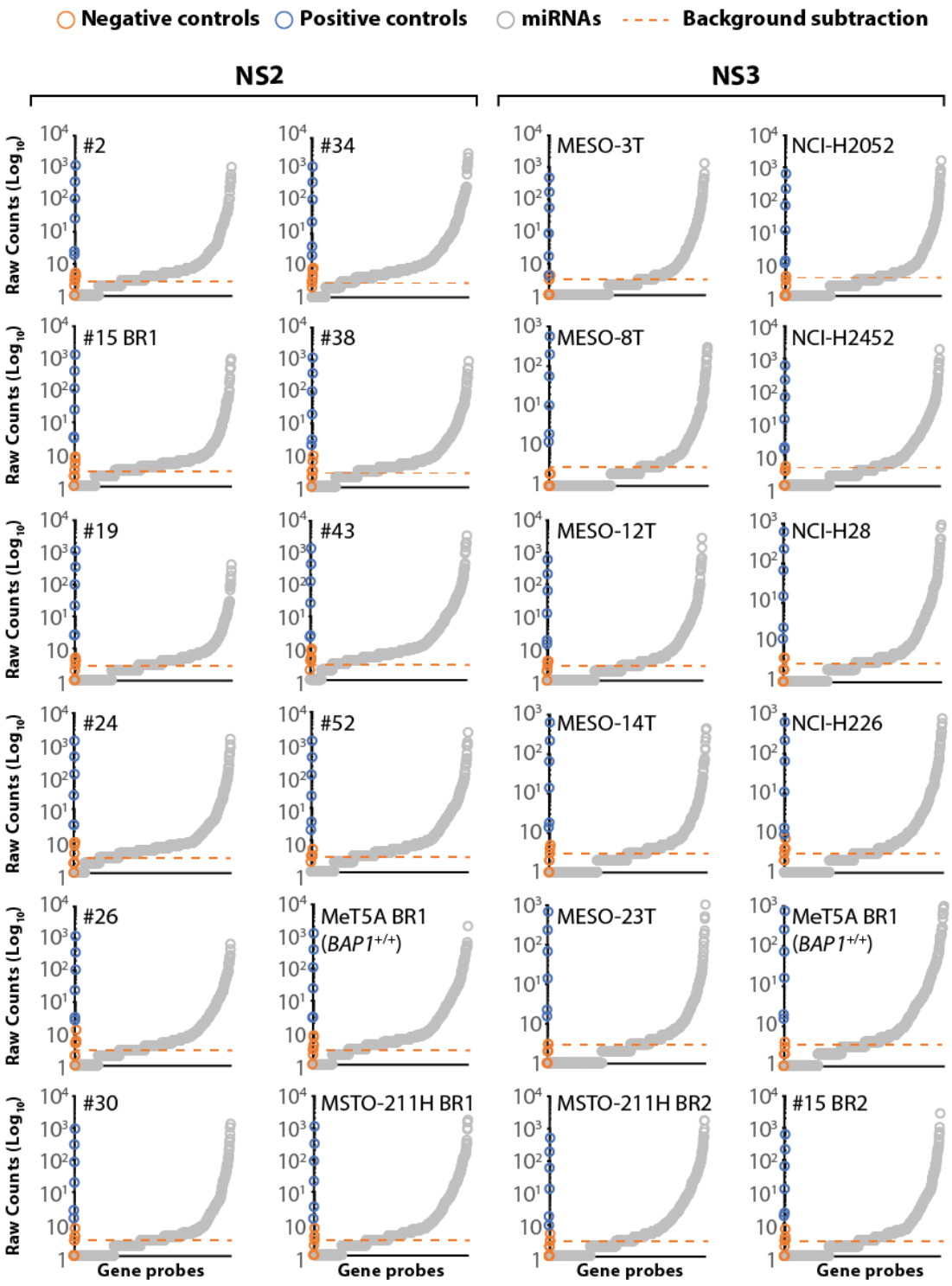

Figure 6.3: Distribution plots of raw counts for miRNAs in nCounter assays NS2 and NS3.

Distribution plots of mean raw counts are shown for RNA from MPM cell lines analysed in NS2 and NS3. For each cell line, the mean raw counts are plotted for 798 miRNAs (grey circles), 6 positive controls (blue circles) and 8 negative controls (orange circles). The orange dashed line indicates the mean counts for negative controls (3 counts) to be applied as background subtraction.

Firstly, the MeT5A (*BAP1*$^{+/+}$) BR1 samples from NS2 and NS3 were plotted against the three biological replicates of MeT5A (*BAP1*$^{+/+}$) from NS1 (Fig. 6.4A), in order to compare miRNA data between technical replicates (Fig. 6.4A, left) and biological replicates (Fig. 6.4A, middle and right) from the three different assays. The six comparisons showed values for the slope of the power trend line ranging between 0.87 – 0.94, and R^2 values between 0.81 – 0.89, indicating good linear relationships between both technical and biological extracts. The segment on the scatter plots outlined by an orange dotted line indicate those miRNAs with counts that fall within the "lower confidence" zone (<23 counts), demonstrated by the larger variability in counts between samples for miRNAs in this range.

Next, cell lines that were represented in both NS2 and NS3 (Fig. 6.4B) were compared. Values for the slope of the power trend line ranged between 0.92 – 1.06, with R^2 values between 0.83 – 0.91, indicating good linear relationships between technical and biological extracts, particularly within the "dynamic range" of the assays. Overall, the nCounter assay and analysis workflows generated reproducible data when profiling technical or biological replicates using the nCounter assay.

6.6 Analysis of miRNAs identified above background in NS2 and NS3

Following background subtraction and data normalisation, approximately one-third of the 798 miRNAs represented on the nCounter assay were identified in each cell line, ranging from 229 – 340 miRNAs (Fig. 6.5). No bias was noted between the number of miRNAs identified in cell lines analysed in NS2 or NS3. The MeT5A (*BAP1*$^{+/+}$) BR1 sample was analysed on all three nCounter assays, so the total number of miRNAs identified in this sample from NS1, NS2 and NS3 provided another measure of inter-assay variability (Fig. 6.6A). Following background subtraction and normalisation, a similar number of miRNAs were identified in each of the nCounter assays for MeT5A (*BAP1*$^{+/+}$) BR1 sample, between a max of 332 miRNAs (NS1) and a min of 296 miRNAs (NS2), with substantial overlap between identified miRNAs (Fig. 6.6B). 63% of 451 miRNAs that were identified in MeT5A (*BAP1*$^{+/+}$) BR1 were common to at least two nCounter assays, NS1 identified 70 (16%) unique miRNAs which were not seen in NS2 and NS3. Similarly, there were 40 (9%) unique miRNAs in NS2 and 55 (12%) unique miRNAs in NS3. However, all except 11 of these unique miRNAs had <10 counts, so fell within the "lower confidence" zone where quantification is less accurate. For the remaining 43% of 451 miRNAs identified in common to all three nCounter assays, the median count per assay was ~80, within the higher confidence "dynamic range" of the assay. Thus, miRNAs with lower counts were less likely to be detected in all replicates.

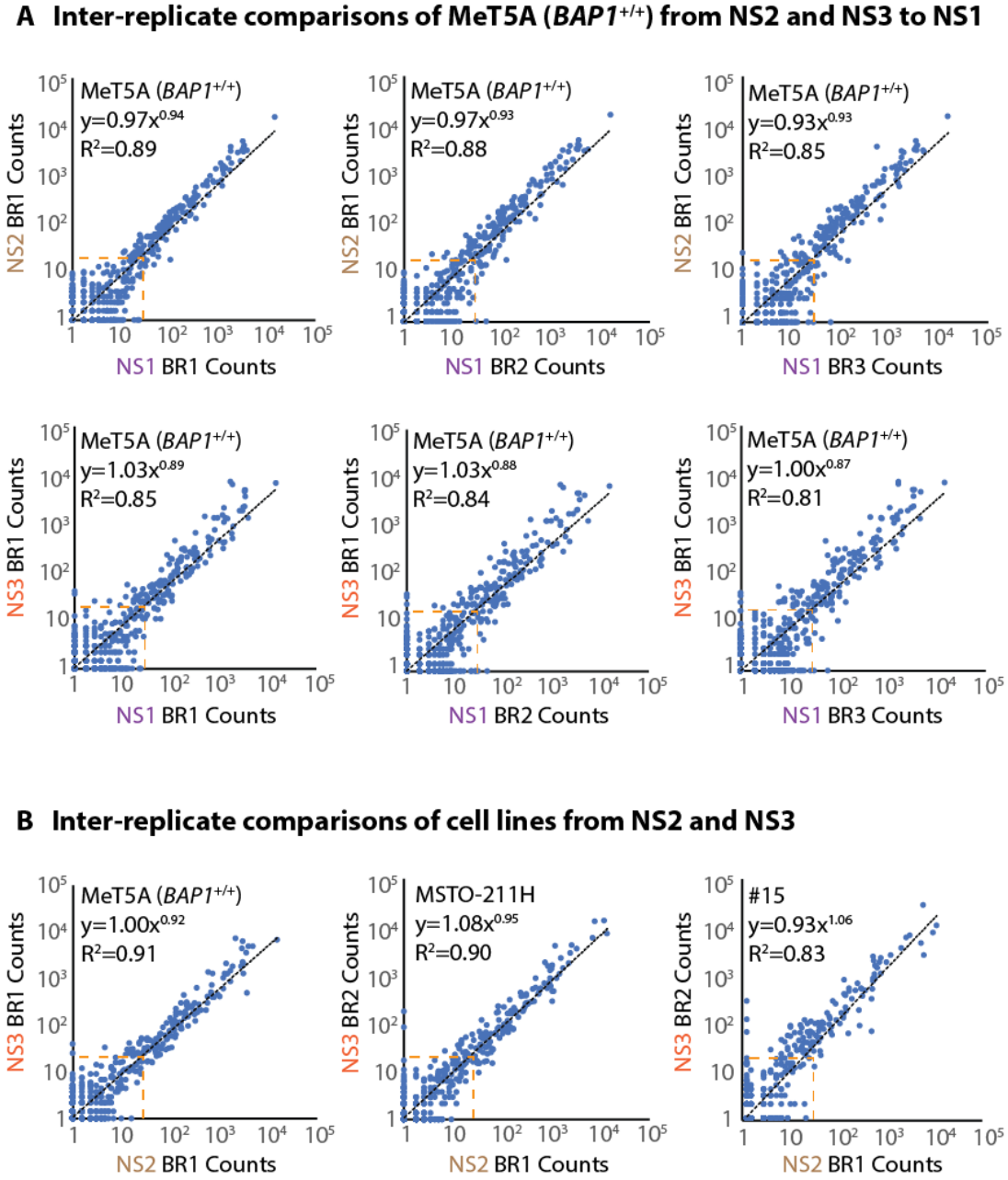

Figure 6.4: Comparisons of biological replicates from cell lines represented in more than one nCounter assay.

Scatter plots show inter-replicate comparisons of counts for 798 miRNAs, following background subtraction and normalisation of miRNA expression to top 100 miRNA genes with the highest counts (NS1) or to all 798 miRNA genes "all genes" (NS2 and NS3). **A** Comparisons between biological replicates are shown for the normal mesothelial cell line MeT5A (*BAP1*$^{+/+}$) from nCounter assays NS2 and NS3 to NS1. **B** Comparisons between biological replicates are shown for the normal mesothelial cell line MeT5A (*BAP1*$^{+/+}$), and MPM cell lines MSTO-211H and #15 from nCounter assays NS2 and NS3. Power regression equation and R^2 value are displayed. BR: biological replicate.

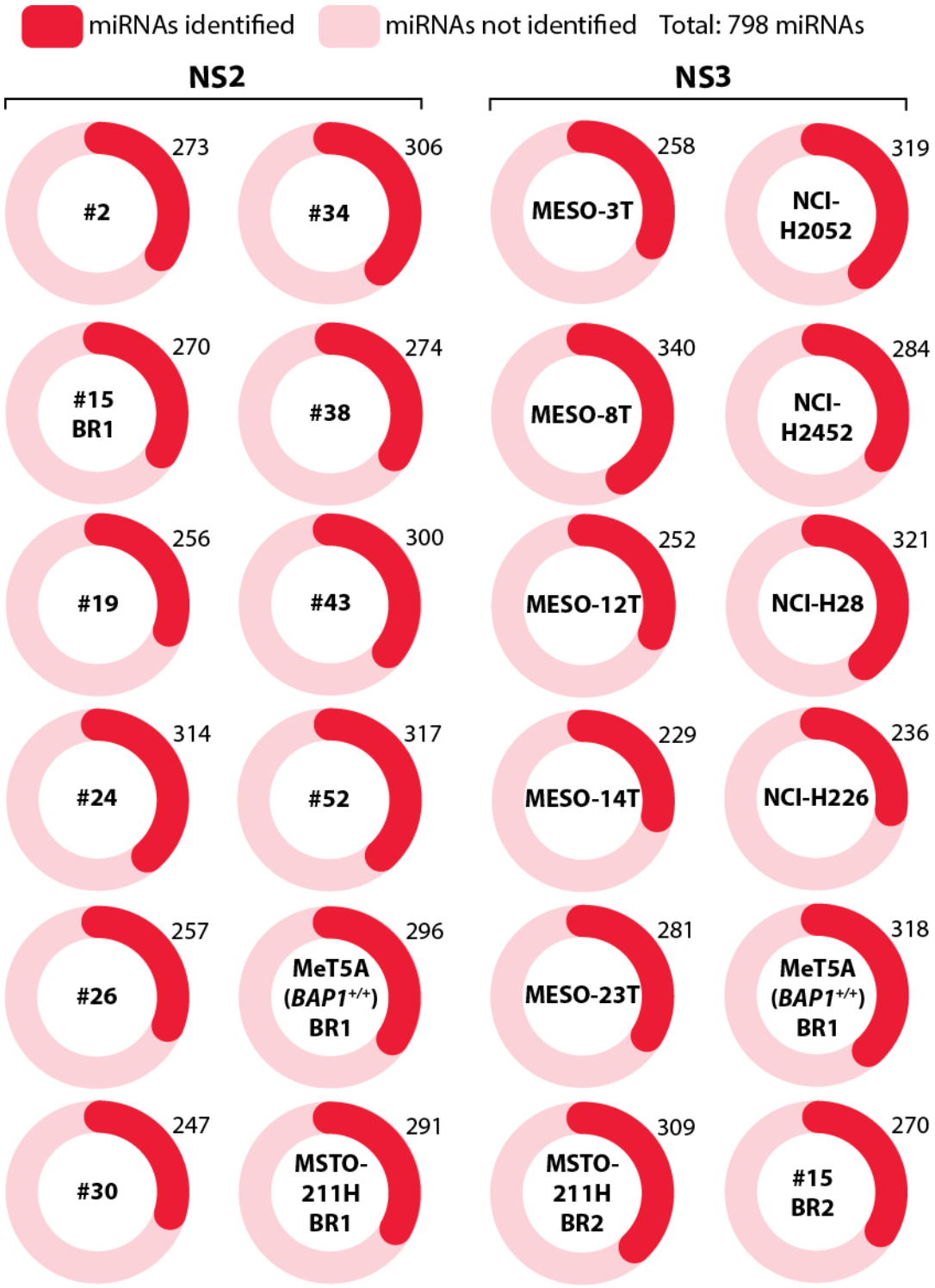

Figure 6.5: Total number of miRNAs identified in MPM cell lines by the NanoString nCounter human v3 miRNA assays NS2 and NS3.
Total number of miRNAs identified in cell lines post-background subtraction and normalisation. miRNAs were classed as "identified" if they showed ≥2 counts after normalisation. BR: biological replicate.

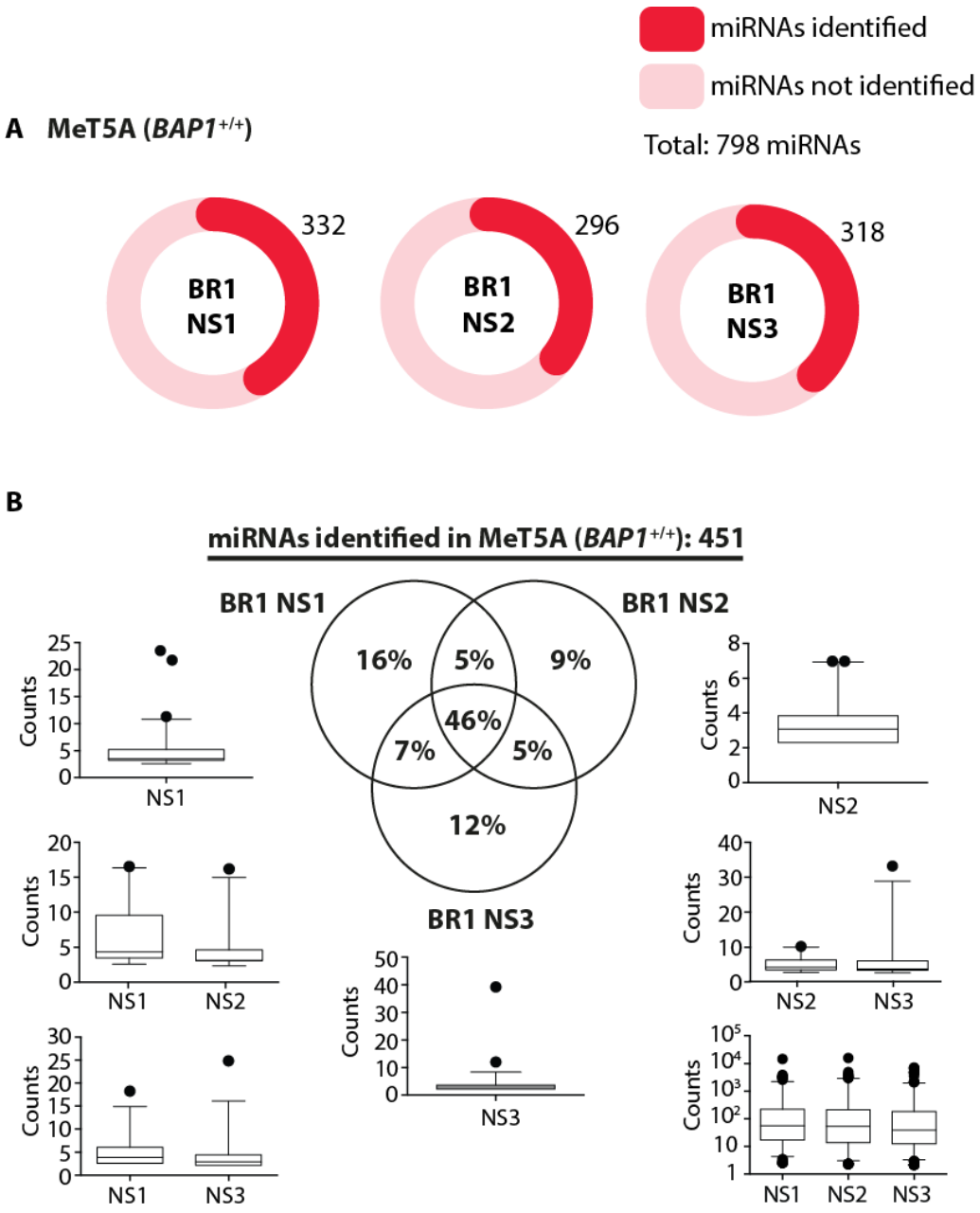

Figure 6.6: Reproducibility of miRNAs identified in MeT5A (*BAP1*$^{+/+}$) across three NanoString nCounter human v3 miRNA assays NS1, NS2 and NS3.
A Number of miRNAs identified in the same MeT5A (*BAP1*$^{+/+}$) sample post-background subtraction and normalisation in three nCounter assays. miRNAs were classed as "identified" if they showed ≥2 counts after normalisation. **B** Three-way Venn diagram shows the overlap between miRNAs identified in MeT5A (*BAP1*$^{+/+}$). The box and whisker plots show the spread of counts for miRNAs identified in each Venn segment. The median and interquartile range are displayed, the whisker boundaries are the 5th and 95th percentile. BR: biological replicate.

6.7 A subset of miRNAs are significantly deregulated in BAP1-negative MPM cell lines

The discovery of differentially expressed miRNA genes in isogenic MeT5A *BAP1*-mutant cell lines (chapter 5) suggested that there could be a BAP1-dependent miRNome in MPM. To explore this idea, NS2/NS3 data were analysed for the MPM cell lines stratified by BAP1 status (see section 3.6). Following background subtraction and normalisation, 293 miRNAs were identified across the two groups (Fig. 6.7A). The majority of these, 239 miRNAs (82%), were identified within both groups of MPM cell lines, however 25 miRNAs (8%) were identified exclusively in BAP1-negative cell lines, and 29 miRNAs (10%) were specific to BAP1-positive cell lines. The scatter plot in Figure 6.7B confirmed good correlation of expression between the two groups for the majority of miRNAs, albeit with some outliers which exhibit differential expression between BAP1 positive and negative cell lines.

To investigate which miRNAs were significantly associated with BAP1 loss, the $\log_2$ fold change was calculated for the BAP1-negative MPM cell line group, using the BAP1-positive group as the comparator sample. Fold change ($\geq$1.5) and significance ($P \leq 0.05$) cut-offs were applied and a volcano plot used to visualise the miRNA expression profile. In total, 52 miRNAs were either significantly upregulated (22 miRNAs) or significantly downregulated (30 miRNAs) in BAP1-negative cell lines compared to BAP1-positive cell lines (Fig. 6.7C, Appendix Table 6.1). Of note, the significantly downregulated miRNAs showed larger magnitude changes in expression than those that were upregulated, with some miRNAs approaching a $\log_2$ 6-fold decrease. The significantly upregulated miRNAs showed smaller fold changes in expression, up to $\log_2$ 2-fold. A similar bias for greater downregulation of miRNAs with loss of BAP1 had previously been observed in isogenic MeT5A *BAP1*-mutant cell lines (*BAP1*$^{w-/KO}$) (Fig 5.7).

The overlap between significantly modulated miRNAs in BAP1-negative MPM cell lines (NS2/NS3) and those identified as BAP1-responsive in isogenic MeT5A *BAP1*-mutant cells (NS1) was also examined (Fig. 6.7D). There were very few commonly responsive miRNAs between the cell models. Of note, miR-10a-5p (C3.1) and miR-628-5p (C3.1 and C5.1) were downregulated in one or both isogenic MeT5A (*BAP1*$^{w-/KO}$) cell lines, and MPM cells. However, five miRNAs showed increased expression in isogenic MeT5A *BAP1*-mutant cells compared to MeT5A (*BAP1*$^{+/+}$), but decreased expression in BAP1-negative compared to BAP1-positive MPM cell lines. Interestingly, these included some of the largest responders highlighted in chapter 5, miR-99a-5p and miR-155-5p (Fig. 5.8).

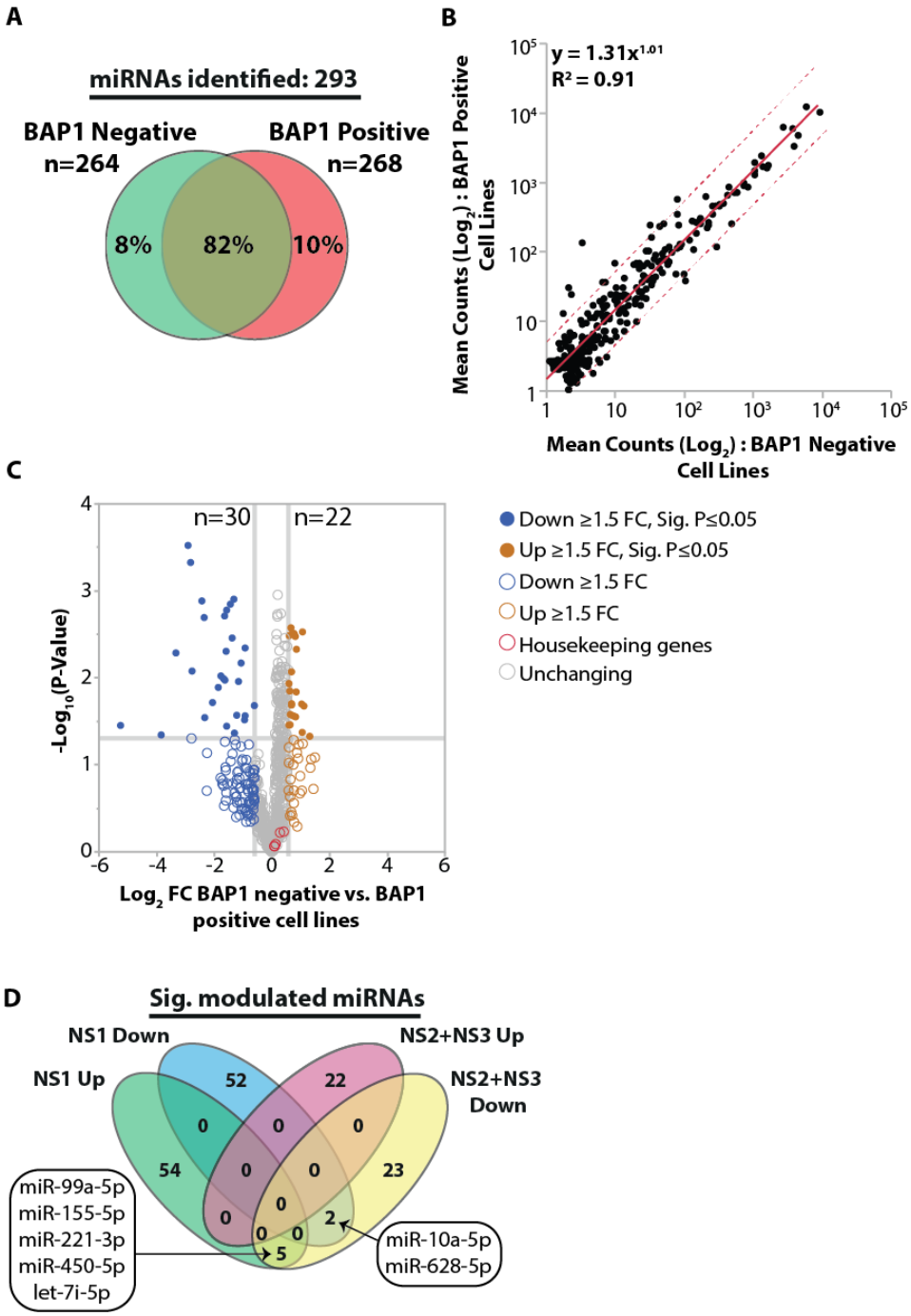

Figure 6.7: Total miRNAs identified in MPM cell lines, grouped by BAP1 status, for the NanoString nCounter human v3 miRNA assays NS2 and NS3.
A Venn diagram shows the overlap between miRNAs identified post-background subtraction and normalisation, across MPM cell lines which have been grouped by their BAP1 status. **B** Scatter plot shows counts for 293 identified miRNAs, plotted for BAP1-positive and BAP1-negative cell lines. Power regression equation and R^2 value is displayed. Dotted lines represent 95% prediction intervals. **C** Volcano plot displays $\log_2$ fold change (FC) in miRNA expression, and $-\log_{10}$ significance values, for BAP1-negative cell lines vs. BAP1 positive cell lines (n=6). The solid grey lines designate 1.5-FC and P=0.05. **D** 4-way Venn diagram showing the overlap of significantly modulated miRNAs that are up- or down-regulated (≥1.5-fold, P≤0.05) in BAP1 negative compared to BAP1 positive comparator cells in NS1 (isogenic MeT5A) and NS2+NS3 (MPM cell panel).

Next, the expression profile for the 52 significantly modulated miRNAs (Fig 6.7C) was assessed in individual MPM cell lines. The cell lines and miRNAs were clustered to distinguish any relationship to histological subtype or BAP1 status (Figure 6.8). Overall, most BAP1-positive MPM cell lines clustered together (cluster 1), whilst the BAP1-negative cell lines were distinct, all falling within two HCL clusters (clusters 2 and 3), although cluster 3 also included MESO-12T and NCI-H2052 which are BAP1-positive. The majority of the MPM cell lines in clusters 2 and 3 were of epithelioid subtype, whereas cluster 1 was populated by biphasic and sarcomatoid MPM cell lines. Of note, the two MSTO-211H biological replicates (BR1 and BR2) clustered closely (cluster 1) and demonstrated highly similar miRNA profiles, whilst the biological replicates for #15 both fell within cluster 3.

Interestingly, following unsupervised hierarchical clustering of the miRNA list, the miRNAs clustered naturally so that that the significantly upregulated miRNAs in BAP1-negative MPM cell lines clustered together in the top half of the heat map, and the significantly downregulated miRNAs in the lower half of the heat map (Fig. 6.8). The miRNAs identified as significantly upregulated in the group of BAP1-negative MPM cell lines (Fig 6.7C), in fact were expressed at similar levels to the MeT5A across most of the MPM cell panel (Fig 6.8). In contrast, there was generally more marked downregulated expression of miRNAs amongst BAP1-negative cell lines (clusters 2 and 3), compared with cluster 1. For example, miR-10a-5p and miR-628-5p are indicated on the heat map by dotted lines (Fig 6.8), these miRNAs were significantly downregulated in both the BAP1-deficient MPM cell lines and isogenic cell model (see Fig. 6.7D). A group of eleven miRNAs are outlined in cluster 1 (Fig 6.8), these miRNAs were significantly downregulated in BAP1-negative cell lines (Fig 6.7C?). It is evident that these miRNAs are highly expressed across the BAP1-positive cell lines in cluster 1 compared with the largely BAP1-negative cell lines in clusters 2 and 3. Overall, this method of analysis had limited success in identifying miRNAs that showed a clear association with BAP1 status within these heterogeneous MPM cell lines.

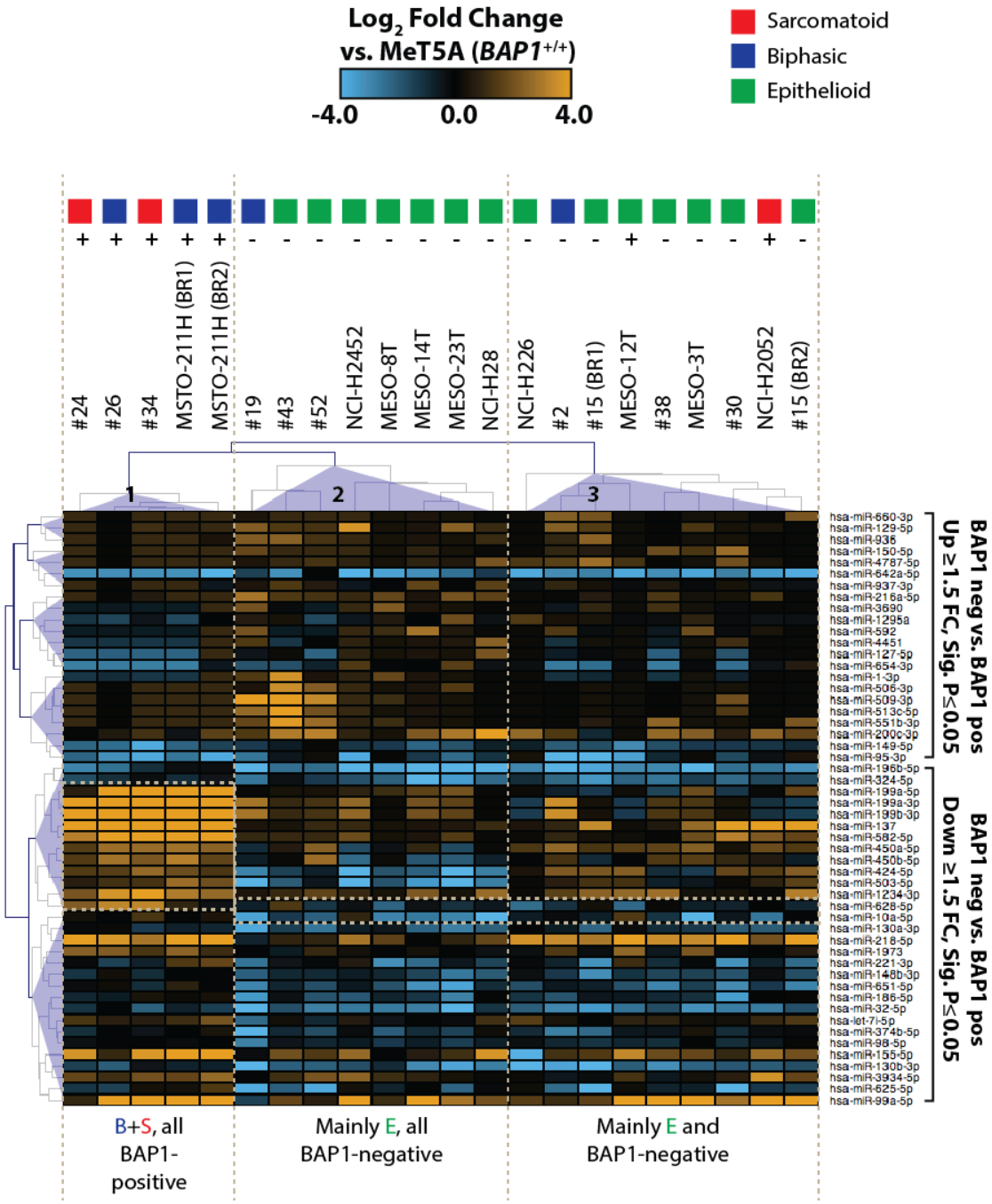

Figure 6.8: Unsupervised hierarchical clustering for 52 significantly modulated miRNAs based on BAP1 status for MPM cell lines on nCounter assays NS2 and NS3. Heat map shows log_2 fold changes for miRNAs where expression ≥1.5-fold and statistical significance (P≤0.05, Welch's unpaired t-test) was detected in BAP1 negative cell lines vs. BAP1 positive cell lines. Log_2 fold changes for NS2 and NS3 cell lines were generated vs. MeT5A (*BAP1*$^{+/+}$) sample from within their own assays. +/- signs indicate BAP1 status. Colour coding indicates the histological subtypes of MPM.

6.8 Chromosome 14q32.31 miRNA locus is downregulated in a subset of BAP1-negative MPM cell lines

I next adopted a different strategy, to examine the NS2/NS3 dataset for specific miRNAs that had already been highlighted as BAP1-dependent in the isogenic MeT5A cell model.
In chapter 5, unsupervised hierarchical clustering analysis for the miRNome of isogenic MeT5A *BAP1*-mutant cell lines in NS1 generated five miRNA clusters (Fig. 5.9). Cluster 3 (C3) displayed predominantly upregulated miRNA expression in isogenic *BAP1*$^{w-/KO}$ cells, and cluster 1 (C1) striking downregulation of miRNAs in isogenic *BAP1*$^{w-/KO}$ cells that mapped to tumour-suppressor locus on ch14q32.31 (see section 5.3.8). I therefore examined the expression profiles for those miRNAs in cluster C3 (Fig. 6.9) and cluster C1 (Fig. 6.10) in the MPM cell line panel from NS2 and NS3 following normalisation to MeT5A (*BAP1*$^{+/+}$).

Unsupervised hierarchical clustering was performed using combined data for the C3 miRNAs from both the MPM cell lines and isogenic MeT5A *BAP1*-mutant cell lines (Fig. 6.9). The cell lines grouped into five major clusters, principally defined by BAP1 status. Overall, BAP1-positive MPM cell lines predominately clustered together (clusters 1 and 2), whilst the majority of BAP1-negative cell lines were positioned in clusters 3, 4 and 5, with the exceptions of NCI-H2052 and #26. Generally, there was increased expression of C3 miRNAs in the isogenic MeT5A *BAP1*-mutant cells compared to the MPM cell line panel. Outlined on the heat map in Fig 6.9 are miRNAs of interest that possess similar expression profiles to the isogenic MeT5A *BAP1*-mutant cells. miR-4516 is predominantly overexpressed in BAP1-negative MPM cell lines from clusters 3-5 compared to MPM cell lines from clusters 1 and 2. miR-4516 was one of the largest responders highlighted in chapter 5 (Fig. 5.8). Furthermore, miR-21-5p, miR-5196-3p, miR-6732-3p and miR-126-3p were all upregulated in MPM cell lines from clusters 4 and 5, but downregulated in MPM cell lines from the remaining clusters. Of note, miR-155-5p, which was another large responder from chapter 5 (Fig. 5.8), showed the highest expression in BAP1-positive MPM cell lines from clusters 1 and 2, although it was also upregulated in most BAP1-negative MPM cell lines in clusters 3-5 relative to MeT5A (*BAP1*$^{+/+}$). Overall, most miRNAs upregulated on *BAP1* mutation in MeT5A cells were not highly expressed in MPM cell lines. However, some were either overexpressed in the majority of MPM cell lines, or were selectively overexpressed in a subset of BAP1-negative MPM cell lines.

Expression data for the HCL C1 miRNAs identified in chapter 5 were also subject to unsupervised hierarchical clustering for both the MPM cell lines and isogenic MeT5A *BAP1*-

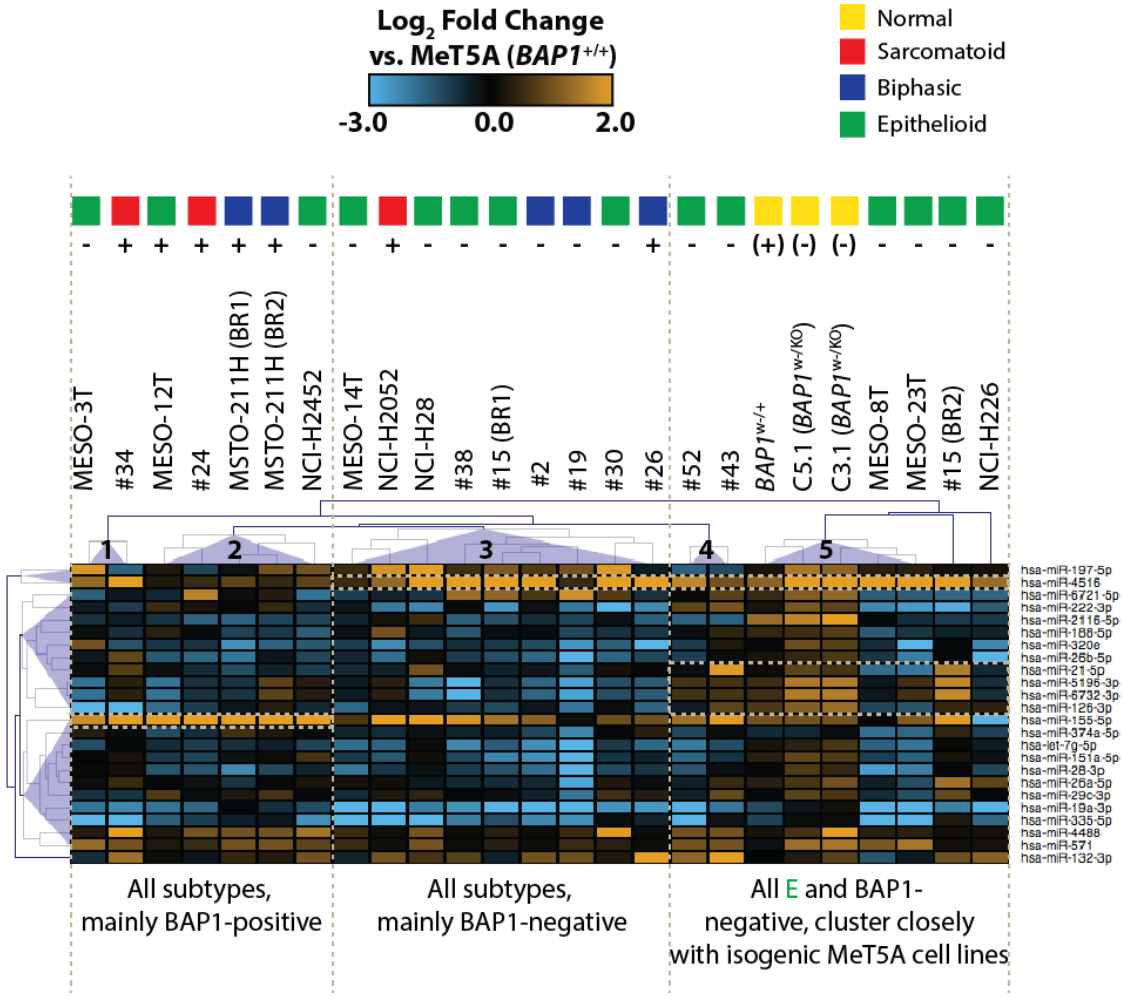

Figure 6.9: Unsupervised hierarchical clustering of HCL C3 miRNAs from nCounter assay NS1, in MPM cell lines from nCounter assays NS2 and NS3.
Heat map shows $\log_2$ fold changes in a panel of MPM cell lines and isogenic *BAP1*-mutant cell lines, relative to MeT5A (*BAP1*$^{+/+}$) from within their own assays. +/- signs indicate BAP1 status. Colour coding indicates the histological subtypes of MPM.

mutant cell lines (Fig. 6.10). The cell lines grouped into five major clusters, largely defined by BAP1 status. Most BAP1-positive MPM cell lines were found within clusters 1 and 4, whilst the majority of the BAP1-negative cell lines were in clusters 2, 3 and 5. Strikingly, a group of BAP1-negative MPM cell lines in cluster 5 show substantial downregulation for the majority of ch14q32.31 miRNAs, thereby phenocopying the expression profiles of the isogenic *BAP1*$^{w-/KO}$ cells. Interestingly, this group of MPM cell lines was predominantly BAP1-negative and epithelioid, with NCI-H2052 the only exception (BAP1-positive, sarcomatoid). Nevertheless, many MPM cell lines in the other clusters also showed downregulation of ch14q32.31 miRNAs, albeit to a lesser extent than cluster 5 where this phenotype was strongest. Of note, three BAP1-negative cell lines, NCI-H2452, #43 and #52 showed an

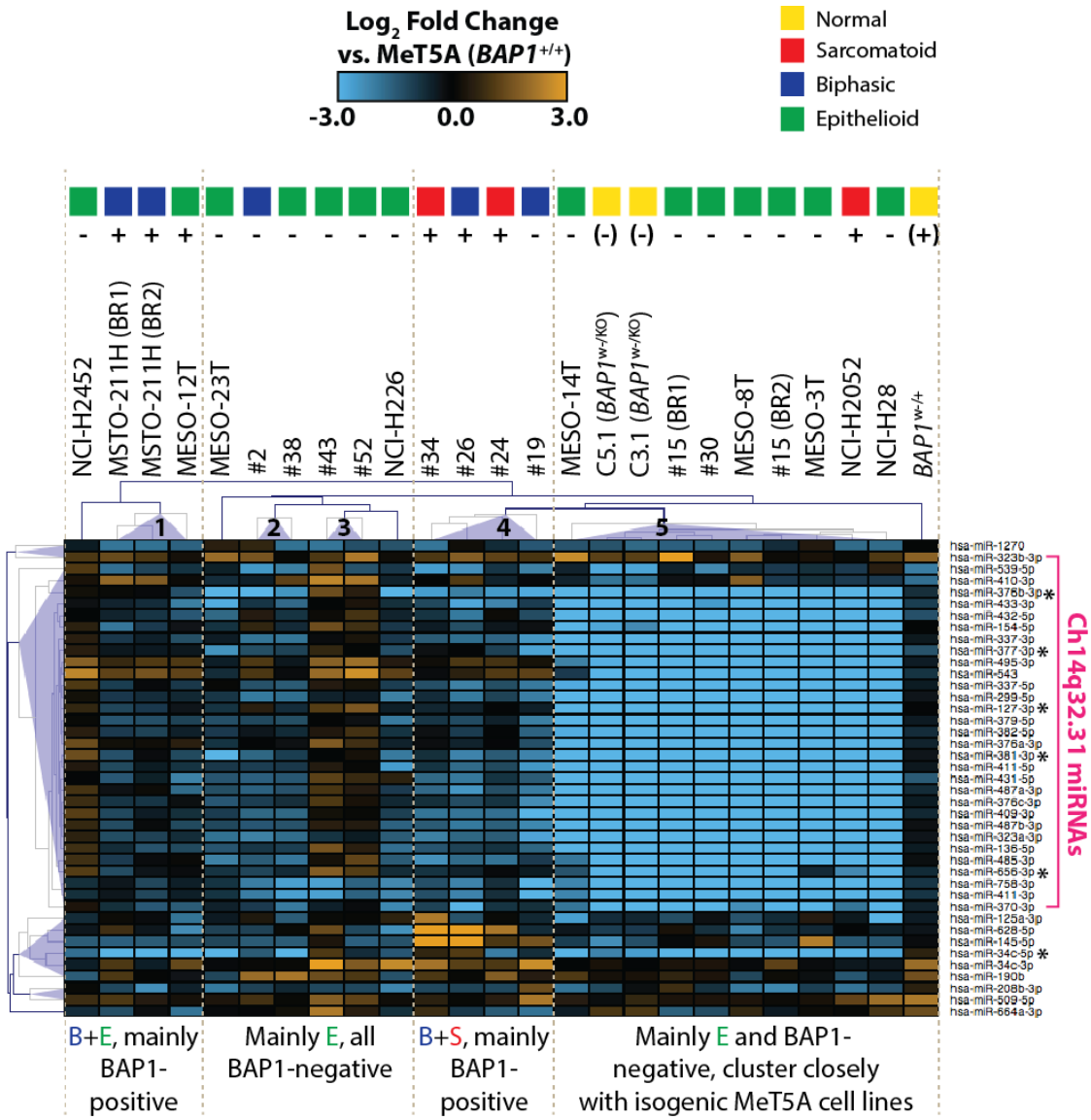

Figure 6.10: Unsupervised hierarchical clustering of HCL C1 miRNAs from nCounter assay NS1, in MPM cell lines from nCounter assays NS2 and NS3.
Heat map shows log_2 fold changes in a panel of MPM cell lines and isogenic BAP1-mutant cell lines for C1 miRNAs from NS1. Log_2 fold changes for NS1, NS2 and NS3 cell lines were generated relative to MeT5A (*BAP1*$^{+/+}$) from within their own assays. miRNAs from chromosome 14q32.31 locus are indicated. *Representative miRNAs selected for qRT-PCR validation. +/- signs indicate BAP1 status. Colour coding indicates the histological subtypes of MPM.

increase in ch14q32.31 miRNAs, relative to MeT5A (*BAP1*$^{+/+}$), implying that in certain cellular contexts BAP1 loss is also compatible with miRNA expression from this locus.

As the ch14q32.31 miRNAs were of particular interest, I explored the counts for each MPM cell line, to determine whether they fell within the "low confidence" or "dynamic range" of the assay (see Fig. 6.2), and how they related to counts for all the other miRNAs detected.

Background-subtracted, normalised counts for all 798 miRNAs and six housekeeping genes on the assay were plotted (Fig. 6.11). Although NS3 reported higher counts for housekeeping genes, overall there was little technical variation between miRNA counts from NS2 and NS3. Across the MPM cell line panel, 57% (17/30) of the ch14q32.31 miRNAs were detected within the dynamic range of the assay in at least one sample, whilst 33% (10/30) fell within the "low confidence" zone where miRNA quantification is less accurate, and 10% (3/30) fell within the "noise" of the assay. It is clear that the majority of ch14q32.31 miRNAs were readily detected in MeT5A (*BAP1*$^{+/+}$) cells, and that their expression was selectively downregulated in seven MPM cell lines.

As the heat map scale in Figure 6.10 did not resolve differential ch14q32.31 miRNA expression well, fold-changes relative to MeT5A (*BAP1*$^{+/+}$) were also plotted in Figure 6.12. This again highlighted differences between the MPM cell lines stratified according to BAP1 status. Based on ch14q32.31 miRNA expression levels, the cell lines fell into three groups, as indicated in Figure 6.12. For the BAP1-positive MPM cell lines, comprised of a mix of all MPM subtypes, the majority (6/7, 86%) exhibited moderately decreased expression of ch14q32.31 miRNAs (up to 16-fold). In contrast, the BAP1-negative MPM cell lines exhibit more variable ch14q32.31 miRNA expression: whilst 33% (5/15, including the 2 biphasic lines) have moderately decreased expression that is comparable to most BAP1-positive cell lines, 20% (3/15) show moderately increased expression. Most notably, 47% (7/15) of BAP1-negative cell lines, but only 14% (1/7) of BAP1-positive cell lines, showed substantially decreased expression of up to 100-fold. Thus, although there appears to be a complex relationship between BAP1 status and ch14q32.31 miRNA expression, silencing of this locus is most common in BAP1-negative MPM cell lines, and was phenocopied by introducing *BAP1* mutations into normal MeT5A mesothelial cells.

6.9 Expression changes for candidate miRNAs are validated by qRT-PCR in isogenic MeT5A and selected MPM cell lines

The observed downregulation of the ch14q32.31 locus in isogenic *BAP1*$^{w-/KO}$ cells and some BAP1-negative MPM cell lines is striking and novel. In order to validate these expression changes, six representative miRNAs were selected for validation by qRT-PCR (Fig. 6.13), including five ch14q32.31 miRNAs (Fig. 5.12) from different clusters within the locus, and miR-34c-5p (similarly downregulated but from a different chromosome), which all showed differential expression across the MPM cell line panel (see Fig. 6.10, asterisks).

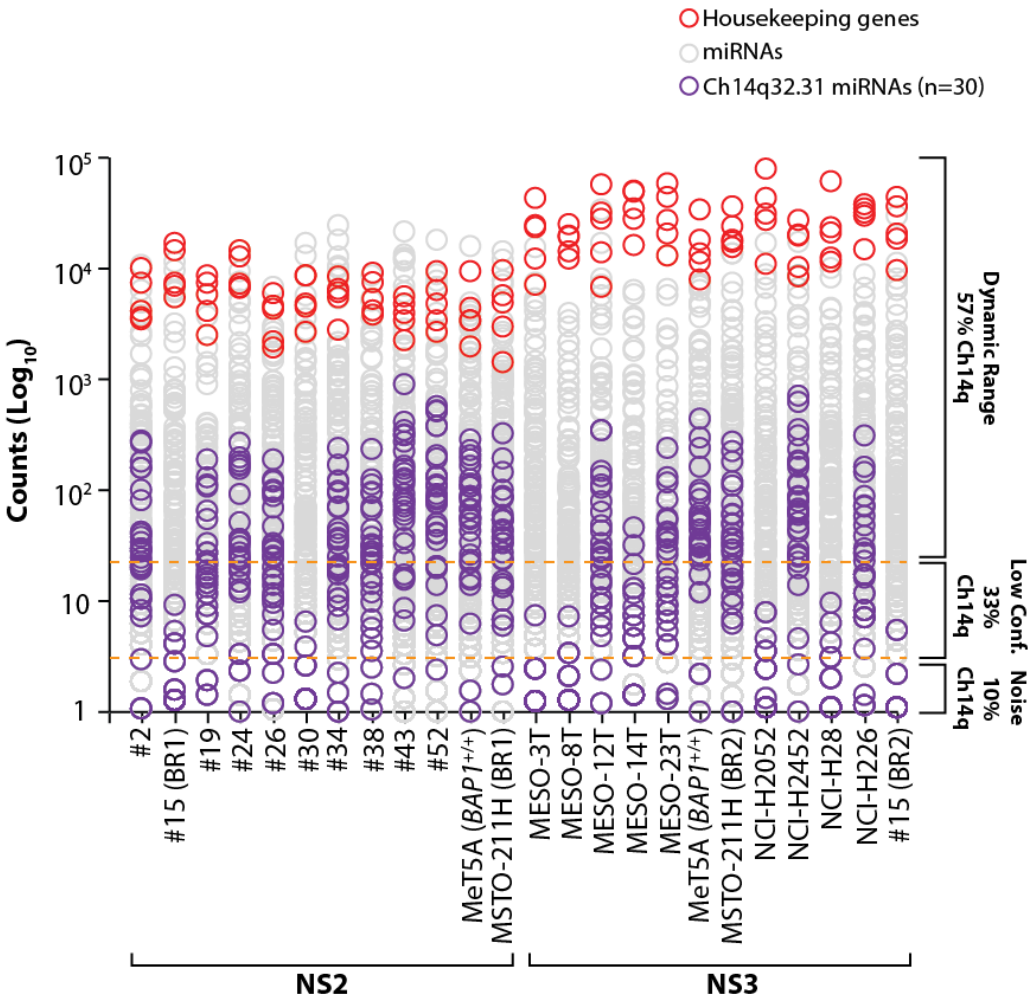

Figure 6.11: Distribution of ch14q32.31 miRNAs across the MPM cell line panel. Line plot displays log_{10} counts, post-background subtraction and normalisation, for 798 miRNAs and six housekeeping genes controls for cell lines from NS2 and NS3. Housekeeping genes are indicated by red hollow circles. Grey hollow circles represent all 798 miRNA genes, of which miRNAs from chromosome 14q32.31 locus are indicated by purple hollow circles.

The quality control measures and choice of reference genes for miRNA qRT-PCR are discussed in detail in chapter 7. The expression profile of the six selected miRNAs was successfully validated in the isogenic *BAP1*$^{w-/KO}$ cell lines and four MPM cell lines, #15, #30, #43 and #52. For each miRNA, decreased expression, relative to MeT5A (*BAP1*$^{+/+}$), was seen in MeT5A *BAP1*$^{w-/KO}$ cells, and in MPM cell lines #15 and #30, whilst increased expression was seen in MPM cell lines #43 and #52. These data confirmed the quantitative changes determined by NanoString analysis.

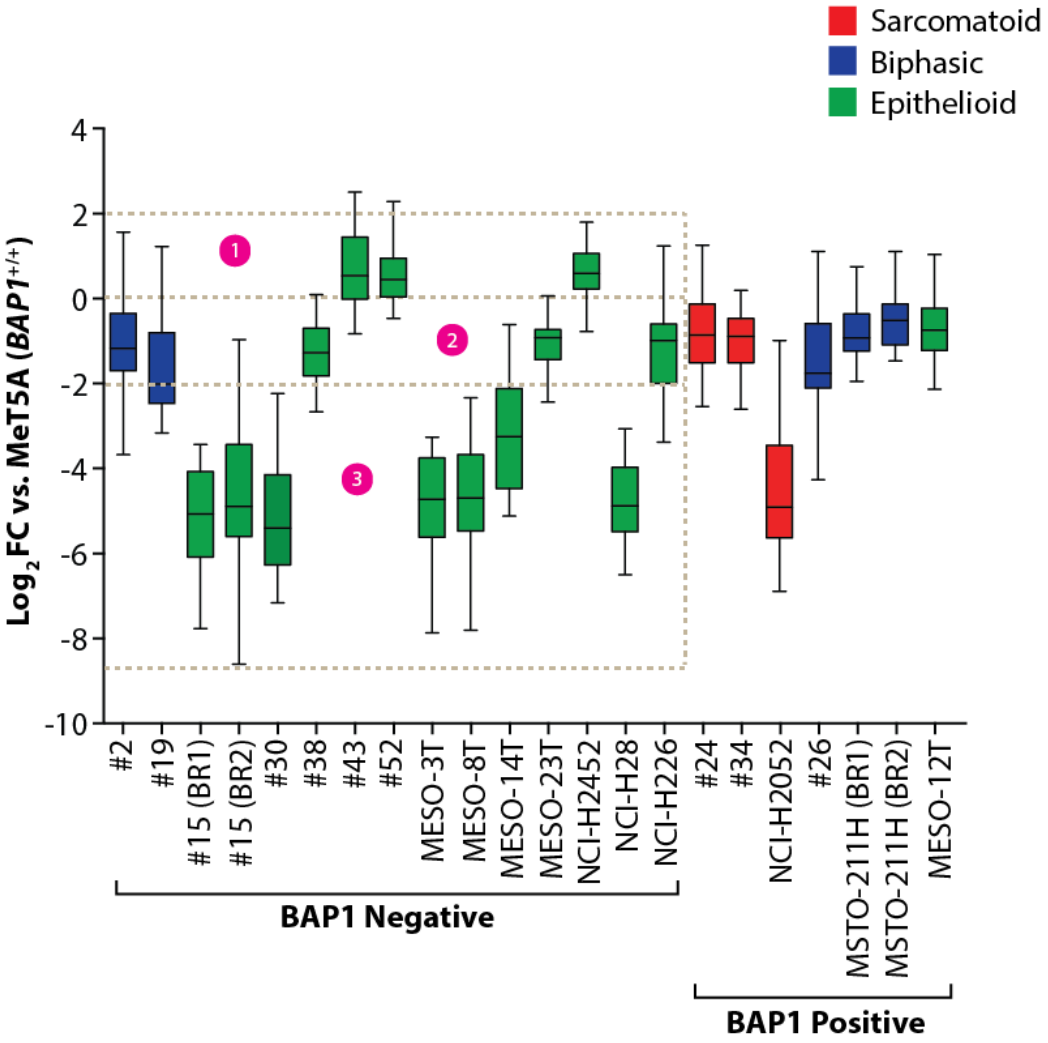

Figure 6.12: Range of ch14q32.31 miRNA locus expression in MPM cell lines from nCounter assays NS2 and NS3.

Box-and-whisker plots showing the range of fold change (FC) expression of ch14q32.31 miRNAs in MPM cell lines grouped by their BAP1 status. Log_2 FC in miRNA expression for MPM cell lines were generated vs. MeT5A (*BAP1*$^{+/+}$) from within their own assays. The median and interquartile range are displayed, the whisker boundaries are the 5th and 95th percentile. Colour coding of the box-and-whisker plots indicate the histological subtypes of MPM.

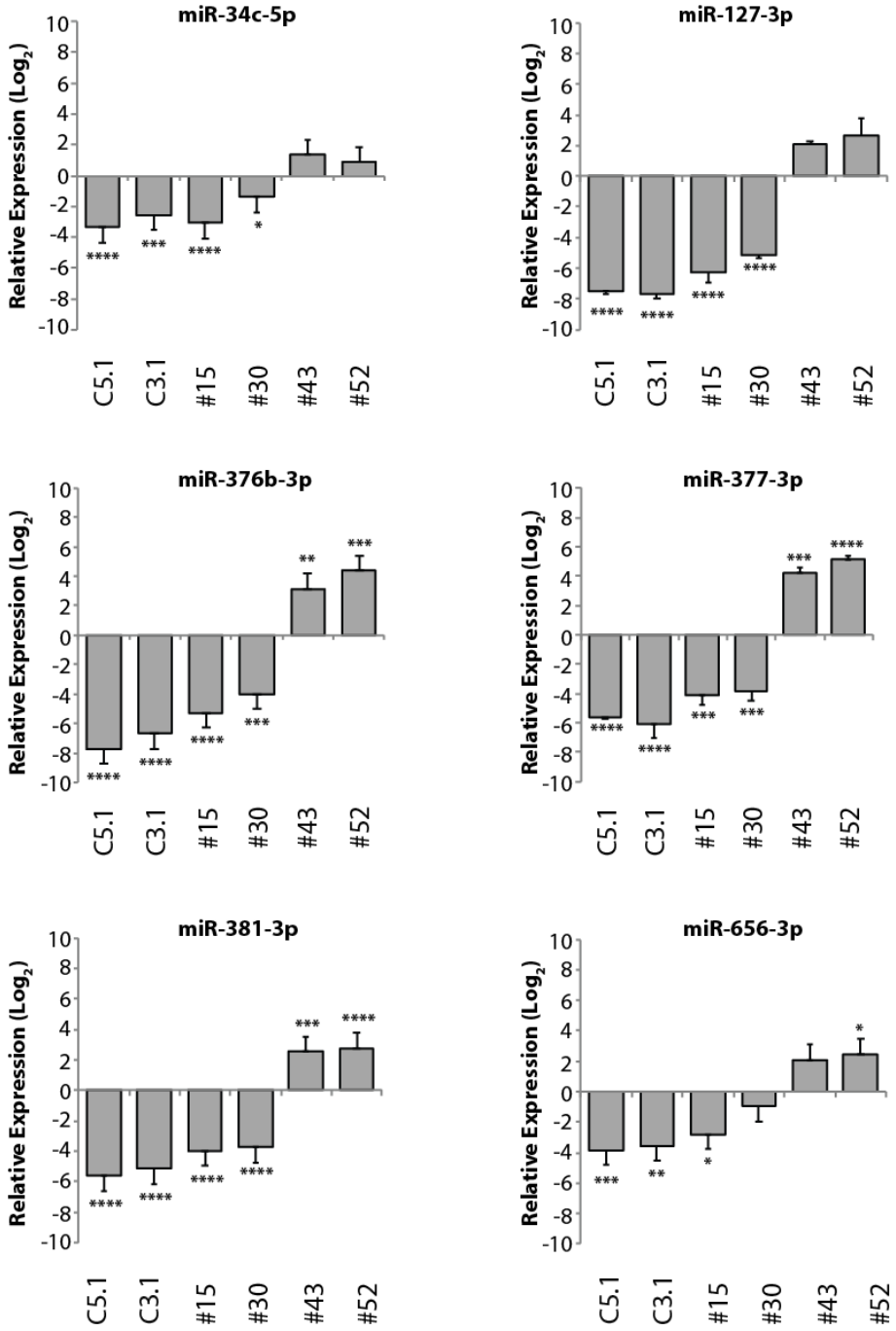

Figure 6.13: Validation of miRNA expression by qRT-PCR for representative HCL cluster C1 miRNAs from nCounter assay NS1.

Bar graphs show log_2 expression of six HCL cluster C1 miRNAs from NS1, as detected by qRT-PCR, normalised to the mean of SNORD95 and SNORD96A and relative to MeT5A (*BAP1*$^{+/+}$), in isogenic BAP1-mutant cell lines and selected MPM cell lines. N = three independent experiments, error bars show SD, one-way ANOVA with Dunnett's post-hoc test, ****P≤0.0001, ***P≤0.001, **P≤0.01, *P≤0.05.

6.10 Discussion

The focus of this chapter was to explore the possibility of a BAP1-dependent miRNome in MPM, by exploring differential miRNA expression between BAP1-negative and BAP1-positive MPM cell lines, and furthermore exploring the clinical relevance of key miRNAs that were differentially expressed in isogenic MeT5A *BAP1*-mutant cell lines as described in chapter 5. From this analysis, I observed a subset of miRNAs that were significantly deregulated in BAP1-negative MPM cell lines compared with BAP1-postive cell lines, however when their expression profiles were assessed in individual MPM cell lines, no clear association with BAP1 status was spotted. In addition, with the exceptions of miR-10a-5p and miR-628-5p which were significantly downregulated in both cell models of BAP1 loss, there were very few commonly responsive miRNAs between isogenic MeT5A cells and BAP1-negative MPM cell lines, with a small number displaying opposing expression profiles in the two cell models. Overall, there was little consistency in miRNA expression profiles between the two cell models, most miRNAs that were upregulated upon *BAP1* mutation in MeT5A cells were not highly expressed in MPM cell lines. However, I observed a group of predominately BAP1-negative, epithelioid MPM cell lines with substantial downregulation of ch14q32.31 miRNAs, phenocopying the expression profiles in the isogenic MeT5A *BAP1*$^{w-/KO}$ cell lines. I successfully validated a group of miRNAs from this locus in the isogenic MeT5A *BAP1*$^{w-/KO}$ cells and in selected MPM cell lines, thus confirming the quantitative expression of these miRNAs as determined by NanoString analysis.

I began the investigation into the BAP1-dependent miRNome in chapter 5, using the NanoString platform to profile isogenic MeT5A *BAP1*-mutated cells and found that BAP1 deficiency profoundly altered the miRNome. In this current chapter, I aimed to validate these differentially expressed miRNAs in a panel of patient-derived MPM cell lines, and to expand the knowledge of miRNA profiles in MPM. The NanoString miRNA analysis of the MPM cell line panel generated points of similarity and difference with previous findings in the isogenic MeT5A cells and from other studies profiling miRNAs in MPM.

Very little was known about the miRNA expression in MPM at the time Guled *et al.* published their study in 2009. They utilised the Agilent microarray-based platform for analysis of miRNA expression profiles in 17 MPM samples compared with normal mesothelial tissue samples (pericardium from healthy subjects) (Guled et al., 2009). Recently published studies have added to this knowledge base by attempting to define sets of miRNAs differentially expressed between MPM and matched normal tissues, and

between *BAP1*-mutant and *BAP1*-WT ccRCC tumours. I will discuss miRNA expression profiles obtained in my study relating to their findings. One of these studies utilised the NanoString platform to investigate miRNA expression in 105 MPM tissue samples and ten healthy pleural samples (De Santi et al., 2017). Another utilised the Agilent microarray platform to profile 27 FFPE tumour biopsy samples from unresected MPM patients and four healthy pleural samples (Truini et al., 2017). Lastly, a recent study re-analysed miRNA expression profiles acquired by the TCGA project on the Illumina HiSeq sequencing platform, for 350 ccRCC tumour samples classified as *BAP1*-mutant (35/350, 10%) or *BAP1*-WT (315/350, 90%) (Ge et al., 2017).

Combining data from chapters 5 and 6, comparison of miRNA profiles for isogenic MeT5A *BAP1*-mutant cells and BAP1-negative MPM cell lines highlighted little overlap of BAP1-responsive miRNAs identified in the two cell models. Of the seven miRNAs differentially expressed in both studies (Fig. 6.7D), five miRNAs (miR-99a-5p, miR-155-5p, miR-221-5p, miR-450-5p and let-7i-5p) showed increased expression in BAP1-negative compared with BAP1-positive MPM cell lines, but decreased expression in isogenic MeT5A *BAP1*-mutant cell lines relative to MeT5A ($BAP1^{+/+}$). Although the two cell models showed opposing responses, it is interesting that the studies by Truini *et al*. and De Santi *et al*. also reported downregulation of miR-99a-5p, let-7i-5p and miR-221-5p in MPM samples compared to healthy controls, although they did not stratify their samples by BAP1 status. In contrast, let-7i-5p expression was upregulated in *BAP1*-mutant ccRCC samples (Ge et al., 2017), which is in agreement with my MPM cell line data from NS2/NS3.

In my study, miR-628-5p and miR-10a-5p expression decreased in both *BAP1*-deficient cell models. Little is known about miR-628-5p function in cancer besides a role in decreasing the tumourigenicity of epithelial ovarian cancer cells by targeting the FGF receptor (Li et al., 2018). On the other hand, miR-10a-5p function is context dependent, acting as an oncomiR in gastric cancer (Lu et al., 2017) or a tumour suppressive miRNA in cervical cancer (Zhai et al., 2017). Neither miRNA has been previously associated with MPM or with *BAP1* mutation.

A group of eleven miRNAs (Fig. 6.8, outlined in cluster 1) were highly expressed in BAP1-positive compared with BAP1-negative MPM cell lines. In the literature, these miRNAs have shown a general trend towards upregulated expression in cancers. For example, miR-199a-3p was highly expressed in ovarian and breast cancer cells (Chen et al., 2008) suggesting

its possible involvement in tumour progression. miR-582-5p is upregulated in colorectal cancer (CRC) specimens and cell lines, and plays an important role in the progression of CRC by increasing cyclin D1 and c-MYC expression in an APC-dependent manner (Shu et al., 2016). miR-450a-5p is upregulated in endometrial carcinosarcomas and is part of a miRNA signature associated with EMT in these cancers (Castilla et al., 2011). miR-424-5p is up-regulated in gastric cancer tissues and cells, its overexpression promotes proliferation of gastric cancer cells (Wei et al., 2016). Although miR-137 expression was variable across MPM cell lines and tissues, high expression was linked to poor patient survival in an MPM survival data set (Johnson et al., 2017). Interestingly, in my study the greatest expression of miR-137 was detected in sarcomatoid and biphasic MPM cell lines; patients with sarcomatoid MPM present with more aggressive disease (Meyerhoff et al., 2015) hinting at a potential prognostic role for miR-137.

A further objective of this study was to explore the expression profiles for miRNAs in NS1 HCL clusters C3 (Fig. 6.9) and C1 (Fig. 6.10) across the MPM cell line panel. C1 miRNA expression was predominantly downregulated in isogenic *BAP1*$^{w-/KO}$ cells, including the striking downregulation of miRNAs that mapped to tumour suppressor locus on ch14q32.31. Consistent with this, many BAP1-negative MPM cell lines also silence expression of ch14q32.31 miRNAs (Fig. 6.10). Decreased expression of a select number of ch14q32.31 miRNAs were also detected in the study by De Santi *et al*. In their study the top five miRNAs statistically deregulated in MPM tissues, compared with healthy pleura, included downregulation of ch14q32.31 miRNAs miR-337-3p, miR-485-3p and miR-299-5p (De Santi et al., 2017). Furthermore, decreased expression of eight other ch14q32.31 miRNAs (miR-154-5p, miR-543, miR-382, miR-411-5p, miR-409-3p, miR-487b-3p, miR-323a-3p, miR-145-5p) was also detected. Although there was no stratification of the MPM cell lines by BAP1 status, ~80% of the MPM tumour samples analysed in the study were of the epithelioid subtype which are more likely to have *BAP1* mutations. This study has also highlighted that ch14q32.31 silencing is not only limited to cell lines as evidenced by their downregulation in tumour tissue, therefore it would be interesting in future to stratify the expression of ch14q32.31 miRNAs in MPM tissue by BAP1 status.

Importantly, my study is the first to report a link between BAP1 loss and the downregulation of ch14q32.31 miRNAs, which I initially discovered upon *BAP1* mutation in the isogenic MeT5A cell model, and successfully validated across a larger panel of BAP1-

negative MPM cell lines, exemplifying the advantages of gene-edited cells for the initial discovery phase of expression profiling.

In the study of differentially expressed miRNAs between *BAP1*-mutant and *BAP1* WT ccRCC tumours (Ge et al., 2017), the authors did not observe differential expression of ch14q32.31 miRNAs, which could be tumour-context dependent as BAP1 loss has contrasting effects in ccRCC, it is associated with worse survival in ccRCC (Minardi et al., 2016) but better prognosis in MPM (Righi et al., 2016). Taken together with my observation that not all BAP1-negative MPM cell lines silenced ch14q32.21 miRNAs, this may suggest this is not exclusively a BAP1-responsive phenotype. This is apparent in NCI-H2052, a BAP1-positive cell line that consistently clusters with BAP1-negative MPM cell lines and displayed a strong downregulation of ch14q32.31 expression, in difference with the moderate downregulation observed in other BAP1-postive MPM cell lines (Fig. 6.10). Of interest, we have previously shown that NCI-H2052 can phenocopy the effect of BAP1 loss in their response to HDACi, as they have a copy number loss of HDAC2 which reduces HDAC2 protein expression (see section 4.5). One potential mechanism of ch14q32.31 silencing is through deacetylation (see section 5.4), and although HDAC2 expression is lost in this cell line, one could speculate that the silencing of this cluster is the result of compensation via another HDAC or an indirect mechanism of HDAC2. Moreover, several studies have shown downregulation of ch14q32.31 miRNAs in different types of cancers where BAP1 mutation is not common (see section 5.4) and loss of ch14q32 is common in MPM (Balsara et al., 1999; Bjorkqvist et al., 1997; De Rienzo et al., 2000). It remains to be elucidated how the mechanism for silencing of ch14q32.31 miRNA genes are connected with *BAP1* mutation in isogenic MeT5A cells, and the loss of functional BAP1 protein in MPM cell lines.

In both isogenic *BAP1*$^{w-/KO}$ cells and BAP1-negative MPM cell lines, significantly upregulated miRNAs showed smaller fold changes in expression compared to miRNAs that decreased in expression with BAP1 loss. The HCL C3 miRNAs were predominantly upregulated in isogenic *BAP1*$^{w-/KO}$ cell lines, but overall this association was not recapitulated across BAP1-negative MPM cell lines (Fig. 6.9). Nonetheless, several miRNAs were upregulated in both BAP1-deficient cell models and are of interest through their association with cancer phenotypes. miR-4516 is one such BAP1-responsive miRNA candidate, which showed increased expression in isogenic *BAP1*$^{w-/KO}$ cells and BAP1-negative MPM cell lines, relative to MeT5A (*BAP1*$^{+/+}$) (Fig 6.9). Its over-expression has been reported in papillary thyroid carcinoma (Borrelli et al., 2017) and prostate cancer (Bell et al., 2015), and its levels are

elevated during stress-induced autophagy in NSCLC A549 cells exposed to heavy metals found in air pollution (Li et al., 2016a).

Increased miR-155-5p expression was observed in isogenic *BAP1*$^{w-/KO}$ cells but it was especially elevated in BAP1-positive MPM cell lines, relative to MeT5A (*BAP1*$^{+/+}$) (Fig. 6.9). miR-155-5p is a pro-inflammatory miRNA, its expression is induced during the macrophage inflammatory response (O'Connell et al., 2007). Of particular interest, miR-155-5p is also upregulated in MeT5A cells after exposure to multi-walled carbon nanofibers (Yin et al., 2016) indicating the presence of inflammation, which frequently occurs after exposure to asbestos fibres and has been linked to the initiation and progression of MPM. Although a link between BAP1 and inflammation in MPM is unspecified, and I observe an increase in miR-155-5p expression with the absence and presence of BAP1, it is possible that both scenarios of BAP1 loss and presence in MPM cells could contribute to the pro-inflammatory phenotype in MPM via an indirect mechanism Importantly, miR-155-5p is upregulated in many types of tumours and acts as an oncomiR, promoting malignant transformation and cancer progression by negatively regulating tumour-suppressive genes including TP53, RhoA and Socs1 (Gironella et al., 2007; Kong et al., 2008; Jiang et al., 2010a). miR-21-5p was similarly increased in isogenic *BAP1*$^{w-/KO}$ cells, relative to MeT5A (*BAP1*$^{+/+}$). Various reports show that the oncogenic miR-21-5p is induced by the IL-6-STAT3 inflammatory pathway, and mediates tumour initiation and malignant progression via targeting the tumour suppressors PTEN, TPM1, and BTG2 (Meng et al., 2007; Zhu et al., 2007; Liu et al., 2009a; Iliopoulos et al., 2010). These results identify a potential link between miRNAs, BAP1, inflammation and cancer, which is unsurprising as the expression of pro-inflammatory miRNAs were detected in cellular models of MPM.

In summary, I have characterised the miRNome of twenty MPM cell lines and explored differential miRNA expression in these cell lines in relation to BAP1 status. In conjunction, I have compared the miRNome of isogenic MeT5A *BAP1*-mutant cell lines to that of MPM cell lines with differing BAP1 status, to determine whether the isogenic model could predict BAP1-responsive miRNAs in patient-derived MPM cell lines. The coordinated expression of BAP1 and ch14q32.31 miRNAs was observed and validated for selected miRNAs. Moreover, this study has identified similar miRNAs to those identified in other miRNA profiling studies, in their attempts to define a set of miRNAs differentially expressed between MPM and healthy controls. My data suggest for the first time that BAP1-dependent miRNAs may in part account for the BAP1-deficient MPM phenotype. In chapter 7, I will adopt a different

line of investigation and explore the idea that miRNAs themselves may potentially regulate BAP1, by examining the correlative relationships between miRNAs and histological subtype and BAP1 status in MPM cell lines.

Chapter 7: Identification of microRNAs regulating BAP1 expression in MPM

7.1 Introduction

Several thousand human genes, representing approximately two-thirds of the protein-coding genes, are potential targets for regulation by miRNAs (Friedman et al., 2009), suggesting that post-transcriptional regulation mediated by miRNAs may be relevant to a large proportion of cellular processes. Several computational tools have been developed to predict mRNA transcripts that are targeted by miRNAs in humans and animals. These algorithms are designed to identify miRNAs that are predicted to target specific gene transcripts, by employing methods such as seed complementarity (Lewis et al., 2003) and the thermodynamic properties of the mRNA-miRNA duplex (Lekprasert et al., 2011). The former method involves identifying miRNAs that show perfect complementarity of their seed region (conserved sequence at positions 2-8 from the miRNA 5′ end) to the seed site found in the 3′UTR of the target mRNA. The latter assesses the stability of the miRNA-mRNA duplex by calculating the free energy of the predicted binding.

One way of conceptualising the action of miRNAs is in the context of a network of interactions between transcription factors (TF), miRNAs and target genes (Fig. 7.1). These gene regulatory networks are made up of basic motifs, such as feedback loops (FBLs) and feedforward loops (FFLs) (Tsang et al., 2007). Conventionally, FFLs are composed of two inputs, one of which (TF) regulates the other (miRNA) yet both jointly regulate the expression of a third component (the target gene) (Mangan and Alon, 2003). This network is "coherent" in that the post-transcriptional repression by the miRNA runs in parallel with transcriptional inhibition of the same target gene by the TF. An "incoherent" FFL is defined as the induction of both the target gene and the miRNA by the TF, which is counterintuitive as two opposing actions are driven by the TF. One biological example of this is c-Myc, which activates transcription of miR-17-5p and miR-20a, along with E2F1, which is post-transcriptionally silenced by these same miRNAs, the (O'Donnell et al., 2005). It has been suggested that these miRNAs contribute towards a homeostatic mechanism to mediate the balance between c-Myc-mediated cell proliferation and the pro-apoptotic functions of E2F1 (Woods et al., 2007).

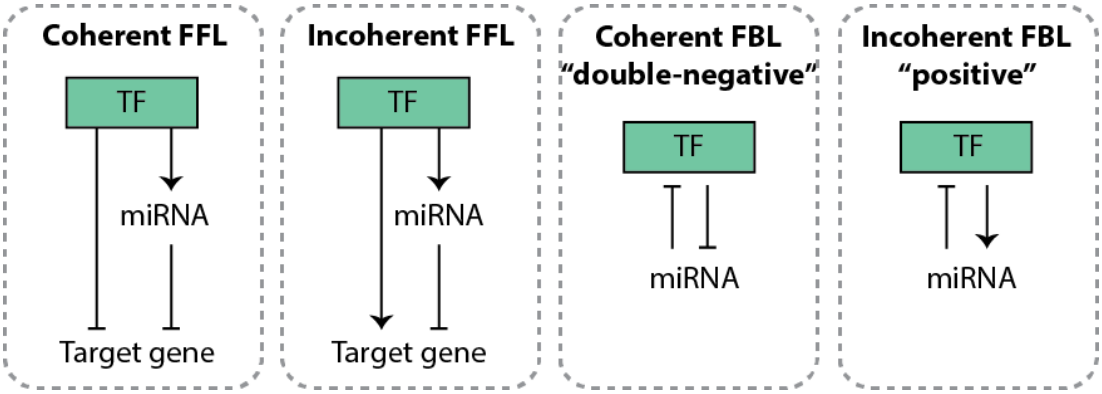

Figure 7.1: Schematic representation of common miRNA-target regulatory networks.
Four major classes of miRNA-associated network motifs are represented. FFL: feedforward loop, FBL: feedback loop, TF: transcription factor.

In a coherent "double-negative" FBL, a miRNA represses a TF, which in turn represses expression of the miRNA itself. In an incoherent "positive" FBL, a TF induces the expression of the miRNA, the miRNA in turn represses the TF (Fig. 7.1). These relatively simple reciprocal FBLs are typically embedded in more complex networks, such that which one of the two inputs remains active will depend on additional inputs to influence the balance of expression in one direction or the other (Tsang et al., 2007).

Loss or inactivation of BAP1 may occur as a result of chromosomal deletion involving the *BAP1* gene locus on ch3p21.1, or due to sequence variation as a result of mutations in the *BAP1* gene (see section 1.3.2). Bi-allelic inactivating mutations or deletions in the *BAP1* gene are consistently described as somatic events in 50% of MPM cases, and the strong correlation between *BAP1* mutation and loss of IHC staining for BAP1 has been reported as a reliable marker of *BAP1* inactivation in tumour cells (Murali et al., 2013; Bott et al., 2011; Yoshikawa et al., 2012; Farzin et al., 2015). However, 25% of MPM tumours without genetic alteration of *BAP1* failed to display IHC staining for BAP1 (Bott et al., 2011), raising the possibility of post-transcriptional or post-translational repression of BAP1 in a subset of MPM tumours.

7.2 Aims and objectives

I am interested in the regulation of BAP1 by miRNAs in MPM. It is known that there are subsets of MPM tumours which lose BAP1 protein expression without an accompanying

BAP1 mutation profile, and the mechanism by which this occurs is still unclear. The aim of this chapter was to investigate whether specific miRNAs post-transcriptionally regulate BAP1 mRNA to reduce its protein expression in MPM, initially taking a correlative approach to this question by profiling the expression of candidate miRNAs across the panel of 15 MPM cell lines with varying BAP1 status that were available that the time this work was undertaken (see Fig. 3.3). Furthermore, I explored the possibility of potential FBL/FFL between BAP1 and candidate miRNAs in MPM, as BAP1 may also regulate miRNAs within a gene regulatory network.

My specific objectives were to:

1. Utilise target prediction algorithms to identify candidate miRNAs that may target BAP1 post-transcriptionally.
2. Profile the expression of candidate miRNAs for BAP1 regulation in a panel of MPM cell lines with varying BAP1 status.
3. Identify correlative relationships between candidate miRNAs and histological subtypes of MPM or BAP1 status.
4. Demonstrate whether candidate miRNAs function in gene regulatory networks with BAP1.

7.3 *In silico* identification of miRNAs predicted to target BAP1

To begin the search for candidate human mature miRNAs predicted to negatively regulate BAP1 expression, four target prediction algorithms (TargetScan, PicTar, miRDB and microRNA.org) were used to identify miRNAs that are predicted to bind the 3' UTR region of the BAP1 mRNA sequence (Fig. 7.2A). Initially, I selected mature miRNA candidates predicted by at least three independent algorithms for experimental validation (Fig. 7.2A). These included members of the miR-125 family (miR-125a/b) and all members of the miR-200 family (miR-141, miR-200a/b/c, miR-429). I was also interested in miR-31-5p, common to two target prediction sites (TargetScan and PicTar) as miR-31-5p was recently reported as a direct regulator of BAP1 in NSCLC (Yu et al., 2016). Additionally, the miR-10 family (miR-10a/b), common to two target prediction algorithms (miRDB and microRNA.org), was included in our candidate list for experimental verification. I was interested in this family as preliminary PCR array data had suggested that they could function in a double-negative FBL with BAP1, as their expression was downregulated in isogenic MeT5A *BAP1*-mutant cell line C5.1 ($BAP1^{w-/KO}$), compared to MeT5A ($BAP1^{+/+}$) (Coulson et al., unpublished data).

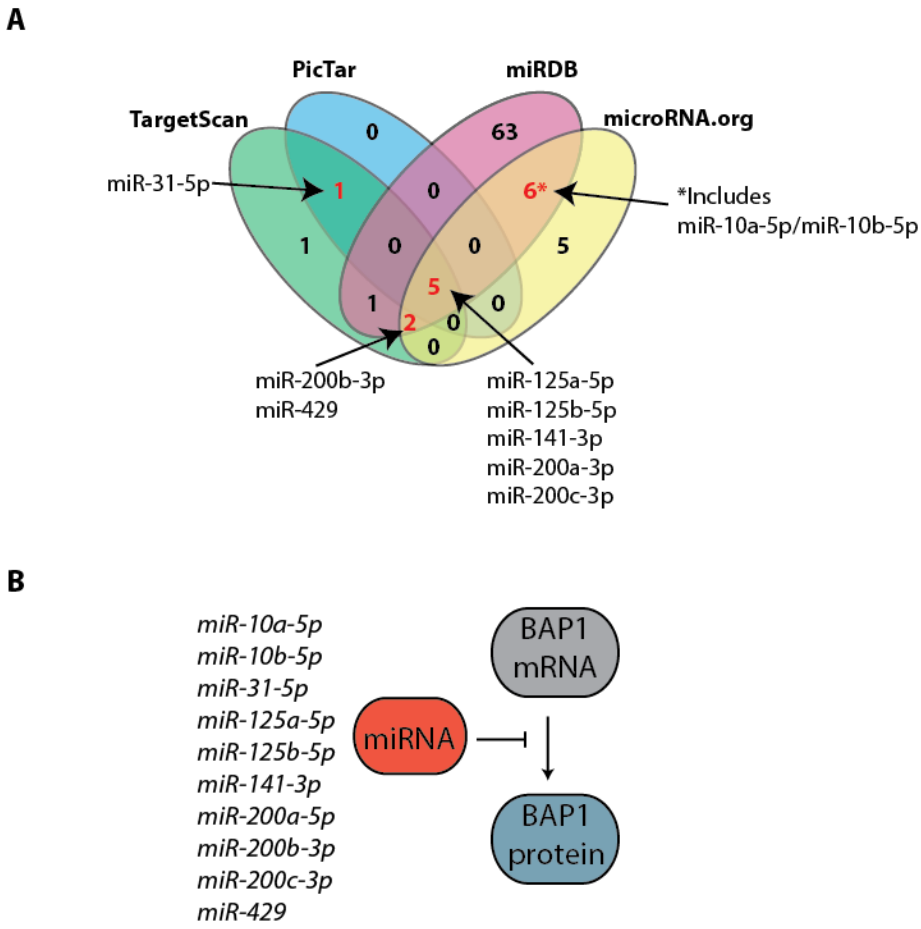

Figure 7.2: Candidate miRNAs predicted to negatively regulate BAP1 expression. **A** Venn diagram of human mature miRNAs predicted to target BAP1 mRNA. Four miRNA prediction algorithms (TargetScan, PicTar, miRDB and microRNA.org, accessed 19/05/16) we used to identify candidate miRNAs predicted to bind the 3' untranslated region (3'UTR) of the BAP1 mRNA sequence. All candidate miRNAs common to ≥3 target prediction sites were selected for experimental verification, in addition to the miR-10 family members miR-10a-5p and miR-10b-5p (miRDB/microRNA.org) and miR-31-5p (TargetScan/PicTar). **B** Schematic of candidate miRNAs predicted to post-transcriptionally downregulate BAP1 protein expression.

The schematic (Fig. 7.2B) summarises the complete list of mature miRNA candidates predicted to post-transcriptionally downregulate BAP1 protein expression, which were selected for experimental investigation. I utilised qRT-PCR to investigate the expression level of these candidate miRNAs in a panel of MPM cell lines with varying BAP1 status and histological subtypes.

7.4 Selection of appropriate miRNA housekeeping genes for normalisation

Accurate determination of miRNA levels by qRT-PCR can be affected by the selection of appropriate housekeeping genes for normalisation between samples. In view of this,

mRNA housekeeping genes such as ß-actin or GAPDH are unsuitable for this application as they are much larger in size and may differ from miRNAs in terms of their stability, extraction efficiency and the process of reverse transcription and PCR amplification. There is no universal miRNA housekeeping gene suitable for all experimental conditions, however small non-coding RNA controls are commonly used as reference RNAs. These include small nucleolar RNAs (SNORDs). Four SNORDs (SNORD61, SNORD68, SNORD95, SNORD96A) were selected from amongst reference SNORDs recommended by the assay manufacturer (Qiagen), as potential housekeeping genes for normalisation of miRNA qRT-PCR data. SNORD genes are closer in size to miRNAs (<200 bp), they belong to the same class of non-coding RNAs as miRNAs, and are relatively abundant and stably expressed genes (Schwarzenbach et al., 2015). I tested the amplification efficiency for each SNORD primer using a two-fold dilution series of cDNA prepared from MSTO-211H cells (Fig. 7.3A - D). The four SNORD primers displayed a linear response to template amount over a 16-fold dilution range. Amplification efficiencies between 90-101% were calculated, which is within acceptable parameters.

A critical aspect of miRNA expression profiling by qRT-PCR is the extraction efficiency, as total RNA sample preparations can differ in the proportion of miRNA extracted. I compared Cq values for each SNORD housekeeping gene from miRNA extracted from MeT5A (*BAP1*$^{+/+}$) cells on three separate occasions, to establish reproducibility (Fig. 7.4A - D). SNORD95 (Fig. 7.4C) was more abundantly expressed than the other SNORDs. Furthermore, similar Cq values for each SNORD across biological replicates were indicative of consistent miRNA extraction efficiency.

Another parameter required for a robust qRT-PCR assay is the invariable expression of the housekeeping gene(s) across the test sample set. Thus, I measured the abundance of all four SNORD genes in the panel of MPM cell lines obtained from ATCC in order to check their suitability for use as housekeeping genes to normalise miRNA expression. In comparison to ß-actin, which displayed Cq values between 15 and 16 (Fig. 7.5A), all four SNORD genes were less abundant, displaying Cq values between 23 and 27 across the cell panel (Fig. 7.5B – E).

However, for each SNORD the Cq values were fairly consistent between cell lines (SNORD61: 25.86 ± 0.52, SNORD68: 25.30 ± 0.57, SNORD95: 24.26 ± 0.53, SNORD96A: 26.35 ± 0.70) with SNORD95 most abundant in each case. Based on these data, we selected one

less abundant (SNORD96A) and one more abundant (SNORD95) housekeeping gene, using their mean value to normalise miRNA expression data.

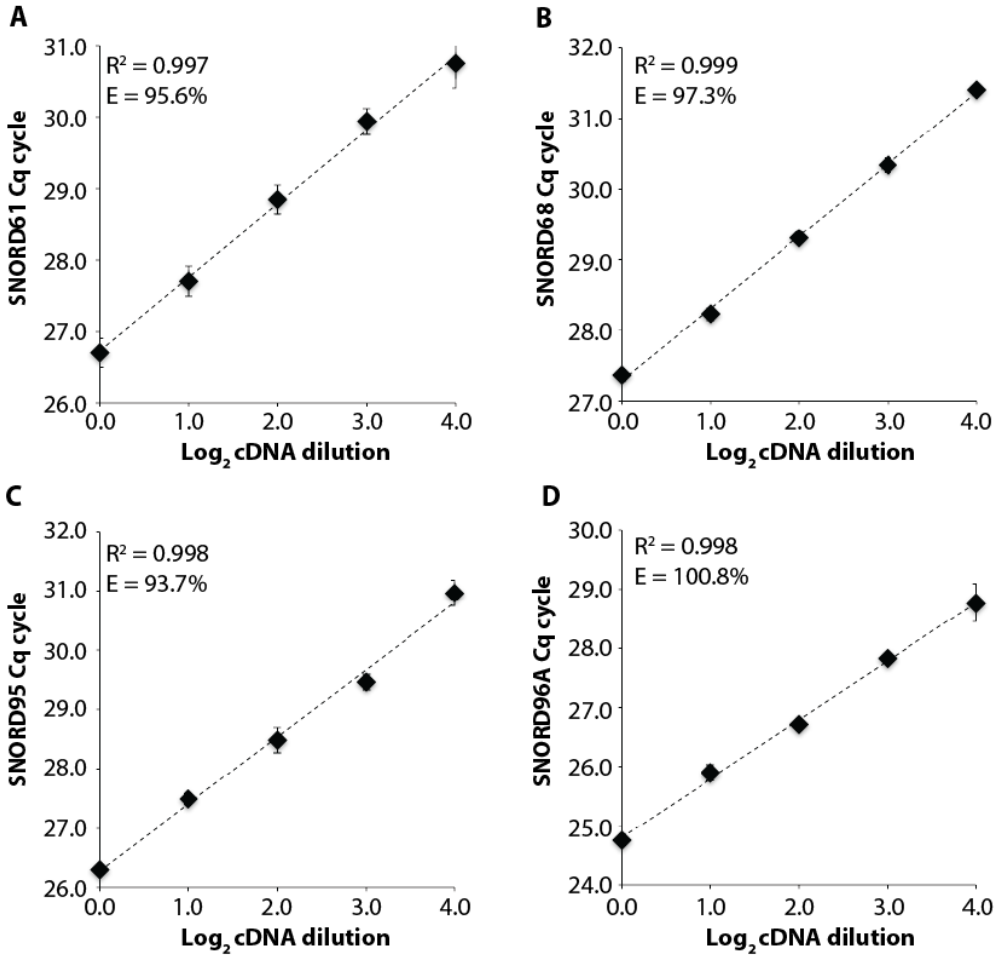

Figure 7.3: Determining SNORD housekeeping gene primer efficiencies for qRT-PCR.
Scatter plots show serial two-fold dilutions of MSTO-211H cDNA on a $\log_2$ scale and corresponding Cq values detected by qRT-PCR for **A** SNORD61, **B** SNORD68, **C** SNORD95 and **D** SNORD96A. E=amplification efficiency, all primers show efficiency values between 90-101%, within acceptable parameters. N=one independent experiment, error bars show SD from three technical replicates for each cDNA dilution.

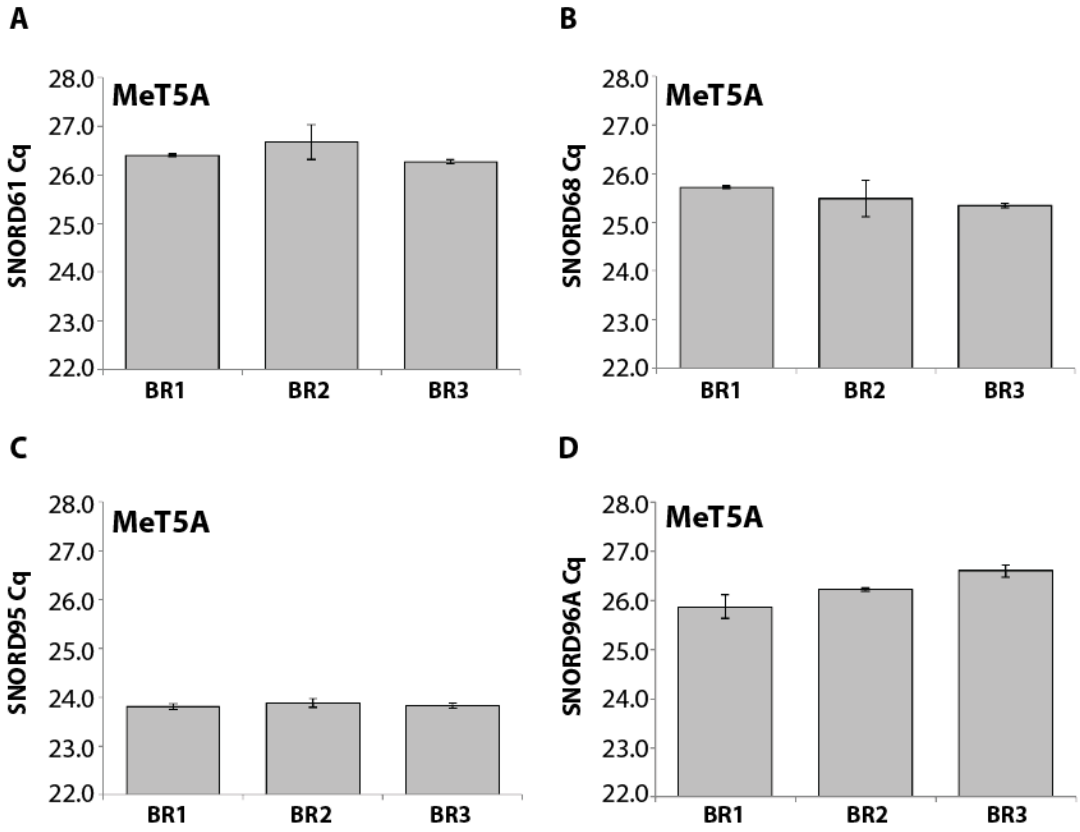

Figure 7.4: Reproducibility of SNORD housekeeping genes across biological replicate miRNA extracts.

Bar graphs show Cq values detected by qRT-PCR for **A** SNORD61, **B** SNORD68, **C** SNORD95 and **D** SNORD96A in three biological replicates (BR) of MeT5A (*BAP1*$^{+/+}$) Error bars show SD from three technical replicates. Y-axis truncated to show the range of 22 – 28 Cq values in all panels. For each housekeeping gene, comparable Cq values across biological replicates was indicative of similar miRNA extraction efficiency.

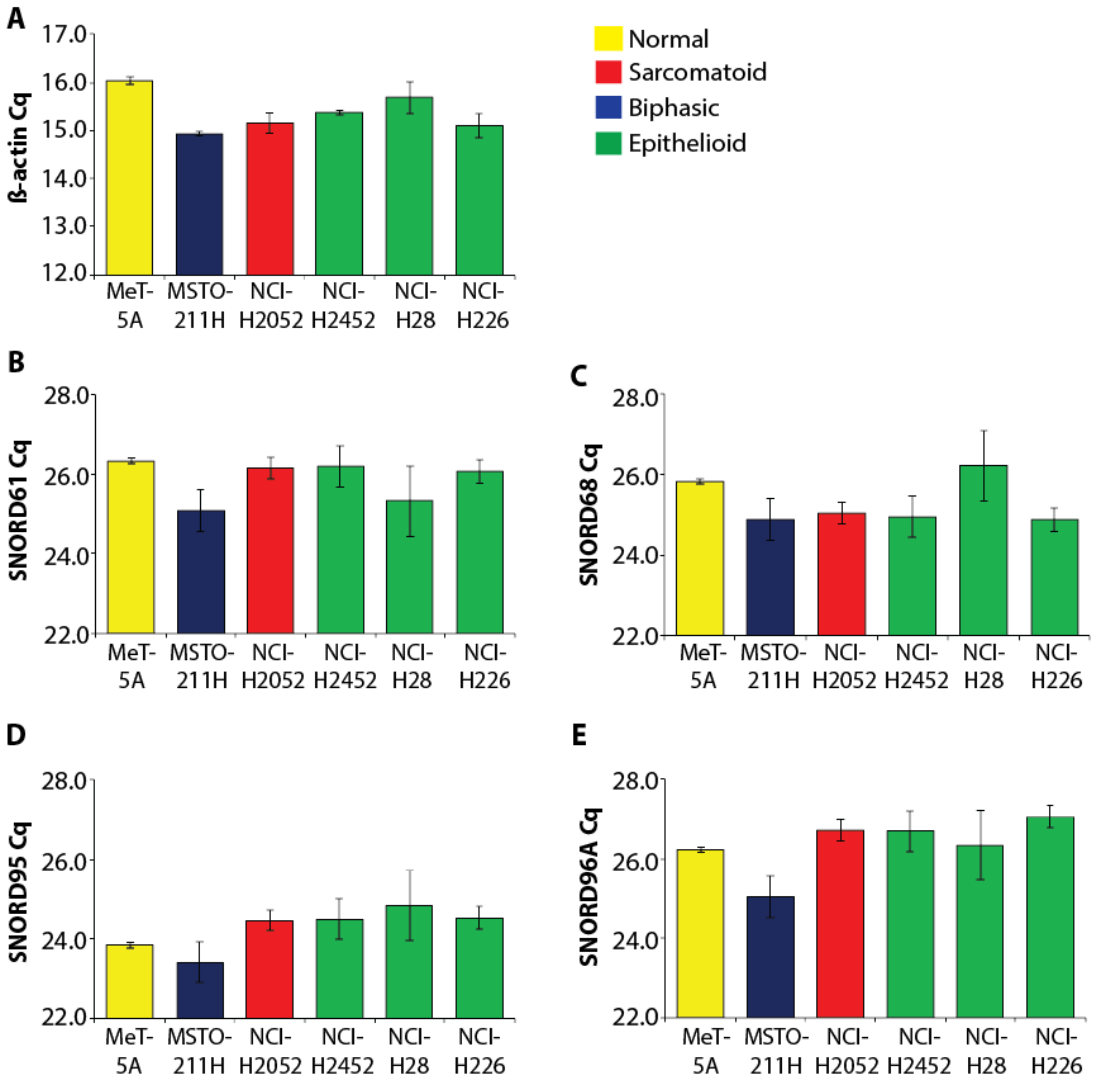

Figure 7.5: Selecting SNORD housekeeping genes for normalising miRNA qRT-PCR data.

Bar graphs show Cq values detected by qRT-PCR for **A** ß-actin, **B** SNORD61, **C** SNORD68, **D** SNORD95 and **E** SNORD96A in MeT5A (*BAP1*$^{+/+}$) and a panel of MPM cell lines from the ATCC. The higher abundance SNORD95 and lower abundance SNORD96A were chosen for normalisation of miRNA qRT-PCR data. Error bars show SD from three biological replicates. Colour coding indicates the histological subtypes of MPM.

7.5 Profiling the expression of candidate miRNAs for BAP1 regulation in MPM cell lines

7.5.1 Analysing expression differences between MPM cell lines and histological subtypes for candidate miRNAs

Using the miScript SYBR Green PCR system, I examined whether the expression of candidate miRNAs (predicted to target BAP1) may be associated with histological subtypes of MPM, to rule out any subtype-specific effects that may affect the regulatory relationship between miRNA and BAP1. I analysed the expression levels of ten mature miRNAs in the panel of MPM cell lines from ATCC and MesobanK. miRNA expression was normalised to the mean value of SNORD95 and SNORD96A for each cell line and expressed relative to the normal mesothelial cell line MeT5A (*BAP1*$^{+/+}$). These data were then ordered from lowest to highest expression to illustrate the range of miRNA expression across the cell lines, which are colour coded by their histological subtype (Fig. 7.6, left panels). In conjunction, the cell lines were stratified according to their histological subtype in order to visualise expression differences between MPM subtypes for candidate miRNAs (Fig. 7.6, right panels).

For the miR-10 family members, approximately half of the cell lines expressed miR-10a-5p (Fig. 7.6A) and miR-10b-5p (Fig. 7.6C) at a similar level to MeT5A (*BAP1*$^{+/+}$), whilst the remaining cell lines showed higher expression of either miRNA compared to MeT5A (*BAP1*$^{+/+}$). Overall, the sarcomatoid MPM cell lines tended towards higher median expression of miR-10a-5p (Fig. 7.6B) and miR-10b-5p (Fig. 7.6D) when compared to the epithelioid and biphasic MPM cell lines. In contrast, miR-31-5p expression was undetectable in a third of MPM cell lines, with the majority showing lower miR-31-5p expression than MeT5A (*BAP1*$^{+/+}$), which would be consistent with a tumour suppressive role for this miRNA (Fig. 7.6E). When the cell lines were grouped by histological subtype, there was little difference in median miR-31-5p expression (Fig. 7.6F).

The miR-125 family members miR-125a-5p and miR-125b-5p had notably different expression patterns across the MPM cell line panel. The majority of MPM cell lines had similar or lower miR-125a-5p expression than MeT5A (*BAP1*$^{+/+}$) (Fig. 7.6G), and there were no trends in miR-125a-5p expression between MPM subtypes (Fig. 7.6H).

Figure 7.6

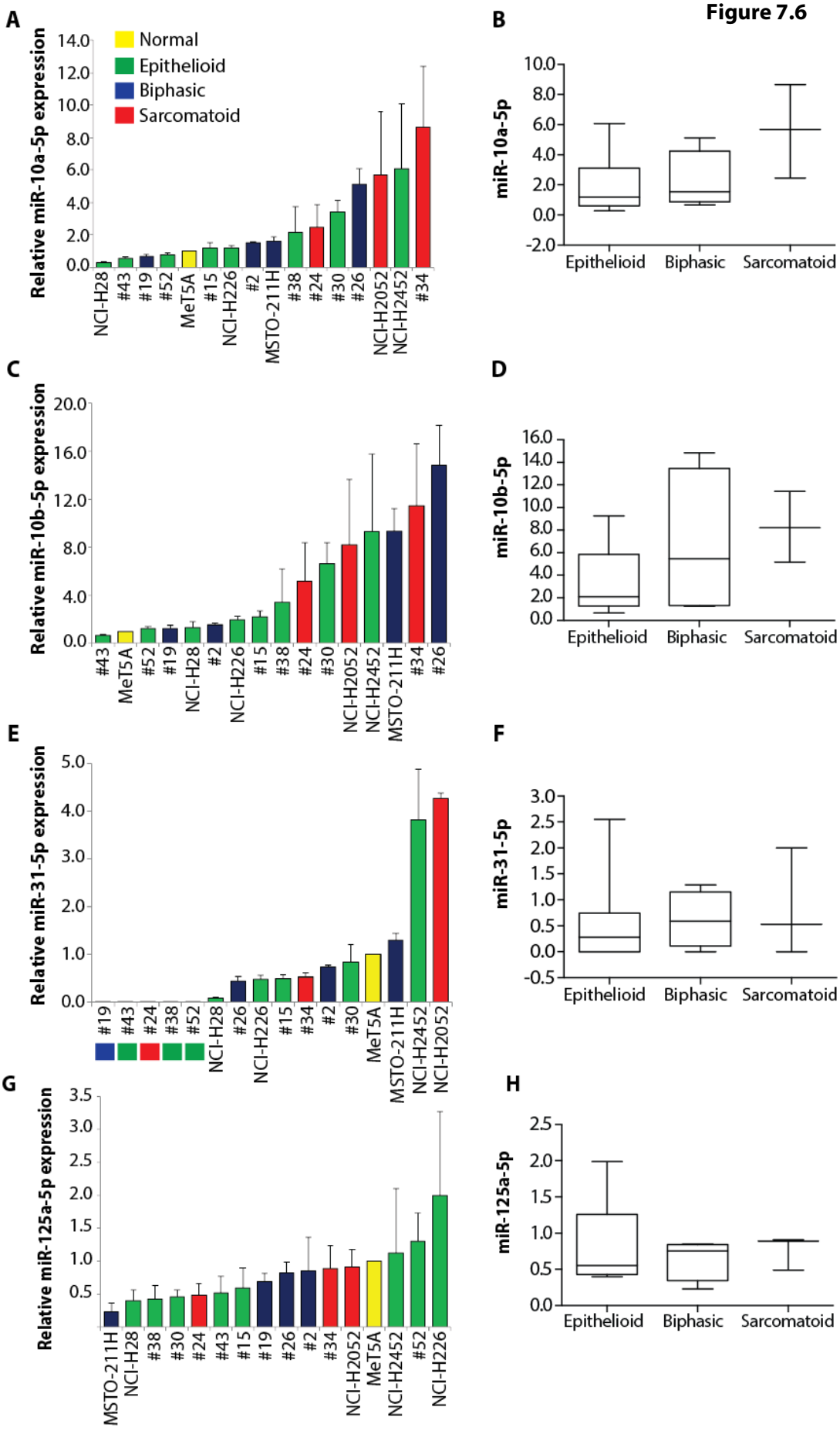
A
Relative miR-10a-5p expression
Normal
Epithelioid
Biphasic
Sarcomatoid
NCI-H28 #43 #19 #52 MeT5A #15 NCI-H226 #2 MSTO-211H #38 #24 #30 #26 NCI-H2052 NCI-H2452 #34
B
miR-10a-5p
Epithelioid Biphasic Sarcomatoid
C
Relative miR-10b-5p expression
#43 MeT5A #52 #19 NCI-H28 #2 NCI-H226 #15 #38 #24 #30 NCI-H2052 NCI-H2452 MSTO-211H #34 #26
D
miR-10b-5p
Epithelioid Biphasic Sarcomatoid
E
Relative miR-31-5p expression
#19 #43 #24 #38 #52 NCI-H28 #26 NCI-H226 #15 #34 #2 #30 MeT5A MSTO-211H NCI-H2452 NCI-H2052
F
miR-31-5p
Epithelioid Biphasic Sarcomatoid
G
Relative miR-125a-5p expression
MSTO-211H NCI-H28 #38 #30 #24 #43 #15 #19 #26 #2 #34 NCI-H2052 MeT5A NCI-H2452 #52 NCI-H226
H
miR-125a-5p
Epithelioid Biphasic Sarcomatoid

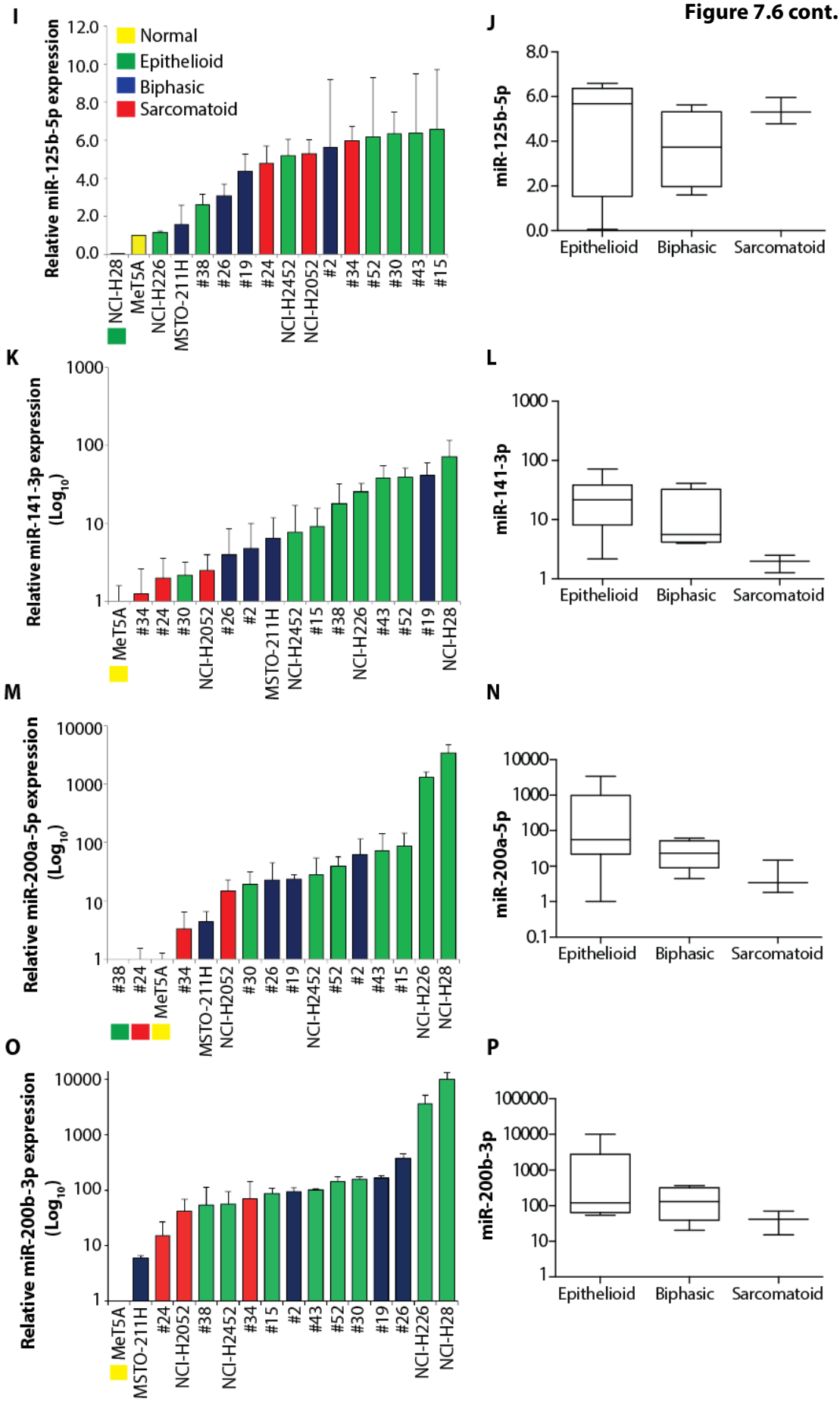
I
Relative miR-125b-5p expression
Normal
Epithelioid
Biphasic
Sarcomatoid
NCI-H28
MeT5A
NCI-H226
MSTO-211H
#38
#26
#19
#24
NCI-H2452
NCI-H2052
#2
#34
#52
#30
#43
#15
J
miR-125b-5p
Epithelioid
Biphasic
Sarcomatoid
K
Relative miR-141-3p expression (Log10)
MeT5A
#34
#24
#30
NCI-H2052
#26
#2
MSTO-211H
NCI-H2452
#15
#38
NCI-H226
#43
#52
#19
NCI-H28
L
miR-141-3p
Epithelioid
Biphasic
Sarcomatoid
M
Relative miR-200a-5p expression (Log10)
#38
#24
MeT5A
#34
MSTO-211H
NCI-H2052
#30
#26
#19
NCI-H2452
#52
#2
#43
#15
NCI-H226
NCI-H28
N
miR-200a-5p
Epithelioid
Biphasic
Sarcomatoid
O
Relative miR-200b-3p expression (Log10)
MeT5A
MSTO-211H
#24
NCI-H2052
#38
NCI-H2452
#34
#15
#2
#43
#52
#30
#19
#26
NCI-H226
NCI-H28
P
miR-200b-3p
Epithelioid
Biphasic
Sarcomatoid

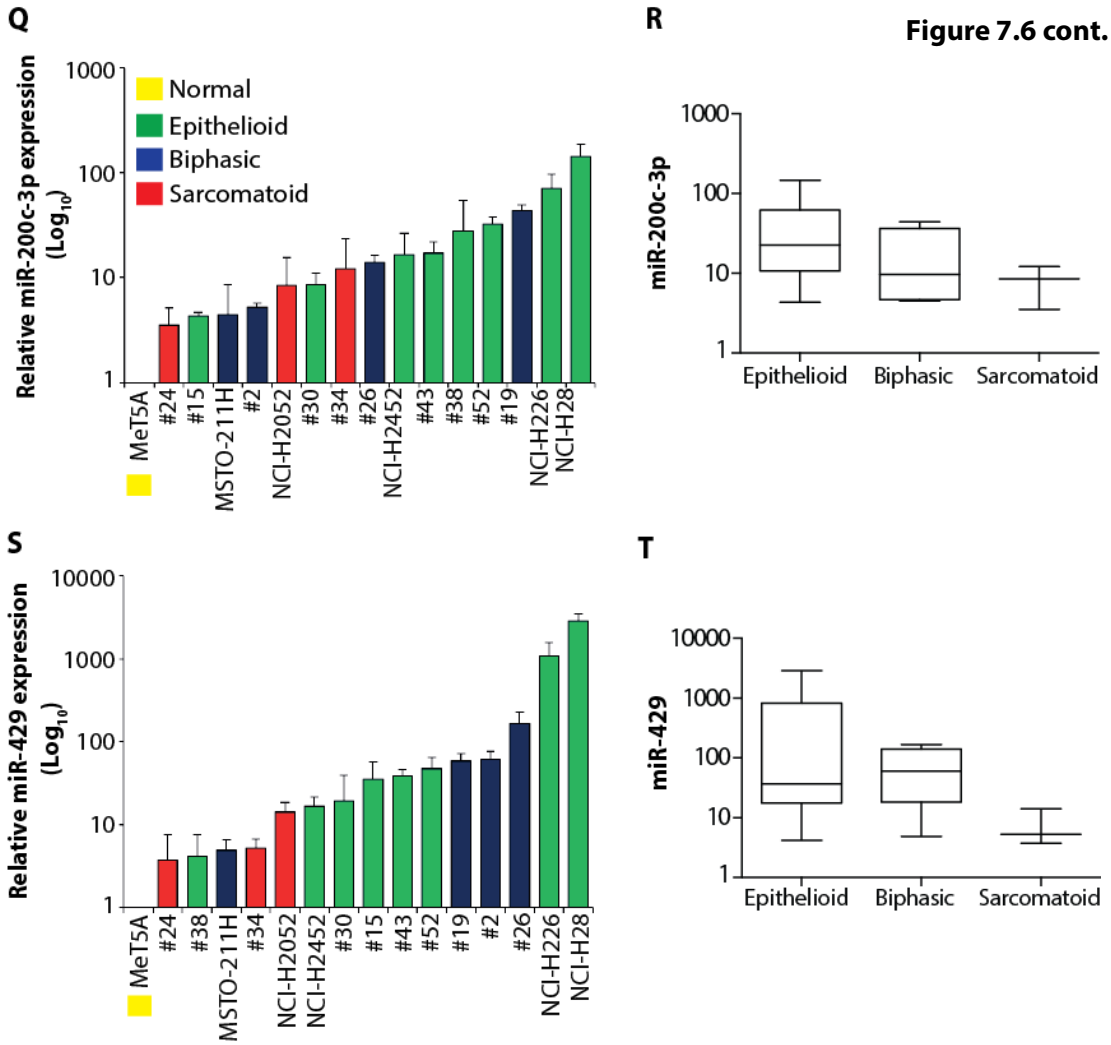

Figure 7.6: Analysis of candidate miRNA expression in a panel of MPM cell lines. Bar graphs show miRNA expression as detected by qRT-PCR, normalised to the mean of SNORD95 and SNORD96A and relative to MeT5A (*BAP1*$^{+/+}$), across the panel of MPM cells from ATCC and MesobanK. The box and whisker plots show the spread of miRNA expression data, normalised to the mean of SNORD95 and SNORD96A and relative to MeT5A (*BAP1*$^{+/+}$), in the MPM cell lines grouped by their histological subtype: the median and interquartile range are displayed, the whisker boundaries are the 5th and 95th percentile. Expression data is visualised in these formats for **A-B** miR-10a-5p, **C-D** miR-10b-5p, **E-F** miR-31-5p, **G-H** miR-125a-5p, **I-J** miR-125b-5p, **K-L** miR-141-3p, **M-N** miR-200a-5p, **O-P** miR-200b-3p, **Q-R** miR-200c-3p, **S-T** miR-429. N = three independent experiments, error bars show SD. Colour coding indicates the histological subtypes of MPM. Differences in miRNA expression between histological sub-types did not reach statistical significance.

In contrast, almost all MPM cell lines had higher expression of miR-125b-5p compared to MeT5A (*BAP1*$^{+/+}$) (Fig. 7.6I). When the cell lines were grouped by histological subtype, the miRNA expression profile for epithelioid and biphasic cell lines shows a wider spread of data compared to the sarcomatoid cell lines (Fig. 7.6J).

The miR-200 family are clustered at two locations in the genome; miR-141-3p and miR-200c-3p are located on chromosome 12, whilst miR-200a-5p, miR-200b-3p and miR-429 are located on chromosome 1 (Humphries and Yang, 2015). The miR-200 family members form two functional groups based on the similarity of their seed sequences, miR-141-3p and miR-200a-5p form one group, and miR-200b-3p, miR-200c-3p and miR-429 form the second. Interestingly, I was unable to detect expression of miR-200 family members in the normal mesothelial cell line MeT5A (*BAP1*$^{+/+}$). Therefore, in almost every MPM cell line there was higher miRNA expression for all family members when compared to MeT5A (*BAP1*$^{+/+}$) (Fig. 7.6K, 7.6M, 7.6O, 7.6Q and 7.6S). Overall, no significant association was found between any candidate miRNAs and histological subtype of MPM. It was important to rule out such subtype-specific associations before exploring correlation between candidate miRNAs and BAP1 status.

7.5.2 Analysing expression differences between BAP1-negative and BAP1-positive MPM cell lines for candidate miRNAs

The ten candidate miRNAs have predicted target sites on the 3'UTR of BAP1 mRNA, therefore it was hypothesised that these miRNAs could negatively regulate BAP1 mRNA expression, leading to a reduction in BAP1 protein levels. If this is the case, then it is predicted that expression of the miRNA would exhibit an inverse correlation with that of their target BAP1. Such correlative studies are often a first step in matching miRNAs to target genes (Yu et al., 2016). However, it should be noted that correlation is a two-way relationship and could also reflect regulation of the miRNA by BAP1, as I have previously explored in chapters 5 and 6. This may be confounded by *BAP1* mutation, in most cases low BAP1 expression is the result of mutation irrespective of miRNA expression, as such it would be more likely to detect the relationship where BAP1 regulates the miRNA, that the other way around. However, I will monitor two candidate MPM cell lines, #15 and #30, where BAP1 mRNA is expressed at 15-30% relative to MeT5A (*BAP1*$^{+/+}$) but have negligible BAP1 protein expression, which suggests post-transcriptional regulation by miRNAs might be important in these cell lines.

To investigate, MPM cell lines were initially grouped by their BAP1 status (see section 3.6) and the spread of candidate miRNA expression in each group was assessed. There was a significant difference in expression of the miR-10 family members when the MPM cell lines were grouped by their BAP1 status. In fact, this analysis revealed significantly lower miR-10a-5p (Fig. 7.7A) and miR-10b-5p (Fig. 7.7B) expression in BAP1-negative cell lines. The expression profile for miR-10a-5p is in agreement with data generated by Nanostring analysis of these cell lines (Fig 6.7D) but would be incompatible with the predicted role as miRNAs that target BAP1 (Fig. 7.2A). Although miR-31-5p expression was slightly lower in BAP1-negative MPM cell lines (Fig. 7.7C), I found no significant difference for miR-31-5p, miR-125a-5p (Fig. 7.7D) or miR-125b-5p (Fig. 7.7E) expression between BAP1-negative and BAP1-positive MPM cell lines. However, with the exception of miR-200c-3p (Fig. 7.7I), miR-200 family members showed significantly higher expression in BAP1-negative MPM cell lines (Fig. 7.7F – J). On the whole, selected members of the miR-200 family displayed an inverse relationship with BAP1, implying that these miRNAs could regulate BAP1 expression.

7.5.3 Inverse correlation between miR-200a-5p, miR-200b-3p, miR-125b-5p and BAP1 in MPM cell lines

As the analysis above is subject to a number of caveats, I next excluded six cell lines with no detectable BAP1, which are either known, or are predicted, to harbour *BAP1* mutations (see section 3.6). For the nine cell lines with any detectable BAP1 expression, I examined correlations between the level of miRNA expression and that of BAP1 mRNA or BAP1 protein; as miRNA action is at the mRNA level but repression of gene expression is most obvious at the protein level (Table 7.1). This revealed few statistically significant correlations for most candidate miRNAs, including those that showed significantly different expression between MPM cell lines stratified by BAP1 status (miR-10a-5p, miR-10b-5p and miR-141-3p) (Fig 7.7). However, for other candidate miRNAs (highlighted in grey in Table 7.1), I have shown their correlation plots with BAP1 mRNA and BAP1 protein (Figures 7.8 to 7.11). Typically, BAP1 mRNA expression correlated well with BAP1 protein expression in MPM cell lines (see Fig. 3.4C). Exceptions to this were NCI-H2452, #15 and #30. Published data show that the NCI-H2452 cell line has a missense mutation in the BAP1 catalytic domain, which results in inactive BAP1 protein that appears

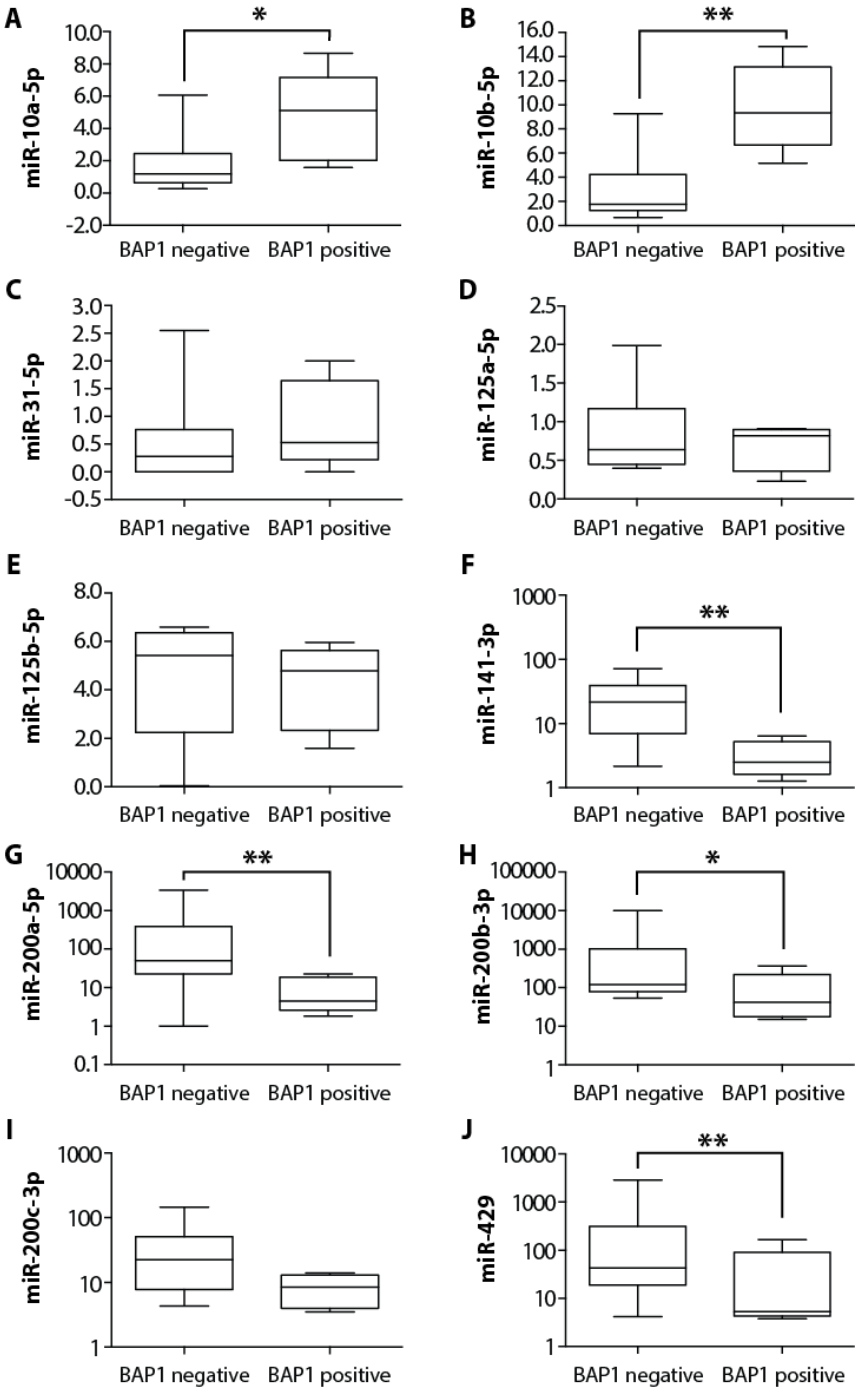

Figure 7.7: miRNA expression differences between BAP1-negative and BAP1-positive MPM cell lines.

The box and whisker plots show the spread of miRNA expression level in MPM cell lines grouped by their BAP1 status (n=10 BAP1-negative and n=5 BAP1-positive). The median and interquartile range are displayed, the whisker boundaries are the 5th and 95th percentile. N = three independent experiments, significant differences between the two groups as determined by unpaired t-test for the miR-10 family members, and by Mann Whitney U test for the miR-200 family members **P<0.01, *P<0.05.

miRNA	Gaussian Distribution (Y/N)	BAP1 mRNA (*r*)	BAP1 Protein (*r*)
miR-10a-5p	Y	-0.24	-0.11
miR-10b-5p	Y	-0.36	-0.13
miR-31-5p	Y	0.15	0.20
miR-125a-5p	Y	0.32	0.13
miR-125b-5p	Y	-0.51	-0.41
miR-141-3p	N	-0.48	-0.62
miR-200a-5p	N	-0.59	-0.68*
miR-200b-3p	N	-0.92***	-0.81**
miR-200c-3p	Y	-0.46	-0.53
miR-429	N	-0.60	-0.54

Table 7.1: Correlation coefficient values for the relationship between miRNA expression and BAP1 mRNA or protein in the MPM cell line panel.
Pearson correlations and Spearman rho correlations were computed for data from Gaussian and non-gaussian distributions, respectively. Gaussian distribution was confirmed by the D'Agostino and Pearson omnibus normality test. Statistically significant relationships are highlighted with asterisks ***P<0.005, **P<0.01, *P<0.05 (two-tailed).

to be unstable (Bott et al., 2011). #15 and #30 retain between 15-30% BAP1 mRNA expression, relative to MeT5A (*BAP1*$^{+/+}$) but have negligible BAP1 protein expression. The mutation status of #15 and #30 is unknown, but another possibility for reduced BAP1 protein in the absence of mutation is the post-transcriptional targeting of BAP1 mRNA by miRNAs. On correlation plots, the data points for MPM cell lines #15 and #30 are indicated with a thick black outline, in order to follow candidate miRNA expression patterns in these cell lines.

Yu *et al*. previously reported inverse correlation between miR-31-5p and BAP1 protein levels in lung cancer tissues (Yu et al., 2016). However, in the context of MPM cell lines, I found no evidence that miR-31-5p and BAP1 expression were inversely correlated (Fig. 7.8A - B). Correlation analysis showed some evidence for an inverse relationship between the miR-200 family members miR-200a-5p and miR-200b-3p, and BAP1 mRNA or protein expression (Table 7.1). Interestingly, MPM cell lines #15 and #30 (where post-transcriptional BAP1 regulation is most likely) were among those that showed the highest miR-200a-5p (Fig. 7.9A – B) and miR-200b-3p (Fig. 7.10A – B) expression.

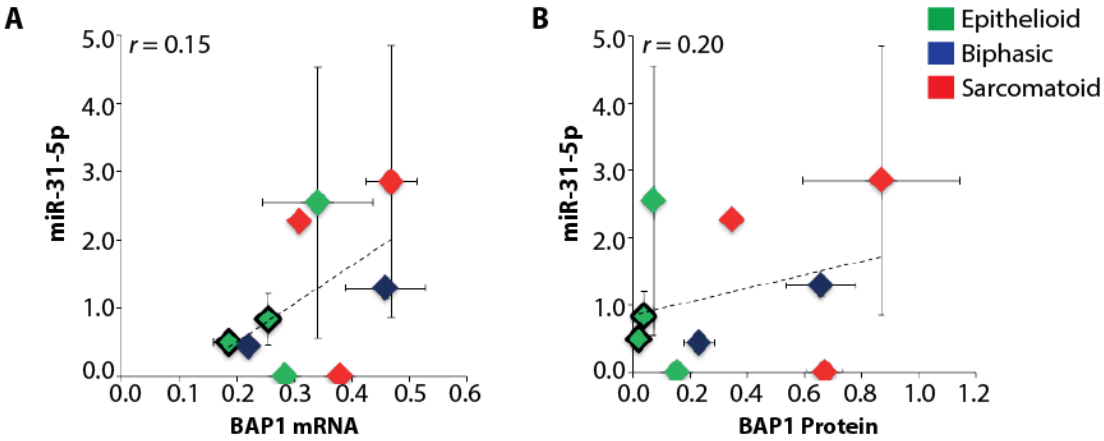

Figure 7.8: miR-31-5p expression does not inversely correlate with BAP1 mRNA or BAP1 protein expression in MPM cell lines.
Scatter plots examining the correlation between miR-31-5p expression and **A** BAP1 mRNA or **B** BAP1 protein. N = three independent experiments, error bars show SD. Colour coding indicates the histological subtypes of MPM. Nine cell lines with detectable BAP1 are included in the analysis, data points for lines #15 and #30 (candidates where BAP1 might be post-transcriptionally regulated) are indicated with a black outline.

No significant correlation was observed between miR-125b-5p and BAP1 mRNA (Fig. 7.11A) or protein expression (Fig. 7.11B). However, MPM cell lines #15 and #30 were among those with the highest miR-125b-5p expression, and the biphasic MPM cell line with higher BAP1 levels showed reduced miR-125b-5p expression. In marked contrast, the sarcomatoid MPM cell lines show high miR-125b-5p expression and BAP1 expression. Consequently, I excluded the sarcomatoid MPM cell lines from the exponential fitted trend line (Fig. 7.11C – D) which highlighted strong inverse correlation between miR-125b-5p and BAP1 expression in the epithelioid and biphasic MPM cell lines. This was most striking for the inverse relationship between miR-125b-5p and BAP1 protein expression (r = -0.83), which would be consistent with miR-125b-5p post-transcriptional regulation of BAP1 expression.

There is a strong suggestion of an inverse relationship between miR-200a-5p, miR-200b-3p and miR-125b-5p and BAP1 expression from correlative studies using qRT-PCR. Next, I extracted the expression profiles for miR-200b-3p and miR-125b-5p from the NanoString NS2/NS3 dataset from chapter 6, to examine whether an inverse relationship between miRNA and BAP1 status could be validated by a different assay (Fig. 7.12). The miR-200a-5p gene probe is not included in NanoString dataset. In the NS2/NS3 dataset, only five MPM cell lines displayed upregulated expression of miR-200b-3p, relative to MeT5A (*BAP1*$^{+/+}$), which included the #30 MPM cell line and two biological replicates of MPM cell line #15

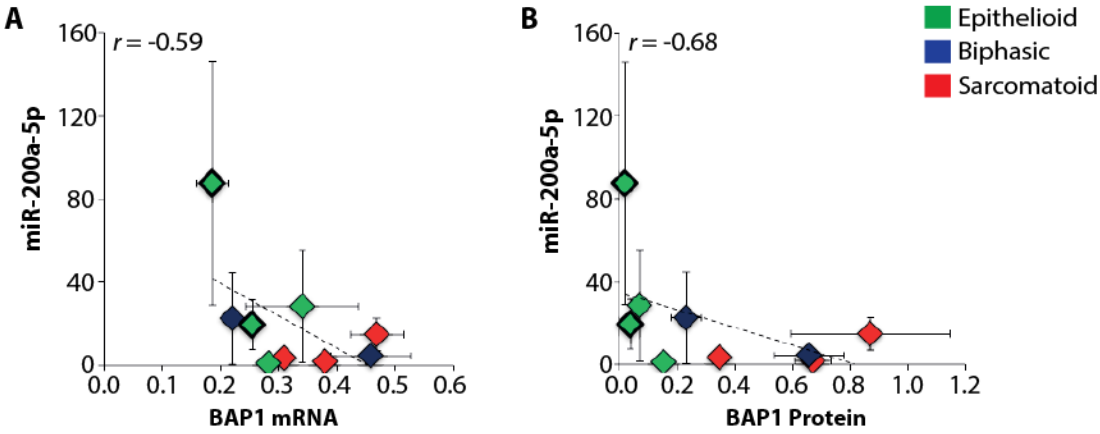

Figure 7.9: miR-200a-5p expression is inversely correlated with BAP1 mRNA and BAP1 protein expression in MPM cell lines.
Scatter plots examining the correlation between miR-200a-5p expression and **A** BAP1 mRNA or **B** BAP1 protein. N = three independent experiments, error bars show SD. Colour coding indicates the histological subtypes of MPM. Nine cell lines with detectable BAP1 are included in the analysis, data points for lines #15 and #30 (candidates where BAP1 might be post-transcriptionally regulated) are indicated with a black outline.

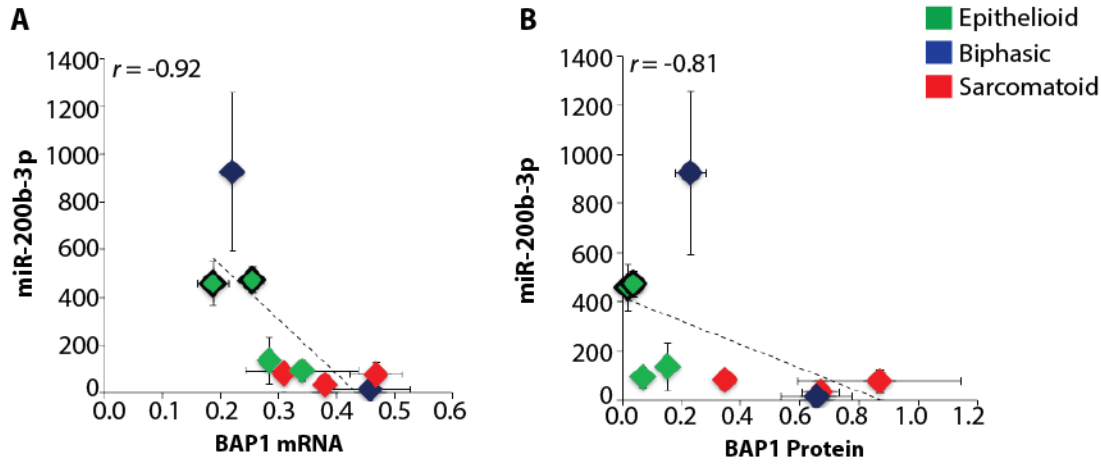

Figure 7.10: miR-200b-3p expression is inversely correlated with BAP1 mRNA and BAP1 protein expression in MPM cell lines.
Scatter plots examining the correlation between miR-200b-3p expression and **A** BAP1 mRNA or **B** BAP1 protein. N = three independent experiments, error bars show SD. Colour coding indicates the histological subtypes of MPM. Nine cell lines with detectable BAP1 are included in the analysis, data points for lines #15 and #30 (candidates where BAP1 might be post-transcriptionally regulated) are indicated with a black outline.

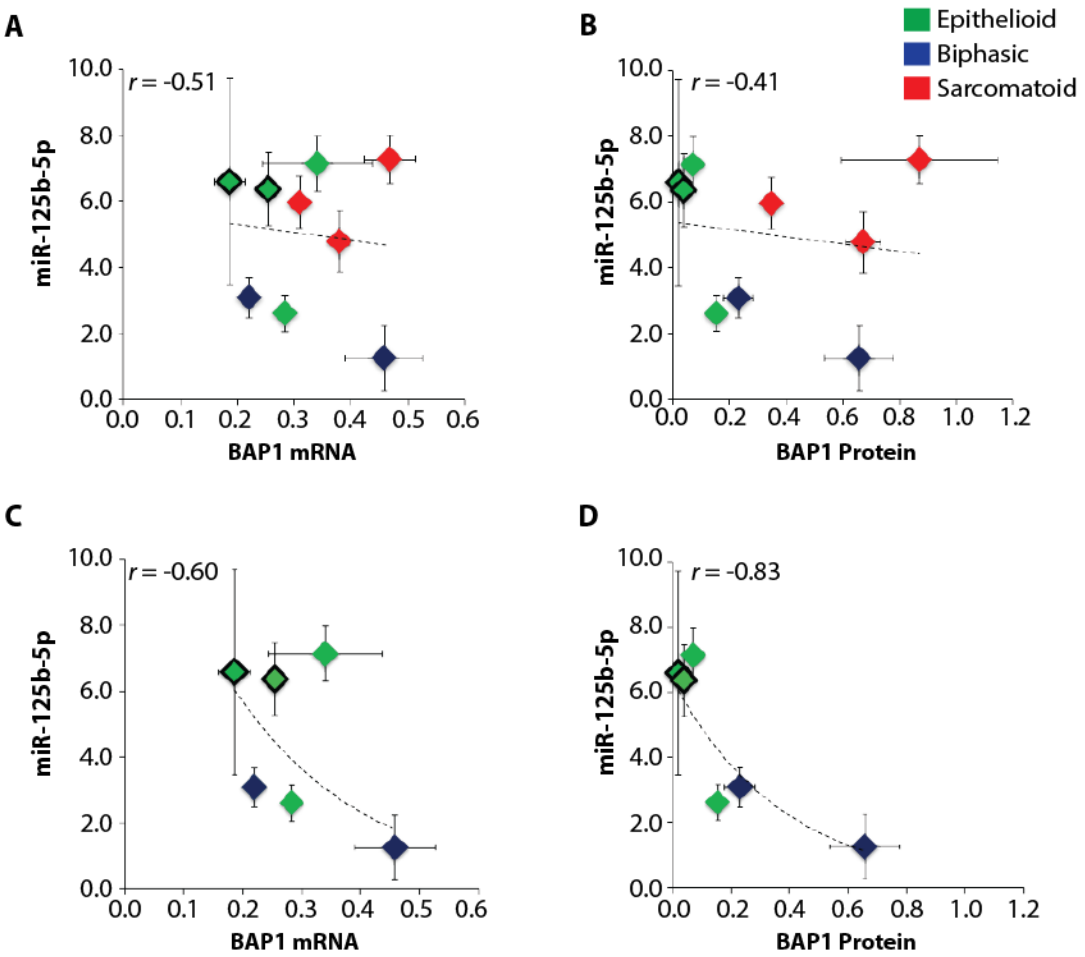

Figure 7.11: miR-125b-5p expression is inversely correlated with BAP1 mRNA and BAP1 protein expression in MPM cell lines.
Scatter plots examining the correlation between miR-125b-5p expression and **A** BAP1 mRNA or **B** BAP1 protein. An exponential trend line is fitted to the data points of **C** and **D**, the sarcomatoid MPM cell lines were excluded from the exponential fitted trend line. N = three independent experiments, error bars show SD. Colour coding indicates the histological subtypes of MPM. Nine cell lines with detectable BAP1 are included in the analysis, data points for lines #15 and #30 (candidates where BAP1 might be post-transcriptionally regulated) are indicated with a black outline.

(where post-transcriptional BAP1 regulation is most likely) (Fig. 7.12A). This was in contrast to the qRT-PCR data in Figure 7.6O, where in every MPM cell line there was higher miRNA expression for miR-200b-3p when compared to MeT5A (*BAP1*$^{+/+}$). miR-125b-5p expression was upregulated >1.5-fold in all MPM cell lines, relative to MeT5A (*BAP1*$^{+/+}$), in agreement with the qRT-PCR expression profiles in Figure 7.6I. Again, #15 and #30 MPM cell lines were among those that showed the highest miR-125b-5p expression (Fig. 7.12B), and I observed a greater expression of miR-125b-5p in BR2 compared to BR1 for the MPM cell line #15. Although there was no clear relationship between candidate miRNAs and BAP1 status in

the NS2/NS3 dataset, I observed increased expression of both miRNAs in MPM cell lines #15 and #30, consistent with the hypothesis that BAP1 expression may be post-transcriptionally targeted by miR-200b-3p and miR-125b-5p in these cell lines.

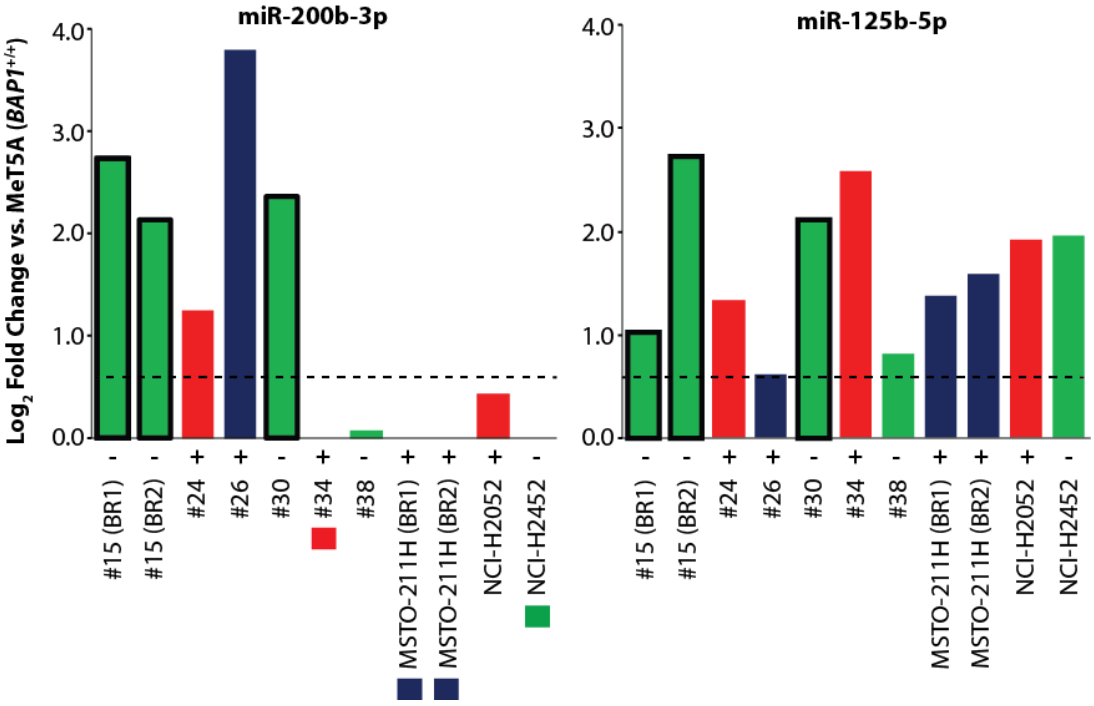

Figure 7.12: miR-200b-3p and miR-125b-5p expression data in MPM cell lines by the NanoString nCounter assay.
Bar graphs shows log_2 fold changes vs. MeT5A (*BAP1*$^{+/+}$) for **A** miR-200b-3p and **B** miR-125b-5p that are predicted to target BAP1. Data was extracted from the NanoString NS2 and NS3 data set (Chapter 6), log_2 fold changes were generated from the MeT5A (*BAP1*$^{+/+}$) sample from within their own assays. Dashed lines designate 1.5-fold change. Colour coding indicates the histological subtypes of MPM. Nine cell lines with detectable BAP1 are included in the analysis, data points for lines #15 and #30 (candidates where BAP1 might be post-transcriptionally regulated) are indicated with a black outline.

7.5.4 Candidate miRNA expression data in isogenic MeT5A *BAP1*-mutant cells by qRT-PCR and NanoString nCounter assay

Thus far, I have explored the correlative relationships between candidate miRNAs predicted to target BAP1, and BAP1 levels, in a panel of MPM cell lines that have endogenous variations in BAP1 expression. However, correlation is a two-way relationship and could also reflect regulation of the miRNA by BAP1. As such, I have attempted to dissociate cause from effect by using the isogenic MeT5A cell model to determine whether BAP1 can regulate candidate miRNA expression.

To explore whether these miRNAs are responsive to BAP1 loss, I examined their expression profiles in the NanoString NS1 data set (chapter 5), extracting the $\log_2$ fold changes for the isogenic *BAP1*-mutant cell line C5.1 (*BAP1*$^{w-/KO}$) vs. MeT5A (*BAP1*$^{+/+}$) for the ten candidate miRNAs (Fig. 7.13A). Three miRNAs, miR-10b-5p, miR-31-5p and miR-125b-5p, showed >1.5-fold increase in their expression upon BAP1 loss, the remaining miRNAs were up- or down-regulated in C5.1 (*BAP1*$^{w-/KO}$) cells relative to MeT5A (*BAP1*$^{+/+}$) but did not reach the fold-change cut-off.

I validated the expression profile for a set of these miRNAs in MeT5A (*BAP1*$^{+/+}$) and isogenic BAP1 mutant cell line C5.1 (*BAP1*$^{w-/KO}$) (Fig. 7.13B – F) by qRT-PCR and compared their profiles across the different assays (Fig. 7.13G). The miR-10 family members were of interest as they showed significantly downregulated expression in BAP1-negative cell lines, compared with BAP1-positive cell lines. miR-31-5p has been reported as a direct regulator of BAP1 in NSCLC, and although I saw no correlation with miR-31-5p and BAP1 in MPM, it would be of interest to observe whether this miRNA is BAP1-responsive. miR-200b-3p and miR-125b-5p were also of interest as these are predicted post-transcriptional regulators of BAP1 from the correlative studies.

Interestingly, miR-10a-5p (Fig. 7.13B), miR-10b-5p (Fig. 7.13C), miR-200b-3p (Fig. 7.13E) and miR-125b-5p (Fig. 7.13F) showed significantly increased expression in C5.1 (*BAP1*$^{w-/KO}$), compared to MeT5A (*BAP1*$^{+/+}$), by qRT-PCR, mirroring the results from the NanoString NS1 assay (Fig. 7.13G) and implying that their expression is indeed BAP1-dependent. However, conflicting data were reported by the two assays for miR-31-5p expression (Fig. 7.13D), which showed increased expression in C5.1 (*BAP1*$^{w-/KO}$) cells as detected by the NanoString platform, but significantly decreased expression in C5.1 (*BAP1*$^{w-/KO}$) cells by qRT-PCR (Fig. 7.13G). Overall, these data highlight that BAP1 may regulate the expression of candidate miRNAs examined through repression, as genetic *BAP1* loss resulted in the upregulation of these miRNAs.

7.6 BAP1 is a target of miR-125b-5p

I have previously shown evidence for inverse correlation between miR-200a-5p, miR-200b-3p, miR-125b-5p and BAP1 in MPM cell lines (Fig. 7.8 – 7.10 and 7.12), suggesting BAP1 could be a target for these miRNAs. To test this further, BAP1 protein expression was evaluated after overexpression of miR-125b-5p. I chose this miRNA as an exemplar to investigate miRNA post-transcriptional targeting of BAP1 it showed the strongest inverse

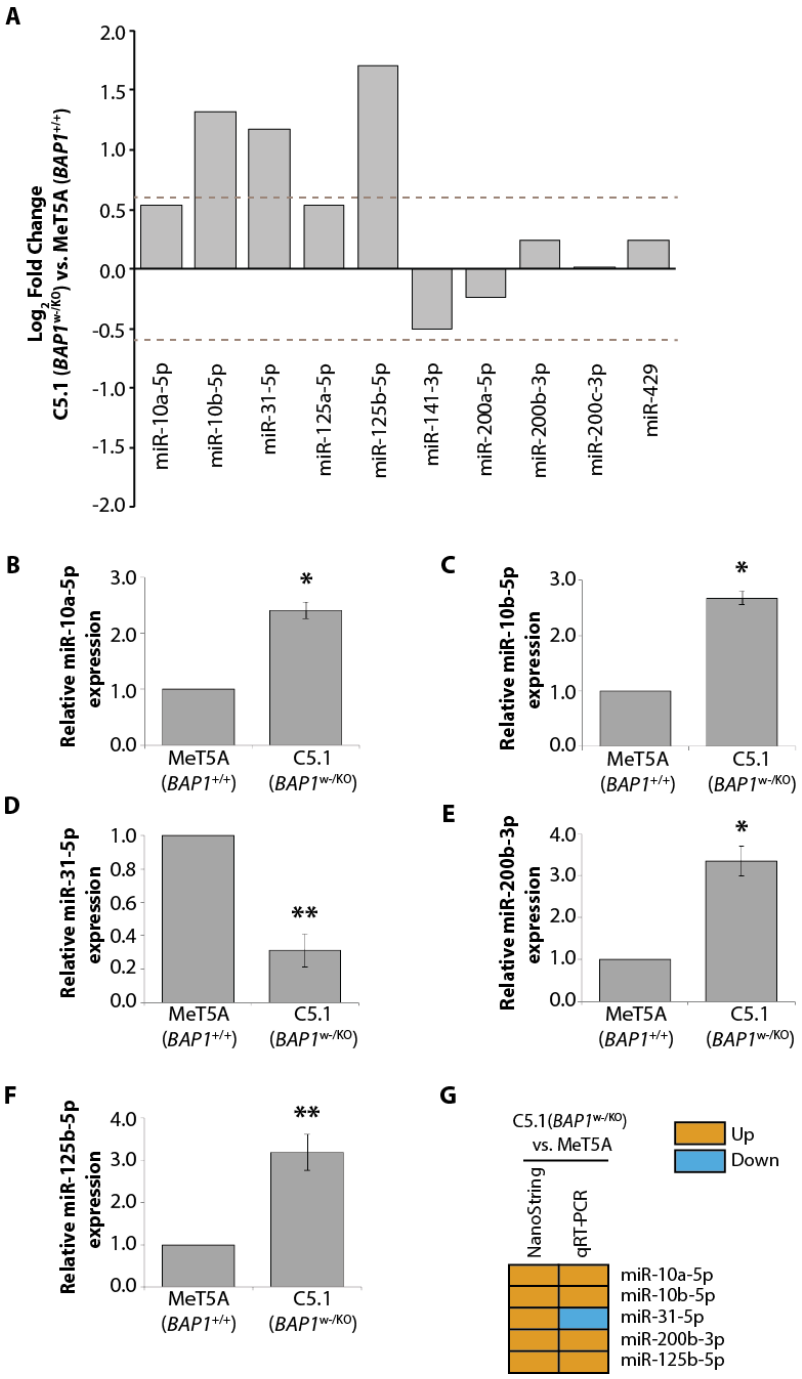

Figure 7.13: BAP1 regulates candidate miRNA expression.
A Bar graph shows log_2 fold changes vs. MeT5A (*BAP1*$^{+/+}$) for ten candidate miRNAs that are predicted to target BAP1, in the isogenic BAP1 mutant cell line C5.1 (*BAP1*$^{w-/KO}$). Data was extracted from the NanoString NS1 data set (Chapter 5), dashed lines designate 1.5-fold change. **B-F** Bar graphs shows quantification for **B** miR-10a-5p, **C** miR-10b-5p, **D** miR-31-5p, **E** miR-200b-3p and **F** miR-125b-5p expression as detected by qRT-PCR, in C5.1 (*BAP1*$^{w-/KO}$) cells relative to MeT5A (*BAP1*$^{+/+}$). **G** Schematic summarising the direction of expression changes for a set of candidate miRNAs across different miRNA profiling assays.

relationship with BAP1 protein expression (r = -0.83). miR-125b-5p overexpression was achieved by transfecting the BAP1-positive MPM cell line MSTO-211H with a miR-125b-5p mimic and measuring expression of BAP1 by immunoblotting (Fig. 7.14). Quantification of protein expression, normalised to β-actin and relative to the mock treatment, confirmed significant reduction in BAP1 protein expression with miR-125b-5p overexpression (Fig. 7.14A and 7.14B). These data confirm that BAP1 levels respond to miR-125b-5p. Together with data in Fig 7.13F, this suggests that BAP1 and miR-125b-5p may operate in a double-negative feedback loop, where BAP1 negatively regulates miR-125b-5p expression (as evidenced by increased expression of miR-125b-5p in *BAP1*$^{w-/KO}$ cells), and is itself a target of miR-125b-5p (Fig. 7.14C). Thus, the dominant mechanism in a cell would contribute towards determining its BAP1 status (Fig. 7.14D).

7.7 Assessing the effect of BAP1 depletion or miR-125b-5p overexpression on predicted and published miR-125b-5p targets

It is well known that one miRNA may regulate many target genes. USP8, Cyclin E1 (CCNE1), B-cell lymphoma 2 (BCL2) and E-cadherin are each potential targets of miR-125b-5p as they contain predicted miR-125b-5p binding sites in their 3'UTR regions. USP8 and CCNE1 were selected for validation as these genes were enriched in significant GO terms from the NanoString NS1 analysis (see Appendix Fig. 5.5). There is also published evidence for BCL2 (Yang et al., 2017) and E-cadherin (Bera et al., 2014) as targets of miR-125b-5p in gallbladder cancer and pancreatic cancer, respectively. I transfected BAP1 siRNA or the miR-125b-5p mimic into the BAP1-positive cell line MSTO-211H and measured the expression of miR-125b-5p gene targets by immunoblotting (Fig. 7.15A).

Relative to the mock treatment, no significant change in USP8 protein expression was observed with BAP1 depletion or miR-125b-5p overexpression (Fig. 7.15B). However, a significant ~3-fold increase in CCNE1 protein expression, relative to the mock treatment, was seen with either BAP1 depletion or miR-125b-5p overexpression (Fig. 7.15B), suggesting that although both can affect CCNE1 expression, this is not a direct effect of the miRNA as CCNE1 level is increased with mimic transfection. Relative to the mock treatment, there was ~50% reduction in BCL2 protein expression with BAP1 depletion, whilst no change in protein expression was detected with miR-125b-5p overexpression (Fig. 7.15B), implying this is a BAP1-dependent effect independent of the miRNA. The loss of E-cadherin and upregulation of Vimentin is associated with EMT where epithelial cells acquire a more migratory and invasive cellular phenotype. Although ~50% reduction in E-cadherin

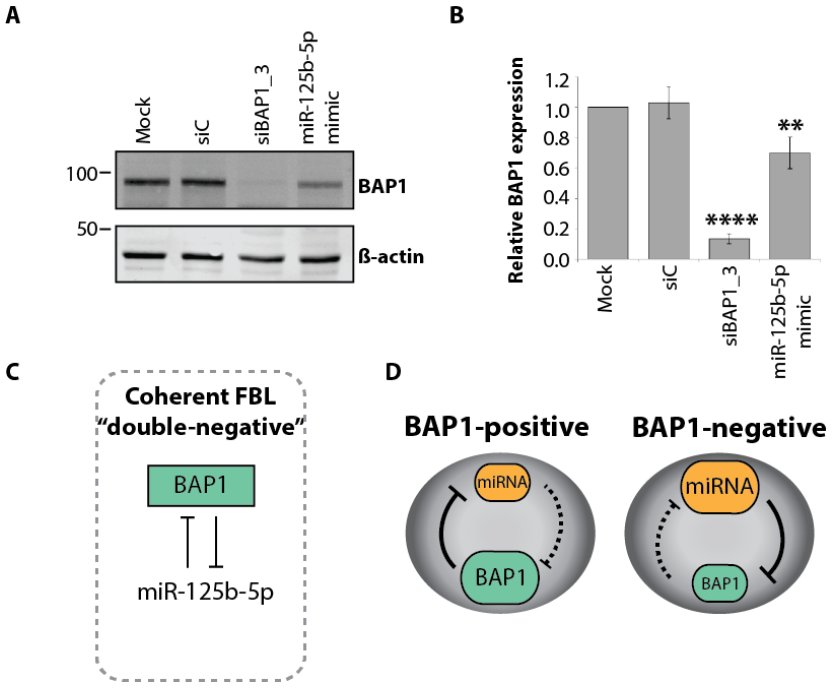

Figure 7.14: miR-125b-5p overexpression reduces BAP1 protein levels.
A Representative immunoblot of MSTO-211H cells transfected with control (siC), BAP1 siRNA, or the miR-125b-5p mimic for 72h prior to cell lysis and immunoblotting. **B** Quantification of BAP1 protein expression normalised to ß-actin and relative to the mock treatment. N = three independent experiments, error bars show SD, one-way ANOVA with Dunnett's post-hoc test, ****P<0.0001, **P<0.01. **C** and **D** Schematics illustrate the hypothesis that miRNAs, such as miR-125b-5p, may function in a feedback loop (FBL) with BAP1 (**C**), and how this network might influence BAP1 status (**D**).

expression was unexpectedly observed in siRNA control (siC)-transfected cells, relative to the mock treatment, there was complete loss of E-cadherin in BAP1-depleted cells and an ~80% reduction in expression with miR-125b-5p overexpression (Fig. 7.15B). However, I did not observe any corresponding changes in Vimentin expression, relative to the mock treatment, in either BAP1-depleted or miR-125b-5p mimic transfected cells (Fig. 7.15B). This suggests that E-cadherin may be a target of miR-125b-5p through miRNA regulation of BAP1.

To establish whether the responses seen were dependent on BAP1, selected proteins were investigated in the isogenic BAP1 mutant cell lines (Fig. 7.15C). Compared to the MeT5A (*BAP1*$^{+/+}$), there was no change in USP8 protein expression in either *BAP1*$^{w-/+}$ or C5.1 (*BAP1*$^{w-/KO}$) cells compared to MeT5A (*BAP1*$^{+/+}$). Consistent with transient depletion of BAP1 (Fig 7.15A and B), in response to mutation of BAP1, CCNE1 protein expression was upregulated in MeT5A C5.1 (*BAP1*$^{w-/KO}$) cells, whereas BCL2 protein expression was greatly reduced in

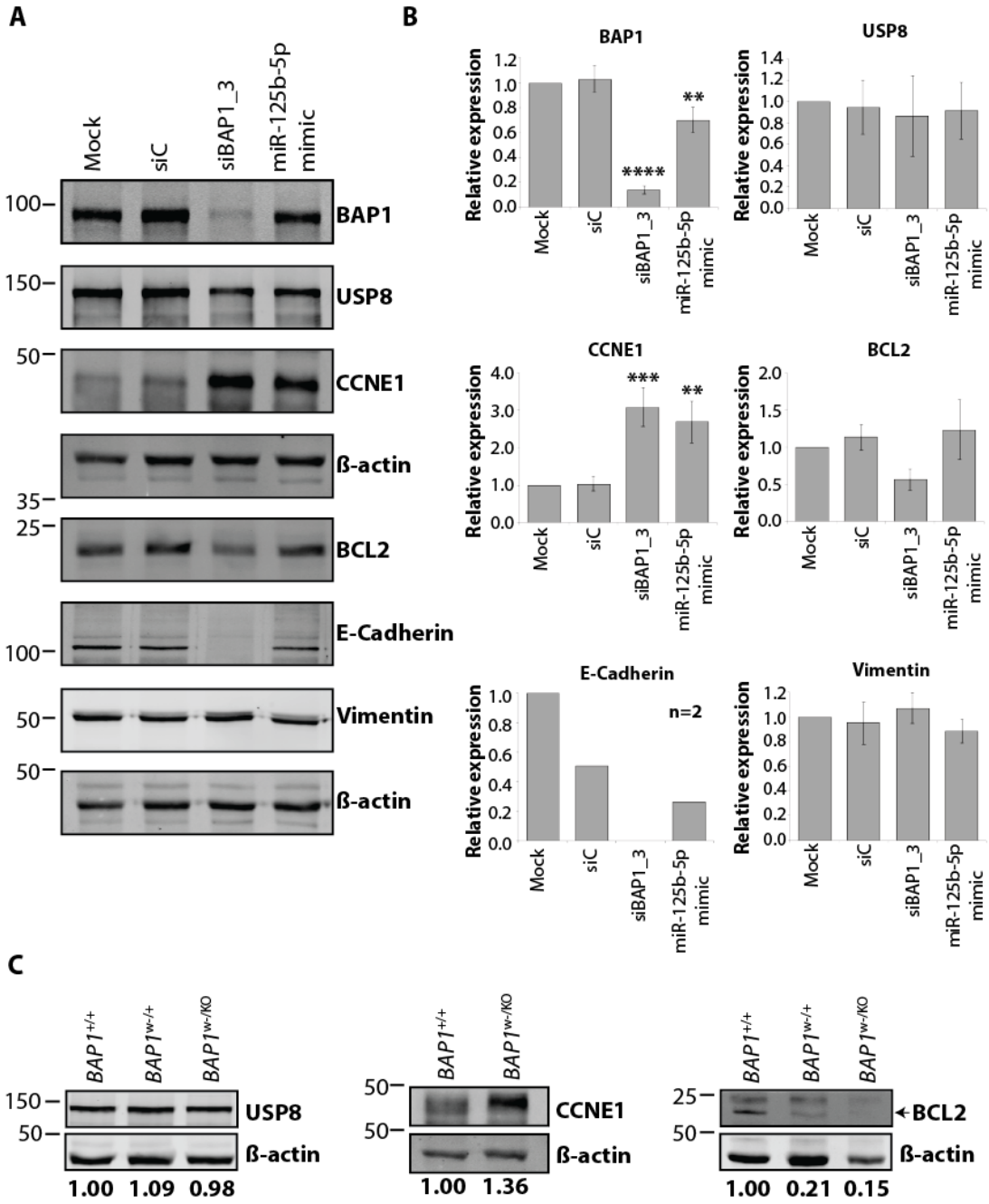

Figure 7.15: BAP1 deficiency or miR-125b-5p overexpression alters CCNE1, BCL2 and E-Cadherin protein expression.

A Representative immunoblots of MSTO-211H cells transfected with control (siC) and BAP1 siRNA, and miR-125b-5p mimic for 72h prior to cell lysis and immunoblotting for BAP1, USP8, CCNE1, BCL2, E-cadherin and Vimentin protein expression. **B** Quantification of protein expression normalised to ß-actin and relative to the mock treatment. N = three independent experiments unless otherwise stated, error bars show SD, one-way ANOVA with Dunnett's post-hoc test, ***P<0.001, **P<0.01. These set of samples are the same as shown in Fig. 7.14. **C** Representative immunoblots showing USP8, CCNE1 and BCL2 protein expression in MeT5A (*BAP1*$^{+/+}$) and isogenic BAP1 mutant cell lines *BAP1*$^{w-/+}$ and C5.1 (*BAP1*$^{w-/KO}$) cells. Protein expression, normalised to ß-actin and relative to MeT5A (*BAP1*$^{+/+}$) from one independent experiment, are stated below each immunoblot.

both *BAP1*$^{w-/+}$ and C5.1 (*BAP1*$^{w-/KO}$) cells, by 79% and 85%, respectively (Fig. 7.15C). These data confirmed that expression of both CCNE1 and BCL2 are influenced by BAP1.

In summary, in this final chapter, I profiled the expression of ten candidate miRNAs predicted to target BAP1 in a panel of MPM cell lines with varying histological subtype and BAP1 status. Although no significant differences in miRNA expression were detected by histological subtype, differential expression was observed based on BAP1 status, with miR-10 family members and miR-141-5p showing significantly altered expression between BAP1-negative and BAP1-positive MPM cell lines. miRNAs are inversely correlated with their gene targets, and I detected an inverse relationship of miR-200a-5p, miR-200b-3p and miR-125b-5p with BAP1 levels in MPM cell lines, suggesting BAP1 could be a target for these miRNAs. As an exemplar, overexpression of miR-125b-5p significantly reduced BAP1 protein expression and, as this miRNA is upregulated C5.1 (*BAP1*$^{w-/KO}$) cells, it is predicted that BAP1 and miR-125b-5p may operate in a double-negative feedback loop. Lastly, BAP1 depletion and miR-125b-5p overexpression caused a decrease in E-cadherin protein expression, implying it is a target of miR-125b-5p and it may be regulated through miRNA-repression of BAP1.

7.8 Discussion

Frequent inactivation of BAP1 through gene loss and/or somatic mutation are observed in MPM; yet there are cases of BAP1 inactivation without detectable mutation, suggesting BAP1 loss can also occur via post-transcriptional and post-translational mechanisms (Bott et al., 2011). Human target prediction analysis was performed to identify candidate miRNAs predicted to negatively regulate BAP1 expression and I sought to examine their expression in a panel of MPM cell lines. I have shown that miR-200a-5p, miR-200b-3p and miR-125b-5p expression was increased in MPM cell lines relative to normal mesothelial cell line MeT5A (*BAP1*$^{+/+}$), and they exhibited a strong inverse correlation with BAP1 mRNA and protein status. I found the inverse relationship to be true in epithelioid MPM cell lines #15 and #30, which show 20-30% BAP1 mRNA expression, relative to MeT5A (*BAP1*$^{+/+}$) but no BAP1 protein, thus it is possible that BAP1 is targeted post-transcriptionally by candidate miRNAs in these cell lines.

At present, this is the first study to have analysed miRNA expression related to BAP1 expression in MPM. Yu *et al.* previously reported upregulated miR-31-5p in NSCLC tissues, where its expression inversely correlated with BAP1 protein (Yu et al., 2016). They analysed

the biological consequences of miR-31-driven repression of BAP1 expression in NSCLC cells and showed that A549 cells transfected with miR-31 mimic increased cell proliferation and inhibited apoptosis by silencing BAP1. Their study strongly indicated that a miR-31-5p-mediated post-transcriptional mechanism was involved in BAP1 repression in NSCLC (Yu et al., 2016), a tumour type where BAP1 is very rarely inactivated by mutation (see Fig. 1.2). However, when I assessed this regulatory relationship in MPM cell lines, no correlation was seen between BAP1 status and miR-31-5p, and any relationship between the two may be obscured by a higher frequency of *BAP1* mutation in MPM (see Fig. 1.2). In contrast with NSCLC, miR-31-5p was generally poorly expressed in MPM cell lines relative to the normal mesothelial cell line MeT5A ($BAP1^{+/+}$), with the lowest expression in BAP1-negative MPM cell lines. In fact, miR-31-5p expression was absent in five MPM cell lines, #19, #43, #24, #38 and #52. The chromosomal fragile site at 9p21.3 that encodes miR-31-5p is often lost in MPM, making this miRNA one of the most commonly deleted in MPM (Ivanov et al., 2009). Indeed, miR-31-5p downregulation resulting from homozygous deletion of miR-31-5p-encoding gene on ch9p21.3 was evident in 54% of MPM patient tumours (Ivanov et al., 2010). Therefore, it is difficult to draw any conclusions concerning the post-transcriptional regulation of BAP1 by miR-31-5p from correlative data in MPM as both undergo frequent genomic losses. In future, it would be interesting to look for exclusivity or otherwise in copy number variation of these two loci in MPM.

Tumour-suppressive effects have been described for miR-31-5p in MPM. The reintroduction of miR-31-5p in patient-derived MPM cells H2595 and HP-1 inhibited their proliferation, migration and invasion (Ivanov et al., 2010). Its reintroduction also inhibited expression of pro-survival phosphatase PPP6C, which had previously been associated with resistance to chemotherapy and radiation therapy. However, conflicting data from another study demonstrated miR-31-5p re-expression in MPM cell line NCI-H2452 promoted chemoresistance to platinum-based therapy *in vitro* (Moody et al., 2017). In a study of solid tumours that metastasise to the brain, DNA losses in ch9p21.3 were among four most frequently detected in 70% of cases (Petersen et al., 2000), demonstrating pro-tumourigenic effects of miR-31-5p loss within the ch9p21.3 locus in cancer.

The miR-200 family is suggested to have diagnostic value for differentiating MPM from its main differential diagnosis, lung adenocarcinoma. Microarray analysis revealed the downregulation of four out of five members of the miR-200 family (miR-200b-3p, miR-200c-3p, miR-141 and miR-429), in MPM compared to lung adenocarcinoma (Gee et al., 2010).

With greater relevance to my study, in a very recent comparison of differentially expressed miRNAs between BAP1-mutant and BAP1-wildtype ccRCC tumours, Ge *et al.* detected 33 significantly modulated miRNAs in BAP1-mutant tumours relative to BAP1-wildtype ccRCC tumours (Ge et al., 2017). Amongst these, miR-200c-3p, miR-10a-5p and miR-10b-3p were upregulated. Consistent with these data, in my study, miR-200c-3p was also significantly upregulated in BAP1-negative MPM cell lines, however the opposite profile was observed for miR-10 family members, with miR-10a-5p and miR-10b-5p significantly downregulated in BAP1-negative MPM cell lines. The expression of miR-10 family may be cancer-specific. The miR-10 family members are deregulated in several types of cancer, miR-10a-5p resides in a region amplified in melanoma and breast cancer (Zhang et al., 2006), and are over expressed in glioblastoma (Gaur et al., 2007), pancreatic cancer (Bloomston et al., 2007) and colon cancer (Volinia et al., 2006), compared with their respective normal tissues.

One concern on analysis of my miRNA expression data was the lack of expression of all miR-200 family members in the normal mesothelial cell line MeT5A (*BAP1*$^{+/+}$). As miRNA expression is presented relative to MeT5A (*BAP1*$^{+/+}$), all miR-200 family members were upregulated in MPM cell lines. MeT5A (*BAP1*$^{+/+}$) was established as a parental clonal cell line for gene editing, so I also examined the expression profiles of the miR-200 family members in the non-clonal MeT5A cell line by qRT-PCR, which verified their absence (data not shown). Nonetheless, it has been reported that TGF-β mediated down-regulation of the miR-200 family in mesothelial cells can promote metastatic behaviour in these cells, implying that these miRNAs could play an essential role in EMT suppression in the normal cellular state (Sugiyama et al., 2014). On the other hand, miR-200b-3p is significantly overexpressed in ovarian cancer tissues versus normal tissues, and it was speculated that miR-200b-3p may negatively regulate BAP1 expression, as BAP1 was also downregulated in these ovarian cancer tissues (Iorio et al., 2007).

Although no significant differences in miR-125b-5p expression were observed of stratification of MPM cell lines by BAP1 status, a strong inverse correlation was detected between miR-125b-5p and BAP1 expression in MPM cell lines, suggestive of post-transcriptional repression of BAP1 by miR-125b-5p. Members of the miR-125 family have opposing roles in cancer; they have been validated as tumour suppressors and oncomiRs in different contexts (Sun et al., 2013). In the panel of MPM cell lines analysed here, overexpression of miR-125b-5p, correlating with decreased BAP1 expression, implied a potential disease-promoting function in MPM, and the notion that miR-125b-5p acts as an

oncomiR by negatively regulating BAP1. It has been reported that members of the miR-125 family, especially miR-125b-5p, act as oncogenes in several cancers; with the overexpression of miR-125b-5p promoting pathogenic events in prostate cancer (Shi et al., 2011), pancreatic cancer (Bloomston et al., 2007) and NSCLC (Ma et al., 2012). In patients with unresected MPM tumours, a miRNA signature consisting of low levels of miR-99a/let-7c/miR-125b-5p indicated significantly shorter overall survival than MPM tumours with high expression of these miRNAs. Of note, BAP1 loss is associated with improved median survival in MPM (Farzin et al., 2015). It would be interesting to examine whether there is any link between BAP1 status, miR-125b-5p expression and survival in MPM tumours.

Through overexpression by miR-125b-5p mimics, I have provided validation for BAP1 as a direct target of miR-125b-5p (Fig. 7.14). To my knowledge, this is the first experiment that demonstrates BAP1 to be modulated by miR-125b-5p, and the observed decrease in BAP1 protein level was robust and significant. Nevertheless, miRNAs often have multiple targets, extra considerations are essential for identification of its direct functional targets. Validation of the miR-125b-5p predicted target site would be important to demonstrate a direct effect, for example using a BAP1 3'UTR luciferase reporter gene assay. Additionally, I could examine whether BAP1 is post-transcriptionally regulated by miRNAs in the MPM cell lines #15 and #30, by introducing a miR-125b-5p inhibitor and testing the hypothesis that this would increase expression of BAP1.

I have also hypothesised that BAP1 and miR-125b-5p may operate in a double-negative FBL. This was based on the observations that (1) in the NanoString NS1 dataset, miR-125b-5p levels were increased ~2.5-fold in C5.1 (*BAP1*$^{w-/KO}$) cells, relative to MeT5A (*BAP1*$^{+/+}$), and (2) miR-125b-5p mimic expression can reduce BAP1 protein levels in a BAP1-positive MPM cell line. TFs are often targets for repression by the miRNAs that they regulate, generating complex networks of interaction (Jansson and Lund 2012). Simple FBLs are found as common motifs in many gene regulatory networks and may provide a means for miRNAs to regulate their own expression. A double-negative FBL has two steady states (Pelaez and Carthew, 2012), in this case it would be the transition from a high BAP1/low miR-125b-5p to a high miR-125b-5p/low BAP1 state, giving rise to the mutually-exclusive expression of the miRNA and target gene (Figure 7.14 C and D). Nevertheless, this feedback loop is likely to contain more components, as miR-125b-5p has the potential to target many genes, and form part of a larger functional network. Delineating how these genes impact on each other may require computational models, as network function can be difficult to assess

experimentally, because the effect of disrupting a single component on a large network may be quite subtle (Martinez and Walhout, 2009).

As miRNAs have the potential to target multiple genes, I assessed the effect of BAP1 depletion (predicting a consequential increase in miR-125b-5p level and function) or miR-125b-5p overexpression on predicted and published miR-125b-5p targets. Interestingly, the predicted miR-125b-5p gene target CCNE1 showed significantly increased expression with both BAP1 siRNA knockdown and miR-125b-5p overexpression, implying that BAP1 depletion through miRNA action may result in this increase. BCL2 is an anti-apoptotic protein and is a published target of miR-125b-5p in gallbladder cancer, where expression of miR-125b-5p and BCL2 are inversely correlated (Yang et al., 2017). In MSTO-211H cells, ~50% decrease in BCL2 expression was detected with BAP1 siRNA knockdown, relative to the mock treatment (Fig. 7.14B), and an 85% decrease in expression was detected in isogenic MeT5A *BAP1*$^{W-/KO}$ cells. It is plausible that the loss of tumour suppressor BAP1 would cause reduced expression of an anti-apoptotic protein, which in the simplest terms would increase the propensity of cells for apoptosis. Indeed, a recent study has shown that a subset of MPM cell lines with loss of function *BAP1* mutations demonstrated increased sensitivity to a death receptor agonist rTRAIL, through alterations in the expression of apoptosis pathway components (Kolluri et al., 2018). It would in future be interesting to examine BCL2 protein expression across the larger panel of MPM cell lines to see if this correlates with genetic BAP1 status. It is unlikely that the decrease in BCL2 expression with BAP1 siRNA knockdown is dependent on miR-125b-5p action as BCL2 levels were unchanged with miR-125b-5p overexpression.

In contrast, E-cadherin expression was reduced by miR-125b-5p overexpression and completely absent in siBAP1-treated cells. These data fit best with the initial hypothesis implying E-cadherin is a target of miR-125b-5p, and it may perhaps be regulated through miRNA-repression of BAP1. In agreement with my data, there is published evidence for E-cadherin as a target of miR-125b-5p in pancreatic cancer (Bera et al., 2014). In this study, significant upregulation of miRNAs including miR-125b-5p were detected in a gemcitabine drug-resistant pancreatic ductal adenocarcinoma (PDAC) cell line compared to the parental cell line. In other PDAC cell lines where miR-125b-5p expression had been determined, E-cadherin expression was inversely related to miR-125b-5p, and PDAC cell lines with more mesenchymal like features displayed higher levels of miR-125b-5p. The authors also analysed clinical tumour data for predicted miR-125b-5p target genes,

including BAP1 and BCL2, showing they were negatively correlated with the expression of miR-125b-5p. However, neither BAP1 nor BCL2 were investigated further, and my data provide the first mechanistic link between these potential network components in cancer. In summary, I have investigated for the first time the miRNA regulation of BAP1 expression in MPM cell lines, and the potential for BAP1-miRNA feedback loops. I have highlighted three miRNAs, miR-200a-5p, miR-200b-3p and miR-125b-5p as potential candidates that may post-transcriptionally repress BAP1, as they were inversely correlated with BAP1 in MPM cell lines. This was validated for miR-125b-5p. Although these miRNAs require further investigation, they could show promise as biomarkers with particular relevance for MPM tumours where BAP1 expression is lost via non-genetic mechanisms.

Chapter 8: Final summary and future perspectives

8.1 Summary of the major findings in this thesis

First characterised in 1998 as a novel TSG (Jensen et al., 1998), interest in *BAP1* has accelerated since 2010 when high rates of *BAP1* mutations were reported in two rare cancers, UVM (Harbour et al., 2010) and MPM (Testa et al., 2011). In recent months, reports have begun to emerge of preclinical studies that aim to exploit *BAP1*-dependencies within tumour cells for therapeutic benefit (Bononi et al., 2017b; Kolluri et al., 2018; Hebert et al., 2017). In this thesis, I have described my contributions to ongoing studies in the Coulson lab (both published and manuscripts in preparation) to profile BAP1-dependencies in *BAP1* mutated isogenic MeT5A cells in order to identify therapeutic targets that may be stratified according to BAP1 status. Importantly, I report the first investigation into the BAP1-dependent miRNome in the isogenic cell model of *BAP1*-deficient MPM and in patient-derived MPM cell lines.

In chapter 3, I verified upregulation of proteins involved in actin cytoskeletal regulatory pathways, and deregulation of cellular metabolism, in isogenic MeT5A cells with genetic *BAP1* deficiency. I demonstrated the clinical relevance of these adaptations by validating expression of candidate proteins across a panel of MPM cell lines with known BAP1 status. Whilst BAP1-dependent metabolic reprogramming was inconsistent between the isogenic and patient-derived cell models, changes in cytoskeletal protein expression (notably ICAM-1) were recapitulated in both. In chapter 4, I have shown for the first time that BAP1 modulates the expression of the chromatin-associated protein HDAC2 in MPM cell lines. I demonstrated that this was not via direct deubiquitylation, but through regulation of the HDAC2 transcript levels. I also highlighted the importance of *BAP1* status in the response of cells HDACi.

Exploring the idea that BAP1 might also regulate miRNAs, in chapter 5 I used the NanoString platform to screen for BAP1-dependent miRNAs in isogenic MeT5A cells. 113 miRNAs were significantly modulated ($P \leq 0.05$, >1.5-fold) in BAP1-deficient cells, amongst these I observed striking downregulation of miRNAs from the ch14q32.31 tumour-suppressor locus in isogenic MeT5A *BAP1*$^{w-/KO}$ cells. Gene ontology analysis suggested these miRNAs may affect the cytoskeleton and transcriptional regulation. In chapter 6, I expanded the analysis of the BAP1-dependent miRNome across a panel of 20 MPM cell lines. This highlighted differential expression of specific miRNAs in MPM cell lines grouped

by BAP1 status, including downregulation of the ch14q32.31 locus. Lastly, in chapter 7, I investigated miRNA post-transcriptional regulation of BAP1 in MPM, and explored BAP1 participation in gene regulatory networks with miRNAs. I identified miR-125b-5p as a novel miRNA that can regulate BAP1. I also demonstrated that expression of this miRNA was significantly increased in isogenic MeT5A *BAP1*$^{w-/KO}$ cells, suggesting the novel hypothesis that BAP1 and miR-125b-5p operate in a double-negative FBL.

In the sections below, I will discuss the implications of my various strands of investigation, as well as suggesting potential future studies to validate and advance my findings.

8.2 Adaptive response of the proteome and miRNome to *BAP1* deficiency in mesothelioma cell models

In chapter 3, I focused on understanding proteome-level adaptation of C5.1 (*BAP1*$^{w-/KO}$) cells compared to normal MeT5A (*BAP1*$^{+/+}$) cells. This isogenic model provides a genetic background of biallelic *BAP1* inactivation, as is frequently seen in MPM (Testa et al., 2011), although the C5.1 (*BAP1*$^{w-/KO}$) cells do retain some expression of BAP1 protein. Intriguingly, although metabolic reprogramming was evident, with the exception of ASS1 the expression of the analysed glycolytic or anaplerotic enzymes in BAP1-negative MPM cell lines did not reflect the profiles from C5.1 (*BAP1*$^{w-/KO}$) cells. This suggests that the metabolic response to loss of BAP1 may be high context-specific. In contrast, the cytoskeletal response to *BAP1* inactivation was recapitulated in both C5.1 (*BAP1*$^{w-/KO}$) MeT5A and BAP1-negative MPM cell lines, as assessed by expression of ICAM1 and ARP complex proteins (Fig. 3.5 and Fig. 3.9). In the pathogenesis of MPM, local invasion is important for tumour progression (Elmes and Simpson, 1976), and our data suggest that BAP1-negative MPM might be more prone to such local invasion.

Consistent with these data, during analysis of the BAP1-responsive miRNome in chapter 5, I observed the greatest enrichment for miRNA-target genes within GO terms describing cytoskeletal regulatory pathways and processes such as cell motility, cell-cell adhesion, focal adhesion and positive regulation of EMT (Fig. 5.10). The genes enriched in these processes are targeted by miRNAs that are both induced and repressed in response to *BAP1* deficiency. In contrast, the gene targets for significantly downregulated miRNAs with *BAP1* deficiency, were highly enriched within the cellular response to glucose, representing the only GO term related to metabolism in this dataset (Fig. 5.10 and Appendix Fig. 5.5. miRNAs are often considered to function as "fine-tuners" of cellular processes, eliminating the

expression of mRNA transcripts that are inappropriate for a particular cell type or cellular state, thereby maintaining dynamic homeostatic control over protein-coding genes and providing robustness to the cellular phenotype (Zhang, 2013). It is likely that the differential miRNA expression profiled in chapter 5 forms part of the adaptive response to *BAP1* deficiency, perhaps helping to maintain normal protein expression, and thus influences the BAP1-dependent proteome (chapter 3), which ultimately drives the cancer phenotype of *BAP1*-deficient MPM.

For analysis of the miRNome, I profiled two *BAP1*$^{w-/KO}$ cell lines C3.1 and C5.1, the latter having the lowest residual level of BAP1 expression. Overall, there was a consistent miRNA response to *BAP1* mutation in both *BAP1*$^{w-/KO}$ cell lines, compared to parental cells. This contrasted somewhat with the proteome response for the two *BAP1*$^{w-/KO}$ cell lines where, compared to the parental cells, the proteome of C5.1 (*BAP1*$^{w-/KO}$) had diverged more than that of C3.1 (*BAP1*$^{w-/KO}$) (Kenyani et al., manuscript in prep). Although the miRNome of both *BAP1*$^{w-/KO}$ cell lines appeared more consistent in their response to BAP1 deficiency, this largely reflected the co-ordinated downregulation of ch14q32.31 miRNAs in both cell lines (Fig. 5.9). It therefore appeared that the ch14q32.31 miRNA locus is sensitive to partial reduction in BAP1 levels, perhaps owing to its highly polycistronic organisation. Whilst the perturbation of a single gene promoter often affects transcription of one protein-coding gene, in comparison this may affect the expression of multiple miRNAs, with consequences for post-transcriptional regulation of their multiple gene targets.

8.3 Overview of the miRNAs linked to BAP1 in this thesis

In chapters 5-7 I discussed in detail several miRNAs of interest that were either significantly up- or down-regulated in *BAP1*-deficient isogenic MeT5A, or MPM cell lines, or were identified as post-transcriptional regulators of BAP1 expression. I have summarised the directions of change for these BAP1-related miRNAs in Table 8.1. Employing a similar strategy to the proteome analysis, we first screened for BAP1-dependent miRNAs in isogenic MeT5A *BAP1*$^{w-/KO}$ cell lines, then validated selected candidate expression using an alternative methodology, and finally defined those miRNAs of most interest based on their correlation with BAP1 expression in patient-derived MPM cell lines. This approach not only relates the expression change to genetic *BAP1* loss, but also provides confidence in their clinical relevance if recapitulated across a panel of MPM cell lines. As discussed above, this approach allowed me to identify and validate downregulation of ch14q32.31 miRNAs in BAP1-deficient cells. A further example of a miRNA that responded to BAP1 loss in both

	miRNA	**NS1** C5.1 (*BAP1* w-/KO) vs. MeT5A (*BAP1*+/+)	**NS1** C3.1 (*BAP1* w-/KO) vs. MeT5A (*BAP1*+/+)	**qRT-PCR** C5.1 (*BAP1* w-/KO) vs. MeT5A (*BAP1*+/+)	**qRT-PCR** C3.1 (*BAP1* w-/KO) vs. MeT5A (*BAP1*+/+)	**qRT-PCR** #15 #30 BAP1 neg MPM cell lines vs. MeT5A (*BAP1*+/+)	**qRT-PCR** #43 #52 BAP1 neg MPM cell lines vs. MeT5A (*BAP1*+/+)	**NS2/NS3** BAP1 neg. vs. BAP1 pos. MPM cell lines
Ch14q32.31 miRNAs	**miR-127-3p**							
	miR-377-3p							
	miR-381-3p							
	miR-656-3p							
	miR-376a-3p							
	miR-376b-3p							
	miR-376c-3p							
	miR-409-3p							
	miR-410-3p							
	miR-34c-5p							
	miR-99a-5p							
	miR-155-5p							
	miR-361-3p							
	miR-664a-3p							
	miR-4516							
	miR-10a-5p							
	miR-628-5p							
	miR-221-3p							
	miR-450a-5p							
	let-7i-5p							
	let-7f-5p							
	miR-21-5p							
	miR-5196-3p							
	miR-6732-3p							
	miR-126-3p							
	miR-199a-5p							
	miR-199a-3p							
	miR-199b-3p							
	miR-137							
	miR-582-5p							
	miR-450a-5p							
	miR-450b-5p							
	miR-424-5p							
	miR-503-5p							
	miR-1234-3p							
	miR-200b-3p							
	miR-125b-5p							
	miR-31-5p							
	miR-10b-5p							

Table 8.1: Directional expression changes for BAP1-related miRNAs as highlighted in chapters 5-7.
Dark red: significantly upregulated (P≤0.05, >1.5-fold) miRNA. Pale red: upregulated miRNA, not significant. Dark blue: significantly downregulated (P≤0.05, >1.5-fold) miRNA. Pale blue: downregulated miRNA, not significant. Black: no change. Grey: No data.

cell models is miR-628-5p (Table 8.1), which showed significantly reduced expression in both *BAP1*$^{w-/KO}$ cell lines compared to MeT5A (*BAP1*$^{+/+}$), and in BAP1-negative compared to BAP1-positive MPM cell lines. It would be of great interest to validate this by qRT-PCR in future. Another miRNA of interest is miR-200b-3p, which increased expression in response to BAP1 loss in both cell models, and was also predicted to target BAP1 (Fig. 7.2). Thus, like miR-125b-5p, miR-200b-3p has the potential to function in a double-negative FBL with BAP1.

8.4 Potential for BAP1-dependent post-transcriptional regulation of HDAC2 by miRNAs

The Coulson lab has established a link between BAP1 and HDAC2 (Sacco et al., 2015), and my work has shown that BAP1 regulates HDAC2 transcript levels (see section 4.4.2). In discussion of these results, I speculated that BAP1-dependent miRNAs might have a role in the post-transcriptional regulation of HDAC2, the hypothesis being that if BAP1 deficiency led to upregulation of miRNAs that target HDAC2, this could decrease HDAC2 transcript abundance (see section 4.6). Several miRNAs have been predicted to target HDAC2 and many of these, including miR-145, miR-455 and miR-223, have been validated experimentally in various disease states (see section 4.6). In my dataset (NS1), expression of these miRNAs was not significantly increased in C5.1 (*BAP1*$^{w-/KO}$) cells compared to MeT5A (*BAP1*$^{+/+}$). In fact, miR-145 expression was significantly decreased in C5.1 (*BAP1*$^{w-/KO}$) cells compared to MeT5A (*BAP1*$^{+/+}$). Nevertheless, let-7f-5p is another candidate miRNA predicted to target HDAC2, and its expression was significantly increased in C5.1 (*BAP1*$^{w-/KO}$) cells compared to MeT5A (*BAP1*$^{+/+}$), with a similar trend in C3.1 (*BAP1*$^{w-/KO}$) cells. It would in future be interesting to validate the predicted target site for let-7f-5p in the HDAC2 3'UTR as the first step in exploring potential mechanistic link.

8.5 Mechanisms by which BAP1 may regulate miRNAs

In both the isogenic MeT5A model and the MPM cell panel, I observed a bias towards downregulation of miRNA expression in BAP1-deficient cells (Fig. 5.7, Fig. 6.7 and Table 8.1). BAP1 can regulate transcription through mechanisms that involve its DUB activity towards histone H2A and chromatin associated factors, or its recruitment to specific promoters in multi-protein complexes that activate transcription (Fig. 1.2). Its diverse roles as a transcriptional activator likely account for the differential miRNA expression upon *BAP1* deficiency in isogenic cell lines (chapter 5) and *BAP1*-negative MPM cell lines (chapter 6). miRNAs are either transcriptionally linked to the expression of their host genes or have their

own gene promoters. It is likely that *BAP1* deficiency within multi-protein complexes, like those with HCF-1 (Machida et al., 2009; Misaghi et al., 2009) that activate gene transcription either at host gene or intergenic miRNA gene promoters, downregulates the transcription of miRNA as well as protein-coding genes. Similarly, loss of BAP1 function within the PR-DUB complex would favour chromatin repression through an increase in H2AK119Ub1. In addition, loss of BAP1 protein increased expression of the histone methyltransferase EZH2 in MPM cells (LaFave et al., 2015) (see section 1.3.4.1). The silencing of ch14q32 miRNA cluster by histone methylation was demonstrated in melanoma cell lines (Zehavi et al., 2012), but whether a similar mechanism governs ch14q32.31 miRNA downregulation in MPM cells, and whether this might be mediated by BAP1-dependent histone methyltransferase activity are hypotheses that will need further exploration.

Whilst we demonstrated that BAP1 deficiency reduced HDAC2 expression (Sacco et al., 2015), the consequences on histone deacetylation and gene transcription were not explored in chapter 4. However, from the literature it could be speculated that ch14q32.31 miRNAs may be regulated by HDACs (see section 5.4). I observed silencing of ch14q32.31 miRNAs in almost half (6/14) of all BAP1-negative MPM cell lines, but only one of six BAP1-positive that intriguingly is known to have copy number loss of HDAC2. Histone deacetylation of miRNA gene promoter regions is a common method of miRNA silencing in cancer (Lee and R, 2013). There is evidence for ch14q32.31 miRNA cluster silencing by histone deacetylation in epithelial ovarian cancer cell lines (Zhang et al., 2008). Preliminary data from the Coulson lab (Ashley Hall) now shows that HDACi treatment of BAP-negative MPM cells can induce expression of ch14q32.31 miRNAs. In the context of my data, I observed BAP1-dependent HDAC2 downregulation, making a direct effect of HDAC2 on ch14q32.31 unlikely. However, we have previously shown isoenzyme compensation when BAP1 is depleted by siRNA in lung cancer cells, such that decreased HDAC2 expression was accompanied by a compensatory increase in HDAC1 expression (Sacco et al., 2015). HDAC1 compensation was less evident in BAP1-negative MPM cell lines (Fig. 4.2A) and isogenic MeT5A *BAP1*-mutant cell lines (Fig. 4.7B), nevertheless it would be important in future to investigate the nature of epigenetic silencing of ch14q32 miRNA cluster in *BAP1*-deficient MPM.

8.6 Regulation of BAP1 by miRNAs

miR-31-5p has previously been shown to regulate BAP1 in NSCLC (Yu et al., 2016), however no correlative relationship was apparent in MPM cells (Fig. 7.8). This may in part be due to

the higher frequency of BAP1 mutation in MPM compared with NSCLC (see Fig. 1.2), meaning that BAP1 expression is often lost through other mechanisms in MPM. Target prediction highlighted several other miRNA binding sites in the BAP1 3'UTR. These miRNAs included miR-200a-5p, miR-200b-3p and miR-125b-5p, expression for all of which showed an inverse correlation with BAP1 in MPM cell lines (chapter 7), suggesting that they may regulate, or be regulated by, BAP1. I was able to demonstrate for the first time that BAP1 is a target of miR-125b-5p, and proposed the idea that BAP1 and miR-125b-5p may operate in a double-negative feedback loop that is highly dependent on the BAP1 status of the cell (Fig. 7.13). As discussed in section 7.1, validation of the predicted miR-125b-5p target site in the BAP1 3'UTR by luciferase reporter gene assays would be required to determine whether BAP1 is directly regulated by miR-125b-5p. If this is shown to be the case, it would raise some interesting questions. Firstly, in MPM tumours which lose BAP1 protein expression without an accompanying *BAP1* mutation, that is non-genetic cases, one could entertain the possibility of therapeutically reactivating BAP1 through inhibiting miR-125b-5p with miRNA inhibitors (see section 1.4.4). Secondly, as miRNA profiles are highly tissue-context specific, it would be interesting to establish whether miR-125b-5p regulation of BAP1 extends beyond MPM, into other tumour types with frequent BAP1 loss, such as UVM and RCC.

8.7 Potential to utilise BAP1-dependent miRNAs as surrogate biomarkers for BAP1 loss

As loss of BAP1 protein can support a diagnosis of MPM (Nasu et al., 2015), surrogate markers for BAP1 loss that are detectable by liquid biopsy, such as miRNAs, could hold value as non-invasive diagnostic or prognostic biomarkers in MPM (see section 1.3.2.3). miRNAs that show increased expression in *BAP1*$^{w-/KO}$ cell lines compared to MeT5A (*BAP1*$^{+/+}$), and in BAP1-negative compared to BAP1-positive MPM cell lines, would provide the best candidate biomarkers. Several miRNAs fit these criteria, including miR-4516, miR-664a-3p, miR-126-3p and miR-200b-3p (Table 8.1). Although their association with BAP1-status does not always reach statistical significance in all models, these miRNAs merit further investigation for their potential to be utilised as surrogate markers for BAP1 loss in MPM. In the short term it would be important to validate their expression by qRT-PCR not only in the isogenic MeT5A *BAP1*$^{w-/KO}$ cell lines, but in an expanded panel of 24 MPM cell lines now available in the lab. The prospect of expanding investigation of these BAP1-dependent miRNAs into clinical samples is another future aim. Tissue microarrays (TMAs) with samples from over 700 MPM patients are available through MesobanK. Another project in the

Coulson lab (Sarah Taylor) will characterise BAP1 expression in these TMAs and it would be of interest to investigate any relationship to the expression of BAP1-dependent miRNAs using BaseScope assays (Advanced Cell Diagnostics). This *in-situ* hybridisation method can be used to detect short (50-300 bp) target sequences such as pre-miRNA (60-70 bp). Probes can be designed against the pre-miRNAs of interest and either fluorescently labelled for direct visualisation, or conjugated to chromogenic dyes. Importantly, matched serum and plasma samples are also available in MesobanK, which would have utility in the clinical investigation of significantly upregulated miRNAs as surrogate liquid biopsy markers for BAP1 loss.

8.8 Potential to drug BAP1-dependent adaptations in MPM

Our search for BAP1-dependencies in MPM that might be targeted through synthetic lethal approaches have highlighted a number of protein targets that are potentially druggable, including ICAM1, SERPINE1, ASS1 (chapter 3) and HDAC2 (chapter 4). We showed that genetic *BAP1* inactivation and reduced HDAC2 expression increased resistance to HDACi (see section 4.5). Although clinical trials of vorinostat in MPM have to date proven unsuccessful (Krug et al., 2015), we speculate that HDACi use might prove more successful if patients were stratified by *BAP1* mutation status and HDAC2 expression. Targeting high ICAM1 or SERPINE1 expression may be of utility in *BAP1*-deficient MPM tumours, indeed there are mAbs against human anti-ICAM1 such as BI-505, which has shown anti-tumour activity in mouse models of multiple myeloma (Veitonmaki et al., 2013). Such approaches may diminish the pro-invasive and metastatic phenotype typically associated with high expression of these proteins (Mendez et al., 2009; Liu et al., 2008; Rosette et al., 2005). ASS1 is the rate-limiting enzyme for arginine biosynthesis, and is already of interest in MPM as ~50% do not express ASS1 (Szlosarek et al., 2006), and show synthetic lethality with arginine deprivation using ADI-PEG20 and with inhibition of polyamine metabolism (Locke et al., 2016). However, in our study, we observed increased expression of ASS1 in *BAP1*-mutant cells (Fig. 3.7 and Fig. 3.11), thus we speculate that MPM with *BAP1*-deficiency might show synthetic lethality with direct ASS1 inhibition. In an ongoing project in the Coulson lab (Sarah Taylor) α-Methyl-DL-aspartic acid, an analogue that can target the arginine biosynthesis pathway, is being used to test this hypothesis.

In addition to their potential to inform diagnosis and patient stratification, BAP1-dependent changes in miRNA expression also highlight other potential protein adaptations to *BAP1*-deficiency, that may not be directly detected by proteomics (due to

relatively low proteome coverage). By interrogating the miRNA-gene targets for significantly regulated miRNAs, such as those belonging to the ch14q32.31 miRNA locus, there is the potential to detect a synthetic lethal phenotype in *BAP1*-deficient MPM cells.

In conclusion, through use of novel isogenic cell models (generated in house) and well characterised low passage MPM cell lines from MesobanK, we have begun to unravel the biology of BAP1-deficient MPM, and established a "discovery" pipeline for synthetic lethal approaches to exploit vulnerabilities on BAP1 loss of function. I have also identified miRNAs that could account for post-transcriptional, rather than genetic, inactivation of BAP1, which may need to be considered when stratifying BAP1-status in MPM patients. The clinical material now available through MesobanK will allow these studies to be moved forwards, but there remains a need for new pre-clinical models of BAP1-deficient MPM, such as *in vitro* 3D cultures/organoids of *BAP1*-deficient MPM cell lines, and *in vivo* mouse models of *BAP1* together other MPM-related mutations, to further advance the discovery of targeted therapies for MPM.

References

Abdel-Rahman, M. H., Pilarski, R., Cebulla, C. M., Massengill, J. B., Christopher, B. N., Boru, G., Hovland, P. & Davidorf, F. H. (2011). Germline BAP1 mutation predisposes to uveal melanoma, lung adenocarcinoma, meningioma, and other cancers. *Journal of Medical Genetics,* 48(12)**,** 856-859.

Abdul Rehman, S. A., Kristariyanto, Y. A., Choi, S. Y., Nkosi, P. J., Weidlich, S., Labib, K., Hofmann, K. & Kulathu, Y. (2016). MINDY-1 Is a Member of an Evolutionarily Conserved and Structurally Distinct New Family of Deubiquitinating Enzymes. *Mol Cell,* 63(1)**,** 146-55.

Abm. (2018). *miRNA cDNA synthesis workflow* [Online]. Available: https://www.abmgood.com/miRNA/images/Workflow-miRNA-cDNA-synthesis-kit-G269-G270.jpg [Accessed Jan 2018].

Akutsu, M., Dikic, I. & Bremm, A. (2016). Ubiquitin chain diversity at a glance. *J Cell Sci,* 129(5)**,** 875-80.

Al-Mamun, M., Ravenhill, L., Srisukkham, W., Hossain, A., Fall, C., Ellis, V. & Bass, R. (2016). Effects of Noninhibitory Serpin Maspin on the Actin Cytoskeleton: A Quantitative Image Modeling Approach. *Microscopy and Microanalysis,* 22(2)**,** 394-409.

Al-Taei, S., Salimu, J., Lester, J. F., Linnane, S., Goonewardena, M., Harrop, R., Mason, M. D. & Tabi, Z. (2012). Overexpression and potential targeting of the oncofoetal antigen 5T4 in malignant pleural mesothelioma. *Lung Cancer,* 77(2)**,** 312-318.

Alix-Panabieres, C. & Pantel, K. (2013). Circulating tumor cells: liquid biopsy of cancer. *Clin Chem,* 59(1)**,** 110-8.

Ambros, V., Bartel, B., Bartel, D. P., Burge, C. B., Carrington, J. C., Chen, X., Dreyfuss, G., Eddy, S. R., Griffiths-Jones, S., Marshall, M., Matzke, M., Ruvkun, G. & Tuschl, T. (2003). A uniform system for microRNA annotation. *Rna,* 9(3)**,** 277-9.

Andrici, J., Parkhill, T. R., Jung, J., Wardell, K. L., Verdonk, B., Singh, A., Sioson, L., Clarkson, A., Watson, N., Sheen, A., Farzin, M., Toon, C. W. & Gill, A. J. (2016). Loss of expression of BAP1 is very rare in non-small cell lung carcinoma. *Pathology,* 48(4)**,** 336-340.

Andrici, J., Sheen, A., Sioson, L., Wardell, K., Clarkson, A., Watson, N., Ahadi, M. S., Farzin, M., Toon, C. W. & Gill, A. J. (2015). Loss of expression of BAP1 is a useful adjunct, which strongly supports the diagnosis of mesothelioma in effusion cytology. *Modern Pathology,* 28(10)**,** 1360-1368.

Angeloni, D. (2007). Molecular analysis of deletions in human chromosome 3p2l and the role of resident cancer genes in disease. *Briefings in Functional Genomics & Proteomics,* 6(1)**,** 19-39.

Aranda, S., Mas, G. & Di Croce, L. (2015). Regulation of gene transcription by Polycomb proteins. *Science Advances,* 1(11).

Baker, R. T. & Board, P. G. (1991). The human ubiquitin-52 amino acid fusion protein gene shares several structural features with mammalian ribosomal protein genes. *Nucleic Acids Res,* 19(5)**,** 1035-40.

Balatti, V., Maniero, S., Ferracin, M., Veronese, A., Negrini, M., Ferrocci, G., Martini, F. & Tognon, M. G. (2011). MicroRNAs dysregulation in human malignant pleural mesothelioma. *J Thorac Oncol,* 6(5)**,** 844-51.

Balkissoon, R., Lommatzsch, S. & Carolan, B. (2011). Chronic Obstructive Pulmonary Disease: A Concise Review. *Medical Clinics of North America,* 95(6)**,** 1125-+.

Balsara, B. R., Bell, D. W., Sonoda, G., De Rienzo, A., du Manoir, S., Jhanwar, S. C. & Testa, J. R. (1999). Comparative genomic hybridization and loss of heterozygosity analyses identify a common region of deletion at 15q11.1-15 in human malignant mesothelioma. *Cancer Res,* 59(2)**,** 450-4.

Baranwal, S. & Alahari, S. K. (2010). miRNA control of tumor cell invasion and metastasis. *International Journal of Cancer,* 126(6)**,** 1283-1290.

Barriere, H., Nemes, C., Du, K. & Lukacs, G. L. (2007). Plasticity of polyubiquitin recognition as lysosomal targeting signals by the endosomal sorting machinery. *Mol Biol Cell,* 18(10)**,** 3952-65.

Bartel, D. P. (2004). MicroRNAs: Genomics, biogenesis, mechanism, and function. *Cell,* 116(2)**,** 281-297.

Bartel, D. P. (2009). MicroRNAs: Target Recognition and Regulatory Functions. *Cell,* 136(2)**,** 215-233.

Baskerville, S. & Bartel, D. P. (2005). Microarray profiling of microRNAs reveals frequent coexpression with neighboring miRNAs and host genes. *Rna,* 11(3)**,** 241-7.

Baughman, J. M., Rose, C. M., Kolumam, G., Webster, J. D., Wilkerson, E. M., Merrill, A. E., Rhoads, T. W., Noubade, R., Katavolos, P., Lesch, J., Stapleton, D. S., Rabaglia, M. E., Schueler, K. L., Asuncion, R., Domeyer, M., Zavala-Solorio, J., Reich, M., DeVoss, J., Keller, M. P., Attie, A. D., Hebert, A. S., Westphall, M. S., Coon, J. J., Kirkpatrick, D. S. & Dey, A. (2016). NeuCode Proteomics Reveals Bap1 Regulation of Metabolism. *Cell Reports,* 16(2)**,** 583-595.

Baumann, F., Flores, E., Napolitano, A., Kanodia, S., Taioli, E., Pass, H., Yang, H. & Carbone, M. (2015). Mesothelioma patients with germline BAP1 mutations have 7-fold improved long-term survival. *Carcinogenesis,* 36(1)**,** 76-81.

Bell, E. H., Kirste, S., Fleming, J. L., Stegmaier, P., Drendel, V., Mo, X., Ling, S., Fabian, D., Manring, I., Jilg, C. A., Schultze-Seemann, W., McNulty, M., Zynger, D. L., Martin, D., White, J., Werner, M., Grosu, A. L. & Chakravarti, A. (2015). A novel miRNA-based predictive model for biochemical failure following post-prostatectomy salvage radiation therapy. *PLoS One,* 10(3)**,** e0118745.

Benjamin, H., Lebanony, D., Rosenwald, S., Cohen, L., Gibori, H., Barabash, N., Ashkenazi, K., Goren, E., Meiri, E., Morgenstern, S., Perelman, M., Barshack, I., Goren, Y., Edmonston, T. B., Chajut, A., Aharonov, R., Bentwich, Z., Rosenfeld, N. & Cohen, D. (2010). A Diagnostic Assay Based on MicroRNA Expression Accurately Identifies Malignant Pleural Mesothelioma. *Journal of Molecular Diagnostics,* 12(6)**,** 771-779.

Bera, A., VenkataSubbaRao, K., Manoharan, M. S., Hill, P. & Freeman, J. W. (2014). A miRNA Signature of Chemoresistant Mesenchymal Phenotype Identifies Novel Molecular Targets Associated with Advanced Pancreatic Cancer. *Plos One,* 9(9).

Bianchi, C. & Bianchi, T. (2014). Global mesothelioma epidemic: Trend and features. *Indian J Occup Environ Med,* 18(2)**,** 82-8.

Bibby, A. C., Tsim, S., Kanellakis, N., Ball, H., Talbot, D. C., Blyth, K. G., Maskell, N. A. & Psallidas, I. (2016). Malignant pleural mesothelioma: an update on investigation, diagnosis and treatment. *European Respiratory Review,* 25(142)**,** 472-486.

Bjorkqvist, A. M., Tammilehto, L., Anttila, S., Mattson, K. & Knuutila, S. (1997). Recurrent DNA copy number changes in 1q, 4q, 6q, 9p, 13q, 14q and 22q detected by comparative genomic hybridization in malignant mesothelioma. *Br J Cancer,* 75(4)**,** 523-7.

Bloomston, M., Frankel, W. L., Petrocca, F., Volinia, S., Alder, H., Hagan, J. P., Liu, C. G., Bhatt, D., Taccioli, C. & Croce, C. M. (2007). MicroRNA expression patterns to differentiate pancreatic adenocarcinoma from normal pancreas and chronic pancreatitis. *Jama-Journal of the American Medical Association,* 297(17)**,** 1901-1908.

Bononi, A., Giorgi, C., Patergnani, S., Larson, D., Verbruggen, K., Tanji, M., Pellegrini, L., Signorato, V., Olivetto, F., Pastorino, S., Nasu, M., Napolitano, A., Gaudino, G., Morris, P., Sakamoto, G., Ferris, L. K., Danese, A., Raimondi, A., Tacchetti, C., Kuchay, S., Pass, H. I., Affar, E. B., Yang, H., Pinton, P. & Carbone, M. (2017a). BAP1 regulates IP3R3-mediated Ca(2+) flux to mitochondria suppressing cell transformation. *Nature,* 546(7659)**,** 549-553.

Bononi, A., Yang, H. N., Giorgi, C., Patergnani, S., Pellegrini, L., Su, M. M., Xie, G. X., Signorato, V., Pastorino, S., Morris, P., Sakamoto, G., Kuchay, S., Gaudino, G., Pass, H. I., Napolitano, A., Pinton, P., Jia, W. & Carbone, M. (2017b). Germline BAP1 mutations induce a Warburg effect. *Cell Death and Differentiation,* 24(10)**,** 1694-1704.

Borchert, G. M., Lanier, W. & Davidson, B. L. (2006). RNA polymerase III transcribes human microRNAs. *Nature Structural & Molecular Biology,* 13(12)**,** 1097-1101.

Borrelli, N., Denaro, M., Ugolini, C., Poma, A. M., Miccoli, M., Vitti, P., Miccoli, P. & Basolo, F. (2017). miRNA expression profiling of 'noninvasive follicular thyroid neoplasms with papillary-like nuclear features' compared with adenomas and infiltrative follicular variants of papillary thyroid carcinomas. *Modern Pathology,* 30(1)**,** 39-51.

Bott, M., Brevet, M., Taylor, B. S., Shimizu, S., Ito, T., Wang, L., Creaney, J., Lake, R. A., Zakowski, M. F., Reva, B., Sander, C., Delsite, R., Powell, S., Zhou, Q., Shen, R., Olshen, A., Rusch, V. & Ladanyi, M. (2011). The nuclear deubiquitinase BAP1 is commonly inactivated by somatic mutations and 3p21.1 losses in malignant pleural mesothelioma. *Nature Genetics,* 43(7)**,** 668-U81.

Boutin, C., Rey, F. & Viallat, J. R. (1995). Prevention of malignant seeding after invasive diagnostic procedures in patients with pleural mesothelioma. A randomised trial of local radiotherapy. *Chest,* 108(3)**,** 754 - 758.

Bremm, A., Freund, S. M. & Komander, D. (2010). Lys11-linked ubiquitin chains adopt compact conformations and are preferentially hydrolyzed by the deubiquitinase Cezanne. *Nat Struct Mol Biol,* 17(8)**,** 939-47.

Bueno, R., Stawiski, E. W., Goldstein, L. D., Durinck, S., De Rienzo, A., Modrusan, Z., Gnad, F., Nguyen, T. T., Jaiswal, B. S., Chirieac, L. R., Sciaranghella, D., Dao, N., Gustafson, C. E., Munir, K. J., Hackney, J. A., Chaudhuri, A., Gupta, R., Guillory, J., Toy, K., Ha, C., Chen, Y. J., Stinson, J., Chaudhuri, S., Zhang, N., Wu, T. D., Sugarbaker, D. J., de Sauvage, F. J., Richards, W. G. & Seshagiri, S. (2016). Comprehensive genomic analysis of malignant pleural mesothelioma identifies recurrent mutations, gene fusions and splicing alterations. *Nat Genet,* 48(4)**,** 407-16.

Burnette, W. N. (1981). "Western blotting": electrophoretic transfer of proteins from sodium dodecyl sulfate--polyacrylamide gels to unmodified nitrocellulose and radiographic detection with antibody and radioiodinated protein A. *Anal Biochem,* 112(2)**,** 195-203.

Burroughs, A. M., Iyer, L. M. & Aravind, L. (2012). The natural history of ubiquitin and ubiquitin-related domains. *Front Biosci (Landmark Ed),* 17**,** 1433-60.

Busacca, S., Germano, S., De Cecco, L., Rinaldi, M., Comoglio, F., Favero, F., Murer, B., Mutti, L., Pierotti, M. & Gaudino, G. (2010). MicroRNA signature of malignant mesothelioma with potential diagnostic and prognostic implications. *Am J Respir Cell Mol Biol,* 42(3)**,** 312-9.

Calin, G. A. & Croce, C. M. (2006). MicroRNA signatures in human cancers. *Nature Reviews Cancer,* 6(11)**,** 857-866.

Calin, G. A., Dumitru, C. D., Shimizu, M., Bichi, R., Zupo, S., Noch, E., Aldler, H., Rattan, S., Keating, M., Rai, K., Rassenti, L., Kipps, T., Negrini, M., Bullrich, F. & Croce, C. M. (2002). Frequent deletions and down-regulation of micro-RNA genes miR15 and miR16 at 13q14 in chronic lymphocytic leukemia. *Proceedings of the National Academy of Sciences of the United States of America,* 99(24)**,** 15524-15529.

Calin, G. A., Ferracin, M., Cimmino, A., Di Leva, G., Shimizu, M., Wojcik, S. E., Iorio, M. V., Visone, R., Sever, N. I., Fabbri, M., Iuliano, R., Palumbo, T., Pichiorri, F., Roldo, C., Garzon, R., Sevignani, C., Rassenti, L., Alder, H., Volinia, S., Liu, C. G., Kipps, T. J., Negrini, M. & Croce, C. M. (2005). A MicroRNA signature associated with prognosis and progression in chronic lymphocytic leukemia. *N Engl J Med,* 353(17)**,** 1793-801.

Calin, G. A., Sevignani, C., Dan Dumitru, C., Hyslop, T., Noch, E., Yendamuri, S., Shimizu, M., Rattan, S., Bullrich, F., Negrini, M. & Croce, C. M. (2004). Human microRNA genes are

frequently located at fragile sites and genomic regions involved in cancers. *Proceedings of the National Academy of Sciences of the United States of America,* 101(9)**,** 2999-3004.

Cancer Research UK. Available: http://www.cancerresearchuk.org/health-professional/cancer-statistics/statistics-by-cancer-type/mesothelioma#heading-Four [Accessed February 2018].

Capotosti, F., Guernier, S., Lammers, F., Waridel, P., Cai, Y., Jin, J., Conaway, J. W., Conaway, R. C. & Herr, W. (2011). O-GlcNAc Transferase Catalyzes Site-Specific Proteolysis of HCF-1. *Cell,* 144(3)**,** 376-388.

Carbone, M., Emri, S., Dogan, A. U., Steele, I., Tuncer, M., Pass, H. I. & Baris, Y. I. (2007). A mesothelioma epidemic in Cappadocia: scientific developments and unexpected social outcomes. *Nature Reviews Cancer,* 7(2)**,** 147-154.

Castilla, M. A., Moreno-Bueno, G., Romero-Perez, L., Van De Vijver, K., Biscuola, M., Lopez-Garcia, M. A., Prat, J., Matias-Guiu, X., Cano, A., Oliva, E. & Palacios, J. (2011). Micro-RNA signature of the epithelial-mesenchymal transition in endometrial carcinosarcoma. *J Pathol,* 223(1)**,** 72-80.

Cerami, E., Gao, J., Dogrusoz, U., Gross, B. E., Sumer, S. O. & Aksoy, B. A. (2012). The cBio Cancer Genomics Portal: An Open Platform for Exploring Multidimensional Cancer Genomics Data (vol 2, pg 401, 2012). *Cancer Discovery,* 2(10)**,** 960-960.

Ceresoli, G. L., Zucali, P. A., Mencoboni, M., Botta, M., Grossi, F., Cortinovis, D., Zilembo, N., Ripa, C., Tiseo, M., Favaretto, A. G., Soto-Parra, H., De Vincenzo, F., Bruzzone, A., Lorenzi, E., Gianoncelli, L., Ercoli, B., Giordano, L. & Santoro, A. (2013). Phase II study of pemetrexed and carboplatin plus bevacizumab as first-line therapy in malignant pleural mesothelioma. *Br J Cancer,* 109(3)**,** 552-8.

Chau, V., Tobias, J. W., Bachmair, A., Marriott, D., Ecker, D. J., Gonda, D. K. & Varshavsky, A. (1989). A multiubiquitin chain is confined to specific lysine in a targeted short-lived protein. *Science,* 243(4898)**,** 1576-83.

Chen, J. & Chen, Z. J. (2013). Regulation of NF-kappaB by ubiquitination. *Curr Opin Immunol,* 25(1)**,** 4-12.

Chen, L. C., Zhang, J. H., Feng, Y., Li, R. Y., Sun, X., Du, W. H., Piao, X. Y., Wang, H., Yang, D. B., Sun, Y., Li, X. F., Jiang, T., Kang, C. S., Li, Y. L. & Jiang, C. L. (2012). MiR-410 regulates MET to influence the proliferation and invasion of glioma. *International Journal of Biochemistry & Cell Biology,* 44(11)**,** 1711-1717.

Chen, R., Alvero, A. B., Silasi, D. A., Kelly, M. G., Fest, S., Visintin, I., Leiser, A., Schwartz, P. E., Rutherford, T. & Mor, G. (2008). Regulation of IKKbeta by miR-199a affects NF-kappaB activity in ovarian cancer cells. *Oncogene,* 27(34)**,** 4712-23.

Chen, W., Wang, J., Liu, S. L., Wang, S. Q., Cheng, Y. D., Zhou, W. L., Duan, C. J. & Zhang, C. F. (2016). MicroRNA-361-3p suppresses tumor cell proliferation and metastasis by directly targeting SH2B1 in NSCLC. *Journal of Experimental & Clinical Cancer Research,* 35.

Chen, Y. X., Gelfond, J. A. L., McManus, L. M. & Shireman, P. K. (2009). Reproducibility of quantitative RT-PCR array in miRNA expression profiling and comparison with microarray analysis. *Bmc Genomics,* 10.

Chernova, T., Sun, X. M., Powley, I. R., Galavotti, S., Grosso, S., Murphy, F. A., Miles, G. J., Cresswell, L., Antonov, A. V., Bennett, J., Nakas, A., Dinsdale, D., Cain, K., Bushell, M., Willis, A. E. & MacFarlane, M. (2016). Molecular profiling reveals primary mesothelioma cell lines recapitulate human disease. *Cell Death and Differentiation,* 23(7)**,** 1152-1164.

Chew, S. H. & Toyokuni, S. (2015). Malignant mesothelioma as an oxidative stress-induced cancer: An update. *Free Radical Biology and Medicine,* 86**,** 166-178.

Chin, L. J., Ratner, E., Leng, S. G., Zhai, R. H., Nallur, S., Babar, I., Muller, R. U., Straka, E., Su, L., Burki, E. A., Crowell, R. E., Patel, R., Kulkarni, T., Homer, R., Zelterman, D., Kidd, K. K.,

Zhu, Y., Christiani, D. C., Belinsky, S. A., Slack, F. J. & Weidhaas, J. B. (2008). A SNP in a let-7 microRNA Complementary Site in the KRAS 3 ' Untranslated Region Increases Non-Small Cell Lung Cancer Risk. *Cancer Research,* 68(20)**,** 8535-8540.

Choi, J. H., Kwon, H. J., Yoon, B. I., Kim, J. H., Han, S. U., Joo, H. J. & Kim, D. Y. (2001). Expression profile of histone deacetylase 1 in gastric cancer tissues. *Japanese Journal of Cancer Research,* 92(12)**,** 1300-1304.

Chomczynski, P. & Sacchi, N. (1987). Single-step method of RNA isolation by acid guanidinium thiocyanate-phenol-chloroform extraction. *Anal Biochem,* 162(1)**,** 156-9.

Christensen, B. C., Godleski, J. J., Marsit, C. J., Houseman, E. A., Lopez-Fagundo, C. Y., Longacker, J. L., Bueno, R., Sugarbaker, D. J., Nelson, H. H. & Kelsey, K. T. (2008). Asbestos exposure predicts cell cycle control gene promoter methylation in pleural mesothelioma. *Carcinogenesis,* 29(8)**,** 1555-9.

Ciechanover, A., Elias, S., Heller, H. & Hershko, A. (1982). "Covalent affinity" purification of ubiquitin-activating enzyme. *J Biol Chem,* 257(5)**,** 2537-42.

Ciechanover, A., Finley, D. & Varshavsky, A. (1984). Ubiquitin dependence of selective protein degradation demonstrated in the mammalian cell cycle mutant ts85. *Cell,* 37(1)**,** 57-66.

Ciechanover, A., Heller, H., Elias, S., Haas, A. L. & Hershko, A. (1980). ATP-dependent conjugation of reticulocyte proteins with the polypeptide required for protein degradation. *Proc Natl Acad Sci U S A,* 77(3)**,** 1365-8.

Cigognetti, M., Lonardi, S., Fisogni, S., Balzarini, P., Pellegrini, V., Tironi, A., Bercich, L., Bugatti, M., Rossi, G., Murer, B., Barbareschi, M., Giuliani, S., Cavazza, A., Marchetti, G., Vermi, W. & Facchetti, F. (2015). BAP1 (BRCA1-associated protein 1) is a highly specific marker for differentiating mesothelioma from reactive mesothelial proliferations. *Mod Pathol,* 28(8)**,** 1043-57.

Clague, M. J., Barsukov, I., Coulson, J. M., Liu, H., Rigden, D. J. & Urbe, S. (2013). Deubiquitylases from genes to organism. *Physiol Rev,* 93(3)**,** 1289-315.

Clague, M. J., Heride, C. & Urbe, S. (2015). The demographics of the ubiquitin system. *Trends Cell Biol,* 25(7)**,** 417-26.

Cleaton, M. A. M., Dent, C. L., Howard, M., Corish, J. A., Gutteridge, I., Sovio, U., Gaccioli, F., Takahashi, N., Bauer, S. R., Charnock-Jones, D. S., Powel, T. L., Smith, G. C. S., Ferguson-Smith, A. C. & Charalambous, M. (2016). Fetus-derived DLK1 is required for maternal metabolic adaptations to pregnancy and is associated with fetal growth restriction. *Nature Genetics,* 48(12)**,** 1473-1480.

Cress, W. D. & Seto, E. (2000). Histone deacetylases, transcriptional control, and cancer. *Journal of Cellular Physiology,* 184(1)**,** 1-16.

D'haene, B., Mestdagh, B., Hellemans, J. & Vandesompelle, J. (2012). miRNA expression profiling: from reference genes to global mean normalization. 822**,** 261-72.

Da Rocha, S. T., Edwards, C. A., Ito, M., Ogata, T. & Ferguson-Smith, A. C. (2008). Genomic imprinting at the mammalian Dlk1-Dio3 domain. *Trends in Genetics,* 24(6)**,** 306-316.

Dai, F. Y., Lee, H., Zhang, Y., Zhuang, L., Yao, H., Xi, Y. X., Xiao, Z. D., You, M. J., Li, W., Su, X. P. & Gan, B. (2017). BAP1 inhibits the ER stress gene regulatory network and modulates metabolic stress response. *Proceedings of the National Academy of Sciences of the United States of America,* 114(12)**,** 3192-3197.

Dalton, L. E., Clarke, H. J., Knight, J., Lawson, M. H., Wason, J., Lomas, D. A., Howat, W. J., Rintoul, R. C., Rassl, D. M. & Marciniak, S. J. (2013). The endoplasmic reticulum stress marker CHOP predicts survival in malignant mesothelioma. *Br J Cancer,* 108(6)**,** 1340-7.

De La Fouchardiere, A., Cabaret, O., Savin, L., Combemale, P., Schvartz, H., Penet, C., Bonadona, V., Soufir, N. & Bressac-de Paillerets, B. (2015). Germline BAP1 mutations predispose also to multiple basal cell carcinomas. *Clin Genet,* 88(3)**,** 273-7.

De Rienzo, A., Jhanwar, S. C. & Testa, J. R. (2000). Loss of heterozygosity analysis of 13q and 14q in human malignant mesothelioma. *Genes Chromosomes Cancer,* 28(3)**,** 337-41.

De Ruijter, A. J. M., Van Gennip, A. H., Caron, H. N., Kemp, S. & Van Kuilenburg, A. B. P. (2003). Histone deacetylases (HDACs): characterization of the classical HDAC family. *Biochemical Journal,* 370**,** 737-749.

De Santi, C., Melaiu, O., Bonotti, A., Cascione, L., Di Leva, G., Foddis, R., Cristaudo, A., Lucchi, M., Mora, M., Truini, A., Tironi, A., Murer, B., Boldorini, R., Cipollini, M., Gemignani, F., Gasparini, P., Mutti, L. & Landi, S. (2017). Deregulation of miRNAs in malignant pleural mesothelioma is associated with prognosis and suggests an alteration of cell metabolism. *Sci Rep,* 7(1)**,** 3140.

Dennis, G., Sherman, B. T., Hosack, D. A., Yang, J., Gao, W., Lane, H. C. & Lempicki, R. A. (2003). DAVID: Database for annotation, visualization, and integrated discovery. *Genome Biology,* 4(9).

Dey, A., Seshasayee, D., Noubade, R., French, D. M., Liu, J., Chaurushiya, M. S., Kirkpatrick, D. S., Pham, V. C., Lill, J. R., Bakalarski, C. E., Wu, J., Phu, L., Katavolos, P., LaFave, L. M., Abdel-Wahab, O., Modrusan, Z., Seshagiri, S., Dong, K., Lin, Z., Balazs, M., Suriben, R., Newton, K., Hymowitz, S., Garcia-Manero, G., Martin, F., Levine, R. L. & Dixit, V. M. (2012). Loss of the Tumor Suppressor BAP1 Causes Myeloid Transformation. *Science,* 337(6101)**,** 1541-1546.

Doran, J. F., Jackson, P., Kynoch, P. A. & Thompson, R. J. (1983). Isolation of PGP 9.5, a new human neurone-specific protein detected by high-resolution two-dimensional electrophoresis. *J Neurochem,* 40(6)**,** 1542-7.

Duffy, M. J., McGowan, P. M. & Gallagher, W. M. (2008). Cancer invasion and metastasis: changing views. *Journal of Pathology,* 214(3)**,** 283-293.

Duncan, L. M., Piper, S., Dodd, R. B., Saville, M. K., Sanderson, C. M., Luzio, J. P. & Lehner, P. J. (2006). Lysine-63-linked ubiquitination is required for endolysosomal degradation of class I molecules. *Embo j,* 25(8)**,** 1635-45.

Duvic, M., Talpur, R., Ni, X., Zhang, C., Hazarika, P., Kelly, C., Chiao, J. H., Reilly, J. F., Ricker, J. L., Richon, V. M. & Frankel, S. R. (2007). Phase 2 trial of oral vorinostat (suberoylanilide hydroxamic acid, SAHA) for refractory cutaneous T-cell lymphoma, (CTCL). *Blood,* 109(1)**,** 31-39.

Eckschlager, T., Plch, J., Stiborova, M. & Hrabeta, J. (2017). Histone Deacetylase Inhibitors as Anticancer Drugs. *Int J Mol Sci,* 18(7).

Edelmann, M. J., Iphofer, A., Akutsu, M., Altun, M., di Gleria, K., Kramer, H. B., Fiebiger, E., Dhe-Paganon, S. & Kessler, B. M. (2009). Structural basis and specificity of human otubain 1-mediated deubiquitination. *Biochem J,* 418(2)**,** 379-90.

Eibel, R., Tuengerthal, S. & Schoenberg, S. O. (2003). The role of new imaging techniques in diagnosis and staging of malignant pleural mesothelioma. *Current Opinion in Oncology,* 15(2)**,** 131-138.

Eletr, Z. M. & Wilkinson, K. D. (2014). Regulation of proteolysis by human deubiquitinating enzymes. *Biochim Biophys Acta,* 1843(1)**,** 114-28.

Eletr, Z. M., Yin, L. M. & Wilkinson, K. D. (2013). BAP1 is phosphorylated at serine 592 in S-phase following DNA damage. *Febs Letters,* 587(24)**,** 3906-3911.

Elmes, P. C. & Simpson, J. C. (1976). The clinical aspects of mesothelioma. *Q J Med,* 45(179)**,** 427-49.

Elmes, P. C. & Wade, O. L. (1965). Relationship between exposure to asbestos and pleural malignancy in Belfast. *Ann N Y Acad Sci,* 132(1)**,** 549-57.

Epizyme Inc (2016). Clinical trial NCT02860286: Study of the EZH2 Inhibitor Tazemetostat in Malignant Mesothelioma.

Esposito, C. L., Cerchia, L., Catuogno, S., De Vita, G., Dassie, J. P., Santamaria, G., Swiderski, P., Condorelli, G., Giangrande, P. H. & de Franciscis, V. (2014). Multifunctional

aptamer-miRNA conjugates for targeted cancer therapy. *Mol Ther,* 22(6)**,** 1151-1163.

Esquela-Kerscher, A., Trang, P., Wiggins, J. F., Patrawala, L., Cheng, A., Ford, L., Weidhaas, J. B., Brown, D., Bader, A. G. & Slack, F. J. (2008). The let-7 microRNA reduces tumor growth in mouse models of lung cancer. *Cell Cycle,* 7(6)**,** 759-64.

Ettinger, D. S., Wood, D. E., Akerley, W., Bazhenova, L. A., Borghaei, H., Camidge, D. R., Cheney, R. T., Chirieac, L. R., D'Amico, T. A., Dilling, T., Dobelbower, M., Govindan, R., Hennon, M., Horn, L., Jahan, T. M., Komaki, R., Lackner, R. P., Lanuti, M., Lilenbaum, R., Lin, J., Loo, B. W., Jr., Martins, R., Otterson, G. A., Patel, J. D., Pisters, K. M., Reckamp, K., Riely, G. J., Schild, S. E., Shapiro, T. A., Sharma, N., Swanson, S. J., Stevenson, J., Tauer, K., Yang, S. C., Gregory, K. & Hughes, M. (2016). NCCN Guidelines Insights: Malignant Pleural Mesothelioma, Version 3.2016. *J Natl Compr Canc Netw,* 14(7)**,** 825-36.

Farazi, T. A., Hoell, J. I., Morozov, P. & Tuschl, T. (2013). MicroRNAs in Human Cancer. *Microrna Cancer Regulation: Advanced Concepts, Bioinformatics and Systems Biology Tools,* 774**,** 1-20.

Farley, M. N., Schmidt, L. S., Mester, J. L., Pena-Llopis, S., Pavia-Jimenez, A., Christie, A., Vocke, C. D., Ricketts, C. J., Peterson, J., Middelton, L., Kinch, L., Grishin, N., Merino, M. J., Metwalli, A. R., Xing, C., Xie, X. J., Dahia, P. L. M., Eng, C., Linehan, W. M. & Brugarolas, J. (2013). A novel germline mutation in BAP1 predisposes to familial clear-cell renal cell carcinoma. *Mol Cancer Res,* 11(9)**,** 1061-1071.

Farzin, M., Toon, C. W., Clarkson, A., Sioson, L., Watson, N., Andrici, J. & Gill, A. J. (2015). Loss of expression of BAP1 predicts longer survival in mesothelioma. *Pathology,* 47(4)**,** 302-7.

Ferreira, J. V., Soares, A. R., Ramalho, J. S., Pereira, P. & Girao, H. (2015). K63 linked ubiquitin chain formation is a signal for HIF1A degradation by Chaperone-Mediated Autophagy. *Sci Rep,* 5**,** 10210.

Feun, L. (2017). Clinical Trial NCT03022565: Vorinostat in patients with class 2 high risk uveal melanoma.

Filipowicz, W., Bhattacharyya, S. N. & Sonenberg, N. (2008). Mechanisms of post-transcriptional regulation by microRNAs: are the answers in sight? *Nat Rev Genet,* 9(2)**,** 102-14.

Finley, D., Ciechanover, A. & Varshavsky, A. (1984). Thermolability of ubiquitin-activating enzyme from the mammalian cell cycle mutant ts85. *Cell,* 37(1)**,** 43-55.

Fire, A., Xu, S., Montgomery, M. K., Kostas, S. A., Driver, S. E. & Mello, C. C. (1998). Potent and specific genetic interference by double-stranded RNA in Caenorhabditis elegans. *Nature,* 391(6669)**,** 806-11.

Fleige, S. & Pfaffl, M. (2006). RNA integrity and the effect on the real-time qRT-PCR performance. *Molecular Aspects of Medicine,* 27(2-3)**,** 126-139.

Forbes, S. A., Beare, D., Boutselakis, H., Bamford, S., Bindal, N., Tate, J., Cole, C. G., Ward, S., Dawson, E., Ponting, L., Stefancsik, R., Harsha, B., Kok, C. Y., Jia, M. M., Jubb, H., Sondka, Z., Thompson, S., De, T. & Campbell, P. J. (2017). COSMIC: somatic cancer genetics at high-resolution. *Nucleic Acids Research,* 45(D1)**,** D777-D783.

Forbes, S. A., Bhamra, G., Bamford, S., Dawson, E., Kok, C., Clements, J., Menzies, A., Teague, J. W., Futreal, P. A. & Stratton, M. R. (2008). The Catalogue of Somatic Mutations in Cancer (COSMIC). *Current protocols in human genetics / editorial board, Jonathan L. Haines ... [et al.],* Chapter 10**,** Unit 10.11-Unit 10.11.

Friedman, R. C., Farh, K. K., Burge, C. B. & Bartel, D. P. (2009). Most mammalian mRNAs are conserved targets of microRNAs. *Genome Res,* 19(1)**,** 92-105.

Fulwyler, M. J. (1965). Electronic separation of biological cells by volume. *Science,* 150(3698)**,** 910-1.

Gaj, T., Epstein, B. E. & Schaffer, D. V. (2016). Genome Engineering Using Adeno-associated Virus: Basic and Clinical Research Applications. *Mol Ther,* 24(3)**,** 458-64.

Gao, J., Aksoy, B. A., Dogrusoz, U., Dresdner, G., Gross, B., Sumer, S. O., Sun, Y., Jacobsen, A., Sinha, R., Larsson, E., Cerami, E., Sander, C. & Schultz, N. (2013). Integrative Analysis of Complex Cancer Genomics and Clinical Profiles Using the cBioPortal. *Science Signaling,* 6(269).

Gaughan, L., Logan, I. R., Neal, D. E. & Robson, C. N. (2005). Regulation of androgen receptor and histone deacetylase 1 by Mdm2-mediated ubiquitylation. *Nucleic Acids Research,* 33(1)**,** 13-26.

Gaur, A., Jewell, D. A., Liang, Y., Ridzon, D., Moore, J. H., Chen, C., Ambros, V. R. & Israel, M. A. (2007). Characterization of microRNA expression levels and their biological correlates in human cancer cell lines. *Cancer Res,* 67(6)**,** 2456-68.

Gazdar, A. F., Girard, L., Lockwood, W. W., Lam, W. L. & Minna, J. D. (2010). Lung Cancer Cell Lines as Tools for Biomedical Discovery and Research. *Jnci-Journal of the National Cancer Institute,* 102(17)**,** 1310-1321.

Ge, Y. Z., Xu, L. W., Zhou, C. C., Lu, T. Z., Yao, W. T., Wu, R., Zhao, Y. C., Xu, X., Hu, Z. K., Wang, M., Yang, X. B., Zhou, L. H., Zhong, B., Xu, Z., Li, W. C., Zhu, J. G. & Jia, R. P. (2017). A BAP1 Mutation-specific MicroRNA Signature Predicts Clinical Outcomes in Clear Cell Renal Cell Carcinoma Patients with Wild-type BAP1. *J Cancer,* 8(13)**,** 2643-2652.

Gee, G. V., Koestler, D. C., Christensen, B. C., Sugarbaker, D. J., Ugolini, D., Ivaldi, G. P., Resnick, M. B., Houseman, E. A., Kelsey, K. T. & Marsit, C. J. (2010). Downregulated microRNAs in the differential diagnosis of malignant pleural mesothelioma. *International Journal of Cancer,* 127(12)**,** 2859-2869.

Geetha, T., Jiang, J. & Wooten, M. W. (2005). Lysine 63 polyubiquitination of the nerve growth factor receptor TrkA directs internalization and signaling. *Mol Cell,* 20(2)**,** 301-12.

Geisler, S., Holmstrom, K. M., Skujat, D., Fiesel, F. C., Rothfuss, O. C., Kahle, P. J. & Springer, W. (2010). PINK1/Parkin-mediated mitophagy is dependent on VDAC1 and p62/SQSTM1. *Nat Cell Biol,* 12(2)**,** 119-31.

Geiss, G. K., Bumgarner, R. E., Birditt, B., Dahl, T., Dowidar, N., Dunaway, D. L., Fell, H. P., Ferree, S., George, R. D., Grogan, T., James, J. J., Maysuria, M., Mitton, J. D., Oliveri, P., Osborn, J. L., Peng, T., Ratcliffe, A. L., Webster, P. J., Davidson, E. H., Hood, L. & Dimitrov, K. (2008). Direct multiplexed measurement of gene expression with color-coded probe pairs (vol 26, pg 317, 2008). *Nature Biotechnology,* 26(6)**,** 709-709.

Gironella, M., Seux, M., Xie, M. J., Cano, C., Tomasini, R., Gommeaux, J., Garcia, S., Nowak, J., Yeung, M. L., Jeang, K. T., Chaix, A., Fazli, L., Motoo, Y., Wang, Q., Rocchi, P., Russo, A., Gleave, M., Dagorn, J. C., Iovanna, J. L., Carrier, A., Pebusque, M. J. & Dusetti, N. J. (2007). Tumor protein 53-induced nuclear protein 1 expression is repressed by miR-155, and its restoration inhibits pancreatic tumor development. *Proceedings of the National Academy of Sciences of the United States of America,* 104(41)**,** 16170-16175.

Git, A., Dvinge, H., Salmon-Divon, M., Osborne, M., Kutter, C., Hadfield, J., Bertone, P. & Caldas, C. (2010). Systematic comparison of microarray profiling, real-time PCR, and next-generation sequencing technologies for measuring differential microRNA expression. *Rna-a Publication of the Rna Society,* 16(5)**,** 991-1006.

Glozak, M. A., Sengupta, N., Zhang, X. H. & Seto, E. (2005). Acetylation and deacetylation of non-histone proteins. *Gene,* 363**,** 15-23.

Goldknopf, I. L. & Busch, H. (1977). Isopeptide linkage between nonhistone and histone 2A polypeptides of chromosomal conjugate-protein A24. *Proc Natl Acad Sci U S A,* 74(3)**,** 864-8.

Goldstein, G., Scheid, M., Hammerling, U., Schlesinger, D. H., Niall, H. D. & Boyse, E. A. (1975). Isolation of a polypeptide that has lymphocyte-differentiating properties and is probably represented universally in living cells. *Proc Natl Acad Sci U S A,* 72(1)**,** 11-5.

Gordon, S., Akopyan, G., Garban, H. & Bonavida, B. (2006). Transcription factor YY1: structure, function, and therapeutic implications in cancer biology. *Oncogene,* 25(8)**,** 1125-1142.

Grassadonia, A., Cioffi, P., Simiele, F., Iezzi, L., Zilli, M. & Natoli, C. (2013). Role of Hydroxamate-Based Histone Deacetylase Inhibitors (Hb-HDACIs) in the Treatment of Solid Malignancies. *Cancers,* 5(3)**,** 919-42.

Greenberg, R. A., Sobhian, B., Pathania, S., Cantor, S. B., Nakatani, Y. & Livingston, D. M. (2006). Multifactorial contributions to an acute DNA damage response by BRCA1/BARD1-containing complexes. *Genes & Development,* 20(1)**,** 34-46.

Griffiths-Jones, S., Grocock, R. J., van Dongen, S., Bateman, A. & Enright, A. J. (2006). miRBase: microRNA sequences, targets and gene nomenclature. *Nucleic Acids Research,* 34**,** D140-D144.

Griffiths-Jones, S., Saini, H. K., van Dongen, S. & Enright, A. J. (2008). miRBase: tools for microRNA genomics. *Nucleic Acids Research,* 36**,** D154-D158.

Grozinger, C. M. & Schreiber, S. L. (2002). Deacetylase enzymes: biological functions and the use of small-molecule inhibitors. *Chemistry & Biology,* 9(1)**,** 3-16.

Gui, C. Y., Ngo, L., Xu, W. S., Richon, V. M. & Marks, P. A. (2004). Histone deacetylase (HDAC) inhibitor activation of p21(WAF1) involves changes in promoter-associated proteins, including HDAC1. *Proceedings of the National Academy of Sciences of the United States of America,* 101(5)**,** 1241-1246.

Guled, M., Lahti, L., Lindholm, P. M., Salmenkivi, K., Bagwan, I., Nicholson, A. G. & Knuutila, S. (2009). CDKN2A, NF2, and JUN Are Dysregulated Among Other Genes by miRNAs in Malignant Mesothelioma-A miRNA Microarray Analysis. *Genes Chromosomes & Cancer,* 48(7)**,** 615-623.

Gulyaeva, L. F. & Kushlinskiy, N. E. (2016). Regulatory mechanisms of microRNA expression. *Journal of Translational Medicine,* 14.

Guo, G. W., Chmielecki, J., Goparaju, C., Heguy, A., Dolgalev, I., Carbone, M., Seepo, S., Meyerson, M. & Pass, H. I. (2015a). Whole-Exome Sequencing Reveals Frequent Genetic Alterations in BAP1, NF2, CDKN2A, and CUL1 in Malignant Pleural Mesothelioma. *Cancer Research,* 75(2)**,** 264-269.

Guo, R. D., Gu, J. H., Zhang, Z. B., Wang, Y. & Gu, C. (2015b). MicroRNA-410 Functions as a Tumor Suppressor by Targeting Angiotensin II Type 1 Receptor in Pancreatic Cancer. *Iubmb Life,* 67(1)**,** 42-53.

Guo, X. E., Ngo, B., Modrek, A. S. & Lee, W. H. (2014). Targeting Tumor Suppressor Networks for Cancer Therapeutics. *Current Drug Targets,* 15(1)**,** 2-16.

Guo, X. Q., Xia, J. Z. & Yan, J. (2015c). Promoter methylated microRNAs: Potential therapeutic targets in gastric cancer. *Molecular Medicine Reports,* 11(2)**,** 759-765.

Hafner, M., Landgraf, P., Ludwig, J., Rice, A., Ojo, T., Lin, C., Holoch, D., Lim, C. & Tuschl, T. (2008). Identification of microRNAs and other small regulatory RNAs using cDNA library sequencing. *Methods,* 44(1)**,** 3-12.

Han, J. J., Lee, Y., Yeom, K. H., Kim, Y. K., Jin, H. & Kim, V. N. (2004). The Drosha-DGCR8 complex in primary microRNA processing. *Genes & Development,* 18(24)**,** 3016-3027.

Han, L., Witmer, P. D., Casey, E., Valle, D. & Sukumar, S. (2007). DNA methylation regulates microRNA expression. *Cancer Biology & Therapy,* 6(8)**,** 1284-1288.

Harbour, J. W., Onken, M. D., Roberson, E. D. O., Duan, S., Cao, L., Worley, L. A., Council, M. L., Matatall, K. A., Helms, C. & Bowcock, A. M. (2010). Frequent Mutation of BAP1 in Metastasizing Uveal Melanomas. *Science,* 330(6009)**,** 1410-1413.

Harms, K. L. & Chen, X. B. (2007). Histone deacetylase 2 modulates p53 transcriptional activities through regulation of p53-DNA binding activity. *Cancer Research,* 67(7)**,** 3145-3152.

Hart, T., Chandrashekhar, M., Aregger, M., Steinhart, Z., Brown, K. R., MacLeod, G., Mis, M., Zimmermann, M., Fradet-Turcotte, A., Sun, S., Mero, P., Dirks, P., Sidhu, S., Roth, F. P., Rissland, O. S., Durocher, D., Angers, S. & Moffat, J. (2015). High-Resolution CRISPR Screens Reveal Fitness Genes and Genotype-Specific Cancer Liabilities. *Cell,* 163(6).

Hassan, R., Broaddus, V. C., Wilson, S., Liewehr, D. J. & Zhang, J. (2007a). Anti-mesothelin immunotoxin SS1P in combination with gemcitabine results in increased activity against mesothelin-expressing tumor xenografts. *Clin Cancer Res,* 13(23)**,** 7166-71.

Hassan, R., Ebel, W., Routhier, E. L., Patel, R., Kline, J. B., Zhang, J., Chao, Q., Jacob, S., Turchin, H., Gibbs, L., Phillips, M. D., Mudali, S., Iacobuzio-Donahue, C., Jaffee, E. M., Moreno, M., Pastan, I., Sass, P. M., Nicolaides, N. C. & Grasso, L. (2007b). Preclinical evaluation of MORAb-009, a chimeric antibody targeting tumor-associated mesothelin. *Cancer Immun,* 7**,** 20.

He, L., Thomson, J. M., Hemann, M. T., Hernando-Monge, E., Mu, D., Goodson, S., Powers, S., Cordon-Cardo, C., Lowe, S. W., Hannon, G. J. & Hammond, S. M. (2005). A microRNA polycistron as a potential human oncogene. *Nature,* 435(7043)**,** 828-833.

Hebert, L., Bellanger, D., Guillas, C., Campagne, A., Dingli, F., Loew, D., Fievet, A., Jacquemin, V., Popova, T., Jean, D., Mechta-Grigoriou, F., Margueron, R. & Stern, M. H. (2017). Modulating BAP1 expression affects ROS homeostasis, cell motility and mitochondrial function. *Oncotarget,* 8(42)**,** 72513-72527.

Hermeking, H. (2010). The miR-34 family in cancer and apoptosis. *Cell Death Differ,* 17(2)**,** 193-9.

Hershko, A., Ciechanover, A., Heller, H., Haas, A. L. & Rose, I. A. (1980). Proposed role of ATP in protein breakdown: conjugation of protein with multiple chains of the polypeptide of ATP-dependent proteolysis. *Proc Natl Acad Sci U S A,* 77(4)**,** 1783-6.

Hershko, A., Heller, H., Elias, S. & Ciechanover, A. (1983). Components of ubiquitin-protein ligase system. Resolution, affinity purification, and role in protein breakdown. *J Biol Chem,* 258(13)**,** 8206-14.

Hicke, L. (2001). Protein regulation by monoubiquitin. *Nat Rev Mol Cell Biol,* 2(3)**,** 195-201.

Hillegass, J. M., Shukla, A., Lathrop, S. A., MacPherson, M. B., Beuschel, S. L., Butnor, K. J., Testa, J. R., Pass, H. I., Carbone, M., Steele, C. & Mossman, B. T. (2010). Inflammation precedes the development of human malignant mesotheliomas in a SCID mouse xenograft model. *Oxidative/Nitrosative Stress and Disease,* 1203**,** 7-14.

Hiramoto, H., Muramatsu, T., Ichikawa, D., Tanimoto, K., Yasukawa, S., Otsuji, E. & Inazawa, J. (2017). miR-509-5p and miR-1243 increase the sensitivity to gemcitabine by inhibiting epithelial-mesenchymal transition in pancreatic cancer. *Scientific Reports,* 7.

Hochstrasser, M. (2009). Origin and function of ubiquitin-like proteins. *Nature,* 458(7237)**,** 422-9.

Hollevoet, K., Reitsma, J. B., Creaney, J., Grigoriu, B. D., Robinson, B. W., Scherpereel, A., Cristaudo, A., Pass, H. I., Nackaerts, K., Portal, J. A. R., Schneider, J., Muley, T., Di Serio, F., Baas, P., Tomasetti, M., Rai, A. J. & van Meerbeeck, J. P. (2012). Serum Mesothelin for Diagnosing Malignant Pleural Mesothelioma: An Individual Patient Data Meta-Analysis. *Journal of Clinical Oncology,* 30(13)**,** 1541-1549.

Howe, E., Holton, K., Nair, S., Schlauch, D., Sinha, R. & Quackenbush, J. (2010). *MeV: MultiExperiment Viewer* (Vol. 18). New York: Springer.

Hsu, P. P. & Sabatini, D. M. (2008). Cancer cell metabolism: Warburg and beyond. *Cell,* 134(5)**,** 703-707.

Huang, B. H., Laban, M., Leung, C. H. W., Lee, L., Lee, C. K., Salto-Tellez, M., Raju, G. C. & Hooi, S. C. (2005). Inhibition of histone deacetylase 2 increases apoptosis and p21(Cip1/WAF1) expression, independent of histone deacetylase 1. *Cell Death and Differentiation,* 12(4)**,** 395-404.

Huang, F., Kirkpatrick, D., Jiang, X., Gygi, S. & Sorkin, A. (2006). Differential regulation of EGF receptor internalization and degradation by multiubiquitination within the kinase domain. *Mol Cell,* 21(6)**,** 737-48.

Hug, N., Longman, D. & Caceres, J. F. (2016). Mechanism and regulation of the nonsense-mediated decay pathway. *Nucleic Acids Res,* 44(4)**,** 1483-95.

Humphries, B. & Yang, C. (2015). The microRNA-200 family: small molecules with novel roles in cancer development, progression and therapy. *Oncotarget,* 6(9)**,** 6472-98.

Husain, A. N., Colby, T. V., Ordonez, N. G., Allen, T. C., Attanoos, R. L., Beasley, M. B., Butnor, K. J., Chirieac, L. R., Churg, A. M., Dacic, S., Galateau-Salle, F., Gibbs, A., Gown, A. M., Krausz, T., Litzky, L. A., Marchevsky, A., Nicholson, A. G., Roggli, V. L., Sharma, A. K., Travis, W. D., Walts, A. E. & Wick, M. R. (2018). Guidelines for Pathologic Diagnosis of Malignant Mesothelioma 2017 Update of the Consensus Statement From the International Mesothelioma Interest Group. *Arch Pathol Lab Med,* 142(1)**,** 89-108.

Hutvagner, G., McLachlan, J., Pasquinelli, A. E., Balint, E., Tuschl, T. & Zamore, P. D. (2001). A cellular function for the RNA-interference enzyme Dicer in the maturation of the let-7 small temporal RNA. *Science,* 293(5531)**,** 834-838.

Hylebos, M., Van Camp, G., van Meerbeeck, J. P. & de Beeck, K. O. (2016). The Genetic Landscape of Malignant Pleural Mesothelioma: Results from Massively Parallel Sequencing. *Journal of Thoracic Oncology,* 11(10)**,** 1615-1626.

Iliopoulos, D., Jaeger, S. A., Hirsch, H. A., Bulyk, M. L. & Struhl, K. (2010). STAT3 activation of miR-21 and miR-181b-1 via PTEN and CYLD are part of the epigenetic switch linking inflammation to cancer. *Mol Cell,* 39(4)**,** 493-506.

Iorio, M. V. & Croce, C. M. (2017). MicroRNA dysregulation in cancer: diagnostics, monitoring and therapeutics. A comprehensive review. *EMBO Mol Med,* 9(6)**,** 852.

Iorio, M. V., Visone, R., Di Leva, G., Donati, V., Petrocca, F., Casalini, P., Taccioli, C., Volinia, S., Liu, C. G., Alder, H., Calin, G. A., Menard, S. & Croce, C. M. (2007). MicroRNA signatures in human ovarian cancer. *Cancer Research,* 67(18)**,** 8699-8707.

Isayeva, T., Brandwein-Gensler, M., Somarathna, M., Moore-Smith, L. & Lee, T. (2017). Micro-RNA profiling as a predictor for clinical outcomes for head and neck patients. *Current Pharmaceutical Design,* 23.

Ismail, I. H., Davidson, R., Gagne, J. P., Xu, Z. Z., Poirier, G. G. & Hendzel, M. J. (2014). Germline mutations in BAP1 impair its function in DNA double-strand break repair. *Cancer Res,* 74(16)**,** 4282-94.

Ito, K., Ito, M., Elliott, W. M., Cosio, B., Caramori, G., Kon, O. M., Barczyk, A., Hayashi, S., Adcock, I. M., Hogg, J. C. & Barnes, P. J. (2005). Decreased histone deacetylase activity in chronic obstructive pulmonary disease. *New England Journal of Medicine,* 352(19)**,** 1967-1976.

Ivanov, S. V., Goparaju, C. M. V., Lopez, P., Zavadil, J., Toren-Haritan, G., Rosenwald, S., Hoshen, M., Chajut, A., Cohen, D. & Pass, H. I. (2010). Pro-tumorigenic Effects of miR-31 Loss in Mesothelioma. *Journal of Biological Chemistry,* 285(30)**,** 22807-22815.

Ivanov, S. V., Miller, J., Lucito, R., Tang, C., Ivanova, A. V., Pei, J., Carbone, M., Cruz, C., Beck, A., Webb, C., Nonaka, D., Testa, J. R. & Pass, H. I. (2009). Genomic events associated with progression of pleural malignant mesothelioma. *Int J Cancer,* 124(3)**,** 589-99.

Jackman, D. M., Kindler, H. L., Yeap, B. Y., Fidias, P., Salgia, R., Lucca, J., Morse, L. K., Ostler, P. A., Johnson, B. E. & Janne, P. A. (2008). Erlotinib plus bevacizumab in previously treated patients with malignant pleural mesothelioma. *Cancer,* 113(4)**,** 808-14.

Jackson, P. K. (2009). Navigating the deubiquitinating proteome with a CompPASS. *Cell,* 138(2)**,** 222-4.

Jacobson, A. D., Zhang, N. Y., Xu, P., Han, K. J., Noone, S., Peng, J. & Liu, C. W. (2009). The lysine 48 and lysine 63 ubiquitin conjugates are processed differently by the 26 s proteasome. *J Biol Chem,* 284(51)**,** 35485-94.

Jansson, M. D. & Lund, A. H. (2012). MicroRNA and cancer. *Mol Oncol,* 6(6)**,** 590-610.

Jean, D., Daubriac, J., Le Pimpec-Barthes, F., Galateau-Salle, F. & Jaurand, M. C. (2012). Molecular changes in mesothelioma with an impact on prognosis and treatment. *Arch Pathol Lab Med,* 136(3)**,** 277-93.

Jensen, D. E., Proctor, M., Marquis, S. T., Gardner, H. P., Ha, S. I., Chodosh, L. A., Ishov, A. M., Tommerup, N., Vissing, H., Sekido, Y., Minna, J., Borodovsky, A., Schultz, D. C., Wilkinson, K. D., Maul, G. G., Barlev, N., Berger, S. L., Prendergast, G. C. & Rauscher, F. J. (1998). BAP1: a novel ubiquitin hydrolase which binds to the BRCA1 RING finger and enhances BRCA1-mediated cell growth suppression. *Oncogene,* 16(9)**,** 1097-1112.

Ji, Z. L., Mohammed, H., Webber, A., Ridsdale, J., Han, N., Carroll, J. S. & Sharrocks, A. D. (2014). The forkhead transcription factor FOXK2 acts as a chromatin targeting factor for the BAP1-containing histone deubiquitinase complex. *Nucleic Acids Research,* 42(10)**,** 6232-6242.

Jiang, S., Zhang, H. W., Lu, M. H., He, X. H., Li, Y., Gu, H., Liu, M. F. & Wang, E. D. (2010a). MicroRNA-155 functions as an OncomiR in breast cancer by targeting the suppressor of cytokine signaling 1 gene. *Cancer Res,* 70(8)**,** 3119-27.

Jiang, S., Zhang, L. F., Zhang, H. W., Hu, S., Lu, M. H., Liang, S., Li, B., Li, Y., Li, D. S., Wang, E. D. & Liu, M. F. (2012). A novel miR-155/miR-143 cascade controls glycolysis by regulating hexokinase 2 in breast cancer cells. *Embo Journal,* 31(8)**,** 1985-1998.

Jiang, S. A., Zhang, H. W., Lu, M. H., He, X. H., Li, Y., Gu, H., Liu, M. F. & Wang, E. D. (2010b). MicroRNA-155 Functions as an OncomiR in Breast Cancer by Targeting the Suppressor of Cytokine Signaling 1 Gene. *Cancer Research,* 70(8)**,** 3119-3127.

Jin, L., Williamson, A., Banerjee, S., Philipp, I. & Rape, M. (2008). Mechanism of ubiquitin-chain formation by the human anaphase-promoting complex. *Cell,* 133(4)**,** 653-65.

Johansson, L. & Linden, C. J. (1996). Aspects of histopathologic subtype as a prognostic factor in 85 pleural mesotheliomas. *Chest,* 109(1)**,** 109-114.

Johnson, T. G., Schelch, K., Cheng, Y. Y., Williams, M., Sarun, K. H., Kirschner, M. B., Kao, S., Linton, A., Klebe, S., McCaughan, B. C., Lin, R. C. Y., Pirker, C., Berger, W., Lasham, A., van Zandwijk, N. & Reid, G. (2017). Dysregulated Expression of the MicroRNA miR-137 and Its Target YBX1 Contribute to the Invasive Characteristics of Malignant Pleural Mesothelioma. *J Thorac Oncol*.

Johnston, S. C., Riddle, S. M., Cohen, R. E. & Hill, C. P. (1999). Structural basis for the specificity of ubiquitin C-terminal hydrolases. *Embo j,* 18(14)**,** 3877-87.

Josson, S., Gururajan, M., Sung, S. Y., Hu, P., Shao, C., Zhau, H. E., Liu, C., Lichterman, J., Duan, P., Li, Q., Rogatko, A., Posadas, E. M., Haga, C. L. & Chung, L. W. K. (2015). Stromal fibroblast-derived miR-409 promotes epithelial-to-mesenchymal transition and prostate tumorigenesis. *Oncogene,* 34(21)**,** 2690-2699.

Jovic, M., Sharma, M., Rahajeng, J. & Caplan, S. (2010). The early endosome: a busy sorting station for proteins at the crossroads. *Histol Histopathol,* 25(1)**,** 99-112.

Jung, H. Y., Fattet, L. & Yang, J. (2015). Molecular pathways: linking tumor microenvironment to epithelial-mesenchymal transition in metastasis. *Clin Cancer Res,* 21(5)**,** 962-968.

Kadariya, Y., Cheung, M., Xu, J., Pei, J., Sementino, E., Menges, C. W., Cai, K. Q., Rauscher, F. J., Klein-Szanto, A. J. & Testa, J. R. (2016). Bap1 Is a Bona Fide Tumor Suppressor: Genetic Evidence from Mouse Models Carrying Heterozygous Germline Bap1 Mutations. *Cancer Res,* 76(9)**,** 2836-44.

Kao, S. C. H., Reid, G., Lee, K., Vardy, J., Clarke, S. & van Zandwijk, N. (2010). Malignant mesothelioma. *Internal Medicine Journal,* 40(11)**,** 742-750.

Katoh, M. (2013). Functional and cancer genomics of ASXL family members. *Br J Cancer,* 109(2)**,** 299-306.

Kemp, C. D., Rao, M., Xi, S. C., Inchauste, S., Mani, H., Fetsch, P., Filie, A., Zhang, M., Hong, J. A., Walker, R. L., Zhu, Y. L. J., Ripley, R. T., Mathur, A., Liu, F., Yang, M. C., Meltzer, P. A., Marquez, V. E., De Rienzo, A., Bueno, R. & Schrump, D. S. (2012). Polycomb Repressor Complex-2 Is a Novel Target for Mesothelioma Therapy. *Clinical Cancer Research,* 18(1)**,** 77-90.

Kenyani, J., Butt, Z., Taylor, S. E., Grosman, R. X., Rusilowicz, E., Prior, I. A., Clague, M. J., Sacco, J. J. & Coulson, J. M. (manuscript in prep). Genome-edited mesothelial cells reveal BAP1-dependent metabolic adaptation and cytoskeletal proteins highlighting actionable pathways in mesothelioma.

Khan, I. F., Hirata, R. K. & Russell, D. W. (2011). AAV-mediated gene targeting methods for human cells. *Nature Protocols,* 6(4)**,** 482-501.

Khodayari, N., Mohammed, K. A., Goldberg, E. P. & Nasreen, N. (2011). EphrinA1 inhibits malignant mesothelioma tumor growth via let-7 microRNA-mediated repression of the RAS oncogene. *Cancer Gene Ther,* 18(11)**,** 806-16.

Kim, V. N., Han, J. & Siomi, M. C. (2009). Biogenesis of small RNAs in animals. *Nature Reviews Molecular Cell Biology,* 10(2)**,** 126-139.

Kindler, H. L., Karrison, T. G., Gandara, D. R., Lu, C., Krug, L. M., Stevenson, J. P., Janne, P. A., Quinn, D. I., Koczywas, M. N., Brahmer, J. R., Albain, K. S., Taber, D. A., Armato, S. G., 3rd, Vogelzang, N. J., Chen, H. X., Stadler, W. M. & Vokes, E. E. (2012). Multicenter, double-blind, placebo-controlled, randomized phase II trial of gemcitabine/cisplatin plus bevacizumab or placebo in patients with malignant mesothelioma. *J Clin Oncol,* 30(20)**,** 2509-15.

Kinnula, V. L., Linnala, A., Viitala, E., Linnainmaa, K. & Virtanen, I. (1998). Tenascin and fibronectin expression in human mesothelial cells and pleural mesothelioma cell-line cells. *Am J Respir Cell Mol Biol,* 19(3)**,** 445-52.

Kloet, S. L., Makowski, M. M., Baymaz, H. I., van Voorthuijsen, L., Karemaker, I. D., Santanach, A., Jansen, P., Di Croce, L. & Vermeulen, M. (2016). The dynamic interactome and genomic targets of Polycomb complexes during stem-cell differentiation. *Nature Structural & Molecular Biology,* 23(7)**,** 682-690.

Kolluri, K. K., Alifrangis, C., Kumar, N., Ishii, Y., Price, S., Michaut, M., Williams, S., Barthorpe, S., Lightfoot, H., Busacca, S., Sharkey, A., Yuan, Z., Sage, E. K., Vallath, S., Le Quesne, J., Tice, D. A., Alrifai, D., von Karstedt, S., Montinaro, A., Guppy, N., Waller, D. A., Nakas, A., Good, R., Holmes, A., Walczak, H., Fennell, D. A., Garnett, M., Iorio, F., Wessels, L., McDermott, U. & Janes, S. M. (2018). Loss of functional BAP1 augments sensitivity to TRAIL in cancer cells. *Elife,* 7.

Komander, D. (2010). Mechanism, specificity and structure of the deubiquitinases. *Subcell Biochem,* 54**,** 69-87.

Komander, D., Clague, M. J. & Urbe, S. (2009a). Breaking the chains: structure and function of the deubiquitinases. *Nat Rev Mol Cell Biol,* 10(8)**,** 550-63.

Komander, D. & Rape, M. (2012). The ubiquitin code. *Annu Rev Biochem,* 81**,** 203-29.

Komander, D., Reyes-Turcu, F., Licchesi, J. D., Odenwaelder, P., Wilkinson, K. D. & Barford, D. (2009b). Molecular discrimination of structurally equivalent Lys 63-linked and linear polyubiquitin chains. *EMBO Rep,* 10(5)**,** 466-73.

Kong, W., Yang, H., He, L., Zhao, J. J., Coppola, D., Dalton, W. S. & Cheng, J. Q. (2008). MicroRNA-155 is regulated by the transforming growth factor beta/Smad pathway and contributes to epithelial cell plasticity by targeting RhoA. *Mol Cell Biol,* 28(22)**,** 6773-84.

Kouzarides, T. (2007). Chromatin modifications and their function. *Cell,* 128(4)**,** 693-705.

Kozomara, A. & Griffiths-Jones, S. (2011). miRBase: integrating microRNA annotation and deep-sequencing data. *Nucleic Acids Research,* 39**,** D152-D157.

Kozomara, A. & Griffiths-Jones, S. (2014). miRBase: annotating high confidence microRNAs using deep sequencing data. *Nucleic Acids Research,* 42(D1)**,** D68-D73.

Kramer, O. H., Zhu, P., Ostendorff, H. P., Golebiewski, M., Tiefenbach, J., Peters, M. A., Brill, B., Groner, B., Bach, I., Heinzel, T. & Gottlicher, M. (2003). The histone deacetylase inhibitor valproic acid selectively induces proteasomal degradation of HDAC2. *Embo Journal,* 22(13)**,** 3411-3420.

Kristariyanto, Y. A., Rehman, S. A. A., Weidlich, S., Knebel, A. & Kulathu, Y. (2017). A single MIU motif of MINDY-1 recognizes K48-linked polyubiquitin chains. *Embo Reports,* 18(3)**,** 392-402.

Krol, J., Loedige, I. & Filipowicz, W. (2010). The widespread regulation of microRNA biogenesis, function and decay. *Nature Reviews Genetics,* 11(9)**,** 597-610.

Krug, L. M., Kindler, H. L., Calvert, H., Manegold, C., Tsao, A. S., Fennell, D., Ohman, R., Plummer, R., Eberhardt, W. E., Fukuoka, K., Gaafar, R. M., Lafitte, J. J., Hillerdal, G., Chu, Q., Buikhuisen, W. A., Lubiniecki, G. M., Sun, X., Smith, M. & Baas, P. (2015). Vorinostat in patients with advanced malignant pleural mesothelioma who have progressed on previous chemotherapy (VANTAGE-014): a phase 3, double-blind, randomised, placebo-controlled trial. *Lancet Oncol,* 16(4)**,** 447-56.

Kubo, T., Toyooka, S., Tsukuda, K., Sakaguchi, M., Fukazawa, T., Soh, J., Asano, H., Ueno, T., Muraoka, T., Yamamoto, H., Nasu, Y., Kishimoto, T., Pass, H. I., Matsui, H., Huh, N. H. & Miyoshi, S. (2011). Epigenetic silencing of microRNA-34b/c plays an important role in the pathogenesis of malignant pleural mesothelioma. *Clin Cancer Res,* 17(15)**,** 4965-74.

Kuehne, A., Emmert, H., Soehle, J., Winnefeld, M., Fischer, F., Wenck, H., Gallinat, S., Terstegen, L., Lucius, R., Hildebrand, J. & Zamboni, N. (2015). Acute Activation of Oxidative Pentose Phosphate Pathway as First-Line Response to Oxidative Stress in Human Skin Cells. *Molecular Cell,* 59(3)**,** 359-371.

Kuninty, P. R., Schnittert, J., Storm, G. & Prakash, J. (2016). MicroRnA Targeting to Modulate Tumor Microenvironment. *Frontiers in Oncology,* 6.

Laemmli, U. K. (1970). Cleavage of structural proteins during the assembly of the head of bacteriophage T4. *Nature,* 227(5259)**,** 680-5.

LaFave, L. M., Beguelin, W., Koche, R., Teater, M., Spitzer, B., Chramiec, A., Papalexi, E., Keller, M. D., Hricik, T., Konstantinoff, K., Micol, J. B., Durham, B., Knutson, S. K., Campbell, J. E., Blum, G., Shi, X., Doud, E. H., Krivtsov, A. V., Chung, Y. R., Khodos, I., de Stanchina, E., Ouerfelli, O., Adusumilli, P. S., Thomas, P. M., Kelleher, N. L., Luo, M., Keilhack, H., Abdel-Wahab, O., Melnick, A., Armstrong, S. A. & Levine, R. L. (2015). Loss of BAP1 function leads to EZH2-dependent transformation. *Nat Med,* 21(11)**,** 1344-9.

Lagger, G., O'Carroll, D., Rembold, M., Khier, H., Tischler, J., Weitzer, G., Schuettengruber, B., Hauser, C., Brunmeir, R., Jenuwein, T. & Seiser, C. (2002). Essential function of histone deacetylase 1 in proliferation control and CDK inhibitor repression. *Embo Journal,* 21(11)**,** 2672-2681.

Lam, Y. A., Xu, W., DeMartino, G. N. & Cohen, R. E. (1997). Editing of ubiquitin conjugates by an isopeptidase in the 26S proteasome. *Nature,* 385(6618)**,** 737-40.

Landgraf, P., Rusu, M., Sheridan, R., Sewer, A., Iovino, N., Aravin, A., Pfeffer, S., Rice, A., Kamphorst, A. O., Landthaler, M., Lin, C., Socci, N. D., Hermida, L., Fulci, V., Chiaretti, S., Foa, R., Schliwka, J., Fuchs, U., Novosel, A., Muller, R. U., Schermer, B., Bissels, U., Inman, J., Phan, Q., Chien, M., Weir, D. B., Choksi, R., De Vita, G., Frezzetti, D., Trompeter, H. I., Hornung, V., Teng, G., Hartmann, G., Palkovits, M., Di Lauro, R., Wernet, P., Macino, G., Rogler, C. E., Nagle, J. W., Ju, J., Papavasiliou, F. N., Benzing, T., Lichter, P., Tam, W., Brownstein, M. J., Bosio, A., Borkhardt, A., Russo, J. J., Sander, C., Zavolan, M. & Tuschl, T. (2007). A mammalian microRNA expression atlas based on small RNA library sequencing. *Cell,* 129(7)**,** 1401-14.

Lauwers, E., Jacob, C. & Andre, B. (2009). K63-linked ubiquitin chains as a specific signal for protein sorting into the multivesicular body pathway. *J Cell Biol,* 185(3)**,** 493-502.

Lavon, I., Zrihan, D., Granit, A., Einstein, O., Fainstein, N., Cohen, M. A., Zelikovitch, B., Shoshan, Y., Spektor, S., Reubinoff, B. E., Felig, Y., Gerlitz, O., Ben-Hur, T., Smith, Y. & Siegal, T. (2010). Gliomas display a microRNA expression profile reminiscent of neural precursor cells. *Neuro-Oncology,* 12(5)**,** 422-433.

Law, M. R., Hodson, M. E. & Heard, B. E. (1982). MALIGNANT MESOTHELIOMA OF THE PLEURA - RELATION BETWEEN HISTOLOGICAL TYPE AND CLINICAL BEHAVIOR. *Thorax,* 37(11)**,** 810-815.

Lee, H. S., Lee, S. A., Hur, S. K., Seo, J. W. & Kwon, J. (2014). Stabilization and targeting of INO80 to replication forks by BAP1 during normal DNA synthesis. *Nature Communications,* 5.

Lee, J. & R, S. H. (2013). Cancer Epigenetics: Mechanisms and Crosstalk of a HDAC Inhibitor, Vorinostat. *Chemotherapy (Los Angel),* 2(111).

Lee, Y., Kim, M., Han, J. J., Yeom, K. H., Lee, S., Baek, S. H. & Kim, V. N. (2004). MicroRNA genes are transcribed by RNA polymerase II. *Embo Journal,* 23(20)**,** 4051-4060.

Leuenberger, C., Schuoler, C., Bye, H., Mignan, C., Rechsteiner, T., Hillinger, S., Opitz, I., Marsland, B., Faiz, A., Hiemstra, P. S., Timens, W., Camici, G. G., Kohler, M., Huber, L. C. & Brock, M. (2016). MicroRNA-223 controls the expression of histone deacetylase 2: a novel axis in COPD. *Journal of Molecular Medicine-Jmm,* 94(6)**,** 725-734.

Lewis, B. P., Shih, I. H., Jones-Rhoades, M. W., Bartel, D. P. & Burge, C. B. (2003). Prediction of mammalian microRNA targets. *Cell,* 115(7)**,** 787-798.

Lewis, E. B. (1978). A gene complex controlling segmentation in Drosophila. *Nature,* 276(5688)**,** 565-70.

Li, M., Qian, Z., Ma, X., Lin, X., You, Y., Li, Y., Chen, T. & Jiang, H. (2018). MiR-628-5p decreases the tumorigenicity of epithelial ovarian cancer cells by targeting at FGFR2. *Biochem Biophys Res Commun,* 495(2)**,** 2085-2091.

Li, M. F., Li, J., Ding, X. F., He, M. A. & Cheng, S. Y. (2010). microRNA and Cancer. *Aaps Journal,* 12(3)**,** 309-317.

Li, W. & Ye, Y. (2008). Polyubiquitin chains: functions, structures, and mechanisms. *Cell Mol Life Sci,* 65(15)**,** 2397-406.

Li, X., Li, Y., Wan, L., Chen, R. & Chen, F. (2017). miR-509-5p inhibits cellular proliferation and migration via targeting MDM2 in pancreatic cancer cells. *Oncotargets and Therapy,* 10**,** 4455-4464.

Li, X., Lv, Y., Hao, J., Sun, H., Gao, N., Zhang, C., Lu, R., Wang, S., Yin, L., Pu, Y. & Chen, R. (2016a). Role of microRNA-4516 involved autophagy associated with exposure to fine particulate matter. *Oncotarget,* 7(29)**,** 45385-45397.

Li, Z., Hao, Q., Luo, J., Xiong, J., Zhang, S., Wang, T., Bai, L., Wang, W., Chen, M., Gu, L., Lv, K. & Chen, J. (2016b). USP4 inhibits p53 and NF-kappaB through deubiquitinating and stabilizing HDAC2. *Oncogene,* 35(22)**,** 2902-12.

Lim, H. Y., Ho, Q. S., Low, J., Choolani, M. & Wong, K. P. (2011). Respiratory competent mitochondria in human ovarian and peritoneal cancer. *Mitochondrion,* 11(3)**,** 437-443.

Liu, A. H. & Xu, X. W. (2011). MicroRNA Isolation from Formalin-Fixed, Paraffin-Embedded Tissues. *Formalin-Fixed Paraffin-Embedded Tissues: Methods and Protocols,* 724**,** 259-267.

Liu, C. J., Liu, T. Y., Kuo, L. T., Cheng, H. W., Chu, T. H., Chang, K. W. & Lin, S. C. (2008). Differential gene expression signature between primary and metastatic head and neck squamous cell carcinoma. *Journal of Pathology,* 214(4)**,** 489-497.

Liu, J., Valencia-Sanchez, M. A., Hannon, G. J. & Parker, R. (2005). MicroRNA-dependent localization of targeted mRNAs to mammalian P-bodies. *Nat Cell Biol,* 7(7)**,** 719-23.

Liu, M., Wu, H., Liu, T., Li, Y., Wang, F., Wan, H., Li, X. & Tang, H. (2009a). Regulation of the cell cycle gene, BTG2, by miR-21 in human laryngeal carcinoma. *Cell Res,* 19(7)**,** 828-37.

Liu, M. L., Xu, A., Yuan, X., Zhang, Q., Fang, T. T., Wang, W. B. & Li, C. L. (2015). Downregulation of microRNA-409-3p promotes aggressiveness and metastasis in colorectal cancer: an indication for personalized medicine. *Journal of Translational Medicine,* 13.

Liu, R., Zheng, H. Q., Zhou, Z., Dong, J. T. & Chen, C. (2009b). KLF5 promotes breast cell survival partially through fibroblast growth factor-binding protein 1-pERK-mediated dual specificity MKP-1 protein phosphorylation and stabilization. *J Biol Chem,* 284(25)**,** 16791-8.

Livak, K. J. & Schmittgen, T. D. (2001). Analysis of relative gene expression data using real-time quantitative PCR and the 2(-Delta Delta C(T)) Method. *Methods,* 25(4)**,** 402-8.

Lo Iacono, M., Monica, V., Righi, L., Grosso, F., Libener, R., Vatrano, S., Bironzo, P., Novello, S., Musmeci, L., Volante, M., Papotti, M. & Scagliotti, G. V. (2015). Targeted next-generation sequencing of cancer genes in advanced stage malignant pleural mesothelioma: a retrospective study. *J Thorac Oncol,* 10(3)**,** 492-9.

Locke, M., Ghazaly, E., Freitas, M. O., Mitsinga, M., Lattanzio, L., Lo Nigro, C., Nagano, A., Wang, J., Chelala, C., Szlosarek, P. & Martin, S. A. (2016). Inhibition of the Polyamine Synthesis Pathway Is Synthetically Lethal with Loss of Argininosuccinate Synthase 1. *Cell Rep,* 16(6)**,** 1604-1613.

Lu, J., Getz, G., Miska, E. A., Alvarez-Saavedra, E., Lamb, J., Peck, D., Sweet-Cordero, A., Ebet, B. L., Mak, R. H., Ferrando, A. A., Downing, J. R., Jacks, T., Horvitz, H. R. & Golub, T. R. (2005). MicroRNA expression profiles classify human cancers. *Nature,* 435(7043)**,** 834-838.

Lu, Y. Y., Wei, G. B., Liu, L. B., Mo, Y. C., Chen, Q. S., Xu, L. F., Liao, R. W., Zeng, D. H. & Zhang, K. Q. (2017). Direct targeting of MAPK8IP1 by miR-10a-5p is a major mechanism for gastric cancer metastasis. *Oncology Letters,* 13(3)**,** 1131-1136.

Ludwig, N., Leidinger, P., Becker, K., Backes, C., Fehlmann, T., Pallasch, C., Rheinheimer, S., Meder, B., Stahler, C., Meese, E. & Keller, A. (2016). Distribution of miRNA expression across human tissues. *Nucleic Acids Res,* 44(8)**,** 3865-77.

Lujambio, A., Ropero, S., Ballestar, E., Fraga, M. F., Cerrato, C., Setien, F., Casado, S., Suarez-Gauthier, A., Sanchez-Cespedes, M., Gitt, A., Spiteri, I., Das, P. P., Caldas, C., Miska, E. & Esteller, M. (2007). Genetic unmasking of an epigenetically silenced microRNA in human cancer cells. *Cancer Research,* 67(4)**,** 1424-1429.

Ma, L., Reinhardt, F., Pan, E., Soutschek, J., Bhat, B., Marcusson, E. G., Teruya-Feldstein, J., Bell, G. W. & Weinberg, R. A. (2010). Therapeutic silencing of miR-10b inhibits metastasis in a mouse mammary tumor model. *Nat Biotechnol,* 28(4)**,** 341-7.

Ma, Y. X., Tian, Z. N. & Zhang, W. (2012). Circulating miR-125b is a novel biomarker for screening non-small-cell lung cancer and predicts poor prognosis. *Journal of Cancer Research and Clinical Oncology,* 138(12)**,** 2045-2050.

MacDiarmid, J. A. & Brahmbhatt, H. (2011). Minicells: versatile vectors for targeted drug or si/shRNA cancer therapy. *Curr Opin Biotechnol,* 22(6)**,** 909-16.

MacFarlane, L. A. & Murphy, P. R. (2010). MicroRNA: Biogenesis, Function and Role in Cancer. *Current Genomics,* 11(7)**,** 537-561.

Machida, Y. J., Machida, Y., Vashisht, A. A., Wohlschlegel, J. A. & Dutta, A. (2009). The Deubiquitinating Enzyme BAP1 Regulates Cell Growth via Interaction with HCF-1. *Journal of Biological Chemistry,* 284(49)**,** 34179-34188.

Mallery, D. L., Vandenberg, C. J. & Hiom, K. (2002). Activation of the E3 ligase function of the BRCA1/BARD1 complex by polyubiquitin chains. *Embo Journal,* 21(24)**,** 6755-6762.

Mangan, S. & Alon, U. (2003). Structure and function of the feed-forward loop network motif. *Proc Natl Acad Sci U S A,* 100(21)**,** 11980-5.

Mao, Q. D., Zhang, W., Zhao, K., Cao, B., Yuan, H., Wei, L. Z., Song, M. Q. & Liu, X. S. (2017). MicroRNA-455 suppresses the oncogenic function of HDAC2 in human colorectal cancer. *Brazilian Journal of Medical and Biological Research,* 50(6).

Martinez, N. J. & Walhout, A. J. (2009). The interplay between transcription factors and microRNAs in genome-scale regulatory networks. *Bioessays,* 31(4)**,** 435-45.

Mashtalir, N., Daou, S., Barbour, H., Sen, N. N., Gagnon, J., Hammond-Martel, I., Dar, H. H., Therrien, M. & Affar el, B. (2014). Autodeubiquitination protects the tumor suppressor BAP1 from cytoplasmic sequestration mediated by the atypical ubiquitin ligase UBE2O. *Mol Cell,* 54(3)**,** 392-406.

Maurer, T. & Wertz, I. E. (2016). Length Matters: MINDY Is a New Deubiquitinase Family that Preferentially Cleaves Long Polyubiquitin Chains. *Mol Cell,* 63(1)**,** 4-6.

McGregor, S. M., Dunning, R., Hyjek, E., Vigneswaran, W., Husain, A. N. & Krausz, T. (2015). BAP1 facilitates diagnostic objectivity, classification, and prognostication in malignant pleural mesothelioma. *Hum Pathol,* 46(11)**,** 1670-8.

Meas, R. & Mao, P. (2015). Histone ubiquitylation and its roles in transcription and DNA damage response. *DNA Repair (Amst),* 36**,** 36-42.

Mendez, E., Houck, J. R., Doody, D. R., Fan, W. H., Lohavanichbutr, P., Rue, T. C., Yueh, B., Futran, N. D., Upton, M. P., Farwell, D. G., Heagerty, P. J., Zhao, L. P., Schwartz, S. M. & Chen, C. (2009). A Genetic Expression Profile Associated with Oral Cancer Identifies a Group of Patients at High Risk of Poor Survival. *Clinical Cancer Research,* 15(4)**,** 1353-1361.

Meng, F., Henson, R., Wehbe-Janek, H., Ghoshal, K., Jacob, S. T. & Patel, T. (2007). MicroRNA-21 regulates expression of the PTEN tumor suppressor gene in human hepatocellular cancer. *Gastroenterology,* 133(2)**,** 647-58.

Meray, R. K. & Lansbury, P. T. (2007). Reversible monoubiquitination regulates the Parkinson disease-associated ubiquitin hydrolase UCH-L1. *Journal of Biological Chemistry,* 282(14)**,** 10567-10575.

Mestdagh, P., Hartmann, N., Baeriswyl, L., Andreasen, D., Bernard, N., Chen, C., Cheo, D., D'Andrade, P., DeMayo, M., Dennis, L., Derveaux, S., Feng, Y., Fulmer-Smentek, S., Gerstmayer, B., Gouffon, J., Grimley, C., Lader, E., Lee, K. Y., Luo, S., Mouritzen, P., Narayanan, A., Patel, S., Peiffer, S., Ruberg, S., Schroth, G., Schuster, D., Shaffer, J. M., Shelton, E. J., Silveria, S., Ulmanella, U., Veeramachaneni, V., Staedtler, F., Peters, T., Guettouche, T., Wong, L. & Vandesompele, J. (2014). Evaluation of quantitative miRNA expression platforms in the microRNA quality control (miRQC) study. *Nat Methods,* 11(8)**,** 809-15.

Meyer, H. J. & Rape, M. (2014). Enhanced protein degradation by branched ubiquitin chains. *Cell,* 157(4)**,** 910-21.

Meyerhoff, R. R., Yang, C. F., Speicher, P. J., Gulack, B. C., Hartwig, M. G., D'Amico, T. A., Harpole, D. H. & Berry, M. F. (2015). Impact of mesothelioma histologic subtype on outcomes in the Surveillance, Epidemiology, and End Results database. *J Surg Res,* 196(1)**,** 23-32.

Mezei, G., Chang, E. T., Mowat, F. S. & Moolgavkar, S. H. (2017). Epidemiology of mesothelioma of the pericardium and tunica vaginalis testis. *Ann Epidemiol,* 27(5)**,** 348-359.e11.

Min, M., Mevissen, T. E., De Luca, M., Komander, D. & Lindon, C. (2015). Efficient APC/C substrate degradation in cells undergoing mitotic exit depends on K11 ubiquitin linkages. *Mol Biol Cell,* 26(24)**,** 4325-32.

Minardi, D., Lucarini, G., Milanese, G., Di Primio, R., Montironi, R. & Muzzonigro, G. (2016). Loss of nuclear BAP1 protein expression is a marker of poor prognosis in patients with clear cell renal cell carcinoma. *Urol Oncol,* 34(8)**,** 338.e11-8.

Misaghi, S., Galardy, P. J., Meester, W. J., Ovaa, H., Ploegh, H. L. & Gaudet, R. (2005). Structure of the ubiquitin hydrolase UCH-L3 complexed with a suicide substrate. *J Biol Chem,* 280(2)**,** 1512-20.

Misaghi, S., Ottosen, S., Izrael-Tomasevic, A., Arnott, D., Lamkanfi, M., Lee, J., Liu, J. F., O'Rourke, K., Dixit, V. M. & Wilson, A. C. (2009). Association of C-Terminal Ubiquitin Hydrolase BRCA1-Associated Protein 1 with Cell Cycle Regulator Host Cell Factor 1. *Molecular and Cellular Biology,* 29(8)**,** 2181-2192.

Mishra, P. J., Banerjee, D. & Bertino, J. R. (2008). MiRSNPs or MiR-polymorphisms, new players in microRNA mediated regulation of the cell - Introducing microRNA pharmacogenomics. *Cell Cycle,* 7(7)**,** 853-858.

Monia, B. P., Ecker, D. J., Jonnalagadda, S., Marsh, J., Gotlib, L., Butt, T. R. & Crooke, S. T. (1989). Gene synthesis, expression, and processing of human ubiquitin carboxyl extension proteins. *J Biol Chem,* 264(7)**,** 4093-103.

Moody, H. L., Lind, M. J. & Maher, S. G. (2017). MicroRNA-31 Regulates Chemosensitivity in Malignant Pleural Mesothelioma. *Mol Ther Nucleic Acids,* 8**,** 317-329.

Morreale, F. E. & Walden, H. (2016). Types of Ubiquitin Ligases. *Cell,* 165(1)**,** 248-248.e1.

Murali, R., Wiesner, T. & Scolyer, R. A. (2013). Tumours associated with BAP1 mutations. *Pathology,* 45(2)**,** 116-126.

Napolitano, A., Pellegrini, L., Dey, A., Larson, D., Tanji, M., Flores, E. G., Kendrick, B., Lapid, D., Powers, A., Kanodia, S., Pastorino, S., Pass, H. I., Dixit, V., Yang, H. & Carbone, M. (2016). Minimal asbestos exposure in germline BAP1 heterozygous mice is associated with deregulated inflammatory response and increased risk of mesothelioma. *Oncogene,* 35(15)**,** 1996-2002.

Nasu, M., Emi, M., Pastorino, S., Tanji, M., Powers, A., Luk, H., Baumann, F., Zhang, Y. A., Gazdar, A., Kanodia, S., Tiirikainen, M., Flores, E., Gaudino, G., Becich, M. J., Pass, H. I., Yang, H. & Carbone, M. (2015). High Incidence of Somatic BAP1 alterations in sporadic malignant mesothelioma. *J Thorac Oncol,* 10(4)**,** 565-76.

Nathan, J. A., Kim, H. T., Ting, L., Gygi, S. P. & Goldberg, A. L. (2013). Why do cellular proteins linked to K63-polyubiquitin chains not associate with proteasomes? *Embo j,* 32(4)**,** 552-65.

Newhouse, M. L. & Thompson, H. (1965). Mesothelioma of pleura and peritoneum following exposure to asbestos in the London area. *Br J Ind Med,* 22(4)**,** 261-9.

Nishikawa, H., Wu, W., Koike, A., Kojima, R., Gomi, H., Fukuda, M. & Ohta, T. (2009). BRCA1-Associated Protein 1 Interferes with BRCA1/BARD1 RING Heterodimer Activity. *Cancer Research,* 69(1)**,** 111-119.

Njauw, C. N., Kim, I., Piris, A., Gabree, M., Taylor, M., Lane, A. M., DeAngelis, M. M., Gragoudas, E., Duncan, L. M. & Tsao, H. (2012). Germline BAP1 inactivation is preferentially associated with metastatic ocular melanoma and cutaneous-ocular melanoma families. *PLoS One,* 7(4)**,** e35295.

Noh, J. H., Chang, Y. G., Kim, M. G., Jung, K. H., Kim, J. K., Bae, H. J., Eun, J. W., Shen, Q., Kim, S. J., Kwon, S. H., Park, W. S., Lee, J. Y. & Nam, S. W. (2013). MiR-145 functions as a tumor suppressor by directly targeting histone deacetylase 2 in liver cancer. *Cancer Letters,* 335(2)**,** 455-462.

Nouraee, N. & Calin, G. A. (2013). MicroRNAs as cancer biomarkers. *Microrna,* 2(2)**,** 102-17.

O'Connell, R. M., Taganov, K. D., Boldin, M. P., Cheng, G. H. & Baltimore, D. (2007). MicroRNA-155 is induced during the macrophage inflammatory response. *Proceedings of the National Academy of Sciences of the United States of America,* 104(5)**,** 1604-1609.

O'Donnell, K. A., Wentzel, E. A., Zeller, K. I., Dang, C. V. & Mendell, J. T. (2005). c-Myc-regulated microRNAs modulate E2F1 expression. *Nature,* 435(7043)**,** 839-43.

Ogundijo, O. E. & Wang, X. (2017). A sequential Monte Carlo approach to gene expression deconvolution. *PLoS One,* 12(10)**,** e0186167.

Oh, Y. M., Kwon, Y. E., Kim, J. M., Bae, S. J., Lee, B. K., Yoo, S. J., Chung, C. H., Deshaies, R. J. & Seol, J. H. (2009). Chfr is linked to tumour metastasis through the downregulation of HDAC1. *Nature Cell Biology,* 11(3)**,** 295-U158.

Ohar, J. A., Cheung, M., Talarchek, J., Howard, S. E., Howard, T. D., Hesdorffer, M., Peng, H., Rauscher, F. J. & Testa, J. R. (2016). Germline BAP1 Mutational Landscape of Asbestos-Exposed Malignant Mesothelioma Patients with Family History of Cancer. *Cancer Res,* 76(2)**,** 206-15.

Ohta, Y., Shridhar, V., Bright, R. K., Kalemkerian, G. P., Du, W., Carbone, M., Watanabe, Y. & Pass, H. I. (1999). VEGF and VEGF type C play an important role in angiogenesis and lymphangiogenesis in human malignant mesothelioma tumours. *Br J Cancer,* 81(1)**,** 54-61.

Ohtake, F., Saeki, Y., Ishido, S., Kanno, J. & Tanaka, K. (2016). The K48-K63 Branched Ubiquitin Chain Regulates NF-kappaB Signaling. *Mol Cell,* 64(2)**,** 251-266.

Okino, Y., Machida, Y., Frankland-Searby, S. & Machida, Y. J. (2015). BRCA1-associated Protein 1 (BAP1) Deubiquitinase Antagonizes the Ubiquitin-mediated Activation of FoxK2 Target Genes. *Journal of Biological Chemistry,* 290(3)**,** 1580-1591.

Ononye, S. N., van Heyst, M., Falcone, E. M., Anderson, A. C. & Wright, D. L. (2012). Toward isozyme-selective inhibitors of histone deacetylase as therapeutic agents for the treatment of cancer. *Pharm Pat Anal,* 1(2)**,** 207-21.

Owen, W. G. (1964). Diffuse Mesothelioma and Exposure to Asbestos Dust in the Merseyside Area. *Br Med J,* 2(5403)**,** 214-8.

Paronetto, M. P., Passacantilli, I. & Sette, C. (2016). Alternative splicing and cell survival: from tissue homeostasis to disease. *Cell Death Differ,* 23(12)**,** 1919-1929.

Parrotta, R., Okonska, A., Ronner, M., Weder, W., Stahel, R., Penengo, L. & Felley-Bosco, E. (2017). A Novel BRCA1-Associated Protein-1 Isoform Affects Response of Mesothelioma Cells to Drugs Impairing BRCA1-Mediated DNA Repair. *J Thorac Oncol,* 12(8)**,** 1309-1319.

Pass, H. I., Goparaju, C., Ivanov, S., Donington, J., Carbone, M., Hoshen, M., Cohen, D., Chajut, A., Rosenwald, S., Dan, H., Benjamin, S. & Aharonov, R. (2010). hsa-miR-29c* Is Linked to the Prognosis of Malignant Pleural Mesothelioma. *Cancer Research,* 70(5)**,** 1916-1924.

Pelaez, N. & Carthew, R. (2012). *MicroRNAs in Development* (Vol. 99).

Pena-Llopis, S., Vega-Rubin-de-Celis, S., Liao, A., Leng, N., Pavia-Jimenez, A., Wang, S., Yamasaki, T., Zhrebker, L., Sivanand, S., Spence, P., Kinch, L., Hambuch, T., Jain, S., Lotan, Y., Margulis, V., Sagalowsky, A. I., Summerour, P. B., Kabbani, W., Wong, S. W. W., Grishin, N., Laurent, M., Xie, X.-J., Haudenschild, C. D., Ross, M. T., Bentley, D. R., Kapur, P. & Brugarolas, J. (2012). BAP1 loss defines a new class of renal cell carcinoma (vol 44, pg 751, 2012). *Nature Genetics,* 44(9)**,** 1072-1072.

Peters, L. & Meister, G. (2007). Argonaute proteins: Mediators of RNA silencing. *Molecular Cell,* 26(5)**,** 611-623.

Petersen, I., Hidalgo, A., Petersen, S., Schluns, K., Schewe, C., Pacyna-Gengelbach, M., Goeze, A., Krebber, B., Knosel, T., Kaufmann, O., Szymas, J. & von Deimling, A. (2000). Chromosomal imbalances in brain metastases of solid tumors. *Brain Pathol,* 10(3)**,** 395-401.

Pollard, T. D. & Beltzner, C. C. (2002). Structure and function of the Arp2/3 complex. *Current Opinion in Structural Biology,* 12(6)**,** 768-774.

Popova, T., Hebert, L., Jacquemin, V., Gad, S., Caux-Moncoutier, V., Dubois-d'Enghien, C., Richaudeau, B., Renaudin, X., Sellers, J., Nicolas, A., Sastre-Garau, X., Desjardins, L., Gyapay, G., Raynal, V., Sinilnikova, O. M., Andrieu, N., Manie, E., de Pauw, A., Gesta, P., Bonadona, V., Maugard, C. M., Penet, C., Avril, M.-F., Barillot, E., Cabaret, O., Delattre, O., Richard, S., Caron, O., Benfodda, M., Hu, H.-H., Soufir, N., Bressac-de Paillerets, B., Stoppa-Lyonnet, D. & Stern, M.-H. (2013). Germline BAP1 Mutations

Predispose to Renal Cell Carcinomas. *American Journal of Human Genetics,* 92(6)**,** 974-980.

Popp, M. W., Artavanis-Tsakonas, K. & Ploegh, H. L. (2009). Substrate filtering by the active site crossover loop in UCHL3 revealed by sortagging and gain-of-function mutations. *J Biol Chem,* 284(6)**,** 3593-602.

Porcu, M. & Chiarugi, A. (2005). The emerging therapeutic potential of sirtuin-interacting drugs: from cell death to lifespan extension. *Trends in Pharmacological Sciences,* 26(2)**,** 94-103.

Price, B. D. & D'Andrea, A. D. (2013). Chromatin remodeling at DNA double-strand breaks. *Cell,* 152(6)**,** 1344-54.

Prins, J. B., Williamson, K. A., Kamp, M. M. K., Van Hezik, E. J., Van der Kwast, T. H., Hagemeijer, A. & Versnel, M. A. (1998). The gene for the cyclin-dependent-kinase-4 inhibitor, CDKN2A, is preferentially deleted in malignant mesothelioma. *International Journal of Cancer,* 75(4)**,** 649-653.

Pritchard, C. C., Cheng, H. H. & Tewari, M. (2012). MicroRNA profiling: approaches and considerations. *Nature Reviews Genetics,* 13(5)**,** 358-369.

Pulford, E., Huilgol, K., Moffat, D., Henderson, D. W. & Klebe, S. (2017). Malignant Mesothelioma, BAP1 Immunohistochemistry, and VEGFA: Does BAP1 Have Potential for Early Diagnosis and Assessment of Prognosis? *Dis Markers,* 2017**,** 1310478.

Qin, J., Zhou, Z., Chen, W., Wang, C., Zhang, H., Ge, G., Shao, M., You, D., Fan, Z., Xia, H., Liu, R. & Chen, C. (2015). BAP1 promotes breast cancer cell proliferation and metastasis by deubiquitinating KLF5. *Nat Commun,* 6**,** 8471.

Rahighi, S., Ikeda, F., Kawasaki, M., Akutsu, M., Suzuki, N., Kato, R., Kensche, T., Uejima, T., Bloor, S., Komander, D., Randow, F., Wakatsuki, S. & Dikic, I. (2009). Specific recognition of linear ubiquitin chains by NEMO is important for NF-kappaB activation. *Cell,* 136(6)**,** 1098-109.

Redman, K. L. & Rechsteiner, M. (1989). Identification of the long ubiquitin extension as ribosomal protein S27a. *Nature,* 338(6214)**,** 438-40.

Reid, G. (2015). MicroRNAs in mesothelioma: from tumour suppressors and biomarkers to therapeutic targets. *Journal of Thoracic Disease,* 7(6)**,** 1031-1040.

Reid, G., Pel, M. E., Kirschner, M. B., Cheng, Y. Y., Mugridge, N., Weiss, J., Williams, M., Wright, C., Edelman, J. J., Vallely, M. P., McCaughan, B. C., Klebe, S., Brahmbhatt, H., MacDiarmid, J. A. & van Zandwijk, N. (2013). Restoring expression of miR-16: a novel approach to therapy for malignant pleural mesothelioma. *Ann Oncol,* 24(12)**,** 3128-35.

Reyes-Turcu, F. E., Ventii, K. H. & Wilkinson, K. D. (2009). Regulation and cellular roles of ubiquitin-specific deubiquitinating enzymes. *Annu Rev Biochem,* 78**,** 363-97.

Righi, L., Duregon, E., Vatrano, S., Izzo, S., Giorcelli, J., Rondon-Lagos, M., Ascoli, V., Ruffini, E., Ventura, L., Volante, M., Papotti, M. & Scagliotti, G. V. (2016). BRCA1-Associated Protein 1 (BAP1) Immunohistochemical Expression as a Diagnostic Tool in Malignant Pleural Mesothelioma Classification: A Large Retrospective Study. *Journal of Thoracic Oncology,* 11(11)**,** 2006-2017.

Rintoul, R. C., Rassl, D. M., Gittins, J., Marciniak, S. J. & Mesoban, K. C. (2016). MesobanK UK: an international mesothelioma bioresource. *Thorax,* 71(4)**,** 380-382.

Rintoul, R. C., Ritchie, A. J., Edwards, J. G., Waller, D. A., Coonar, A. S., Bennett, M., Lovato, E., Hughes, V., Fox-Rushby, J. A. & Sharples, L. D. (2014). Efficacy and cost of video-assisted thoracoscopic partial pleurectomy versus talc pleurodesis in patients with malignant pleural mesothelioma (MesoVATS): an open-label, randomised, controlled trial. *Lancet,* 384(9948)**,** 1118-27.

Ritorto, M. S., Ewan, R., Perez-Oliva, A. B., Knebel, A., Buhrlage, S. J., Wightman, M., Kelly, S. M., Wood, N. T., Virdee, S., Gray, N. S., Morrice, N. A., Alessi, D. R. & Trost, M. (2014).

Screening of DUB activity and specificity by MALDI-TOF mass spectrometry. *Nat Commun,* 5**,** 4763.

Roberts, D. J. & Miyamoto, S. (2015). Hexokinase II integrates energy metabolism and cellular protection: Akting on mitochondria and TORCing to autophagy. *Cell Death and Differentiation,* 22(2)**,** 248-257.

Robinson, B. M. (2012). Malignant pleural mesothelioma: an epidemiological perspective. *Ann Cardiothorac Surg,* 1(4)**,** 491-6.

Robinson, B. W., Creaney, J., Lake, R., Nowak, A., Musk, A. W., de Klerk, N., Winzell, P., Hellstrom, K. E. & Hellstrom, I. (2003). Mesothelin-family proteins and diagnosis of mesothelioma. *Lancet,* 362(9396)**,** 1612-6.

Rodriguez, A., Griffiths-Jones, S., Ashurst, J. L. & Bradley, A. (2004). Identification of mammalian microRNA host genes and transcription units. *Genome Res,* 14(10a)**,** 1902-10.

Rosette, C., Roth, R. B., Oeth, P., Braun, A., Kammerer, S., Ekblom, J. & Denissenko, M. F. (2005). Role of ICAM1 in invasion of human breast cancer cells. *Carcinogenesis,* 26(5)**,** 943-950.

Rothschild, S. I. (2014). microRNA therapies in cancer. *Mol Cell Ther,* 2**,** 7.

Royo, H. & Cavaille, J. (2008). Non-coding RNAs in imprinted gene clusters. *Biology of the Cell,* 100(3)**,** 149-166.

Russell, D. W. & Hirata, R. K. (1998). Human gene targeting by viral vectors. *Nature Genetics,* 18(4)**,** 325-330.

Sacco, J. J., Kenyani, J., Butt, Z., Carter, R., Chew, H. Y., Cheeseman, L. P., Darling, S., Denny, M., Urbe, S., Clague, M. J. & Coulson, J. M. (2015). Loss of the deubiquitylase BAP1 alters class I histone deacetylase expression and sensitivity of mesothelioma cells to HDAC inhibitors. *Oncotarget,* 6(15)**,** 13757-13771.

Sahtoe, D. D., van Dijk, W. J., Ekkebus, R., Ovaa, H. & Sixma, T. K. (2016). BAP1/ASXL1 recruitment and activation for H2A deubiquitination. *Nature Communications,* 7.

Saiki, R. K., Scharf, S., Faloona, F., Mullis, K. B., Horn, G. T., Erlich, H. A. & Arnheim, N. (1985). Enzymatic amplification of beta-globin genomic sequences and restriction site analysis for diagnosis of sickle cell anemia. *Science,* 230(4732)**,** 1350-4.

Santarelli, L., Strafella, E., Staffolani, S., Amati, M., Emanuelli, M., Sartini, D., Pozzi, V., Carbonari, D., Bracci, M., Pignotti, E., Mazzanti, P., Sabbatini, A., Ranaldi, R., Gasparini, S., Neuzil, J. & Tomasetti, M. (2011). Association of MiR-126 with soluble mesothelin-related peptides, a marker for malignant mesothelioma. *PLoS One,* 6(4)**,** e18232.

Scherpereel, A. (2017). Nivolumab Monotherapy or Nivolumab Plus Ipilimumab, for Unresectable Malignant Pleural Mesothelioma (MPM) Patients (MAPS2). *ASCO.* Chicago.

Scherpereel, A., Astoul, P., Baas, P., Berghmans, T., Clayson, H., de Vuyst, P., Dienemann, H., Galateau-Salle, F., Hennequin, C., Hillerdal, G., Le Pechoux, C., Mutti, L., Pairon, J. C., Stahel, R., van Houtte, P., van Meerbeeck, J., Waller, D. & Weder, W. (2010). Guidelines of the European Respiratory Society and the European Society of Thoracic Surgeons for the management of malignant pleural mesothelioma. *European Respiratory Journal,* 35(3)**,** 479-495.

Scheuermann, J. C., Alonso, A. G. D., Oktaba, K., Ly-Hartig, N., McGinty, R. K., Fraterman, S., Wilm, M., Muir, T. W. & Muller, J. (2010). Histone H2A deubiquitinase activity of the Polycomb repressive complex PR-DUB. *Nature,* 465(7295)**,** 243-U138.

Schipper, P. H., Nichols, F. C., Thomse, K. M., Deschamps, C., Cassivi, S. D., Allen, M. S. & Pairolero, P. C. (2008). Malignant pleural mesothelioma: surgical management in 285 patients. *Ann Thorac Surg,* 85(1)**,** 257-64; discussion 264.

Schmittgen, T. D., Lee, E. J., Jiang, J. M., Sarkar, A., Yang, L. Q., Elton, T. S. & Chen, C. F. (2008). Real-time PCR quantification of precursor and mature microRNA. *Methods,* 44(1)**,** 31-38.

Schramm, A., Opitz, I., Thies, S., Seifert, B., Moch, H., Weder, W. & Soltermann, A. (2010). Prognostic significance of epithelial-mesenchymal transition in malignant pleural mesothelioma. *Eur J Cardiothorac Surg,* 37(3)**,** 566-72.

Schroeder, A., Mueller, O., Stocker, S., Salowsky, R., Leiber, M., Gassmann, M., Lightfoot, S., Menzel, W., Granzow, M. & Ragg, T. (2006). The RIN: an RNA integrity number for assigning integrity values to RNA measurements. *Bmc Molecular Biology,* 7.

Schwarz, D. S., Hutvagner, G., Du, T., Xu, Z. S., Aronin, N. & Zamore, P. D. (2003). Asymmetry in the assembly of the RNAi enzyme complex. *Cell,* 115(2)**,** 199-208.

Schwarzenbach, H., da Silva, A. M., Calin, G. & Pantel, K. (2015). Data Normalization Strategies for MicroRNA Quantification. *Clinical Chemistry,* 61(11)**,** 1333-1342.

Scott, D. A., Richardson, A. D., Filipp, F. V., Knutzen, C. A., Chiang, G. G., Ronai, Z. A., Osterman, A. L. & Smith, J. W. (2011). Comparative Metabolic Flux Profiling of Melanoma Cell Lines BEYOND THE WARBURG EFFECT. *Journal of Biological Chemistry,* 286(49)**,** 42626-42634.

Segre, C. V. & Chiocca, S. (2011). Regulating the Regulators: The Post-Translational Code of Class I HDAC1 and HDAC2. *Journal of Biomedicine and Biotechnology*.

Seitz, H., Royo, H., Bortolin, M. L., Lin, S. P., Ferguson-Smith, A. C. & Cavaille, J. (2004). A large imprinted microRNA gene cluster at the mouse Dlkl-Gtl2 domain. *Genome Research,* 14(9)**,** 1741-1748.

Sekido, Y., Pass, H. I., Bader, S., Mew, D. J., Christman, M. F., Gazdar, A. F. & Minna, J. D. (1995). Neurofibromatosis type 2 (NF2) gene is somatically mutated in mesothelioma but not in lung cancer. *Cancer Res,* 55(6)**,** 1227-31.

Shah, M. Y., Ferrajoli, A., Sood, A. K., Lopez-Berestein, G. & Calin, G. A. (2016). microRNA Therapeutics in Cancer - An Emerging Concept. *EBioMedicine,* 12**,** 34-42.

Shahar, T., Granit, A., Zrihan, D., Canello, T., Charbit, H., Einstein, O., Rozovski, U., Elgavish, S., Ram, Z., Siegal, T. & Lavon, I. (2016). Expression level of miRNAs on chromosome 14q32.31 region correlates with tumor aggressiveness and survival of glioblastoma patients. *Journal of Neuro-Oncology,* 130(3)**,** 413-422.

Shalem, O., Sanjana, N. E., Hartenian, E., Shi, X., Scott, D. A., Mikkelsen, T. S., Heckl, D., Ebert, B. L., Root, D. E., Doench, J. G. & Zhang, F. (2014). Genome-Scale CRISPR-Cas9 Knockout Screening in Human Cells. *Science,* 343(6166)**,** 84-87.

Shapiro, A. L., Vinuela, E. & Maizel, J. V., Jr. (1967). Molecular weight estimation of polypeptide chains by electrophoresis in SDS-polyacrylamide gels. *Biochem Biophys Res Commun,* 28(5)**,** 815-20.

Shen, J. J., Niu, W. N., Zhou, M., Zhang, H. B., Ma, J., Wang, L. & Zhang, H. Y. (2014). MicroRNA-410 Suppresses Migration and Invasion by Targeting MDM2 in Gastric Cancer. *Plos One,* 9(8).

Shi, X. B., Xue, L. R., Ma, A. H., Tepper, C. G., Kung, H. J. & White, R. W. D. (2011). miR-125b Promotes Growth of Prostate Cancer Xenograft Tumor Through Targeting Pro-Apoptotic Genes. *Prostate,* 71(5)**,** 538-549.

Shi, Y. (2007). Histone lysine demethylases: emerging roles in development, physiology and disease. *Nat Rev Genet,* 8(11)**,** 829-33.

Shi, Y., Bo, Z., Pang, G., Qu, X., Bao, W., Yang, L. & Ma, Y. (2017). MiR-99a-5p regulates proliferation, migration and invasion abilities of human oral carcinoma cells by targeting NOX4. *Neoplasma,* 64(5)**,** 666-673.

Shu, Z. B., Chen, L. B. & Ding, D. Y. (2016). miR-582-5P induces colorectal cancer cell proliferation by targeting adenomatous polyposis coli. *World Journal of Surgical Oncology,* 14.

Simon, J. A. & Kingston, R. E. (2009). Mechanisms of polycomb gene silencing: knowns and unknowns. *Nat Rev Mol Cell Biol,* 10(10)**,** 697-708.

Smith, P. K., Krohn, R. I., Hermanson, G. T., Mallia, A. K., Gartner, F. H., Provenzano, M. D., Fujimoto, E. K., Goeke, N. M., Olson, B. J. & Klenk, D. C. (1985). MEASUREMENT OF PROTEIN USING BICINCHONINIC ACID. *Analytical Biochemistry,* 150(1)**,** 76-85.

Song, H., Tao, L., Chen, C., Pan, L., Hao, J., Ni, Y., Li, D., Li, B. & Shi, G. (2015). USP17-mediated deubiquitination and stabilization of HDAC2 in cigarette smoke extract-induced inflammation. *Int J Clin Exp Pathol,* 8(9)**,** 10707-15.

Song, J., Noh, J. H., Lee, J. H., Eun, J. W., Ahn, Y. M., Kim, S. Y., Lee, S. H., Park, W. S., Yoo, N. J., Lee, J. Y. & Nam, S. W. (2005). Increased expression of historic deacetylase 2 is found in human gastric cancer. *Apmis,* 113(4)**,** 264-268.

Song, Y. H., Wang, J., Nie, G., Chen, Y. J., Li, X., Jiang, X. & Cao, W. H. (2017). MicroRNA-509-5p functions as an anti- oncogene in breast cancer via targeting SOD2. *European Review for Medical and Pharmacological Sciences,* 21(16)**,** 3617-3625.

Sowa, M. E., Bennett, E. J., Gygi, S. P. & Harper, J. W. (2009). Defining the Human Deubiquitinating Enzyme Interaction Landscape. *Cell,* 138(2)**,** 389-403.

Spence, J., Sadis, S., Haas, A. L. & Finley, D. (1995). A ubiquitin mutant with specific defects in DNA repair and multiubiquitination. *Mol Cell Biol,* 15(3)**,** 1265-73.

Stokes, M. P., Rush, J., Macneill, J., Ren, J. M., Sprott, K., Nardone, J., Yang, V., Beausoleil, S. A., Gygi, S. P., Livingstone, M., Zhang, H., Polakiewicz, R. D. & Comb, M. J. (2007). Profiling of UV-induced ATM/ATR signaling pathways. *Proc Natl Acad Sci U S A,* 104(50)**,** 19855-60.

Strell, C., Lang, K., Niggemann, B., Zaenker, K. S. & Entschladen, F. (2007). Surface molecules regulating rolling and adhesion to endothelium of neutrophil granulocytes and MDA-MB-468 breast carcinoma cells and their interaction. *Cellular and Molecular Life Sciences,* 64(24)**,** 3306-3316.

Sugarbaker, D. & Wolf, A. (2010). Surgery for malignant pleural mesothelioma. *Expert Review of Respiratory Medicine,* 4(3)**,** 363-372.

Sugiyama, K., Kajiyama, H., Shibata, K., Yuan, H., Kikkawa, F. & Senga, T. (2014). Expression of the miR200 Family of microRNAs in Mesothelial Cells Suppresses the Dissemination of Ovarian Cancer Cells. *Molecular Cancer Therapeutics,* 13(8)**,** 2081-2091.

Sun, Y. M., Lin, K. Y. & Chen, Y. Q. (2013). Diverse functions of miR-125 family in different cell contexts. *J Hematol Oncol,* 6**,** 6.

Swatek, K. N. & Komander, D. (2016). Ubiquitin modifications. *Cell Res,* 26(4)**,** 399-422.

Szlosarek, P. W., Klabatsa, A., Pallaska, A., Sheaff, M., Smith, P., Crook, T., Grimshaw, M. J., Steele, J. P., Rudd, R. M., Balkwill, F. R. & Fennell, D. A. (2006). In vivo loss of expression of argininosuccinate synthetase in malignant pleural mesothelioma is a biomarker for susceptibility to arginine depletion. *Clin Cancer Res,* 12(23)**,** 7126-31.

Takamizawa, J., Konishi, H., Yanagisawa, K., Tomida, S., Osada, H., Endoh, H., Harano, T., Yatabe, Y., Nagino, M., Nimura, Y., Mitsudomi, T. & Takahashi, T. (2004). Reduced expression of the let-7 microRNAs in human lung cancers in association with shortened postoperative survival. *Cancer Research,* 64(11)**,** 3753-3756.

Tam, S., de Borja, R., Tsao, M. S. & McPherson, J. D. (2014). Robust global microRNA expression profiling using next-generation sequencing technologies. *Laboratory Investigation,* 94(3)**,** 350-358.

Tekirdag, K. A., Akkoc, Y., Kosar, A. & Gozuacik, D. (2016). MIR376 family and cancer. *Histology and Histopathology,* 31(8)**,** 841-855.

Temin, H. M. & Mizutani, S. (1992). RNA-dependent DNA polymerase in virions of Rous sarcoma virus. 1970. *Biotechnology,* 24**,** 51-6.

Testa, J. R., Cheung, M., Pei, J., Below, J. E., Tan, Y., Sementino, E., Cox, N. J., Dogan, A. U., Pass, H. I., Trusa, S., Hesdorffer, M., Nasu, M., Powers, A., Rivera, Z., Comertpay, S.,

Tanji, M., Gaudino, G., Yang, H. & Carbone, M. (2011). Germline BAP1 mutations predispose to malignant mesothelioma. *Nature Genetics,* 43(10)**,** 1022-U140.

Tomasetti, M., Nocchi, L., Staffolani, S., Manzella, N., Amati, M., Goodwin, J., Kluckova, K., Nguyen, M., Strafella, E., Bajzikova, M., Peterka, M., Lettlova, S., Truksa, J., Lee, W., Dong, L. F., Santarelli, L. & Neuzil, J. (2014). MicroRNA-126 suppresses mesothelioma malignancy by targeting IRS1 and interfering with the mitochondrial function. *Antioxid Redox Signal,* 21(15)**,** 2109-25.

Towbin, H., Staehelin, T. & Gordon, J. (1979). Electrophoretic transfer of proteins from polyacrylamide gels to nitrocellulose sheets: procedure and some applications. *Proc Natl Acad Sci U S A,* 76(9)**,** 4350-4.

Travis, W. D. (2014). The 2015 WHO classification of lung tumors. *Pathologe,* 35**,** 188-188.

Treasure, T., Lang-Lazdunski, L., Waller, D., Bliss, J. M., Tan, C., Entwisle, J., Snee, M., O'Brien, M., Thomas, G., Senan, S., O'Byrne, K., Kilburn, L. S., Spicer, J., Landau, D., Edwards, J., Coombes, G., Darlison, L. & Peto, J. (2011). Extra-pleural pneumonectomy versus no extra-pleural pneumonectomy for patients with malignant pleural mesothelioma: clinical outcomes of the Mesothelioma and Radical Surgery (MARS) randomised feasibility study. *Lancet Oncol,* 12(8)**,** 763-72.

Truini, A., Coco, S., Alama, A., Genova, C., Sini, C., Dal Bello, M. G., Barletta, G., Rijavec, E., Burrafato, G., Boccardo, F. & Grossi, F. (2014). Role of microRNAs in malignant mesothelioma. *Cellular and Molecular Life Sciences,* 71(15)**,** 2865-2878.

Truini, A., Coco, S., Nadal, E., Genova, C., Mora, M., Dal Bello, M. G., Vanni, I., Alama, A., Rijavec, E., Biello, F., Barletta, G., Merlo, D. F., Valentino, A., Ferro, P., Ravetti, G. L., Stigliani, S., Vigani, A., Fedeli, F., Beer, D. G., Roncella, S. & Grossi, F. (2017). Downregulation of miR-99a/let-7c/miR-125b miRNA cluster predicts clinical outcome in patients with unresected malignant pleural mesothelioma. *Oncotarget,* 8(40)**,** 68627-68640.

Tsang, J., Zhu, J. & van Oudenaarden, A. (2007). MicroRNA-mediated feedback and feedforward loops are recurrent network motifs in mammals. *Mol Cell,* 26(5)**,** 753-67.

Tsuji, K., Kawauchi, S., Saito, S., Furuya, T., Ikemoto, K., Nakao, M., Yamamoto, S., Oka, M., Hirano, T. & Sasaki, K. (2010). Breast cancer cell lines carry cell line-specific genomic alterations that are distinct from aberrations in breast cancer tissues: comparison of the CGH profiles between cancer cell lines and primary cancer tissues. *BMC Cancer,* 10(15).

Tyagi, S., Chabes, A. L., Wysocka, J. & Herr, W. (2007). E2F activation of S phase promoters via association with HCF-1 and the MLL family of histone H3K4 methyltransferases. *Molecular Cell,* 27(1)**,** 107-119.

van der Bij, S., Schaake, E., Koffijberg, H., Burgers, J. A., de Mol, B. & Moons, K. G. M. (2011). Markers for the non-invasive diagnosis of mesothelioma: a systematic review. *British Journal of Cancer,* 104(8)**,** 1325-1333.

van Meerbeeck, J. P., Bass, P., Debruyne, C., Groen, H. J., Manegold, C., Ardizzoni, A., Gridelli, C., van Marck, E. A., Lentz, M., Giaccone, G. & European Org Res Treatment Canc Lung Canc, C. (1999). A phase II study of gemcitabine in patients with malignant pleural mesothelioma. *Cancer,* 85(12)**,** 2577-2582.

van Meerbeeck, J. P., Scherpereel, A., Surmont, V. F. & Baas, P. (2011). Malignant pleural mesothelioma: The standard of care and challenges for future management. *Critical Reviews in Oncology Hematology,* 78(2)**,** 92-111.

van Zandwijk, N., Clarke, C., Henderson, D., Musk, A. W., Fong, K., Nowak, A., Loneragan, R., McCaughan, B., Boyer, M., Feigen, M., Currow, D., Schofield, P., Nick Pavlakis, B. I., McLean, J., Marshall, H., Leong, S., Keena, V. & Penman, A. (2013). Guidelines for the diagnosis and treatment of malignant pleural mesothelioma. *J Thorac Dis,* 5(6)**,** E254-307.

van Zandwijk, N., Pavlakis, N., Kao, S. C., Linton, A., Boyer, M. J., Clarke, S., Huynh, Y., Chrzanowska, A., Fulham, M. J., Bailey, D. L., Cooper, W. A., Kritharides, L., Ridley, L., Pattison, S. T., MacDiarmid, J., Brahmbhatt, H. & Reid, G. (2017). Safety and activity of microRNA-loaded minicells in patients with recurrent malignant pleural mesothelioma: a first-in-man, phase 1, open-label, dose-escalation study. *Lancet Oncol,* 18(10)**,** 1386-1396.

Veitonmaki, N., Hansson, M., Zhan, F., Sundberg, A., Lofstedt, T., Ljungars, A., Li, Z. C., Martinsson-Niskanen, T., Zeng, M., Yang, Y., Danielsson, L., Kovacek, M., Lundqvist, A., Martensson, L., Teige, I., Tricot, G. & Frendeus, B. (2013). A human ICAM-1 antibody isolated by a function-first approach has potent macrophage-dependent antimyeloma activity in vivo. *Cancer Cell,* 23(4)**,** 502-15.

Veldman-Jones, M. H., Brant, R., Rooney, C., Geh, C., Emery, H., Harbron, C. G., Wappett, M., Sharpe, A., Dymond, M., Barrett, J. C., Harrington, E. A. & Marshall, G. (2015). Evaluating Robustness and Sensitivity of the NanoString Technologies nCounter Platform to Enable Multiplexed Gene Expression Analysis of Clinical Samples. *Cancer Res,* 75(13)**,** 2587-93.

Ventii, K. H., Devi, N. S., Friedrich, K. L., Chernova, T. A., Tighiouart, M., Van Meir, E. G. & Wilkinson, K. D. (2008). BRCA1-associated protein-1 is a tumor suppressor that requires deubiquitinating activity and nuclear localization. *Cancer Research,* 68(17)**,** 6953-6962.

Vijay-Kumar, S., Bugg, C. E. & Cook, W. J. (1987). Structure of ubiquitin refined at 1.8 A resolution. *J Mol Biol,* 194(3)**,** 531-44.

Vogelzang, N. J., Rusthoven, J. J., Symanowski, J., Denham, C., Kaukel, E., Ruffie, P., Gatzemeier, U., Boyer, M., Emri, S., Manegold, C., Niyikiza, C. & Paoletti, P. (2003). Phase III study of pemetrexed in combination with cisplatin versus cisplatin alone in patients with malignant pleural mesothelioma. *J Clin Oncol,* 21(14)**,** 2636-44.

Volinia, S., Calin, G. A., Liu, C. G., Ambs, S., Cimmino, A., Petrocca, F., Visone, R., Iorio, M., Roldo, C., Ferracin, M., Prueitt, R. L., Yanaihara, N., Lanza, G., Scarpa, A., Vecchione, A., Negrini, M., Harris, C. C. & Croce, C. M. (2006). A microRNA expression signature of human solid tumors defines cancer gene targets. *Proc Natl Acad Sci U S A,* 103(7)**,** 2257-61.

Wadt, K. A., Aoude, L. G., Johansson, P., Solinas, A., Pritchard, A., Crainic, O., Andersen, M. T., Kiilgaard, J. F., Heegaard, S., Sunde, L., Federspiel, B., Madore, J., Thompson, J. F., McCarthy, S. W., Goodwin, A., Tsao, H., Jonsson, G., Busam, K., Gupta, R., Trent, J. M., Gerdes, A. M., Brown, K. M., Scolyer, R. A. & Hayward, N. K. (2015). A recurrent germline BAP1 mutation and extension of the BAP1 tumor predisposition spectrum to include basal cell carcinoma. *Clin Genet,* 88(3)**,** 267-72.

Wang, P., Deng, Y. & Fu, X. N. (2017). MiR-509-5p suppresses the proliferation, migration, and invasion of non-small cell lung cancer by targeting YWHAG. *Biochemical and Biophysical Research Communications,* 482(4)**,** 935-941.

Wang, Y. F., Shi, J., Chai, K. Q., Ying, X. H. & Zhou, B. H. P. (2013). The Role of Snail in EMT and Tumorigenesis. *Current Cancer Drug Targets,* 13(9)**,** 963-972.

Wang, Z. Y., Reddy, G. P., Gotway, M. B., Higgins, C. B., Jablons, D. M., Ramaswamy, M., Hawkins, R. A. & Webb, W. R. (2004). Malignant pleural mesothelioma: Evaluation with CT, MR imaging, and PET. *Radiographics,* 24(1)**,** 105-119.

Warburg, O., Wind, F. & Negelein, E. (1927). The metabolism of tumors in the body. *Journal of General Physiology,* 8(6)**,** 519-530.

Weber, J. A., Baxter, D. H., Zhang, S. L., Huang, D. Y., Huang, K. H., Lee, M. J., Galas, D. J. & Wang, K. (2010). The MicroRNA Spectrum in 12 Body Fluids. *Clinical Chemistry,* 56(11)**,** 1733-1741.

Wei, S., Li, Q., Li, Z., Wang, L., Zhang, L. & Xu, Z. (2016). miR-424-5p promotes proliferation of gastric cancer by targeting Smad3 through TGF-beta signaling pathway. *Oncotarget,* 7(46)**,** 75185-75196.

Wertz, I. E. & Dixit, V. M. (2010). Signaling to NF-kappaB: regulation by ubiquitination. *Cold Spring Harb Perspect Biol,* 2(3)**,** a003350.

Wiborg, O., Pedersen, M. S., Wind, A., Berglund, L. E., Marcker, K. A. & Vuust, J. (1985). The human ubiquitin multigene family: some genes contain multiple directly repeated ubiquitin coding sequences. *Embo j,* 4(3)**,** 755-9.

Wiesner, T., Obenauf, A. C., Murali, R., Fried, I., Griewank, K. G., Ulz, P., Windpassinger, C., Wackernagel, W., Loy, S., Wolf, I., Viale, A., Lash, A. E., Pirun, M., Socci, N. D., Ruetten, A., Palmedo, G., Abramson, D., Offit, K., Ott, A., Becker, J. C., Cerroni, L., Kutzner, H., Bastian, B. C. & Speicher, M. R. (2012). Germline mutations in BAP1 predispose to melanocytic tumors. *Experimental Dermatology,* 21(3)**,** e22-e22.

Wilkinson, K. D., Lee, K. M., Deshpande, S., Duerksen-Hughes, P., Boss, J. M. & Pohl, J. (1989). The neuron-specific protein PGP 9.5 is a ubiquitin carboxyl-terminal hydrolase. *Science,* 246(4930)**,** 670-3.

Wilkinson, K. D., Urban, M. K. & Haas, A. L. (1980). Ubiquitin is the ATP-dependent proteolysis factor I of rabbit reticulocytes. *J Biol Chem,* 255(16)**,** 7529-32.

Wilson, A. J., Byun, D. S., Popova, N., Murray, L. B., L'Italien, K., Sowa, Y., Arango, D., Velcich, A., Augenlicht, L. H. & Mariadason, J. M. (2006). Histone deacetylase 3 (HDAC3) and other class IHDACs regulate colon cell maturation and p21 expression and are deregulated in human colon cancer. *Journal of Biological Chemistry,* 281(19)**,** 13548-13558.

Winborn, B. J., Travis, S. M., Todi, S. V., Scaglione, K. M., Xu, P., Williams, A. J., Cohen, R. E., Peng, J. & Paulson, H. L. (2008). The deubiquitinating enzyme ataxin-3, a polyglutamine disease protein, edits Lys63 linkages in mixed linkage ubiquitin chains. *J Biol Chem,* 283(39)**,** 26436-43.

Woods, K., Thomson, J. M. & Hammond, S. M. (2007). Direct regulation of an oncogenic micro-RNA cluster by E2F transcription factors. *J Biol Chem,* 282(4)**,** 2130-4.

Xu, J., Kadariya, Y., Cheung, M., Pei, J., Talarchek, J., Sementino, E., Tan, Y., Menges, C. W., Cai, K. Q., Litwin, S., Peng, H., Karar, J., Rauscher, F. J. & Testa, J. R. (2014). Germline mutation of Bap1 accelerates development of asbestos-induced malignant mesothelioma. *Cancer Res,* 74(16)**,** 4388-97.

Xu, P., Duong, D. M., Seyfried, N. T., Cheng, D., Xie, Y., Robert, J., Rush, J., Hochstrasser, M., Finley, D. & Peng, J. (2009). Quantitative proteomics reveals the function of unconventional ubiquitin chains in proteasomal degradation. *Cell,* 137(1)**,** 133-45.

Xu, X., Chen, H., Lin, Y. W., Hu, Z. H., Mao, Y. Q., Wu, J., Xu, X. L., Zhu, Y., Li, S. Q., Zheng, X. Y. & Xie, L. P. (2013). MicroRNA-409-3p inhibits migration and invasion of bladder cancer cells via targeting c-Met. *Molecules and Cells,* 36(1)**,** 62-68.

Yang, D., Zhan, M., Chen, T., Chen, W., Zhang, Y. H., Xu, S. W., Yan, J. C., Huang, Q. H. & Wang, J. (2017). miR-125b-5p enhances chemotherapy sensitivity to cisplatin by down-regulating Bcl2 in gallbladder cancer. *Scientific Reports,* 7.

Yin, X. H., Ju, L., Wu, W., Xiao, Y., Ying, S. B., Zhang, M., Lou, J. L., Jia, Z. Y., Xia, H. L., Zhu, L. J. & Zhang, X. (2016). [Changes of microRNAs profiling in mesothelial cells exposed to multi-walled carbon nanotubes]. *Zhonghua Lao Dong Wei Sheng Zhi Ye Bing Za Zhi,* 34(7)**,** 531-534.

Yoshikawa, Y., Sato, A., Tsujimura, T., Emi, M., Morinaga, T., Fukuoka, K., Yamada, S., Murakami, A., Kondo, N., Matsumoto, S., Okumura, Y., Tanaka, F., Hasegawa, S., Nakano, T. & Hashimoto-Tamaoki, T. (2012). Frequent inactivation of the BAP1 gene in epithelioid-type malignant mesothelioma. *Cancer Science,* 103(5)**,** 868-874.

Yu, H., Mashtalir, N., Daou, S., Hammond-Martel, I., Ross, J., Sui, G., Hart, G. W., Rauscher, F. J., III, Drobetsky, E., Milot, E., Shi, Y. & Affar, E. B. (2010). The Ubiquitin Carboxyl

Hydrolase BAP1 Forms a Ternary Complex with YY1 and HCF-1 and Is a Critical Regulator of Gene Expression. *Molecular and Cellular Biology,* 30(21)**,** 5071-5085.

Yu, H., Pak, H., Hammond-Martel, I., Ghram, M., Rodrigue, A., Daou, S., Barbour, H., Corbeil, L., Hebert, J., Drobetsky, E., Masson, J. Y., Di Noia, J. M. & Affar, E. B. (2014). Tumor suppressor and deubiquitinase BAP1 promotes DNA double-strand break repair. *Proceedings of the National Academy of Sciences of the United States of America,* 111(1)**,** 285-290.

Yu, M. C., Liang, H. W., Fu, Z., Wang, X. L., Liao, Z. C., Zhou, Y., Liu, Y. Q., Wang, Y. B., Hong, Y. T., Zhou, X. Y., Yan, X., Yu, M., Ma, M., Zhang, W. J., Guo, B. L., Zhang, J. G., Zen, K., Zhang, C. Y., Wang, T., Zhang, Q. P. & Chen, X. (2016). BAP1 suppresses lung cancer progression and is inhibited by miR-31. *Oncotarget,* 7(12)**,** 13742-13753.

Zalcman, G., Mazieres, J., Margery, J., Greillier, L., Audigier-Valette, C., Moro-Sibilot, D., Molinier, O., Corre, R., Monnet, I., Gounant, V., Riviere, F., Janicot, H., Gervais, R., Locher, C., Milleron, B., Tran, Q., Lebitasy, M. P., Morin, F., Creveuil, C., Parienti, J. J. & Scherpereel, A. (2016). Bevacizumab for newly diagnosed pleural mesothelioma in the Mesothelioma Avastin Cisplatin Pemetrexed Study (MAPS): a randomised, controlled, open-label, phase 3 trial. *Lancet,* 387(10026)**,** 1405-1414.

Zauderer, M. G., Bott, M., McMillan, R., Sima, C. S., Rusch, V., Krug, L. M. & Ladanyi, M. (2013). Clinical characteristics of patients with malignant pleural mesothelioma harboring somatic BAP1 mutations. *J Thorac Oncol,* 8(11)**,** 1430-3.

Zehavi, L., Avraham, R., Barzilai, A., Bar-Ilan, D., Navon, R., Sidi, Y., Avni, D. & Leibowitz-Amit, R. (2012). Silencing of a large microRNA cluster on human chromosome 14q32 in melanoma: biological effects of mir-376a and mir-376c on insulin growth factor 1 receptor. *Molecular Cancer,* 11.

Zhai, L. C., Li, Y. L., Lan, X. Z. & Ai, L. (2017). MicroRNA-10a-5p suppresses cancer proliferation and division in human cervical cancer by targeting BDNF. *Experimental and Therapeutic Medicine,* 14(6)**,** 6147-6151.

Zhang, J., Kan, S., Huang, B., Hao, Z., Mak, T. W. & Zhong, Q. (2011). Mule determines the apoptotic response to HDAC inhibitors by targeted ubiquitination and destruction of HDAC2. *Genes & Development,* 25(24)**,** 2610-2618.

Zhang, L., Huang, J., Yang, N., Greshock, J., Megraw, M. S., Giannakakis, A., Liang, S., Naylor, T. L., Barchetti, A., Ward, M. R., Yao, G., Medina, A., O'Brien-Jenkins, A., Katsaros, D., Hatzigeorgiou, A., Gimotty, P. A., Weber, B. L. & Coukos, G. (2006). microRNAs exhibit high frequency genomic alterations in human cancer. *Proc Natl Acad Sci U S A,* 103(24)**,** 9136-41.

Zhang, L., Volinia, S., Bonome, T., Calin, G. A., Greshock, J., Yang, N., Liu, C. G., Giannakakis, A., Alexiou, P., Hasegawa, K., Johnstone, C. N., Megraw, M. S., Adams, S., Lassus, H., Huang, J., Kaur, S., Liang, S., Sethupathy, P., Leminen, A., Simossis, V. A., Sandaltzopoulos, R., Naomoto, Y., Katsaros, D., Gimotty, P. A., DeMichele, A., Huang, Q., Butzow, R., Rustgi, A. K., Weber, B. L., Birrer, M. J., Hatzigeorgiou, A. G., Croce, C. M. & Coukos, G. (2008). Genomic and epigenetic alterations deregulate microRNA expression in human epithelial ovarian cancer. *Proceedings of the National Academy of Sciences of the United States of America,* 105(19)**,** 7004-7009.

Zhang, Y. (2013). MicroRNA Regulation Networks. *In:* Dubitzky, W., Wolkenhauer, O., Cho, K. H. & Yokota, H. (eds.) *Encyclopedia of Systems Biology*. New York: Springer.

Zhang, Y. F., Yu, Y., Song, W. Z., Zhang, R. M., Jin, S., Bai, J. W., Kang, H. B., Wang, X. & Cao, X. C. (2016). miR-410-3p suppresses breast cancer progression by targeting Snail. *Oncology Reports,* 36(1)**,** 480-486.

Zhang, Z. H., Yamashita, H., Toyama, T., Sugiura, H., Ando, Y., Mita, K., Hamaguchi, M., Hara, Y., Kobayashi, S. & Iwase, H. (2005). Quantitation of HDAC1 mRNA expression in invasive carcinoma of the breast. *Breast Cancer Research and Treatment,* 94(1)**,** 11-16.

Zheng, B., Liang, L., Huang, S., Zha, R., Liu, L., Jia, D., Tian, Q., Wang, Q., Wang, C., Long, Z., Zhou, Y., Cao, X., Du, C., Shi, Y. & He, X. (2012). MicroRNA-409 suppresses tumour cell invasion and metastasis by directly targeting radixin in gastric cancers. *Oncogene,* 31(42)**,** 4509-4516.

Zheng, H. Q., Zhou, Z., Huang, J., Chaudhury, L., Dong, J. T. & Chen, C. (2009). Kruppel-like factor 5 promotes breast cell proliferation partially through upregulating the transcription of fibroblast growth factor binding protein 1. *Oncogene,* 28(42)**,** 3702-13.

Zhu, P., Martin, E., Mengwasser, J., Schlag, P., Janssen, K. P. & Gottlicher, M. (2004). Induction of HDAC2 expression upon loss of APC in colorectal tumorigenesis. *Cancer Cell,* 5(5)**,** 455-463.

Zhu, S., Si, M. L., Wu, H. & Mo, Y. Y. (2007). MicroRNA-21 targets the tumor suppressor gene tropomyosin 1 (TPM1). *J Biol Chem,* 282(19)**,** 14328-36.

Zupkovitz, G., Grausenburger, R., Brunmeir, R., Senese, S., Tischler, J., Jurkin, J., Rembold, M., Meunier, D., Egger, G., Lagger, S., Chiocca, S., Propst, F., Weitzer, G. & Seiser, C. (2010). The Cyclin-Dependent Kinase Inhibitor p21 Is a Crucial Target for Histone Deacetylase 1 as a Regulator of Cellular Proliferation. *Molecular and Cellular Biology,* 30(5)**,** 1171-1181.

Appendices

Appendix Figure 5.1: Relationships between biological replicates following normalisation of miRNA expression using "all genes"

Scatter plots show inter-replicate comparisons of counts for 798 miRNAs from NS1, following background subtraction and normalisation of miRNA expression to all 798 miRNA genes "all genes". Comparisons for cell lines MeT5A (*BAP1*$^{+/+}$) and isogenic *BAP1*-mutant cell lines *BAP1*$^{w-/+}$, C5.1 (*BAP1*$^{w-/KO}$) and C3.1 (*BAP1*$^{w-/KO}$) are shown. Power regression equation and R^2 values are displayed. BR: biological replicate.

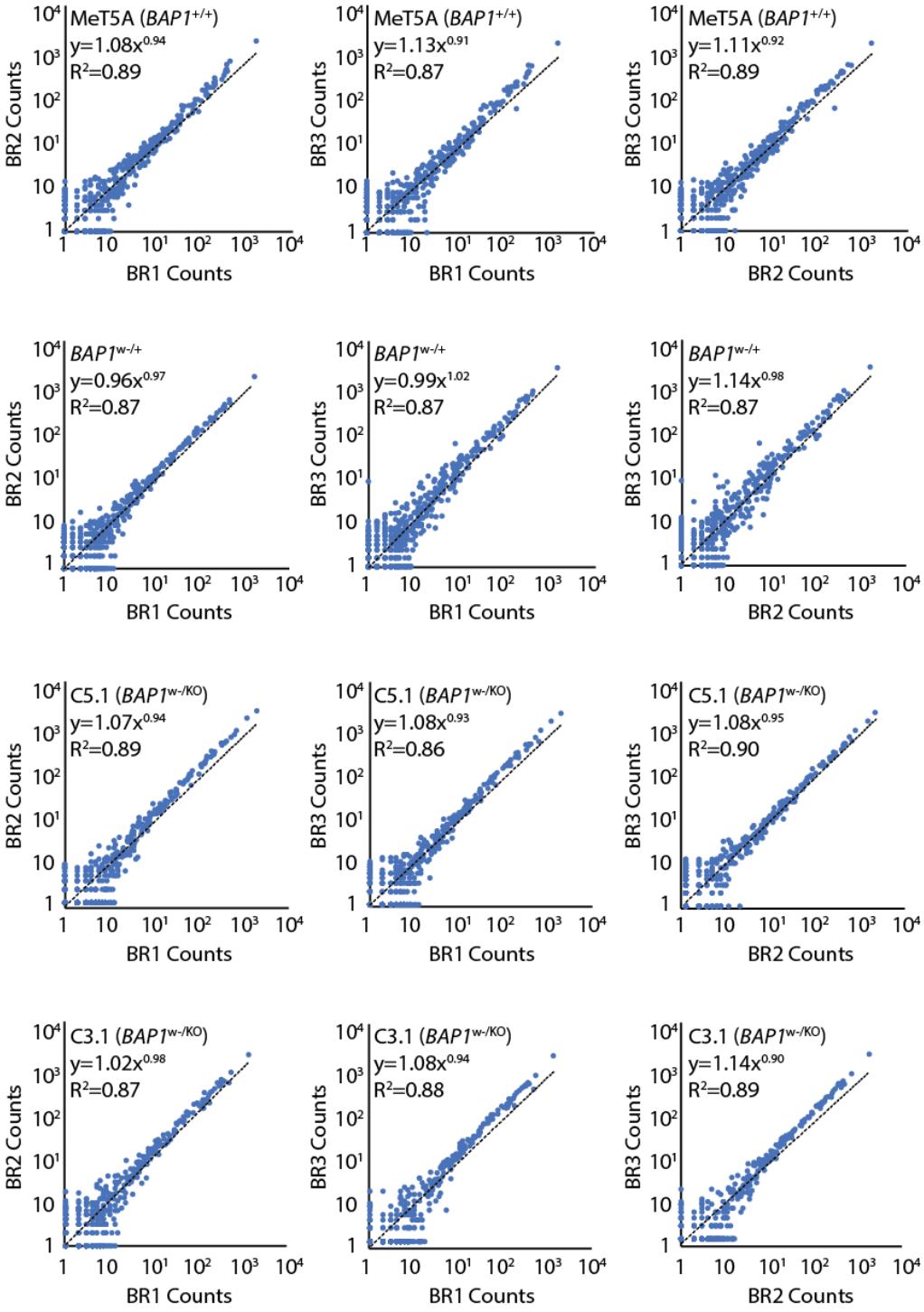

Appendix Figure 5.2: Relationships between biological replicates following normalisation of miRNA expression using "housekeeping genes"

Scatter plots show inter-replicate comparisons of counts for 798 miRNAs from NS1, following background subtraction and normalisation of miRNA expression to the housekeeping genes (B2M, GAPDH, ACTB, RPLP0, RPL19). Comparisons for cell lines MeT5A (*BAP1*$^{+/+}$) and isogenic *BAP1*-mutant cell lines *BAP1*$^{w-/+}$, C5.1 (*BAP1*$^{w-/KO}$) and C3.1 (*BAP1*$^{w-/KO}$) are shown. Power regression equation and R^2 values are displayed. BR: biological replicate.

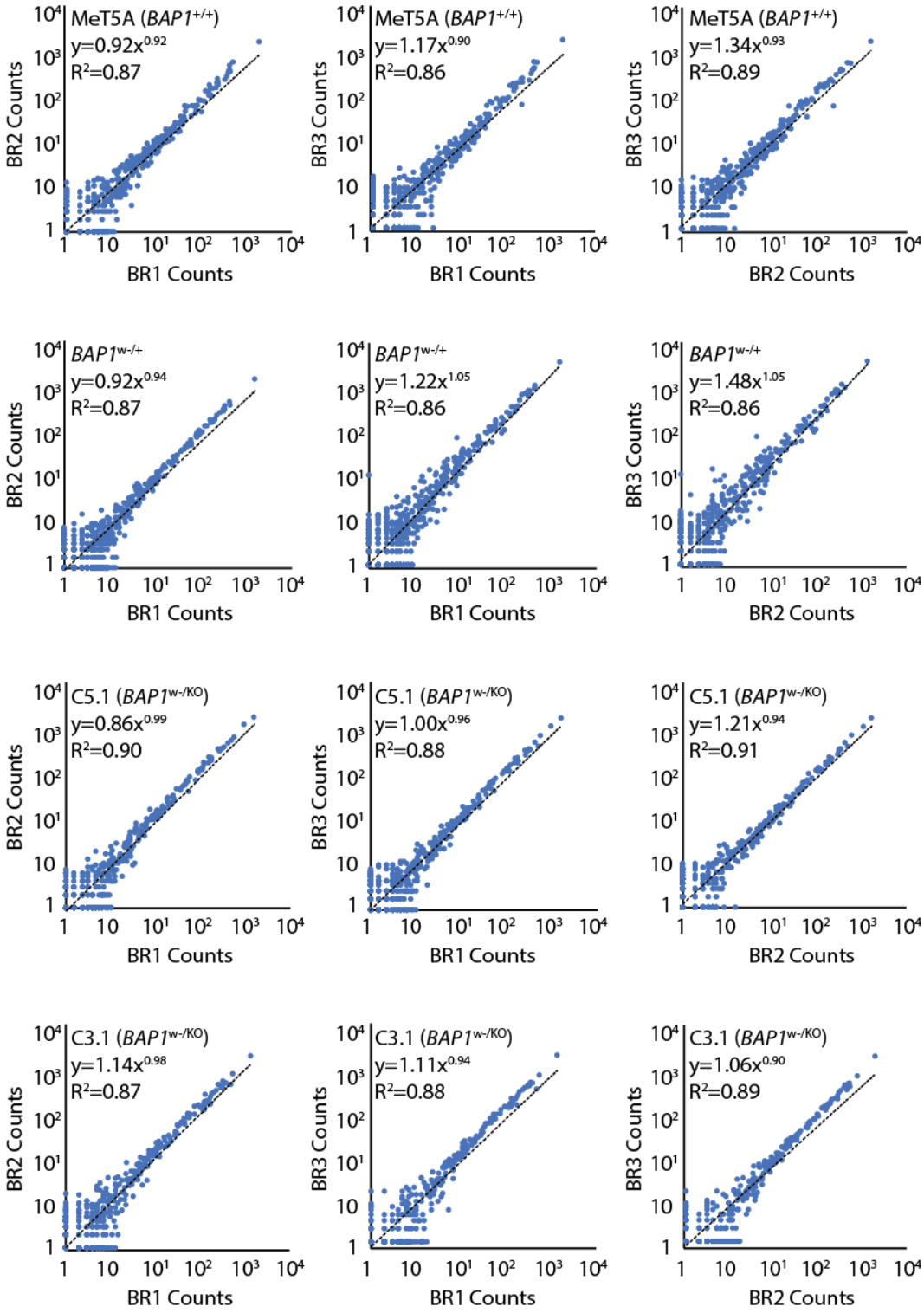

Appendix Figure 5.3: Relationships between biological replicates following normalisation of miRNA expression using "combined positive and negative ligation genes"

Scatter plots show inter-replicate comparisons of counts for 798 miRNAs from NS1, following background subtraction and normalisation of miRNA expression to the six combined positive and negative ligation genes. Comparisons for cell lines MeT5A (*BAP1*$^{+/+}$) and isogenic *BAP1*-mutant cell lines *BAP1*$^{w-/+}$, C5.1 (*BAP1*$^{w-/KO}$) and C3.1 (*BAP1*$^{w-/KO}$) are shown. Power regression equation and R^2 values are displayed. BR: biological replicate.

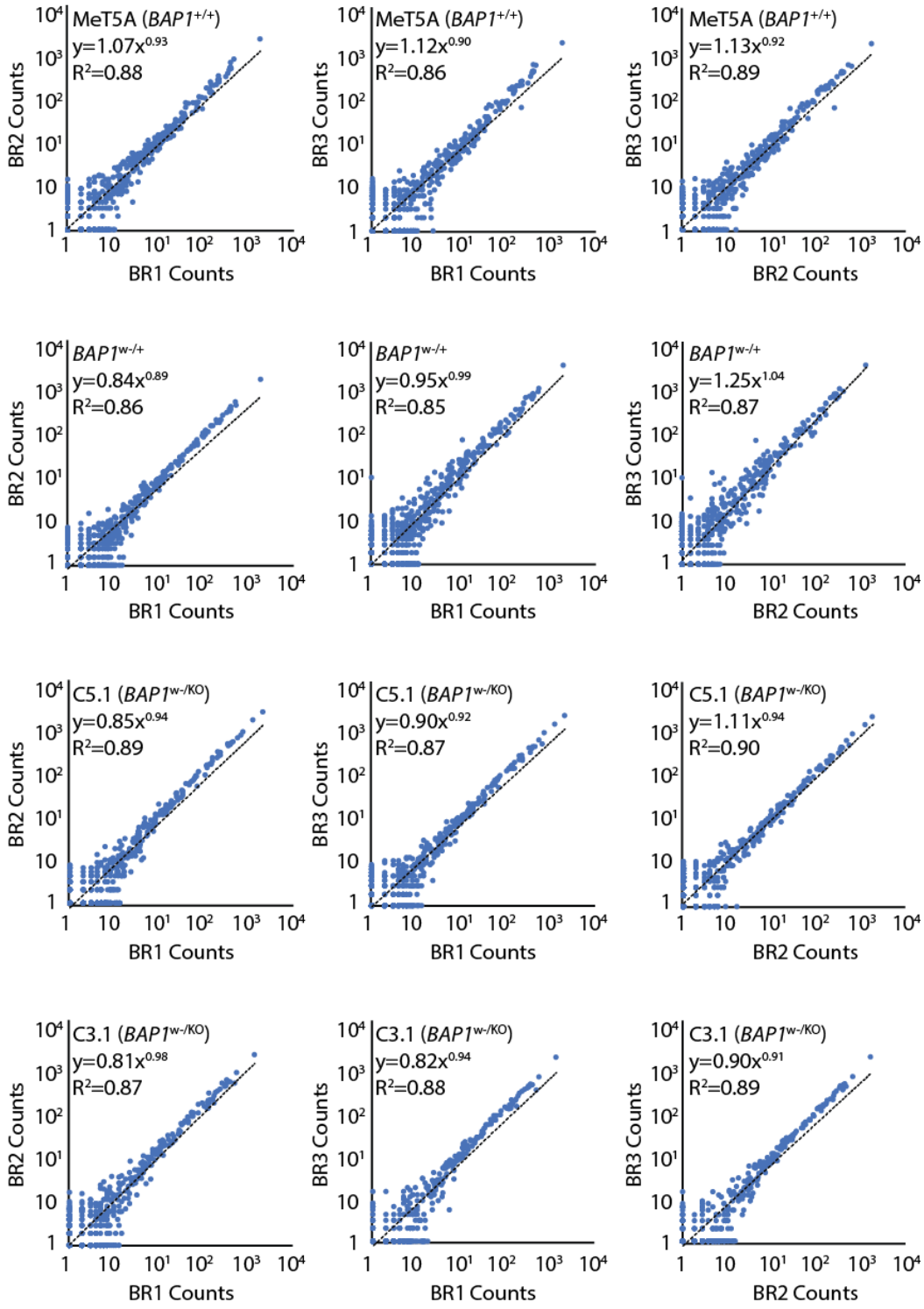

Appendix Figure 5.4: Relationships between biological replicates following normalisation of miRNA expression using "positive controls"

Scatter plots show inter-replicate comparisons of counts for 798 miRNAs from NS1, following background subtraction and normalisation of miRNA expression to the positive controls. Comparisons for cell lines MeT5A (*BAP1*$^{+/+}$) and isogenic *BAP1*-mutant cell lines *BAP1*$^{w-/+}$, C5.1 (*BAP1*$^{w-/KO}$) and C3.1 (*BAP1*$^{w-/KO}$) are shown. Power regression equation and R^2 values are displayed. BR: biological replicate.

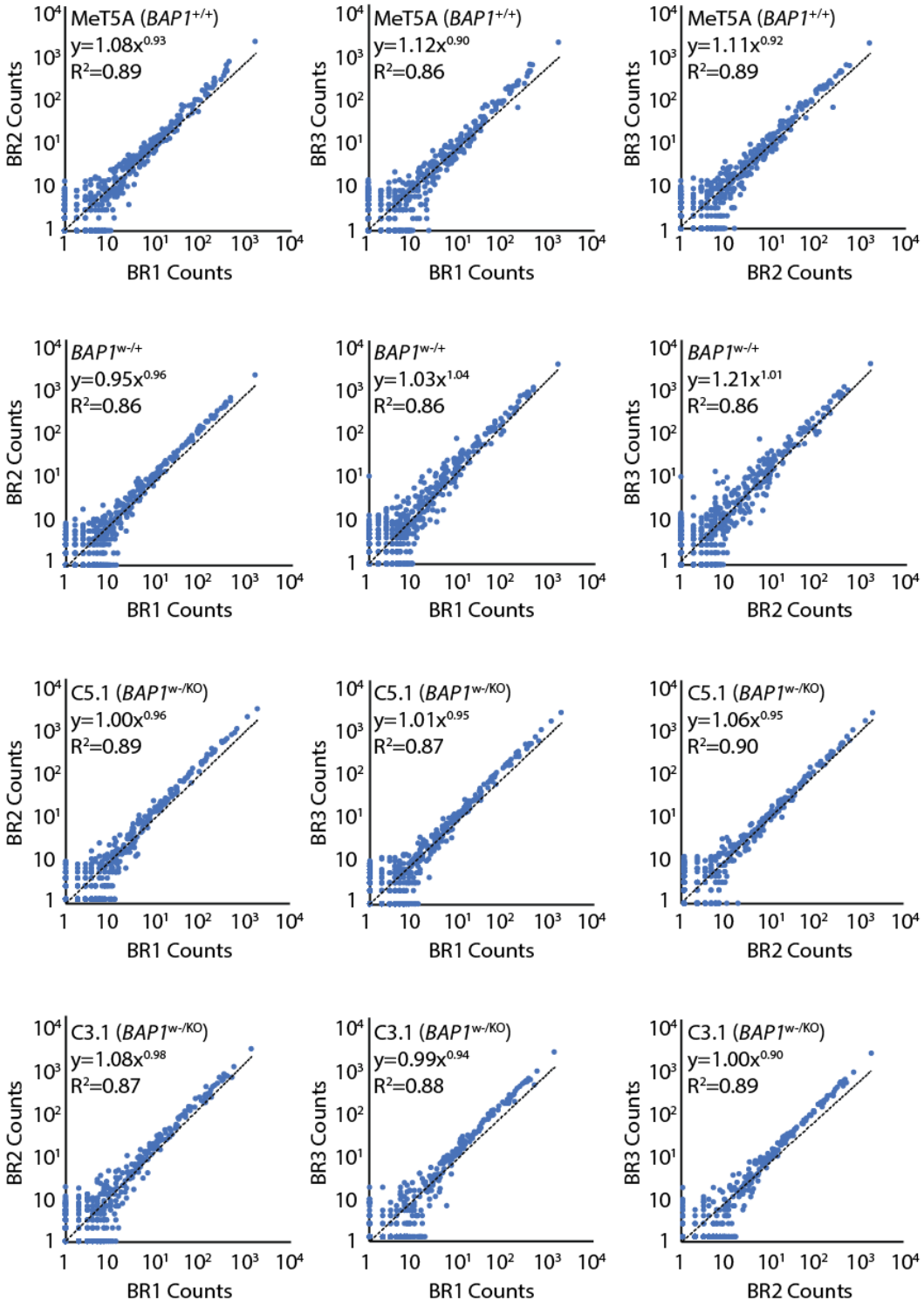

Appendix Figure 5.5: Visualisation of miRNA-gene target networks for representative GO terms.
miRNA-gene target interactions for clusters C1 and C5 were extracted from miRWalk2.0 database (http://zmf.umm.uni-heidelberg.de/apps/zmf/mirwalk2 /index.html). Network maps for gene lists enriched within significant GO terms "Cell motility", "G1/S transition of mitotic cell cycle", "Protein deubiquitylation" and "RISC complex" are illustrated. The box beneath each miRNA indicates whether the miRNA was up-regulated (orange) or down-regulated (blue), in both isogenic *BAP1*$^{w-/KO}$ cell lines (cluster 1), or in C5.1 (*BAP1*$^{w-/KO}$) cells (cluster C5).

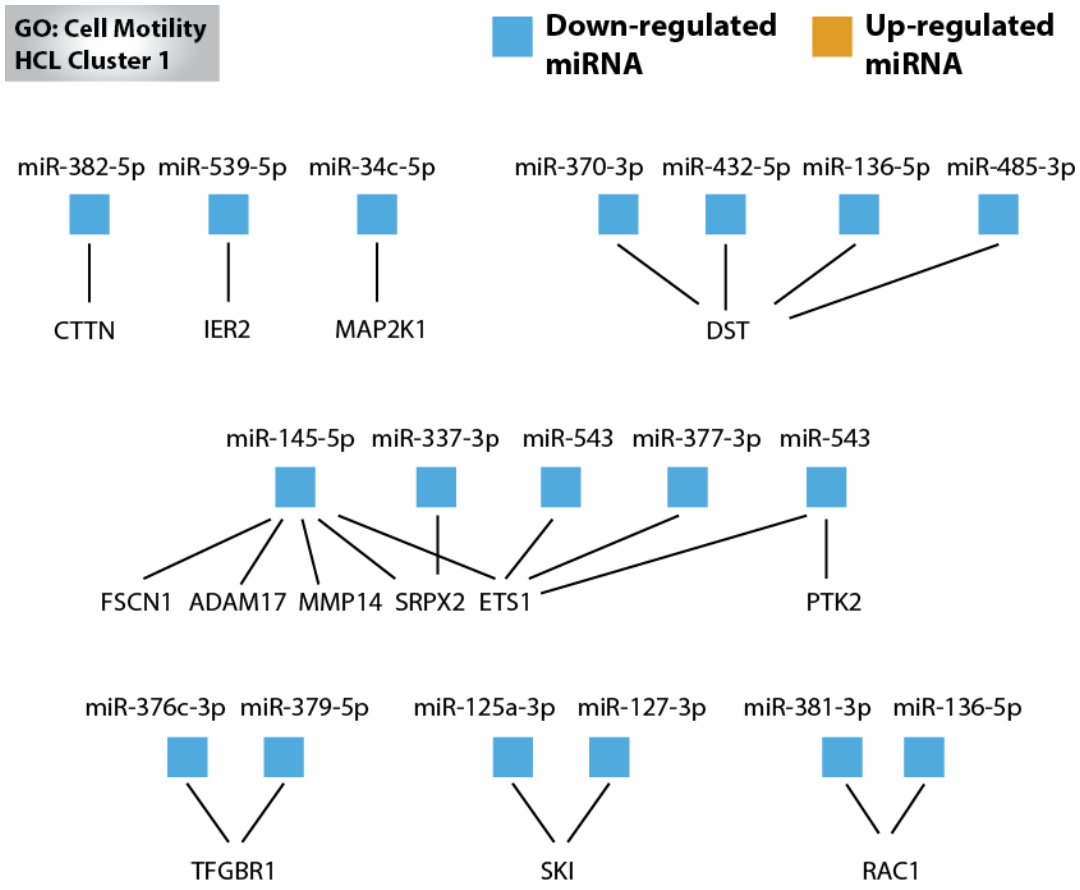

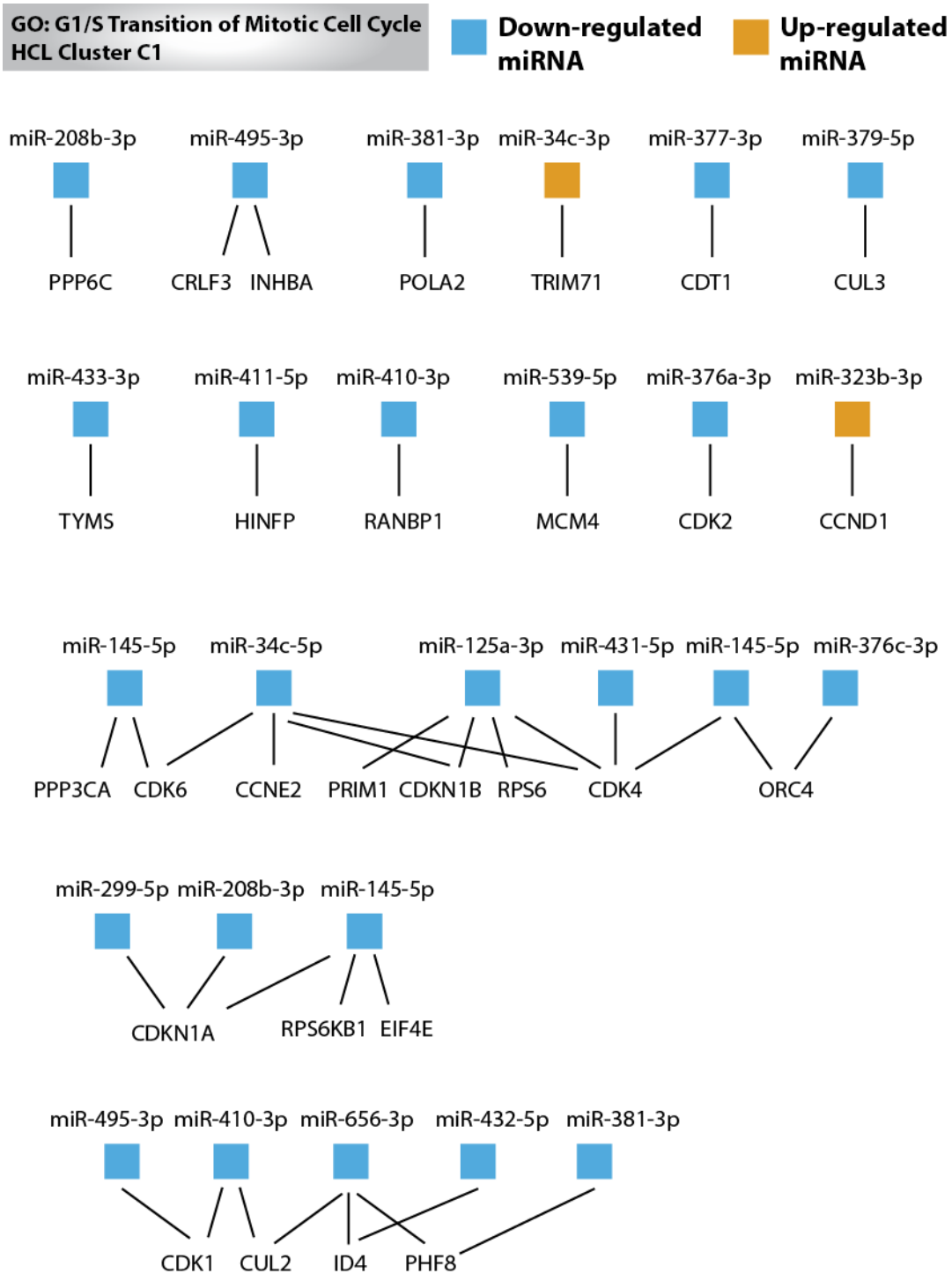
GO: G1/S Transition of Mitotic Cell Cycle
HCL Cluster C1
Down-regulated miRNA
Up-regulated miRNA
miR-208b-3p
PPP6C
miR-495-3p
CRLF3
INHBA
miR-381-3p
POLA2
miR-34c-3p
TRIM71
miR-377-3p
CDT1
miR-379-5p
CUL3
miR-433-3p
TYMS
miR-411-5p
HINFP
miR-410-3p
RANBP1
miR-539-5p
MCM4
miR-376a-3p
CDK2
miR-323b-3p
CCND1
miR-145-5p
PPP3CA
CDK6
miR-34c-5p
CCNE2
miR-125a-3p
PRIM1
CDKN1B
RPS6
miR-431-5p
CDK4
miR-145-5p
ORC4
miR-376c-3p
miR-299-5p
CDKN1A
miR-208b-3p
miR-145-5p
RPS6KB1
EIF4E
miR-495-3p
CDK1
miR-410-3p
CUL2
miR-656-3p
ID4
miR-432-5p
PHF8
miR-381-3p

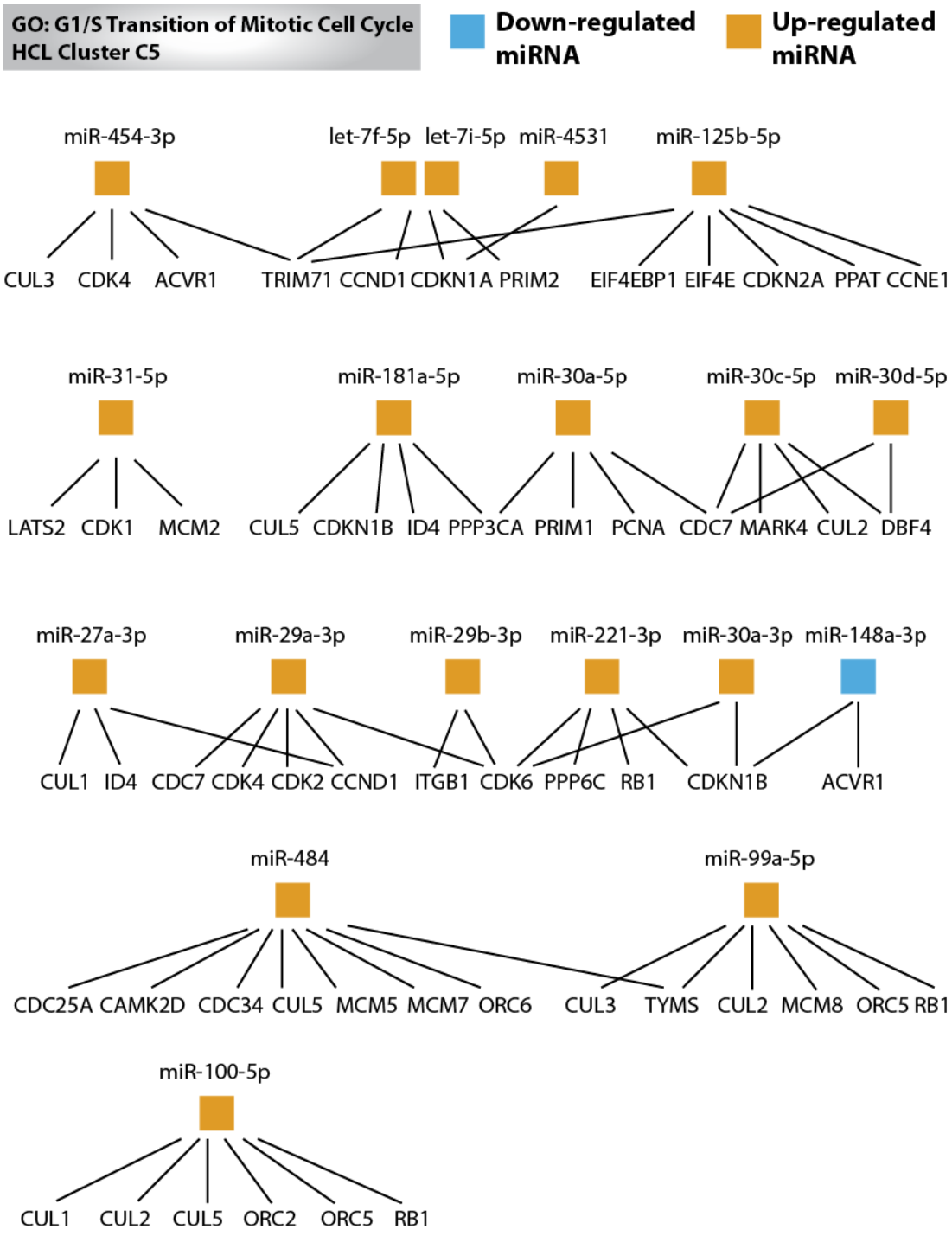
GO: G1/S Transition of Mitotic Cell Cycle
HCL Cluster C5
Down-regulated miRNA
Up-regulated miRNA
miR-454-3p
let-7f-5p
let-7i-5p
miR-4531
miR-125b-5p
CUL3
CDK4
ACVR1
TRIM71
CCND1
CDKN1A
PRIM2
EIF4EBP1
EIF4E
CDKN2A
PPAT
CCNE1
miR-31-5p
miR-181a-5p
miR-30a-5p
miR-30c-5p
miR-30d-5p
LATS2
CDK1
MCM2
CUL5
CDKN1B
ID4
PPP3CA
PRIM1
PCNA
CDC7
MARK4
CUL2
DBF4
miR-27a-3p
miR-29a-3p
miR-29b-3p
miR-221-3p
miR-30a-3p
miR-148a-3p
CUL1
ID4
CDC7
CDK4
CDK2
CCND1
ITGB1
CDK6
PPP6C
RB1
CDKN1B
ACVR1
miR-484
miR-99a-5p
CDC25A
CAMK2D
CDC34
CUL5
MCM5
MCM7
ORC6
CUL3
TYMS
CUL2
MCM8
ORC5
RB1
miR-100-5p
CUL1
CUL2
CUL5
ORC2
ORC5
RB1

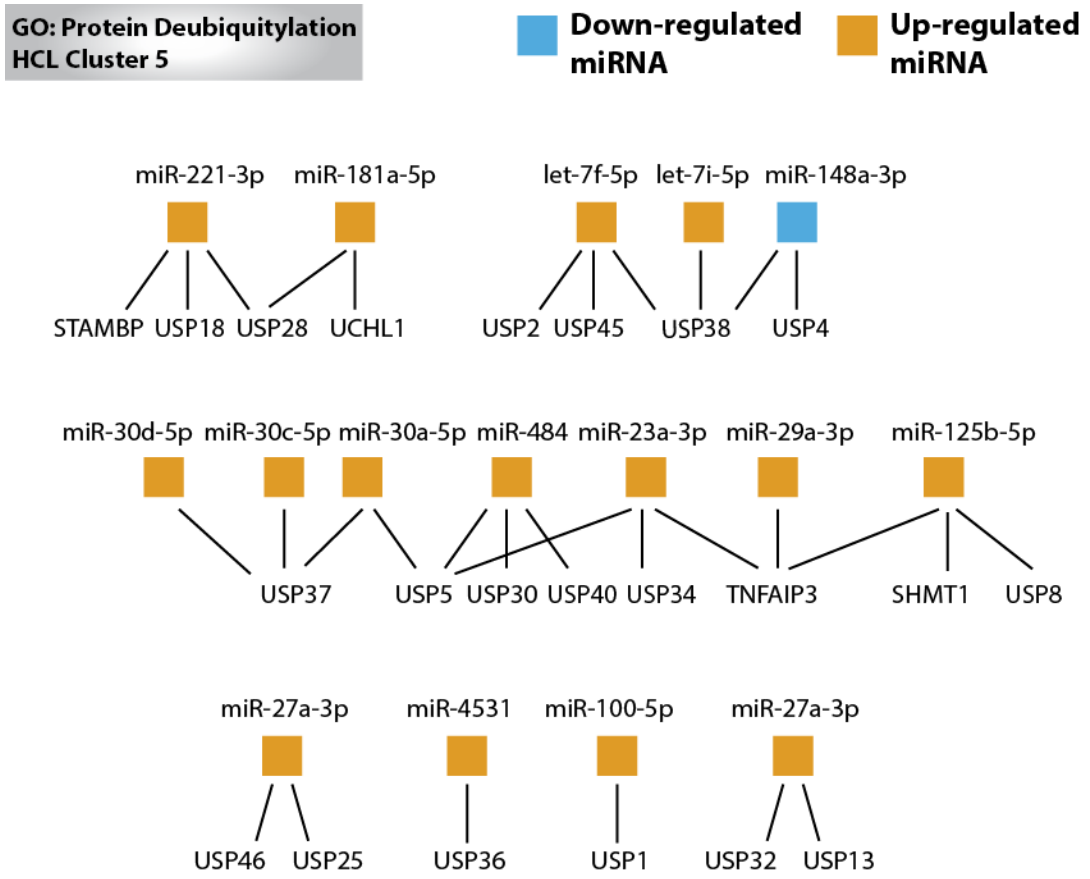
GO: Protein Deubiquitylation
HCL Cluster 5
Down-regulated miRNA
Up-regulated miRNA
miR-221-3p
miR-181a-5p
let-7f-5p
let-7i-5p
miR-148a-3p
STAMBP
USP18
USP28
UCHL1
USP2
USP45
USP38
USP4
miR-30d-5p
miR-30c-5p
miR-30a-5p
miR-484
miR-23a-3p
miR-29a-3p
miR-125b-5p
USP37
USP5
USP30
USP40
USP34
TNFAIP3
SHMT1
USP8
miR-27a-3p
miR-4531
miR-100-5p
miR-27a-3p
USP46
USP25
USP36
USP1
USP32
USP13

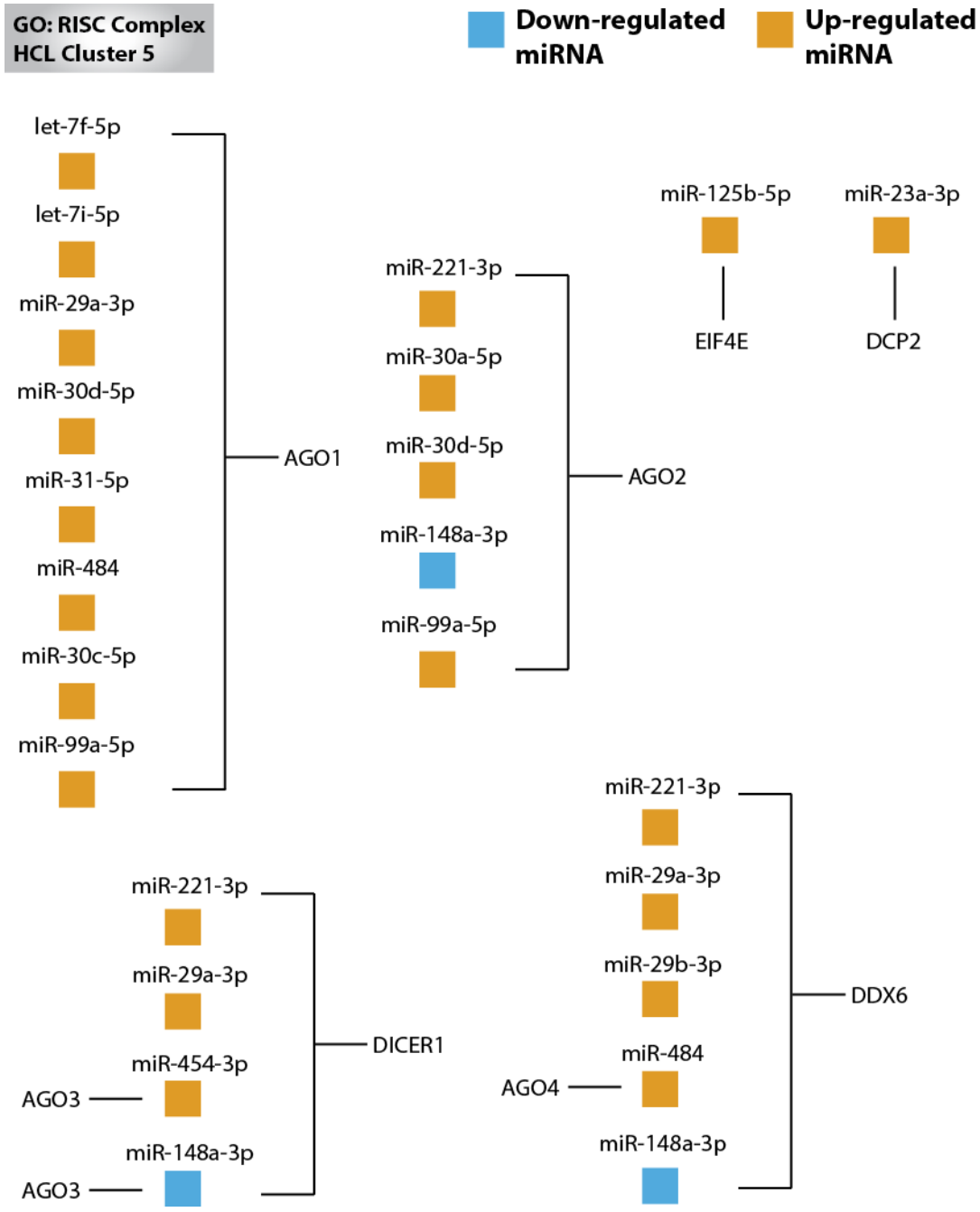
GO: RISC Complex
HCL Cluster 5
Down-regulated miRNA
Up-regulated miRNA
let-7f-5p
let-7i-5p
miR-29a-3p
miR-30d-5p
miR-31-5p
miR-484
miR-30c-5p
miR-99a-5p
AGO1
miR-221-3p
miR-30a-5p
miR-30d-5p
miR-148a-3p
miR-99a-5p
AGO2
miR-125b-5p
EIF4E
miR-23a-3p
DCP2
miR-221-3p
miR-29a-3p
miR-454-3p
AGO3
miR-148a-3p
AGO3
DICER1
miR-221-3p
miR-29a-3p
miR-29b-3p
miR-484
AGO4
miR-148a-3p
DDX6

Appendix Table 5.1: Log_2 ratios of significantly modulated miRNAs from the venn diagrams in Fig. 5.8A and B.

The tables list the significantly modulated miRNAs vs. MeT5A (*BAP1*$^{+/+}$) in individual isogenic MeT5A *BAP1*-mutant cell lines, significantly modulated miRNAs in common to isogenic *BAP1*$^{w-/KO}$ cell lines C3.1 and C5.1 only, and significantly modulated miRNAs in common to all three isogenic MeT5A *BAP1*-mutant cell lines (NS1).

Significantly modulated miRNAs: *BAP1*$^{w-/+}$		
miRNA	**Target Sequence**	**Log_2 Fold Change vs. MeT5A (*BAP1*$^{+/+}$)**
hsa-miR-509-5p	UACUGCAGACAGUGGCAAUCA	2.25
hsa-miR-34c-3p	AAUCACUAACCACACGGCCAGG	2.02
hsa-miR-323b-3p	CCCAAUACACGGUCGACCUCUU	1.82
hsa-miR-3168	GAGUUCUACAGUCAGAC	1.54
hsa-miR-190b	UGAUAUGUUUGAUAUUGGGUU	1.47
hsa-miR-664a-3p	UAUUCAUUUAUCCCCAGCCUACA	1.40
hsa-miR-1246	AAUGGAUUUUUGGAGCAGG	1.25
hsa-miR-361-3p	UCCCCCAGGUGUGAUUCUGAUUU	1.08
hsa-miR-155-5p	UUAAUGCUAAUCGUGAUAGGGGU	0.99
hsa-miR-181a-5p	AACAUUCAACGCUGUCGGUGAGU	0.79
hsa-miR-1306-5p	CCACCUCCCCUGCAAACGUCCA	0.63
hsa-miR-342-3p	UCUCACACAGAAAUCGCACCCGU	0.58
hsa-miR-374a-5p	UUAUAAUACAACCUGAUAAGUG	-0.69
hsa-miR-148a-3p	UCAGUGCACUACAGAACUUUGU	-0.71
hsa-miR-340-5p	UUAUAAAGCAAUGAGACUGAUU	-0.96
hsa-miR-335-5p	UCAAGAGCAAUAACGAAAAAUGU	-1.11
hsa-miR-301b-3p	CAGUGCAAUGAUAUUGUCAAAGC	-1.23
hsa-miR-19a-3p	UGUGCAAAUCUAUGCAAAACUGA	-1.24
hsa-miR-302a-5p	ACUUAAACGUGGAUGUACUUGCU	-1.70
hsa-miR-410-3p	AAUAUAACACAGAUGGCCUGU	-1.83

Significantly modulated miRNAs: C5.1 (*BAP1*$^{w-/KO}$)		
miRNA	**Target Sequence**	**Log_2 Fold Change vs. MeT5A (*BAP1*$^{+/+}$)**
hsa-miR-99a-5p	AACCCGUAGAUCCGAUCUUGUG	3.37
hsa-miR-4531	AUGGAGAAGGCUUCUGA	2.71
hsa-miR-221-5p	ACCUGGCAUACAAUGUAGAUUU	2.45
hsa-miR-515-5p	UUCUCCAAAAGAAAGCACUUUCUG	1.88
hsa-miR-181a-5p	AACAUUCAACGCUGUCGGUGAGU	1.78

hsa-miR-30a-5p	UGUAAACAUCCUCGACUGGAAG	1.74
hsa-miR-125b-5p	UCCCUGAGACCCUAACUUGUGA	1.71
hsa-miR-100-5p	AACCCGUAGAUCCGAACUUGUG	1.65
hsa-miR-5196-3p	UCAUCCUCGUCUCCCUCCCAG	1.51
hsa-miR-6732-3p	UCAUCCUCGUCUCCCUCCCAG	1.51
hsa-miR-197-5p	CGGGUAGAGAGGGCAGUGGGAGG	1.48
hsa-miR-571	UGAGUUGGCCAUCUGAGUGAG	1.35
hsa-miR-1827	UGAGGCAGUAGAUUGAAU	1.30
hsa-miR-30a-3p	CUUUCAGUCGGAUGUUUGCAGC	1.28
hsa-miR-31-5p	AGGCAAGAUGCUGGCAUAGCU	1.17
hsa-miR-30c-5p	UGUAAACAUCCUACACUCUCAGC	1.15
hsa-miR-361-3p	UCCCCCAGGUGUGAUUCUGAUUU	1.14
hsa-miR-450a-5p	UUUUGCGAUGUGUUCCUAAUAU	1.13
hsa-miR-222-3p	AGCUACAUCUGGCUACUGGGU	1.08
hsa-miR-484	UCAGGCUCAGUCCCCUCCCGAU	1.06
hsa-miR-30e-3p	CUUUCAGUCGGAUGUUUACAGC	1.04
hsa-miR-155-5p	UUAAUGCUAAUCGUGAUAGGGGU	1.01
hsa-miR-27a-3p	UUCACAGUGGCUAAGUUCCGC	0.98
hsa-miR-378i	ACUGGACUUGGAGUCAGAAGG	0.98
hsa-miR-30d-5p	UGUAAACAUCCCCGACUGGAAG	0.97
hsa-miR-664a-3p	UAUUCAUUUAUCCCCAGCCUACA	0.97
hsa-miR-320e	AAAGCUGGGUUGAGAAGG	0.94
hsa-miR-454-3p	UAGUGCAAUAUUGCUUAUAGGGU	0.87
hsa-miR-151a-5p	UCGAGGAGCUCACAGUCUAGU	0.86
hsa-miR-29a-3p	UAGCACCAUCUGAAAUCGGUUA	0.84
hsa-miR-342-3p	UCUCACACAGAAAUCGCACCCGU	0.83
hsa-miR-29b-3p	UAGCACCAUUUGAAAUCAGUGUU	0.82
hsa-let-7f-5p	UGAGGUAGUAGAUUGUAUAGUU	0.81
hsa-miR-21-5p	UAGCUUAUCAGACUGAUGUUGA	0.80
hsa-miR-23a-3p	AUCACAUUGCCAGGGAUUUCC	0.80
hsa-miR-29c-3p	UAGCACCAUUUGAAAUCGGUUA	0.79
hsa-miR-28-3p	CACUAGAUUGUGAGCUCCUGGA	0.70
hsa-miR-221-3p	AGCUACAUUGUCUGCUGGGUUUC	0.65
hsa-let-7i-5p	UGAGGUAGUAGUUUGUGCUGUU	0.64
hsa-miR-26a-5p	UUCAAGUAAUCCAGGAUAGGCU	0.64
hsa-miR-345-5p	GCUGACUCCUAGUCCAGGGCUC	0.60
hsa-miR-1260b	AUCCCACCACUGCCACCAU	-0.59
hsa-miR-374a-5p	UUAUAAUACAACCUGAUAAGUG	-0.66
hsa-miR-196a-5p	UAGGUAGUUUCAUGUUGUUGGG	-0.74
hsa-miR-590-5p	GAGCUUAUUCAUAAAAGUGCAG	-1.04
hsa-miR-628-5p	AUGCUGACAUAUUUACUAGAGG	-1.04
hsa-miR-208b-3p	AUAAGACGAACAAAAGGUUUGU	-1.24
hsa-miR-340-5p	UUAUAAAGCAAUGAGACUGAUU	-1.25
hsa-miR-4286	ACCCCACUCCUGGUACC	-1.55

hsa-miR-135b-5p	UAUGGCUUUUCAUUCCUAUGUGA	-1.76
hsa-miR-410-3p	AAUAUAACACAGAUGGCCUGU	-1.93
hsa-miR-891a-5p	UGCAACGAACCUGAGCCACUGA	-2.08
hsa-miR-34c-5p	AGGCAGUGUAGUUAGCUGAUUGC	-2.18
hsa-miR-3161	CUGAUAAGAACAGAGGCCCAGAU	-2.21
hsa-miR-766-3p	ACUCCAGCCCCACAGCCUCAGC	-2.36
hsa-miR-145-5p	GUCCAGUUUUCCCAGGAAUCCCU	-2.37
hsa-miR-154-5p	UAGGUUAUCCGUGUUGCCUUCG	-2.77
hsa-miR-539-5p	GGAGAAAUUAUCCUUGGUGUGU	-2.82
hsa-miR-495-3p	AAACAAACAUGGUGCACUUCUU	-2.94
hsa-miR-433-3p	AUCAUGAUGGGCUCCUCGGUGU	-3.21
hsa-miR-432-5p	UCUUGGAGUAGGUCAUUGGGUGG	-3.32
hsa-miR-656-3p	AAUAUUAUACAGUCAACCUCU	-3.41
hsa-miR-758-3p	UUUGUGACCUGGUCCACUAACC	-3.47
hsa-miR-411-3p	UUUGUGACCUGGUCCACUAACC	-3.47
hsa-miR-337-3p	CUCCUAUAUGAUGCCUUUCUUC	-3.59
hsa-miR-136-5p	ACUCCAUUUGUUUUGAUGAUGGA	-3.96
hsa-miR-377-3p	AUCACACAAAGGCAACUUUUGU	-3.97
hsa-miR-381-3p	UAUACAAGGGCAAGCUCUCUGU	-4.00
hsa-miR-411-5p	UAGUAGACCGUAUAGCGUACG	-4.09
hsa-miR-376b-3p	AUCAUAGAGGAAAAUCCAUGUU	-4.21
hsa-miR-370-3p	GCCUGCUGGGGUGGAACCUGGU	-4.25
hsa-miR-485-3p	GUCAUACACGGCUCUCCUCUCU	-4.39
hsa-miR-543	AAACAUUCGCGGUGCACUUCUU	-4.99
hsa-miR-299-5p	UGGUUUACCGUCCCACAUACAU	-5.05
hsa-miR-337-5p	GAACGGCUUCAUACAGGAGUU	-5.08
hsa-miR-431-5p	UGUCUUGCAGGCCGUCAUGCA	-5.11
hsa-miR-379-5p	UGGUAGACUAUGGAACGUAGG	-5.17
hsa-miR-323a-3p	CACAUUACACGGUCGACCUCU	-5.30
hsa-miR-127-3p	UCGGAUCCGUCUGAGCUUGGCU	-5.36
hsa-miR-487a-3p	AAUCAUACAGGGACAUCCAGUU	-5.41
hsa-miR-487b-3p	AAUCGUACAGGGUCAUCCACUU	-5.43
hsa-miR-382-5p	GAAGUUGUUCGUGGUGGAUUCG	-6.18
hsa-miR-409-3p	GAAUGUUGCUCGGUGAACCCCU	-6.85
hsa-miR-376c-3p	AACAUAGAGGAAAUUCCACGU	-7.11
hsa-miR-376a-3p	AUCAUAGAGGAAAAUCCACGU	-7.62

Significantly modulated miRNAs: C3.1 (*BAP1*$^{w-/KO}$)		
miRNA	**Target Sequence**	**Log_2 Fold Change vs. MeT5A (*BAP1*$^{+/+}$)**
hsa-miR-4516	GGGAGAAGGGUCGGGGC	5.16
hsa-miR-2116-5p	GGUUCUUAGCAUAGGAGGUCU	2.65
hsa-miR-4488	AGGGGGCGGGCUCCGGCG	2.16
hsa-miR-1246	AAUGGAUUUUUGGAGCAGG	2.10
hsa-miR-5196-3p	UCAUCCUCGUCUCCCUCCCAG	1.55
hsa-miR-6732-3p	UCAUCCUCGUCUCCCUCCCAG	1.55
hsa-miR-126-3p	UCGUACCGUGAGUAAUAAUGCG	1.32
hsa-miR-6721-5p	UGGGCAGGGGCUUAUUGUAGGAG	1.27
hsa-miR-155-5p	UUAAUGCUAAUCGUGAUAGGGGU	1.02
hsa-miR-664a-3p	UAUUCAUUUAUCCCCAGCCUACA	1.01
hsa-miR-26a-5p	UUCAAGUAAUCCAGGAUAGGCU	0.98
hsa-miR-361-3p	UCCCCCAGGUGUGAUUCUGAUUU	0.90
hsa-miR-222-3p	AGCUACAUCUGGCUACUGGGU	0.83
hsa-miR-301a-3p	CAGUGCAAUAGUAUUGUCAAAGC	0.80
hsa-miR-132-3p	UAACAGUCUACAGCCAUGGUCG	0.77
hsa-miR-188-5p	CAUCCCUUGCAUGGUGGAGGG	0.73
hsa-miR-30a-5p	UGUAAACAUCCUCGACUGGAAG	0.69
hsa-miR-1306-5p	CCACCUCCCCUGCAAACGUCCA	0.68
hsa-miR-26b-5p	UUCAAGUAAUUCAGGAUAGGU	0.67
hsa-miR-30d-5p	UGUAAACAUCCCCGACUGGAAG	0.67
hsa-miR-29c-3p	UAGCACCAUUUGAAAUCGGUUA	0.65
hsa-let-7g-5p	UGAGGUAGUAGUUUGUACAGUU	0.63
hsa-miR-454-3p	UAGUGCAAUAUUGCUUAUAGGGU	0.63
hsa-miR-183-5p	UAUGGCACUGGUAGAAUUCACU	0.62
hsa-miR-125a-3p	ACAGGUGAGGUUCUUGGGAGCC	-0.65
hsa-miR-148a-3p	UCAGUGCACUACAGAACUUUGU	-0.79
hsa-miR-10a-5p	UACCCUGUAGAUCCGAAUUUGUG	-0.87
hsa-miR-135b-5p	UAUGGCUUUUCAUUCCUAUGUGA	-0.90
hsa-miR-628-5p	AUGCUGACAUAUUUACUAGAGG	-0.99
hsa-miR-455-3p	GCAGUCCAUGGGCAUAUACAC	-1.05
hsa-miR-146b-5p	UGAGAACUGAAUUCCAUAGGCU	-1.47
hsa-miR-1270	CUGGAGAUAUGGAAGAGCUGUGU	-1.74
hsa-miR-410-3p	AAUAUAACACAGAUGGCCUGU	-1.88
hsa-miR-539-5p	GGAGAAAUUAUCCUUGGUGUGU	-2.76
hsa-miR-495-3p	AAACAAACAUGGUGCACUUCUU	-3.14
hsa-miR-433-3p	AUCAUGAUGGGCUCCUCGGUGU	-3.15
hsa-miR-370-3p	GCCUGCUGGGGUGGAACCUGGU	-3.27
hsa-miR-432-5p	UCUUGGAGUAGGUCAUUGGGUGG	-3.27
hsa-miR-377-3p	AUCACACAAAGGCAACUUUUGU	-3.59

hsa-miR-136-5p	ACUCCAUUUGUUUUGAUGAUGGA	-3.91
hsa-miR-337-3p	CUCCUAUAUGAUGCCUUUCUUC	-4.03
hsa-miR-381-3p	UAUACAAGGGCAAGCUCUCUGU	-4.15
hsa-miR-758-3p	UUUGUGACCUGGUCCACUAACC	-4.19
hsa-miR-411-3p	UUUGUGACCUGGUCCACUAACC	-4.19
hsa-miR-656-3p	AAUAUUAUACAGUCAACCUCU	-4.20
hsa-miR-411-5p	UAGUAGACCGUAUAGCGUACG	-4.37
hsa-miR-337-5p	GAACGGCUUCAUACAGGAGUU	-4.43
hsa-miR-376b-3p	AUCAUAGAGGAAAAUCCAUGUU	-4.82
hsa-miR-299-5p	UGGUUUACCGUCCCACAUACAU	-4.94
hsa-miR-543	AAACAUUCGCGGUGCACUUCUU	-5.25
hsa-miR-487b-3p	AAUCGUACAGGGUCAUCCACUU	-5.37
hsa-miR-323a-3p	CACAUUACACGGUCGACCUCU	-5.70
hsa-miR-431-5p	UGUCUUGCAGGCCGUCAUGCA	-5.72
hsa-miR-485-3p	GUCAUACACGGCUCUCCUCUCU	-5.96
hsa-miR-379-5p	UGGUAGACUAUGGAACGUAGG	-5.99
hsa-miR-127-3p	UCGGAUCCGUCUGAGCUUGGCU	-6.17
hsa-miR-487a-3p	AAUCAUACAGGGACAUCCAGUU	-6.20
hsa-miR-382-5p	GAAGUUGUUCGUGGUGGAUUCG	-6.27
hsa-miR-409-3p	GAAUGUUGCUCGGUGAACCCCU	-6.80
hsa-miR-376c-3p	AACAUAGAGGAAAUUCCACGU	-7.06
hsa-miR-376a-3p	AUCAUAGAGGAAAAUCCACGU	-7.24

1 significantly downregulated miRNA in common *BAP1*$^{w-/+}$, C5.1 (*BAP1*$^{w-/KO}$) and C3.1 (*BAP1*$^{w-/KO}$)

	Log_2 Fold Change vs. MeT5A (*BAP1*$^{+/+}$)		
miRNA	***BAP1*$^{w-/+}$**	**C5.1 (*BAP1*$^{w-/KO}$)**	**C3.1 (*BAP1*$^{w-/KO}$)**
hsa-miR-410-3p	-1.83	-1.93	-1.88

30 significantly downregulated miRNAs in common C5.1 (*BAP1*$^{w-/KO}$) and C3.1 (*BAP1*$^{w-/KO}$)

	Log_2 Fold Change vs. MeT5A (*BAP1*$^{+/+}$)	
miRNA	**C5.1 (*BAP1*$^{w-/KO}$)**	**C3.1 (*BAP1*$^{w-/KO}$)**
hsa-miR-127-3p	-5.36	-6.17
hsa-miR-135b-5p	-1.76	-0.90
hsa-miR-136-5p	-3.96	-3.91
hsa-miR-299-5p	-5.05	-4.94
hsa-miR-323a-3p	-5.30	-5.70
hsa-miR-337-3p	-3.59	-4.03
hsa-miR-337-5p	-5.08	-4.43
hsa-miR-370-3p	-4.25	-3.27
hsa-miR-376a-3p	-7.62	-7.24
hsa-miR-376b-3p	-4.21	-4.82

hsa-miR-376c-3p	-7.11	-7.06
hsa-miR-377-3p	-3.97	-3.59
hsa-miR-379-5p	-5.17	-5.99
hsa-miR-381-3p	-4.00	-4.15
hsa-miR-382-5p	-6.18	-6.27
hsa-miR-409-3p	-6.85	-6.80
hsa-miR-411-5p	-4.09	-4.37
hsa-miR-431-5p	-5.11	-5.72
hsa-miR-432-5p	-3.32	-3.27
hsa-miR-433-3p	-3.21	-3.15
hsa-miR-485-3p	-4.39	-5.96
hsa-miR-487a-3p	-5.41	-6.20
hsa-miR-487b-3p	-5.43	-5.37
hsa-miR-495-3p	-2.94	-3.14
hsa-miR-539-5p	-2.82	-2.76
hsa-miR-543	-4.99	-5.25
hsa-miR-628-5p	-1.04	-0.99
hsa-miR-656-3p	-3.41	-4.20
hsa-miR-758-3p	-3.47	-4.19
hsa-miR-411-3p	-3.47	-4.19

3 significantly upregulated miRNAs in common *BAP1*$^{w-/+}$, C5.1 (*BAP1*$^{w-/KO}$) and C3.1 (*BAP1*$^{w-/KO}$)

	Log_2 Fold Change vs. MeT5A (*BAP1*$^{+/+}$)		
miRNA	***BAP1***$^{w-/+}$	**C5.1 (*BAP1*$^{w-/KO}$)**	**C3.1 (*BAP1*$^{w-/KO}$)**
hsa-miR-155-5p	0.99	1.01	1.02
hsa-miR-361-3p	1.08	1.14	0.90
hsa-miR-664a-3p	1.40	0.97	1.01

8 significantly upregulated miRNAs in common C5.1 (*BAP1*$^{w-/KO}$) and C3.1 (*BAP1*$^{w-/KO}$)

	Log_2 Fold Change vs. MeT5A (*BAP1*$^{+/+}$)	
miRNA	**C5.1 (*BAP1*$^{w-/KO}$)**	**C3.1 (*BAP1*$^{w-/KO}$)**
hsa-miR-26a-5p	0.64	0.98
hsa-miR-29c-3p	0.79	0.65
hsa-miR-30a-5p	1.74	0.69
hsa-miR-30d-5p	0.97	0.67
hsa-miR-222-3p	1.08	0.83
hsa-miR-454-3p	0.87	0.63
hsa-miR-5196-3p	1.51	1.55
hsa-miR-6732-3p	1.51	1.55

Appendix Table 5.2: Log_2 fold changes vs. MeT5A (*BAP1*$^{+/+}$) of 113 significantly modulated miRNAs in isogenic MeT5A *BAP1*-mutant cell lines (NS1).

miRNA	*BAP1*$^{w-/+}$	C3.1 (*BAP1*$^{w-/KO}$)	C5.1 (*BAP1*$^{w-/KO}$)
hsa-let-7f-5p	0.17	0.51	0.81
hsa-let-7g-5p	0.21	0.63	0.38
hsa-let-7i-5p	0.03	0.21	0.64
hsa-miR-100-5p	0.44	0.31	1.65
hsa-miR-10a-5p	0.4	-0.87	0.53
hsa-miR-1246	1.25	2.1	-0.45
hsa-miR-125a-3p	-0.48	-0.65	-0.74
hsa-miR-125b-5p	0.22	-0.08	1.71
hsa-miR-126-3p	0.67	1.32	1.14
hsa-miR-1260b	0.36	0.09	-0.59
hsa-miR-127-3p	-0.06	-6.17	-5.36
hsa-miR-1270	0.02	-1.74	-1.38
hsa-miR-1306-5p	0.63	0.68	0.11
hsa-miR-132-3p	0.01	0.77	0.29
hsa-miR-135b-5p	-0.62	-0.9	-1.76
hsa-miR-136-5p	-0.46	-3.91	-3.96
hsa-miR-145-5p	-0.21	-1.34	-2.37
hsa-miR-146b-5p	-1.28	-1.47	-1.2
hsa-miR-148a-3p	-0.71	-0.79	-0.43
hsa-miR-151a-5p	0.34	0.7	0.86
hsa-miR-154-5p	-0.02	-2.31	-2.77
hsa-miR-155-5p	0.99	1.02	1.01
hsa-miR-181a-5p	0.79	0.68	1.78
hsa-miR-1827	0.28	-0.53	1.3
hsa-miR-183-5p	0.18	0.62	-0.01
hsa-miR-188-5p	0.46	0.73	0.54
hsa-miR-190b	1.47	0.29	0.24
hsa-miR-196a-5p	-0.22	0.21	-0.74
hsa-miR-197-5p	0.2	1.23	1.48
hsa-miR-19a-3p	-1.24	0.13	-0.31
hsa-miR-208b-3p	0.58	-0.25	-1.24
hsa-miR-21-5p	0.08	0.59	0.8
hsa-miR-2116-5p	1.34	2.65	1.65
hsa-miR-221-3p	-0.44	0.17	0.65
hsa-miR-221-5p	1.68	1.24	2.45
hsa-miR-222-3p	0.21	0.83	1.08
hsa-miR-23a-3p	0.2	0.45	0.8
hsa-miR-26a-5p	0.33	0.98	0.64
hsa-miR-26b-5p	0.19	0.67	0.45
hsa-miR-27a-3p	-0.05	0.41	0.98
hsa-miR-28-3p	-0.05	0.47	0.7
hsa-miR-299-5p	-0.33	-4.94	-5.05
hsa-miR-29a-3p	-0.06	0.29	0.84
hsa-miR-29b-3p	-0.09	0.43	0.82

hsa-miR-29c-3p	0.01	0.65	0.79
hsa-miR-301a-3p	0.48	0.8	0.07
hsa-miR-301b-3p	-1.23	-0.41	0.09
hsa-miR-302a-5p	-1.7	-0.89	-0.34
hsa-miR-30a-3p	0.24	-0.06	1.28
hsa-miR-30a-5p	0.71	0.69	1.74
hsa-miR-30c-5p	0.27	0.3	1.15
hsa-miR-30d-5p	0.6	0.67	0.97
hsa-miR-30e-3p	0.67	0.14	1.04
hsa-miR-31-5p	0.33	0.51	1.17
hsa-miR-3161	-1.78	-1.62	-2.21
hsa-miR-3168	1.54	1.06	1.69
hsa-miR-320e	-0.04	0.77	0.94
hsa-miR-323a-3p	-0.35	-5.7	-5.3
hsa-miR-323b-3p	1.82	1.16	1.17
hsa-miR-335-5p	-1.11	-0.21	-0.16
hsa-miR-337-3p	-0.42	-4.03	-3.59
hsa-miR-337-5p	-0.46	-4.43	-5.08
hsa-miR-340-5p	-0.96	-0.22	-1.25
hsa-miR-342-3p	0.58	-0.06	0.83
hsa-miR-345-5p	0.12	-0.43	0.6
hsa-miR-34c-3p	2.02	-0.06	0.3
hsa-miR-34c-5p	0.62	-2.64	-2.18
hsa-miR-361-3p	1.08	0.9	1.14
hsa-miR-370-3p	-0.6	-3.27	-4.25
hsa-miR-374a-5p	-0.69	-0.13	-0.66
hsa-miR-376a-3p	-0.61	-7.24	-7.62
hsa-miR-376b-3p	-0.79	-4.82	-4.21
hsa-miR-376c-3p	-0.47	-7.06	-7.11
hsa-miR-377-3p	-1.38	-3.59	-3.97
hsa-miR-378i	-0.18	0.4	0.98
hsa-miR-379-5p	-0.44	-5.99	-5.17
hsa-miR-381-3p	-0.33	-4.15	-4
hsa-miR-382-5p	-0.75	-6.27	-6.18
hsa-miR-409-3p	-0.68	-6.8	-6.85
hsa-miR-410-3p	-1.83	-1.88	-1.93
hsa-miR-411-3p	-0.9	-4.19	-3.47
hsa-miR-411-5p	-0.41	-4.37	-4.09
hsa-miR-4286	-0.19	0.22	-1.55
hsa-miR-431-5p	-1.52	-5.72	-5.11
hsa-miR-432-5p	-1.35	-3.27	-3.32
hsa-miR-433-3p	-1.07	-3.15	-3.21
hsa-miR-4488	0.2	2.16	0.6
hsa-miR-450a-5p	0.25	0.65	1.13
hsa-miR-4516	1.22	5.16	2.13
hsa-miR-4531	1.69	2.06	2.71
hsa-miR-454-3p	0.54	0.63	0.87
hsa-miR-455-3p	-0.44	-1.05	0.27
hsa-miR-484	-0.38	0.02	1.06
hsa-miR-485-3p	-0.24	-5.96	-4.39

hsa-miR-487a-3p	-0.72	-6.2	-5.41
hsa-miR-487b-3p	-0.26	-5.37	-5.43
hsa-miR-495-3p	-0.48	-3.14	-2.94
hsa-miR-509-5p	2.25	0.69	-0.22
hsa-miR-515-5p	0.06	0.61	1.88
hsa-miR-5196-3p	0.55	1.55	1.51
hsa-miR-539-5p	-2.05	-2.76	-2.82
hsa-miR-543	-0.86	-5.25	-4.99
hsa-miR-571	-0.26	1.46	1.35
hsa-miR-590-5p	-0.68	0.25	-1.04
hsa-miR-628-5p	-0.36	-0.99	-1.04
hsa-miR-656-3p	-0.71	-4.2	-3.41
hsa-miR-664a-3p	1.4	1.01	0.97
hsa-miR-6721-5p	0.51	1.27	1.13
hsa-miR-6732-3p	0.55	1.55	1.51
hsa-miR-758-3p	-0.9	-4.19	-3.47
hsa-miR-766-3p	-0.4	-0.61	-2.36
hsa-miR-891a-5p	-1.85	-1.79	-2.08
hsa-miR-99a-5p	1.66	1.17	3.37

Appendix Table 5.3: Log_2 fold changes vs. MeT5A (*BAP1*$^{+/+}$) for significantly modulated ch14q32.31 miRNAs identified in HCL cluster C1 (NS1).

Chromosome 14q32.31 miRNAs in HCL Cluster C1 (NS1)			
	Log_2 Fold Change vs. MeT5A (*BAP1*$^{+/+}$)		
miRNA	***BAP1***$^{w-/+}$	**C5.1 (*BAP1*$^{w-/KO}$)**	**C3.1 (*BAP1*$^{w-/KO}$)**
hsa-miR-127-3p	-0.06	-5.36	-6.17
hsa-miR-136-5p	-0.46	-3.96	-3.91
hsa-miR-154-5p	-0.02	-2.77	-2.31
hsa-miR-299-5p	-0.33	-5.05	-4.94
hsa-miR-323a-3p	-0.35	-5.30	-5.70
hsa-miR-323b-3p	1.82	1.17	1.16
hsa-miR-337-3p	-0.42	-3.59	-4.03
hsa-miR-337-5p	-0.46	-5.08	-4.43
hsa-miR-370-3p	-0.60	-4.25	-3.27
hsa-miR-376a-3p	-0.61	-7.62	-7.24
hsa-miR-376b-3p	-0.79	-4.21	-4.82
hsa-miR-376c-3p	-0.47	-7.11	-7.06
hsa-miR-377-3p	-1.38	-3.97	-3.59
hsa-miR-379-5p	-0.44	-5.17	-5.99
hsa-miR-381-3p	-0.33	-4.00	-4.15
hsa-miR-382-5p	-0.75	-6.18	-6.27
hsa-miR-409-3p	-0.68	-6.85	-6.80
hsa-miR-410-3p	-1.83	-1.93	-1.88
hsa-miR-411-3p	-0.90	-3.47	-4.19
hsa-miR-411-5p	-0.41	-4.09	-4.37
hsa-miR-431-5p	-1.52	-5.11	-5.72
hsa-miR-432-5p	-1.35	-3.32	-3.27
hsa-miR-433-3p	-1.07	-3.21	-3.15
hsa-miR-485-3p	-0.24	-4.39	-5.96
hsa-miR-487a-3p	-0.72	-5.41	-6.20
hsa-miR-487b-3p	-0.26	-5.43	-5.37
hsa-miR-495-3p	-0.48	-2.94	-3.14
hsa-miR-539-5p	-2.05	-2.82	-2.76
hsa-miR-543	-0.86	-4.99	-5.25
hsa-miR-656-3p	-0.71	-3.41	-4.20
hsa-miR-758-3p	-0.90	-3.47	-4.19

Appendix Table 6.1: Log_2 fold changes for 52 significantly modulated miRNAs in BAP1-negative MPM cell lines vs. BAP1-positive MPM cell lines (NS2/NS3)

miRNA	Log_2 Fold Change BAP1-negative vs. BAP1-positive MPM cell lines
hsa-miR-654-3p	0.67
hsa-miR-551b-3p	1.07
hsa-miR-150-5p	0.73
hsa-miR-127-5p	0.78
hsa-miR-937-3p	0.61
hsa-miR-4451	0.82
hsa-miR-1295a	0.86
hsa-miR-936	0.69
hsa-miR-660-3p	0.6
hsa-miR-3690	0.63
hsa-miR-129-5p	0.85
hsa-miR-4787-5p	0.69
hsa-miR-509-3p	1.04
hsa-miR-592	0.69
hsa-miR-149-5p	1.12
hsa-miR-642a-5p	0.65
hsa-miR-513c-5p	0.75
hsa-miR-1-3p	0.83
hsa-miR-216a-5p	0.64
hsa-miR-506-3p	0.6
hsa-miR-200c-3p	1.06
hsa-miR-95-3p	1.32
hsa-miR-199a-5p	-3.83
hsa-miR-1234-3p	-1.29
hsa-miR-628-5p	-1.56
hsa-miR-199a-3p	-5.24
hsa-miR-199b-3p	-5.24
hsa-miR-130a-3p	-0.94
hsa-miR-99a-5p	-2.32
hsa-miR-324-5p	-0.92
hsa-miR-32-5p	-1.21
hsa-miR-98-5p	-0.6
hsa-miR-10a-5p	-2.05
hsa-miR-218-5p	-1.85
hsa-miR-148b-3p	-1.15
hsa-miR-221-3p	-1.62
hsa-miR-625-5p	-1.67
hsa-miR-450b-5p	-1.76
hsa-miR-582-5p	-2.76
hsa-miR-374b-5p	-1.06
hsa-miR-137	-3.32
hsa-miR-1973	-1.58
hsa-let-7i-5p	-0.92
hsa-miR-651-5p	-1.37

hsa-miR-155-5p	-2.34
hsa-miR-130b-3p	-1.63
hsa-miR-450a-5p	-1.56
hsa-miR-3934-5p	-1.43
hsa-miR-196b-5p	-2.42
hsa-miR-186-5p	-1.31
hsa-miR-424-5p	-2.81
hsa-miR-503-5p	-2.9